IMPACT FORCES ON BRIDGE PIERS

IN THE EVENT OF SHIP COLLISIONS

Berend Meijer

MSc. Thesis report

November 2020

TU Delft

Rijkswaterstaat

NOBLEO bouw & infra

Impact forces on bridge piers in the event of ship collisions

by

Berend Meijer

to obtain the degree of Master of Science

at the Delft University of Technology,

to be defended publicly on Thursday December 3, 2020 at 2:30 PM.

Student number:	4317599	
Project duration:	January 6, 2020 – December 3, 2020	
Thesis committee:	Prof. dr. M. Veljkovic,	Steel and Composite Structures, TU Delft
	Prof. dr. ir. L.J. Sluys,	Materials, Mechanics, Management and Design, TU Delft
	Dr. C. Walters,	Ship and Offshore Structures, TU Delft
	Ir. M. de Hertog,	Nobleo Bouw & Infra
	Ir. J.W. Vreugdenhil,	Rijkswaterstaat

An electronic version of this thesis is available at `http://repository.tudelft.nl/`.

Rijkswaterstaat
Ministerie van Infrastructuur en Milieu

TU Delft Delft University of Technology

NOBLEO bouw & infra

A man knocked at the Heavenly gate
his face was scarred and old
He stood before the Man of Fate
for permission to the fold
What have you done? St. Peter asked
to gain admission here?
I've been a Sea-Captain, sir,
for many and many a year!
The Pearly gates swung open wide,
St. Peter touched the bell:
come in and choose your harp, he said;
you've had your share of hell!

(Poet unknown)

Preface

The origin of this thesis is initiated by Nobleo Bouw & Infra during the design phase of the Schinkelbruggen, where the problem is proposed to Rijkswaterstaat. When I found out about this problem I was directly enthusiastic to put obtained knowledge from the Civil Engineering curriculum into practice and combine it with my interests in ships. The beauty of this problem is that it is on the interface of two disciplines; structural engineering and maritime engineering. These two disciplines meet both literally and metaphorically in this problem. My passion for complexity has driven me to tackle this problem.

I am very glad that I could use the broad expertise of the graduation committee, which is asked for this particular problem. First, I would like to express my gratitude to my supervisors from the Delft University of Technology, Milan Veljkovic, Carey Walters and Bert Sluys. Milan Veljkvovic provided me the relevant knowledge on steel structures in one of his courses and helped me with critical remarks on this topic in my research, where he took the time to discuss and help me with the problem. Carey Walters has been very helpful to provide me with knowledge on crashworthiness, ship structures and material modelling. Carey was always ready to help me out with the problems I faced. His passion for crashworthiness is infectious. The expertise of Bert Sluys on computational modelling was very helpful for me, where his knowledge was specifically useful during discussions in meetings with the committee to inform all members. I would like to thank Matthijs de Hertog from Nobleo in particular, for his time and dedication. I found our weekly meetings on the Friday afternoon very helpful, where we could discuss things I found and decisions which should be made. Matthijs has a pile of practical experience which would put my feet back on the ground when I got lost in my research. Thereby, I've enjoyed my involvement in Nobleo Bouw & Infra and the enthusiasm of colleagues. Moreover, I would like to thank Jan Willem Vreugdenhil for his involvement and to welcome me at Rijkswaterstaat. Jan Willem has a lot of knowledge about the background of the problem origin of this research and we could discuss policy-related considerations comprehensively.

Lastly, I would like to thank my friends and family for their support and welcome distractions in the pandemic times where working from home has been the norm. My roommates, which provided welcome (and unwelcome) distraction and coffee breaks. My friends from Stud, which where always ready to get some fresh air together. And my study mates where I could discuss my findings and considerations with, both relevant and irrelevant for my thesis.

Berend Meijer
Rotterdam, November 2020

Abstract

The aim of this thesis is to propose a simple technique to estimate the maximum impact forces acting on bridge piers in the event of ship collisions. This technique is determined for Dutch commercial inland waterway ships (CEMT classes) and set up to be applied by bridge engineers to determine the required bridge pier strength. Many collision events on bridge piers have occurred in history where some led to a major failure of the bridge deck due to insufficient strength of the bridge pier. The accuracy of the Dutch guideline on calculating these impact forces (ROK 1.4) is questioned, mainly regarding the generalisation of the guideline to different ship types. Therefore, an investigation on this topic has been initiated to provide more accuracy in the estimations on bridge pier impact forces in the event of ship collisions.

The background of the collision event is explained to provide basic knowledge and understanding of the origination of the impact forces. A dynamic nonlinear finite element model has been created using ABAQUS/Explicit to simulate the ship-bridge pier collision event. The bridge pier is assumed to be rigid and fixed, while the ship structure is assumed to dissipate all initial kinetic energy through plastic deformation (crushing of the structure). Material properties have been obtained from a test database and include rate effects. The output of the simulations is presented in the form of impact force versus penetration depth.

Existing analytical calculation methods on the crushing strength of a ship's bow structure are presented and studied for the verification of the numerical finite element model. A sensitivity analysis was performed and showed expected behaviour with no singularities. The correlation between the results of numerical simulations and analytical calculation methods showed good agreement. It has been concluded that the numerical calculation model is verified as stable, and results are in agreement with existing calculation methods.

Numerical simulations have been performed on one class IV and two class V ship's bow structures. The deformation process resulting from these simulations showed visually comparable failure behaviour with a real case. Moreover, a thorough analysis of the reaction forces per structural element of the ship's bow was performed where local forces are compared with deformation processes. This showed good correlation.

A relationship between initial kinetic energy levels and maximum impact force has been developed based on the results of the numerical calculations. The global form of the relationship was determined by analysing the results and using found relationships. This form was fitted on the result data through curve fitting techniques. With the established expression, the estimated impact force can be calculated for the event of a ship collision, given an initial kinetic energy level involved in the collision event.

Using this expression, maximum impact force values have been presented for different ship classes. For ships smaller than a medium-sized ship (CEMT IV), the impact force values are higher than is found in the current Dutch guideline. However, lower impact forces are estimated for ships larger than this medium-sized ship. This difference mainly originate from the relatively stiff response of the frontal part of the analysed ship's bows, compared to the ship's bow structure that led to the current Dutch guideline.

With the proposed impact force expression, the maximum impact force on bridge piers in the event of ship collisions could be estimated with increased accuracy.

Contents

1 Introduction

1.1. General

When designing a waterway structure, impact forces should be taken into account. For the design of bridge piers on a waterway, impact forces in the event of ship collisions can often be the normative design load and are therefore essential to incorporate into the design process.

In the Netherlands, rules to determine the impact forces of inland waterway ships on bridges have been determined by Rijkswaterstaat and are published in *'Richtlijnen Ontwerpen Kunstwerken'* (ROK). In this guideline, one general equation is presented to determine the impact force exhibited on bridge piers, based on the initial kinetic energy of the ship, before the collision. The general equation from this guideline is based on a TU Delft Master's Thesis of Joustra and Pater [35], where hand calculations and a finite element analysis are performed on a CEMT class IV inland waterway ship. The concluding equation from this study is critically reviewed by the authors on applying it for other types of ships. Therefore, remarks are added about the application of the equation. One of the remarks is that the equation can only be used with caution for ships classified as CEMT IV (medium-sized ships). And when this is done, it should only be applied to collisions with kinetic energy levels up to 50 MNm (meganewton meter, 1 MNm = 1 MJ), or an impact force of 29 MN. However, where the equation is adopted into the ROK, the remarks about the application of the formula are not present in the ROK.

A preliminary study performed by Nobleo Bouw & Infra indicates that the guideline of Rijkswaterstaat underestimates impact forces for small ships, and overestimates the forces for large ships [27]. The problem surfaced during the design of the new *Schinkelbruggen* (Schinkelbridges) in Amsterdam.

Due to the misalignment between initial kinetic energy and impact force as a result of the general equation, Nobleo Bouw & Infra, in collaboration with Rijkswaterstaat, initiated an investigation on the development of a new set of equations to determine the impact force exhibited by inland waterway ships on bridge piers.

With that, a study is found necessary where the impact forces on bridge piers – or other (rigid) waterway structures – in the event of a ship collision is investigated more accurately and for more ship sizes than is done before for Dutch waterways. The goal is to revisit the current guidelines on impact forces and give advice for an update if necessary.

This report presents an estimation method for determining the collision impact forces on bridge piers in the event of a collision, for Dutch inland waterway ships. The ships on Dutch waterways are classified within CEMT waterway classes (see section 2.1).

1.2. Importance

Usually, ships sail precisely on course. However, there are chances that they get off course during their trip, for all sorts of reasons. If it is getting off course, it may collide with a bridge pier. This event can have disastrous consequences, for example casualties, reduced availability or closure of waterway and rail- or traffic bridge.

An extreme example of a bridge collapse caused by a ship collision is the collapse of the Sunshine Skyway

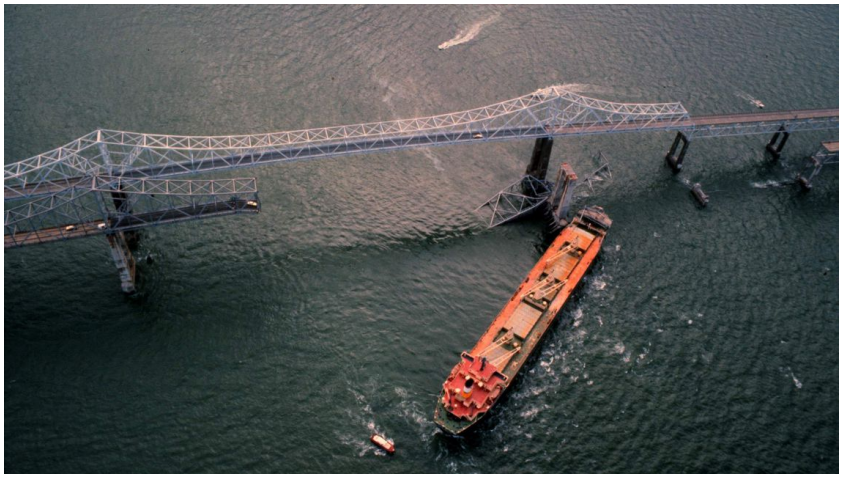

Figure 1.1: An aerial photo from May 9, 1980, shows the freighter Summit Venture after it collided with the Sunshine Skyway bridge. The bridge collapse killed 35 people. [22]

Bridge. On the day of May 9, 1980, the freighter Summit Venture collided with a bridge pier of the Sunshine Skyway Bridge. The collision was caused by a thunderstorm with a sudden squall, resulting in the ship hitting the bridge pier and eventually structural collapse of the bridge deck and the deaths of 35 people when vehicles sunk in Tampa Bay [48].

Figure 1.2: The collapsed section of the Interstate 40 bridge, May 31, 2002 [75]

A more recent example is the I40 Bridge disaster. The picture shown in figure 1.2 shows the consequences of the ship collision with the bridge pier supporting the Interstate 40 road bridge crossing the Arkansas River in 2002. The resulting failure of the supports caused a section of the bridge to collapse, killing 14 people and injuring 11 people [74]. It is found that the collision resulted from a loss of consciousness on the part of the captain of the ship's towboat.

These are examples of bridges which are designed with insufficient strength which have collapsed as result of the accidents. The desired state is a sufficiently strong bridge which will therefore not fail as result of a ship collision. To make sure the bridge will not fail, the bridge (pier) should be stiffer than the colliding structure, and energy should be dissipated through distortion of the colliding (ship) structure.

Figure 1.3: Dutch ship the "Eeemshorn" after colliding with the *Oosterscheldekering* (Eastern Scheldt storm surge barrier). [76]

This is shown by a more recent accident in the Netherlands. On the 5th of May 2018, a Dutch ship collided with high speed onto a surge barrier, the *Oosterscheldekering* (Eastern Scheldt storm surge barrier). The ship, "*Eemshorn*", showed massive damage at the ship's bow after the collision (see figure 1.3). The ship was built in 1983 and has the capacity to carry 875 t, with a length of 56 meters and width of 9.1 meters. From AIS satellite tracking data it is obtained that this ship had an velocity of 11.7 knots (6.0 m/s) just before the collision. Hence, the kinetic energy level before impact is estimated on 22 MNm – assuming that the ship was fully loaded. The picture shows highly plastic distortion of the ship's structure, where the collided structure is only damaged locally, see figure 1.4. This shows the rigid character of a waterway structure during a ship collision, when sufficient stiffness is provided in the waterway structure. Figure 1.3 is used to compare the visual results with of simulations in this study, shown in appendix G.

Figure 1.4: Damaged part of *Oosterscheldekering* after collision of Eemshorn ship [77]

Rijkswaterstaat keeps the figures of collisions on infrastructure or shore on Dutch waterways and calculated a chance of 6.9E-07 these accidents per ship-kilometres, excluding minor accidents. This might seem not significant at first glance. However, this results in an average of 30 major accidents per year. In the diagram of figure 1.5, the amount of ship-bridge accidents found in history are shown for different years. Note that this includes also collision of ships onto bridge decks.

Given these chances of a ship-bridge accident, it is of high importance to consider the impact force in the design phase of the bridge. Not including sufficient strength (or stiffness) in the bridge pier could have profound consequences, since these piers support the superstructure.

1.3. General collision analysis

To provide some initial understanding for the determination of the scope, general information about collision analyses is explained in this section.

The most accurate approach to determine the impact force on a bridge pier in the event of a ship collision is doing full-scale experimental tests on all ship types which could possibly collide with the bridge pier. Or in a

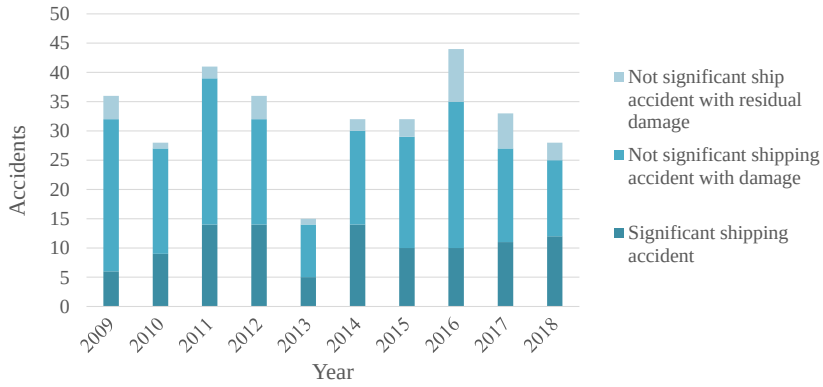

Figure 1.5: Ship-bridge collisions 2009-2018, data received from Rijkswaterstaat

simpler manner, these experiments can be conducted on just a range of ships with different sizes, and results could be extrapolated. Nevertheless, this kind of experimental research is not feasible for this study since the available financial resources are insufficient. Therefore, the analysis will be conducted theoretically.

To theoretically determine the maximum impact force a bridge pier should resist, the collision process of a ship onto a rigid structure should be studied thoroughly. During the collision process, different forces are exhibited onto the pier over a short time, depending on the structure of the ship. With calculation methods, the force-displacement data of the ship collision should be obtained to determine the impact force on the bridge pier.

Just before the collision, the ship has a kinetic energy level E_{kin} which is determined by the mass and the velocity of the ship and the influence of the moving water around the ship. This energy will be dissipated into other forms of energy, of which mainly plastic dissipation energy of the ship's bow. Minorsky [46] proposed a decoupled method to approach the problem of ship-ship collisions. This method could be applied to ship-bridge collisions as well. The collision of a ship could be divided into two problems:

- External dynamics: This problem deals with the energy released for dissipation and the impact impulse of the collision by analysing the rigid motion of the colliding ship, considering the effect of the surrounding water.
- Internal mechanics: The structural response and damage caused by the energy released to be dissipated by crushing of the ship structure during the collision.

These two problems can be treated independently and will hence be treated independently to simplify the problem of this research. Eventually, an energy balance can be used to link the two problems and determine the force distribution during the collision process. The main goal of this study is to determine the impact force for different ship sizes. Therefore, the focus of this research is on the internal mechanics where the factors influencing the external dynamics are assumed as given.

Principle of Conservatism In the analysis of this problem, the principle of conservatism should always be taken into consideration. The principle of conservatism posits that engineers have an obligation to make conservative decisions where uncertainty reigns. In the case of this study, this means that where a decision should be made about matters of high uncertainty and significant impact on the outcome, or matters outside of the scope of this study, the option which results in the highest collision impact force should be taken. By using this principle, it is essential to note where the principle is introduced in order to allow the reader to give his own interpretation to it. It is expected from an engineer to take this conservatism into account for further decisions following up on this study.

1.3.1. External dynamics

The external dynamics include many uncertainties since a ship can collide with a bridge pier for all kind of reasons and in all kind of conditions. For example, a ship with engine problems can sail with full speed into a bridge pier. Beyond the fact that these risks are important to take into consideration when designing a bridge

pier, this research does not have the purpose of evaluating the risks and probabilities behind the collision. The purpose is to find a relation between the ship size properties and given velocity, in normal conditions, and the collision impact force. When this is known, it is up to the reader to evaluate on this value by taking the risks and probabilities into consideration.

Since the external dynamics do not lie within the scope of this research, a value for the kinetic energy will be calculated using a simple calculation. The main equation that will be used is the following, a variant on the well-known equation to calculate the kinetic energy of a moving object from Leibniz and Bernoulli:

$$E_{kin} = C_m C_d \frac{1}{2} m v^2 \tag{1.1}$$

With:

E_{kin} = kinetic energy [kNm]
m = mass (of the ship) [t]
v = velocity of ship [m/s]
C_m = hydrodynamic mass coefficient [-]
C_d = damping coefficient [-]

The most critical variables of the external dynamics are the mass and the velocity. The mass is defined as displacement, or displacement tonnage, in shipbuilding industries. It is generally measured indirectly by calculating the volume of water displaced by the ship and then converting it into weight using Archimedes principle. The displacement is commonly measured as metric tonnes. Since ships are designed for a given *deadweight* tonnage (DWT), the displacement tonnage is not always known. In that case, a factor of 1.4 is generally used, where 40% of the DWT is added to incorporate the own weight of the ship into the mass variable. This is also recommended by Rijkswaterstaat [59]. To meet the principle of conservatism, the maximum mass of a ship (fully loaded) will be used.

The to be considered velocity v of the ship is dependent on the waterway specifications where the regarded waterway structure is placed, and its determined (CEMT) class. According to the ROK [59], the velocity to consider in a collision analysis should be the maximum sailing speed of a loaded ship in open water, increased with the flow velocity of the waterway. The flow velocity is disregarded in the present study, this could eventually be implemented into the input parameters of the concluding advice of this report. The velocities used in this study will be taken from the recommended impact velocities per CEMT class waterway according to the ROK [59].

The hydrodynamic mass coefficient C_m is a factor to incorporate water surrounding the ships which moves together with the ship. The factor is usually taken between 1.05 and 1.10 and depends among others on the ratio between the cross-section of the ship and the waterway and the shape of the ship. To be conservative, a factor of 1.1 could be assumed where needed. The damping coefficient C_d is determined by the damping effect of the water in front of the ship. This is highly dependent on the geometry of the ship and the collided structure. It is expected that this effect is not significant when considering a conventional ship's bow (straight stem) and moreover, the effect is complex and hard to quantify. Therefore, it is usually neglected for frontal collisions in literature, and a coefficient of 1.0 is taken.

Other hydrodynamic factors contributing to the energy (dissipation) at the collision, such as wave generation and reflection of waves onto the construction, are considered as insignificant and will be disregarded in this research.

Another influencing factor, which is not yet found in literature, is the added energy of a running ship engine during the collision. If the collision is a consequence of, for example, an unresponsive ship, the chances are that the engine is still running and the ship propeller is still creating thrust. Since this factor would be included in the external dynamics, this occurrence is not within the scope of this research. Moreover, given the duration of the collision and its high forces, this factor is expected to be of no significance.

According to Saul and Svensson [71], a head-on (frontal) collision condition results in the maximum energy to be absorbed by crumpling of the ship, which would lead to a maximum deformation of the ship which in their turn results in an upper limit of the impact force. Therefore, it is assumed that the ship is sailing with its centre-line aligned with the centre-line of the bridge pier, to establish a frontal collision and upper limit solution.

1.3.2. Internal mechanics

The kinetic energy dissipation in the distortion of the ship is dependent on the strength and stiffness of the bow of the ship. The energy is dissipated in the form of energy absorption through crushing and distortion of the ship's structure during the collision. This is the main contributor of the kinetic energy dissipation since the distortion of the structure will be mainly plastic. It is complex to obtain a precise calculation of the internal mechanics since collision strength of a ship is governed by a mixture mechanical phenomena, such as buckling, yielding, tearing and rupture failure of the materials. There are two classes of theoretical methods used to approach this complex problem, which predict the damage caused by a collision [44]:

1. Analytical method
2. Finite Element Method (FEM)

The analytical method is an approximate calculation of simplified reality. The failure progress is thoroughly analysed by doing (full-scale) experiments, and local failure modes are observed and described using known equations. By combining all these equations, a global approximation can be established about the force which is required to cause failure of all elements of a certain cross-section. This calculation method could be used for estimating the collision impact force of a ship's bow. However, this method can be applied only if the structure of the ship's bow is known. When designing a bridge, the structure of the ships passing the bridge pier is generally not known and could therefore not be used to calculate the collision impact force. However, in this study, the ship's bow structure is known and therefore used in analytical calculations to determine the impact force of the analysed bow structure. This method is elaborated further in chapter 5, where studies which conclude with analytical (semi-empirical) expression are described and applied.

The finite element method (FEM), or finite element analysis (FEA), is the most widely used method for solving problems of engineering and mathematical models. Usually, the behaviour of nature can be described by equations expressed in differential or integral form. The FEM is a numerical technique for solving partial differential or integral equations [49]. In FEM for structural analysis, a structural system is modelled by a set of appropriate finite elements interconnected at discrete points called nodes, with equations of physics forming a link between the nodes. The FEM is a powerful tool for the analysis of structural response in collisions. Therefore, it is widely used to investigate the topic of this thesis.

Different commercial codes are generally used for this problem, such as LS-DYNA, ABAQUS and MSC Dytran. The FEM is considered as an accurate calculation, and it may replace model experiments in some cases. However, attention must be paid to the input and the validation of the output. In addition, due to a large number of elements and the need to solve a dynamic problem step by step, it is very time-consuming to simulate collisions using FEM, with results in high computational costs. However, since the FEM is considered as an accurate calculation and considerable computational power is available for this research, the FEM will be the primary method for determining the collision impact force of ships. Naturally, much effort is necessary for choosing the right input parameters and validation of the outcome. This is done and explained in chapter 4 and chapter 6, respectively.

In the calculations, the ship's structure will be divided into two categories, consisting of a rigid structure (schematised as mass) and a deformable structure (the bow) that is capable of absorbing energy during the collision event.

1.3.3. Ship Structure

When sufficient stiffness is provided by the collided structure, the determining factor for the impact force is the structure of the ship. And for a frontal collision, it is the structure of the ship's bow. Therefore, it is of high relevance to consult information about the structure of a ship, and in particular, of a ship's bow, to determine the strengths and stiffnesses during the collision process and eventually the collision impact force. The ship design company Concordia-Damen is found to be willing to provide drawings of ship's bows from modern inland waterway ships.

1.3.4. Colliding object

The considered colliding object in the analysis of this research is a pier of a bridge spanning over a Dutch waterway. Geometric and structural information about the bridge pier is considered as unknown, since the purpose of this study is to find the impact force which should be incorporated into the design of the bridge. The impact force is often governing for the design of bridge piers where a collision risk is present and will

therefore determine the bridge pier design. Conversely, the design of the bridge pier could influence the magnitude of the impact force as a collision is always about the interaction of multiple objects. However, since the design of the bridge pier is not known, and the design impact force calculation must be generally applicable, a conservative approach is appropriate here.

To ensure this conservatism, the bridge pier is assumed as a rigid and immovable (fixed) wall. In this way, the crushing load of a ship's bow is treated as an upper limit for the impact force on the bridge [40]. Thereby, according to Vrouwenvelder, by assuming the bridge as rigid structure, the upper limit of the impact load can be obtained [81]. According to the Eurocode provision [47], impact by ships against solid structures, such as concrete bridge piers, should, in general, be considered as 'hard' impact, where the kinetic energy is dissipated in the ship structure itself. On top of this assumption on conservatism, this creates a simplification in the collision process since no energy is dissipated in the bridge pier, which makes the calculations less complicated.

Technically, the regarded bridge pier in this study could be considered as a different waterway structure with a sufficiently high stiffness, such that it could be assumed as rigid. Since the geometry and precise structural properties of the bridge pier are neglected, the outcome of this study could be used for other types of structures in waterways which respond in a similar manner as a bridge pier in an event of a ship collision, for example piers of flood defenses, weirs.

The application of protective measures in front of the bridge piers to decrease the impact force magnitude is disregarded in this thesis.

1.4. Problem Statement

The main problem of this study is the lack of substantiation of the correctness of the guidelines of Rijkswaterstaat on ship impact forces for inland waterway ships.

Since Rijkswaterstaat has adopted the impact force expression, without the critical remarks about the applicability on different ship sizes, questions could be asked about generalising the equation for each CEMT ship class. Conform the conclusion of preliminary study by Nobleo Bouw & Infra, it could be that the general equation to determine the impact forces of inland waterway ships may overestimate the impact force of small inland waterway ships and may underestimate the impact force of large inland waterway ships [27].

The solution to this problem should be presented in a way which is suitable for a bridge engineer. In other words, the estimate of impact forces should be dependent on information which is available to a bridge engineer. According to Rijkswaterstaat, the following relevant information is openly available for bridge engineers:

- Type and class of ship
- Weight (both loaded and unloaded)
- Velocity
- Length
- Width
- Draft

The knowledge gap of this study lies in the collision type and considered ship types. Many studies are performed on ship-ship collisions, where a (rigid) striking ship's bow collides with the side hull of a struck ship (for example: [53, 65, 30, 25]). Collisions of sea ships with offshore structures are investigated thoroughly (for example: [5, 11]). And collisions of barge ships with bridge piers (for example: [15, 91]). However, the problem considered in these studies shows only partial overlap with the problem of the present study. The side hull structure of a ship is very different from the considered ship's bow structures which are to be analysed in this thesis. Furthermore, sea ships are substantially heavier and larger and have a different kind of bow structure than CEMT class inland ships. Beside the study of Joustra and Pater [35], no other study is performed on the impact force of Dutch inland waterway ships.

1.4.1. Scope

The scope of this study lies completely on the *impact force* of the ship's bow on a bridge pier during a collision. The probability of the collision and hydrodynamics are hence not within the scope. The following statements define the scope of this research:

- Dutch (commercial) inland CEMT class ships are regarded
- The centre-line of the ship is aligned with the centre-line of the pier, before and during the collision
- The collision event occurs during normal environmental conditions

1.4.2. Research question

To achieve the research objective, the following research question is formulated:

Research Question: *What is the magnitude of the impact force on bridge piers in the event of a ship collision, for ships on Dutch inland waterways based on the information available to bridge engineers?*

To be able to give a complete answer to the research question, some sub-questions are formulated that each treat an integral part of the problem:

- ***Subquestion 1:*** *Which existing calculation methods are present for determining the impact force of ship collisions?*
- ***Subquestion 2:*** *What input parameters should be applied when doing an non-linear finite element simulation on ship collisions with bridge piers?*
- ***Subquestion 3:*** *Does the non-linear finite element simulation set-up show satisfactory results with verification and validation techniques?*
- ***Subquestion 4:*** *What is the force-displacement curve for a class IV and class V ship collision?*

1.5. Report Structure

The remainder of this report first discusses the (theoretical) background of the problem and reviews current standards with recommendations on this problem in chapter 2: Background. In 3: Methodology the research approach is explained with an explanation of the calculation method which is utilised and shows how the calculations model is verified and validated. The methodology chapter is followed by a thorough explanation of the calculation model properties and parameters in chapter 4: Nonlinear Finite Element Analysis. Simplified calculation methods to verify calculation results are explained in 5: Simplified Analytical Calculation Methods, and applied for one example in this chapter. Chapter 6: Verification and Validation, elaborates upon the verification and validation methods applied to the calculation method of the problem. The final results of the calculations are presented in chapter 7: Results, where the results are interpreted as well. The thesis ends with conclusions, limitations and recommendations for further research in chapter 8: Conclusion and Discussion.

2

Background

Background information of the research topic is described in this chapter, to provide the necessary understanding of the topic for answering the research question.

The collision of bodies in this research is assumed as 'hard collision', which means that a moving object collides with a rigid, immovable object. The moving object in the considered collision is an inland waterway ship, which sails on a Dutch waterway. Since the hit structure stands still, it contains no (kinetic) energy. Assumed is that the moving ship contains all the energy involved in the collision, and will dissipate all the energy involved in the collision. The energy will dissipate mainly into distortion energy of the plastic deformation of the ship structure, by, for example, folding and bending of elements. For this reason, information about the structure of the ship is of high relevance for this research. Furthermore, since the collision is considered as a frontal collision, where the ship's bow will have the first contact with the hit structure, the structure of the frontal part of the ship is the relevant part.

First, relevant ships (structures) are described in this chapter after which more information about the ship's bow is given. This is continued with mechanics of a ship-bridge collision, first on a global scale and then on a more local scale. Thereafter, the current relevant guidelines are treated and compared. To eventually end with a description of, and a review on, the background study behind the current guideline of Rijkswaterstaat.

2.1. Ships on Dutch waterways

The majority of Dutch waterways are managed by Rijkswaterstaat. With that, Rijkswaterstaat defines requirements for these waterways. And moreover, defines the maximum ship sizes which are admitted to sail on each waterway. For all large navigable waterways, the maximum ship size is defined by the 'Classification of European Inland Waterways'. It was created by the *Conférence Européenne des Ministres des Transports* (CEMT) in 1992. Hence the range of dimensions is also referred to as CEMT Class I-VII. The admitted ship size of each waterway is limited by the dimensions of the structures, including the locks and bridges, on the route. Rijkswaterstaat defines displacement tonnages and maximum velocities for all CEMT Classes in the Netherlands, shown in table 2.1.

In this study, ships are referred to according to a CEMT class. However, ships are actually classified according to RWS classes in the Netherlands, and waterways according to CEMT classes. Nevertheless, since all parameters are defined for CEMT classes, in this study this class system is used for the ships. More info about the ships of the different CEMT Classes is provided in appendix A.

This thesis considers only ships which are defined with a CEMT class, this means that small (recreational) ships are disregarded. Moreover, both ships and barges are classified within the CEMT classes. However, only (uncoupled) ships are considered in this study since the barges or coupled ships show a different collision behaviour which asks for a different estimation approach. This lies not within the scope of this research.

Class-Type	Length[1] [m]	Width[1] [m]	Draught[1] [m]	Water displacement[2] [t]	Velocity[2] [m/s]
I-Bulk	38.5	4.05	2.2	400	4.1
II-Bulk	55.0	6.60	2.6	560	4.8
III-Bulk	67.0	8.20	2.5	1000	5.1
IV-Bulk	85.0	9.50	2.5	1500	5.3
Vb-Bulk	135.0	11.40	3.5	3000	4.5
Vb-Tanker	135.0	21.80	4.4	3000	4.5
Va-Bulk	110.0	11.40	3.0	3000	5.5
Va-Tanker	110.0	11.40	3.5	3000	5.5

Table 2.1: CEMT Class ships considered in this study and their general characteristics relevant for collision analyses.

[1] From bureauvoorlichtingbinnenvaart.nl (see appendix A)
[2] Values recommended by Rijkswaterstaat [59].

2.1.1. Dutch inland waterway ships figures

Data about the current ships in the Netherlands is analysed to gain information about ship lengths, tonnages and their construction year. Relationships are determined, which can be useful in the analysis process and conclusion of this study.

The data is extracted from the website of the Dutch association for inland navigation ships ("*Vereniging 'De Binnenvaart'*), where a database consisting of 16758 Dutch navigation ships of different types from about 1875 up to 2020 is presented [78]. The complete database is not publicly available to download as an analysable data set and therefore, 5085 ships are extracted from the website code for analysis. This collection is gathered from the pages of ship names starting with an 'A' or a 'D', which is considered as random sample. The columns of most relevance in the data set are the year, tonnage and length. Data about the construction years is depicted in figures 2.1a and 2.1b.

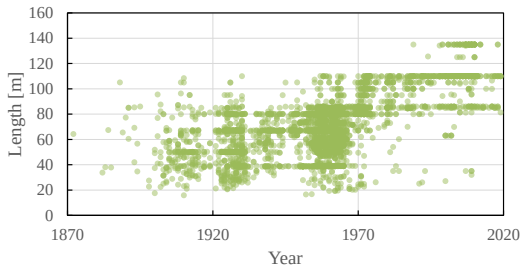

(a) Ship length vs. construction year (data source: debinnenvaart.nl)

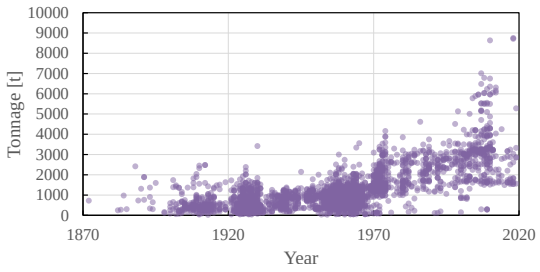

(b) Ship tonnage vs. construction year (data source: debinnenvaart.nl)

The lengths of navigation ships show a relatively high spread up to a construction year of around 1975. In general, longer ships are built after this year. The tonnage data shows a more linear character, which is increasing up to 2020. Valuable information can be extracted from the ratio of the tonnage and length of the ships. A common thought is that ships are increasingly large and pushed to their boundaries in terms of tonnage. This can confirmed by observing the graph in figure 2.2.

From around 1950, the ratios increase with time, with some extremes occurring in the past decades. This means that the cargo capacity per meter length of the ships is increasing. A logical cause for this increase is an increase in width. This can partly be the case, but the shown amount of difference could not only be reached with the increased width of the ships, as width limits are easily met. Nonetheless, the graph shows the trend in pushing the cargo capacity to the boundaries of the ship geometry, implicitly.

2.1.2. Ship structure

To provide some insight on the main structural elements of the analysed ships, this section elaborates on the different structural parts of the ship and their elements.

The bow of an inland waterway ship is formed of steel members. Usually, the part in front of the collision bulkhead is considered as fore-end, or bow structure. On many conventional ships a stem bar, which is a

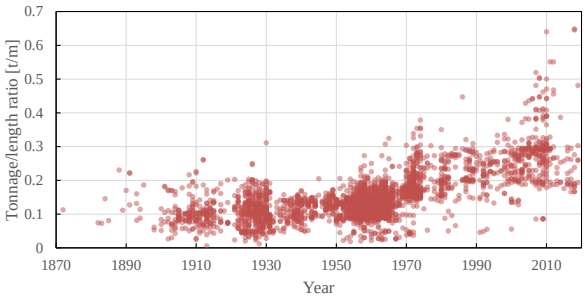

Figure 2.2: Ship length vs. tonnage/length-ratio (data source: debinnenvaart.nl)

solid round bar, is fitted from the keel to the waterline region, and a radiused plate fitted to form the upper part of the stem [20]. This forms what is referred to as a 'soft nose' stem, which in the event of a collision should buckle under load, keeping the impact damage to a minimum. Older ships had a more rigid stem which could cause considerable damage on the hit structure during an impact. An overall view of the fore-end structure is shown in figures 2.3 and 2.4.

The mid-ship section of the ship starts from the foremost bulkhead. Bulkheads are vertical partitions arranged transversely in the length of the ship. The bulkheads divide the ship into watertight compartments to prevent full flooding of the inside of the ship and provide fire safety. Structurally, the bulkheads serve as hull strength members, not only carrying some of the ship's vertical loading but also resisting any tendency for transverse deformation of the ship. A typical mid-ship section is drawn in figure 2.5.

The shell plating forms the outer watertight skin of the ship and contributes strongly to the longitudinal strength and stiffness of the ship. Internal strengthening of the shell plating might be either transversal or longitudinal and provides protection to the collapse of the plating under variate loads the ship is subjected to.

The bottom and side shell plating consist of a series of flat and curved steel plates usually with a greater width than length which are butt welded together. The vertical welded joints are referred to as 'butts' and horizontal welded joints as 'seams'. Stiffening members, both longitudinal and transverse, are generally welded to the shell by continuous fillet welds. Where the bending stresses are the highest, generally presumed as the middle 40% length of the mid-ship section, the bottom and side shell plating are at their greatest thickness. The plating then tapers to a lesser thickness at the ends of the ship. The side shell plating thickness is usually increased at the stern frame connection, at any shaft brackets and in the way of the hawse pipes, where considerable shafting occurs. Further shell plate thickness increases are found in the panting region.

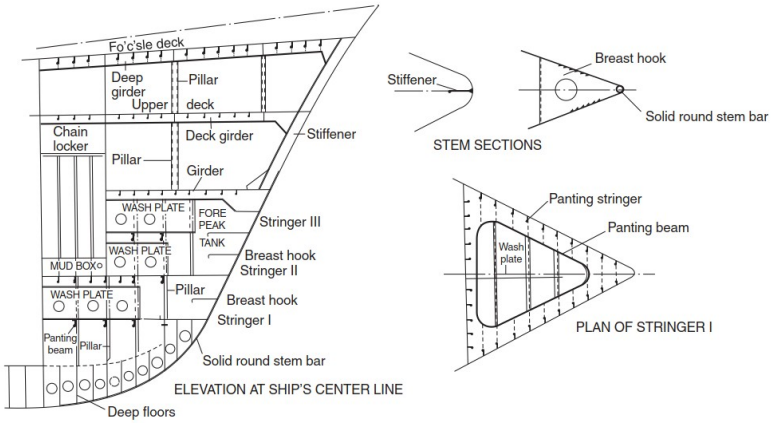

Figure 2.3: Fore end construction [20]

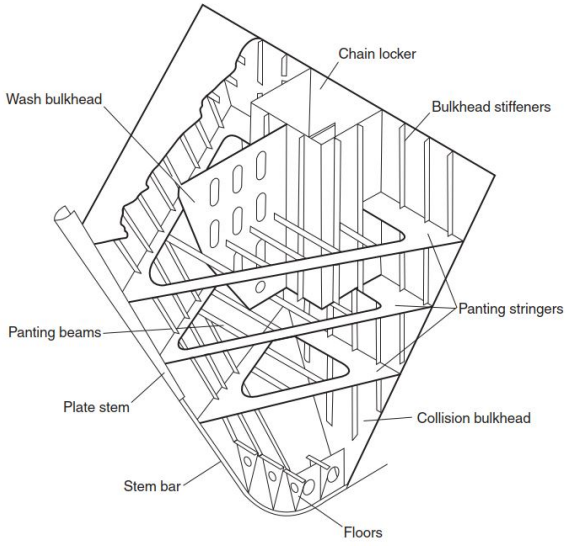

Figure 2.4: Fore end structure [20]

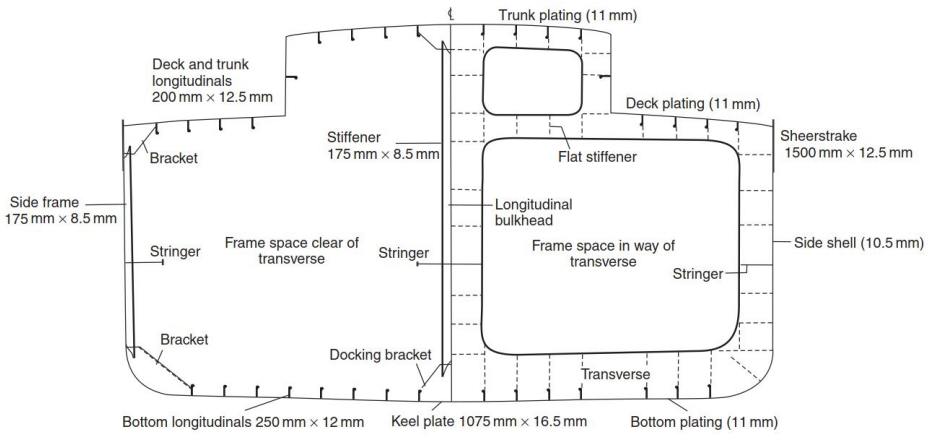

Figure 2.5: Midship section of a coastal tanker < 5000 tonnes [20]

2.1.3. Ship's bow geometry

The bow is the forward part of the hull of a ship, the structure which is usually most forward when the ship is underway. Since this is the fore-end of the ship, this is the first structure of the ship colliding with the bridge pier in case of a ship-bridge collision. This is, therefore, a greatly relevant structure involved in this study.

Nowadays, ships are designed with different bow shapes depending on the purpose of the ship. Bulbous bows are for example developed to decrease the drag of the ship hull. Dutch inland waterways are almost in all cases designed with a straight stern, also referred to as conventional bow. Therefore, this is the type of bow that is investigated in this study.

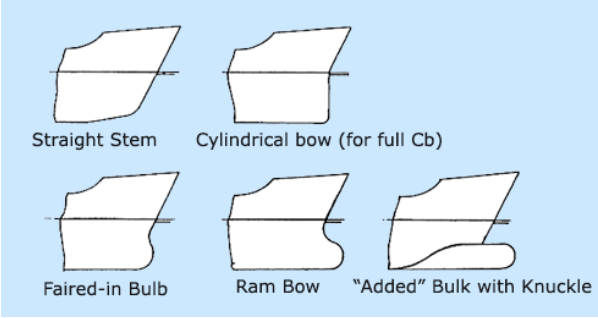

Figure 2.6: Common types of ship's bows [37]

Ship designs could either be transversely framed or longitudinally framed. The name defines the direction of the hull stiffeners. A longitudinally framed design employs stiffeners that run longitudinally, that is along the length of the ship. This is generally used for sea going ships having a length more than 120 meter. The inland waterway ships considered in this study are presumed to be designed with transverse frames. From structural point of view, this results in a lower strength and stiffness in longitudinal direction of the ship. In other words, generally speaking, transversely framed ships will have a lower impact force in the event of frontal collisions to waterway structures than longitudinal framed ships with the same properties.

Plate thicknesses

Since the thickness of the plates in the bow structure will have a significant influence on both the impact force and energy dissipation, it is of high value to look into the recommendations for these thicknesses. Just as for geometric properties of ships, Det Norske Veritas Germanischer Lloyd (DNV GL) determines rules on thicknesses of plates of the ship structure. These rules will be treated here.

The DNVGL document on Rules for Classification of Inland navigation vessels [17] gives insight about the general determination of the element thicknesses. The side shell plating of the fore-end is mainly dependent on either the material factor, rule length (length of the ship) and spacing of the stiffeners, or the design load of the bottom structure and the side structure of the fore-end with the spacing of the stiffeners. The design load is determined by the wave height and draught of the ship. Since wave heights are not significantly high on Dutch waterways, the design load is mainly determined by the draught of the ship. The other factors determining the element thicknesses are thus based on the geometry. A short study on these requirements with different parameters gives results which show that for a wave height up to, for example, 10 meters, the geometric factors are the governing factors for the element thicknesses. Since the wave heights acting on inland waterways are marginal, the geometric factors are governing for inland waterway ships. The primary variable in the rules for thicknesses is the ship length of which a linear relationship with the element thickness is defined. For a transverse framed design, the minimum thickness for the side plating is formulated as:

$$t = 1.68 + 0.02Lk^{0.5} + 3.6s \tag{2.1}$$

Where L is the ship length, k the material factor and s the stiffener spacing.

In figure 2.7, minimum element thicknesses are depicted for a range of ship lengths, as specified in the rules of DNVGL. Material factor k is according to DNVGL for Grade A steel equal to 1 and stiffener spacing s is for this analysis assumed on 0.5 meters. From eq. 2.1 and figure 2.7, a linear relationship is found between the ship length and element thickness. This is important to note, since the element thickness is a governing factor for the structural stiffness and thus the collision force. In practice, the element thickness could be higher

since other factors could govern the design, such as workability and minimum thickness for establishing connections. Nonetheless, the minimum element thickness is considered as giving good qualitative information about the relation between element thickness and ship length.

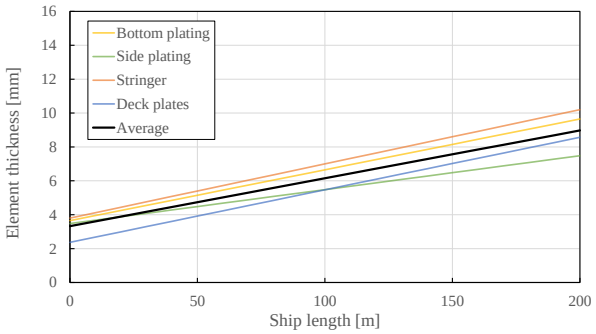

Figure 2.7: Minimum plate thickness vs ship length according to DNVGL Rules [17]

By combining this information with the obtained ship data presented in section 2.1.1, the element thickness could be determined with a given ship tonnage. Data about the length of the ships and their tonnages are combined to the graph in figure 2.8

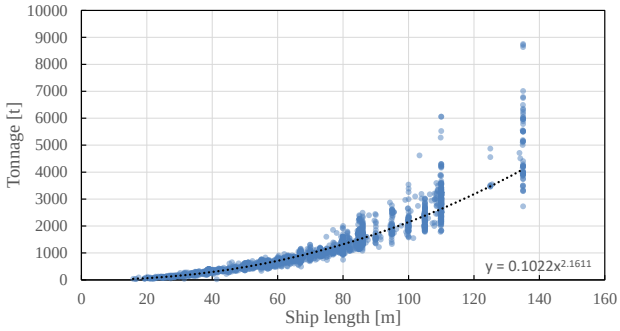

Figure 2.8: Ship length vs. tonnage, including a fitted curve (data source: debinnenvaart.nl)

The graph shows what is expected. A clear correlation is observed between the ship length and cargo tonnage. The correlation shows the behaviour of a power function. The spread of the tonnage increases with increasing ship length as well. To find a correlation between the ship length and tonnage, curve fitting is conducted. A relation is found in terms of the following expression:

$$\text{DWT} = 0.1022L^{2.611} \tag{2.2}$$

With tonnage as DWT and ship length L.

A relation between the ship tonnage and element thickness is found by substituting eq. 2.2 in eq. 2.1. This is done for different elements and is depicted in figure 2.9a. By using the kinetic energy calculation for the external dynamics (eq. 1.1), the kinetic energy for a given tonnage is calculated. This is done by assuming a velocity of 5.5 m/s and a mass of 1.4 times the tonnage, as formulated by Rijkswaterstaat. The element thickness for a range of kinetic energy levels is depicted in figure 2.9b.

With this calculation, an informative relationship is obtained for an approximation of the relation between the collision force and ship energy level since the element thickness is an important structural parameter which is expected to have a strong influence on the collision force. This is further on studied in chapter 6.

The analysis on plate thicknesses shows a non-linear relationship between the ship tonnage and the minimal plate thicknesses. This being said, an increase of a factor two in tonnage, does not lead to a increase of a factor two in minimal plate thicknesses. The collision force is assumed to be mainly determined by the strength and stiffness of the ship's bow, and plate thicknesses have a high impact on these factors. This means that small

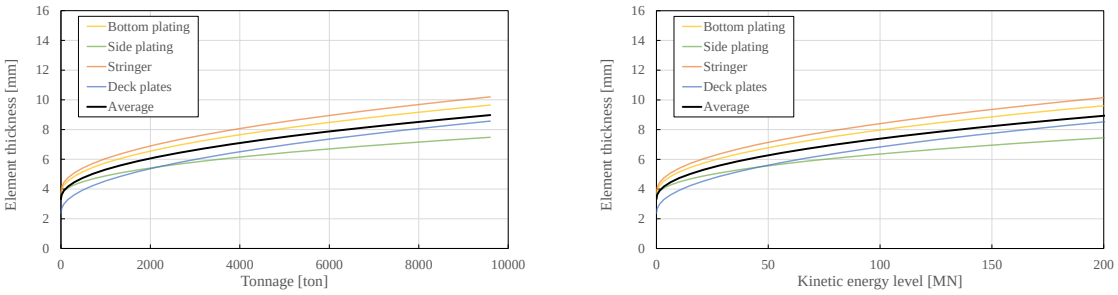

(a) Tonnage vs. element thicknesses

(b) Kinetic energy level vs. element thicknesses

Figure 2.9: Element thickness relationships (data sources [78, 17]).

ships have a relatively high strength and stiffness in the ship's bow compared to large ships, because of the minimal plate thicknesses, and will cause relatively high collision forces. Despite their lower mass and initial kinetic energy level.

Material

Since 1959, standardisation is defined for the used steel in the shipbuilding industry. There are now five different qualities of steel used in ship construction, often referred to as IACS steels [20]. These are graded A, B, C D and E. Grade A being the ordinary mild steel according to Lloyd's Register requirements (shipbuilding standardisation society) and usually employed in shipbuilding. Grade B has better quality than Grade A and specified where thicker plates are required at more critical parts of the structure. Grades C, D, and E possess increasing notch-tough characteristics. Lloyd's Register requirements for Grades A, B, D, and E steels may be found in Chapter 3 of LLoyd's Rules for the Manufacture, Testing and Certification of Materials [43]. LLoyd's Register provides results from steel tensile tests of different steel grades in this document. The IACS steels have a typical steel stress-strain relationship with elastic and plastic strain, as shown in figure 2.10.

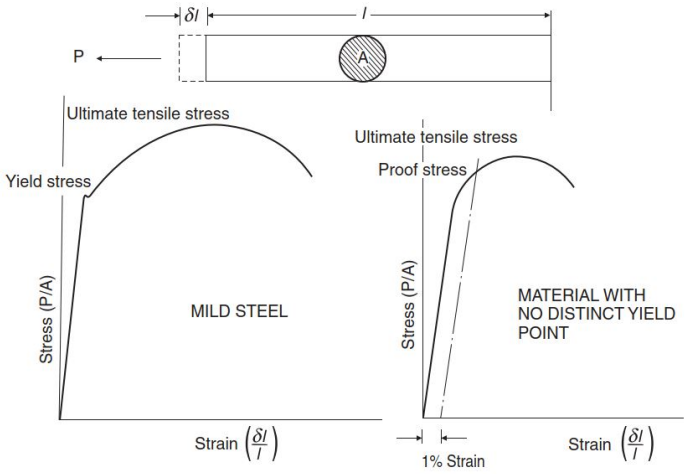

Figure 2.10: Stress–strain relationship of shipbuilding materials [20]

2.2. Ship collision mechanics

The determination of the impact load on a bridge pier during a ship-bridge collision accident is very complex as it depends on the ship characteristics and the bridge structure, as well as the circumstances of the collision accident. The problem is simplified to find a manageable solution.

A collision is an isolated event in which two or more bodies exert on each other in about a relatively short time [32]. In the case of a ship-bridge collision, the magnitude of these forces is relatively high. The term *ship collision* generally refers to at least two moving maritime vessels hitting each other, where the related term *allision* refers to a moving ship striking a stationary ship. In this thesis, the term ship collision is adopted to

refer to a ship-bridge pier collision. A general collision causes a change in motion of the bodies involved due to internal forces acting between them during the collision. Different types of collisions are determined by their conservation of kinetic energy. However, all collisions conserve momentum. Specifically, collisions can be either *elastic*, meaning they conserve both momentum and kinetic energy, or *plastic*(inelastic), meaning they conserve momentum but not kinetic energy.

The ship-bridge collision observed in this thesis is considered an elastic-plastic collision, as the kinetic energy is assumed to be almost fully dissipated, with some elasticity left in the ship structure which results in 'negative' motion of the ship. Some important parameters involved in a ship-bridge collision are:

- For the colliding vessel: type, size, shape, speed, loading condition, and strength and stiffness of the bow, hull and deckhouse.
- For the bridge elements in contact with the colliding vessel: size, shape, mass and lateral resistance characteristics.
- For the collision circumstances: eccentricity of impact and water depth.

In the present study, simplifications are included to decrease the number of parameters. This is described in chapter 1. The remaining parameters of relevance are exclusively about the colliding ship: speed, mass and structural properties (shape, size, et cetera.).

2.2.1. Basics of impact analysis

The mechanics of a collision are relatively complex [80]. The initial energy of the colliding object can be transferred into many other forms of kinetic energy and elastic-plastic deformation or fracture of structural elements in both hit structure and the colliding object. Small differences in the precise impact location and angle can result in substantial changes in the effects of the impact. This external factor, however, is neglected and the analysis is limited to the elementary case, where the colliding object hits a rigid, immovable wall under a right angle. To find the forces at the interface one should consider object and structure as one closed system. The assumption that the hit structure, the bridge pier, is rigid and immovable makes the problem more manageable.

When considering a collision as elastic, it could be simplified to a elastic single degree of freedom system. Which is described by the second order ordinary differential equation:

$$M\ddot{x} + kx = 0 \tag{2.3}$$

Where M is the mass of the object, k the spring stiffness and x the displacement. $\ddot{x}$ is the second derivative of the displacement with respect to time, which is acceleration in terms of physics. The first derivative defines the velocity of the object. By setting two initial conditions, the equation can be solved:

$$\begin{aligned} x(0) &= 0 \\ \dot{x}(0) &= v_0 \end{aligned} \tag{2.4}$$

$$x(t) = \frac{v_0 M}{k} - \frac{v_0 M e^{-\frac{kt}{M}}}{k} \tag{2.5}$$

Using the law of energy conservation and equating the initial kinetic energy to the potential energy at maximum compression, the maximum force can be determined:

$$\frac{1}{2} M v_0^2 - \frac{1}{2k} F^2 = 0 \tag{2.6}$$

Substitute:

$$F = -kx \tag{2.7}$$

Results in the equation for the maximum force:

$$F = v_0 \sqrt{Mk} \tag{2.8}$$

Considering a plastic-elastic collision involves a more complex single degree of freedom system, with the following ordinary differential equation:

$$M\ddot{x} + c\dot{x} + kx = 0 \tag{2.9}$$

Where coefficient c is added which is associated to the damping of the motion. This brings extra complexity to the problem, but is a good description for (simple) plastic-elastic problems. The system is then schematised according to figure 2.11.

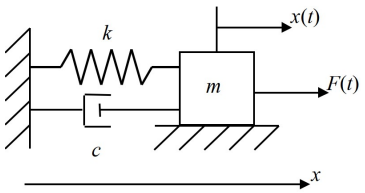

Figure 2.11: Mass-spring SDOF system

An alternative model for the colliding object is the continuous elastic rod (figure 2.12) with mass density ρ, modulus of elasticity E, cross sectional area A and length L [80]. The interaction at a collision could then be presented as:

$$F = Z v_0 \tag{2.10}$$

Z = EA/c, the rod impedance
$c = \sqrt{E/\rho}$, the wave propagation velocity

Substituting Z and c:

$$F = v_0 A \sqrt{E\rho} \tag{2.11}$$

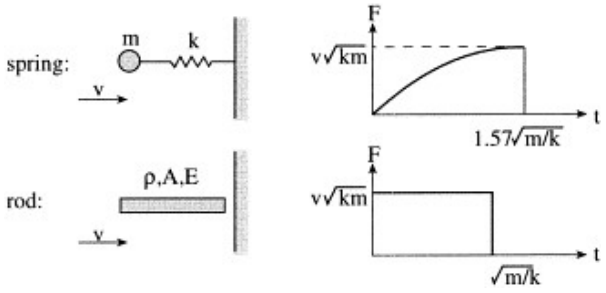

Figure 2.12: Spring and rod models for the colliding objects [82]

By taking $k = EA/L$ and $m = \rho AL$ we get equation 2.8 again. So as far as the maximum force concerned, there is no difference between the spring and rod model. Nevertheless, considering the load time history, there is a significant difference. The spring has a linearly increasing force over deformation where the rod has a constant load over deformation.

In practice, the colliding ship will not behave elastically, but responds by a mix of elastic deformations, yielding and buckling. The load-deformation curve, however, will still have the nature of a quasi-elastic single degree of freedom system and equation 2.8 could still be used for first approximations. This is true for the loading branch but does not account for the unloading branch, which will usually be much steeper. This fact has an important effect on load time history. For example, for perfectly plastic material, there will be an infinite stiffness of the unloading branch as no elasticity is present. For the spring model, this means that at the top load the spring stiffness becomes infinitely great and the interaction force drops down to zero immediately. With this in mind, the total duration could be calculated as:

$$\Delta t = 0.5\pi \sqrt{\frac{m}{k}} = 1.57 \sqrt{\frac{m}{k}} \tag{2.12}$$

For the rod model, the end of the loading curve is reached as soon as the pressure wave reaches the end of the rod. The reflecting wave will have an infinite propagation velocity. So the load duration in this case is:

$$\Delta t = \frac{L}{c} = L \sqrt{\frac{\rho}{E}} = \sqrt{\frac{m}{k}} \tag{2.13}$$

The total impulse $\int F dt = mv$ is an easy verification which confirms the correctness of both methods.

2.2.2. Crushing Strength of Plate Assemblies

The frontal part of the ship, the ship's bow, is the part which will dissipate most of the kinetic energy involved in a collision onto a bridge pier. The energy dissipation will almost completely be provided by plastic deformation of structural elements, as a result of crushing of the structure. The crushing behaviour is covered in this section to provide insight into this crushing phenomenon.

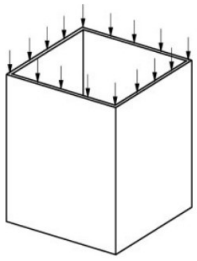

Figure 2.13: A plated structure under predominantly axial compressive loads [51]

Fundamentals of Crushing Behaviour

Consider a box column structure under predominantly compressive loads, as shown in figure 2.13. The plot in figure 2.14 shows a typical load response over displacement curve of this structure. As the compressive load increases, the structure eventually reaches the ultimate strength, which is the first peak in the graph [45]. If the displacement continues to increase, when kinetic energy is still present, the internal load will decrease rapidly. During this decrease, some parts of the structure may bend or stretch. A lobe emerges, and the walls begin to fold. As the deformation continues, eventually, walls make contact with each other. This contact ends the folding mechanism of one fold and initiates a new fold.

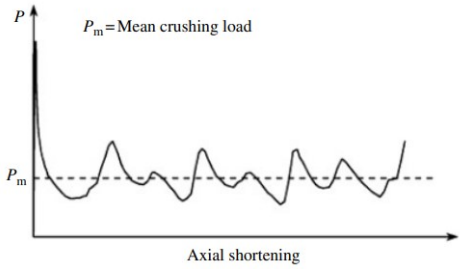

Figure 2.14: Typical crushing response curve of a thin-walled structure under predominantly compressive loads [53]

The internal load increases until the adjacent walls buckle. The structure begins to fold in a similar manner to the previous one. The repetition of this process can be seen in the load-displacement curve of the graph. Each through-peak pair in this graph is associated with the formation of one structural fold. This process repeats itself until either the end of the structure is reached, or the kinetic energy is fully dissipated by the plastic deformation. If the entire structure is completely folded, the structure behaves as a rigid body until gross yielding occurs by compression.

Figure 2.15 shows a crushed box column structure after cutting it in half. The folding mechanisms can be clearly seen. It is apparent that many folds form during the crushing process. The formation of these folds results in large axial compressive displacements. If the structure is uniform over the length, the folds develop sequentially from one end of the tube, so the phenomenon is known as progressive crushing. A ship's bow can be designed to force this kind of deformation patterns, to achieve high energy absorption capacity in a collision accident. One can imagine this structure as part of the ship's bow, on a local level. For example, the outer hull combined with a stiffener could form a similar structure as one of the corners of the box column.

For ship-bridge pier collisions, the peak forces are of most interest as these are the forces to which the bridge pier will be exposed. The considered box column is, naturally, a highly simplified structure of the ship's bow. Many more factors will influence the crushing behaviour of the bow structure and thereby the load-displacement curve. Mainly, the tapered shape over the length of the bow has a significant influence on the crushing force over the displacement. The magnitude of the first peak (which is observed in figure 2.14), initiated by buckling, will be decreased significantly relative to the following peaks as the first part of the structure contains only few material compared to the structure 'deeper' into the ship. This means that depending on the geometry, the highest peak in crushing force will be developed later on in the crushing process, where more material is present.

2.3. Review on existing standards regarding bridge pier impact forces

During the present study, the current Dutch guidelines on collision forces are evaluated. However, other guidelines are set up on this topic too. As a comparative pre-study, these guidelines are observed and com-

Figure 2.15: A plated structure crushed under axial compressive loads and cut at its midsection [53]

pared to the *Richtlijnen Ontwerpen Kunstwerken*. The relevant standards are treated and compared to get an overview of international coherence. But first, the Dutch guideline is described.

2.3.1. Richtlijnen Ontwerpen Kunstwerken

As introduced in the problem origin in chapter 1, the Richtlijnen Ontwerp Kunstwerken (ROK) document contains general requirements for public work projects commissioned by Rijkswaterstaat. In the current document (ROK 1.4 from April 2017), the requirement for the to be used collision force on a bridge pier is written as follows:

"The frontal, representative equivalent static force F_{dx} trough an impact load from river and canal traffic against rigid obstacles is:"

$$F_{dx} = 3.3\sqrt{E} + 5.6 \tag{2.14}$$

where:

E = kinetic energy level of the ship $E = 0.55mv^2$ [MNm]
F_{dx} = collision force for a frontal collision [MN]

Additional explanation is added, of which the following is relevant for this research:

- The formula assumes a collision with a rigid object. The energy is therefore dissipated completely by the distortion of the ship structure. With that, the ship will be (heavily) damaged. The "crumple zone" will be excessively large in such order that the share of the elastic or plastic distortion of the hit structure is not relevant.
- The kinetic energy level E of the ship is $0.55mv^2$ instead of $0.5mv^2$ to take into account the mass of the surrounding water moving together with the ship.
- The displacement tonnage of the ship is defined by the mass of the ship, plus the cargo (deadweight tonnage).
- On CEMT class 0 waterways, where only small or recreational ship traffic takes place, the frontal collision force is defined as constant, $F_{dx} = 500$ kN.

As mentioned in section 1.4, the focus of this research is on the internal mechanics of the ship and not on the external dynamics. Therefore, the energy level is assumed as given, and the collision force will be calculated from this value. Accordingly, the method to calculate the energy level for eq. 2.14 is not within the scope of this research but is defined as input for the force calculation.

The origin of equation 2.14 is treated in section 2.4. Here, a short analysis on the equation is provided. The equation expresses a relation between the kinetic energy level and the collision force in the form of a square root. With this, it is assumed that for an increased energy level (heavier ships and/or higher velocities), the collision force will increase as well. However, the same difference in energy levels with higher values will result in a relatively smaller change in collision force, than for energy levels with lower values, given a decreasing gradient behaviour of the square root relation. Noticeable is the constant of 5.6 in the equation, which defines a lower limit for the impact force, independently from the energy level. This constant is a result of curve fitting

of the force-displacement peak curve where the curve is assumed linear and starting at a non-zero value. The non-zero starting value is included in the conversion to force-energy. The constant implies that for very small ships, the value 5.6 is determinant for the collision force. The explanation note in the ROK partly resolves this on class 0 waterways. However, for ships on, for example, waterway class I, this could have a high impact. This cannot be substantiated by logic, since a ship with a velocity of zero and therefore, an kinetic energy level of zero will still have a collision force of 5.6 MN. However, since the curve starts at a higher value with this constant, a better fit is found considering the constant provides freedom on the tangent of the curve.

2.3.2. Eurocode

The eurocodes are ten European standards which specify how structural design should be conducted within the European Union. Dutch organisation NEN manages and publishes the standards applicable to the Netherlands. Eurocode 1 (NEN-EN 1991) is of most relevance for this research. In this document, actions on structures are defined. In other words, the loads to implement during the design phase of the structure. Part 1-7 of Eurocode 1 [47] defines the accidental actions for structures, including accidental loads on bridge piers. The standard describes general dynamic calculations for impact loads. Moreover, it describes impact loads from ships on structures. The Eurocode states that the collision forces acting by ships on fixed structures on inland waterways needs to be considered as hard collisions, where the kinetic energy is dissipated into elastic and plastic deformation of the ship structure itself. In the absence of a dynamic calculation, a table is given with indicative dynamic values for the collision forces on inland waterways.

With these indicative values, the following notes are added:

- The indicative values could be adjusted depending on the consequences of failure as a result of a ship impact force.
- In the absence of a dynamic calculation of the hit structure, it is recommended to multiply the indicative values with a proper dynamic multiplication factor. In the given values, dynamic effects are incorporated. However, this is not the case for the hit structure. For a frontal collision, an indicative dynamic magnification factor is 1.3.

For a more advanced calculation, a calculation method is given in section C.4.3. of the document. Equations are given, depending on the deformation energy E_{def} which is equal to the kinetic energy ($\frac{1}{2}mv^2$) at a frontal collision. Here, it is advised to use the average mass for the regarded ship as defined in Eurocode and a velocity of 3 m/s increased by the water flow velocity. An added (hydrodynamic) mass of 10% should be incorporated into the kinetic energy equation when considering a frontal collision. A distinction is made between collisions with deformation (or kinetic) energy lower than 0.21 MNm and higher than 0.21 MNm. If the deformation energy is lower than 0.21 MNm, the collision is considered as elastic, and the dynamic collision force should be calculated as follows:

$$F_{dyn,el} = 10.95\sqrt{E_{def}} \tag{2.15}$$

Since all considered collisions in this study contain a higher amount of deformation energy than this limit, the deformations are defined to be plastic, and equation 2.16 is provided to calculate the design value of the dynamic collision force.

$$F_{dyn,pl} = 5.0\sqrt{1 + 0.128E_{def}} \tag{2.16}$$

The background document of this equation is not available for the author; the origin is therefore not reviewed. Nonetheless, the characteristics of the formula are described here. Similar to the ROK force formula, this formula gives a square root relation between the energy level and the force. However, the European standard adds a multiplication factor in the square root to decrease the energy level dependency, which results in a flatter curve. The Eurocode defines just as the ROK a minimum force higher than zero for an energy level of zero. However, in this case, the collision force starts at 5.0 MN.

2.3.3. American guideline

In the United States, guidelines used in highway design and construction are published by the American Association of State Highway and Transportation Officials (AASHTO). Despite its name, the association represents

not only highways but air, rail, water and public transportation as well. A comprehensive guide on vessel collisions is published in the book "Guide Specifications and Commentary for Vessel Collision Design of Highway Bridges"[2]. In section 3.9 of the book, guidelines on the ship impact force are formulated. This guideline reads: "The ship collision equivalent static impact force associated with a head-on collision with a rigid object shall be computed by the following for Product Carrier/Tanker, Bulk Carrier, and Freighter/Container vessels":

$$P_S = 220DWT^{1/2}\left(\frac{V}{27}\right) \tag{2.17}$$

Where:

P_s = equivalent static ship impact force [kips]
DWT = deadweight tonnage of ship [tons]
V = ship impact speed [ft/s]

This equation is primarily developed from research conducted by Woisin [87] in Hambrug. Collision data was generated by doing experimental tests on physical (scale) models. From Woisin's data, Saul and Svensson [71] developed a basic equation for mean ship impact forces for bulk carriers larger than 40.000 DWT colliding with a rigid body at a speed of appr. 8.2 m/s. This equation is reduced after a review for the development of the Guide Specifications for speeds between 4.1 and 8.2 m/s. Here, the scatter of ± 50% was still in use. This scatter was simplified to a single force using the 70 per cent fractile of the force distribution, which resulted in the eventual eq. 2.17.

Limitations coming from the background research on the minimum size of the vessel (40.000 DWT), type of vessel and a minimum impact speed of 4.1 m/s were not imposed. In order to provide flexibility to the designer, eq. 2.17 remains recommended until further research results are available. It is noted that the use of eq. 2.17 for shallow speed levels may underestimate the actual force levels.

A conversion is necessary to compare the American guideline with the ROK because for eq. 2.17, US customary units are used. This differs from the ROK formula where metric units are used. Moreover, the American expression uses deadweight tonnage as variable, where the ROK uses the mass (displacement) of the ship as variable incorporated in the energy level. Eq. 2.17 is converted to be compared with the ROK by using the following relations:

$$V[\text{ft/s}] = 3.28V[\text{m/s}]$$
$$F[\text{kips}] = 4448.20F[\text{N}]$$
$$DWT = 1.40\text{Mass}$$

And substituting it in eq. 2.17:

$$\frac{F}{4448.2} = 220\sqrt{\frac{M}{1.4}}\left(\frac{3.28V}{27}\right) \tag{2.18}$$

Which gives:

$$F = 0.1V\sqrt{M} \tag{2.19}$$

With the force in meganewtons, mass in tonnes and velocity in m/s.

To finalise this an equation where it will depend on energy level, similar to the ROK, the kinetic energy equation, $E_{kin} = 0.5MV^2$ is inserted, in meganewtonmeter (MNm):

$$F = 4.5\sqrt{E} \tag{2.20}$$

Important to note is that some round off inaccuracies have occurred with the numerical conversion of the equations above. This is, however, not significant (0.15%). Moreover, the relation between the deadweight tonnage and total displacement of the ship is assumed as 1.4, which could differ for different ship sizes.

However, with the formula of eq. 2.20, a quick comparison is possible with the ROK. The American guideline assumes a square root relationship, similarly to the ROK and Eurocode. A multiplication factor of 4.5 scales

the square root, which is higher than the 3.3 of the ROK although the American standard does not include a lower limit. Consequently, the American standard starts lower at zero energy but will increase steeper than the ROK. From up to about 22 MNm, the calculated forces are higher by using the American standard than by using the ROK guideline.

2.3.4. Norwegian guideline

Other relevant documents are the standards from Norway. The Norwegian oil and gas industry introduced NORSOK Standards in 1994, to promote knowledge, expertise and competitiveness. Since the oil and gas industry is an essential sector in Norway, these standards are widely supported. NORSOK stands for "Norsk Sokkels Konkurranseposisjon", which means "Norwegian shelf's competitive position" in English. The standards are now used worldwide, replacing oil company specifications and are also used as references in authorities regulations.

The relevant guidelines for the present study are defined in the NORSOK Standard N-004 "Design of steel structures"[66] . Annex A.3 presents information about the approach for ship collisions. A recommended standard force deformation curve for bow impact is given (see figure 2.16), which was developed in 1981. It is based on a raked bow where crushing occurs in the relatively weak bow superstructure. The curve is based upon collision with an infinitely rigid, plane wall.

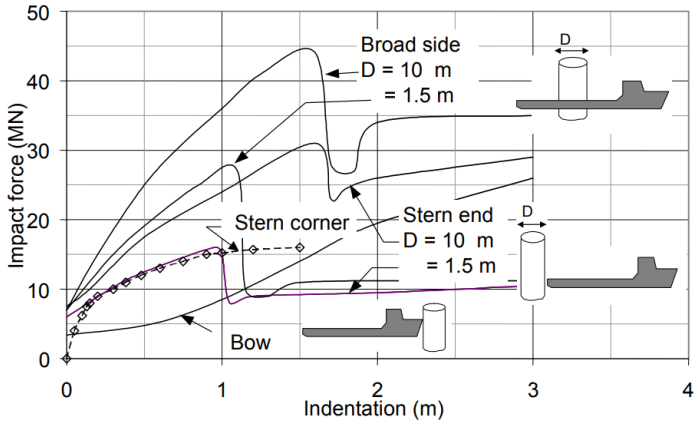

Figure 2.16: Force–deformation curves for a 5000-DWT supply vessel [66]

The curves for a broad side, stern corner, or stern end impact are not relevant for the present study. The bow impact curve, depicted in figure 2.16, shows impact forces over a given indentation depth. Other information given in the NORSOK Standard considers a non-rigid collided object and ships the size of sea-going ships which is therefore not relevant for the present study.

2.3.5. General comparison of standards

The guidelines of the ROK, Eurocode (NEN) and American standard (AAHSTO) are depicted in figure 2.17. Similar behaviour is observed in the curves, which originates in the square root relation of the kinetic energy with the force which is defined in each guideline. A common agreement is found in the decreasing gradient. Both the ROK and Eurocode start at an initial force level, where the AAHSTO starts at zero.

2.4. Background study on current Rijkswaterstaat guideline

In 1993, a study conducted by Joustra and Pater [35] resulted in the current guideline of Rijkswaterstaat on collision forces of ships on bridge piers. As mentioned in chapter 1, this study does not draw a general conclusion for ships of different sizes than the CEMT Class IV ship considered in the study. A force-energy relationship is found solely for one ship. Although this relationship could be right for this particular ship, it is not appropriate to assume this relationship for other kinds of ship. This is also mentioned by the involved authors. Therefore, more research should be conducted. However, to find out where the current guideline is originated from, a summary of this report is written in this section.

The report is found in the repository of the TU Delft. It is a summarising and concluding report of three

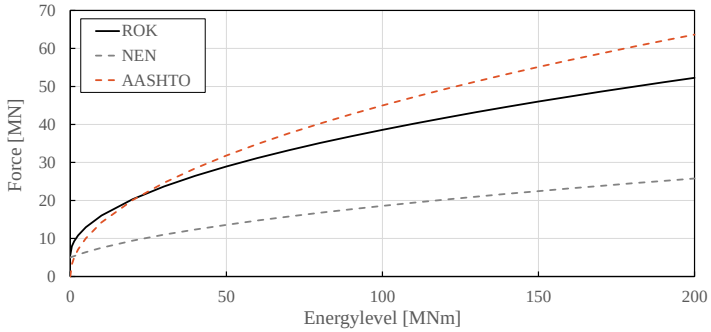

Figure 2.17: Comparison of guidelines on ship collision forces with variable energy level.

subreports: a literature study on this topic, a hand calculation for two Dutch inland ships and computer simulation for one of the two ships (Thomar, CEMT class IV).

The hand calculations are based on the collapse mechanism of each individual structural element per frame. The frames consist mainly of a combination of steel plates, with the outer hull as the most important plate for this calculation. The collapse mechanisms are either buckling, yielding or wrinkling of the plate. The type of mechanism is among others dependent on the type of support of the plate. For each plate, the failure load is calculated and combined to create a force-displacement diagram, see figure 2.18.

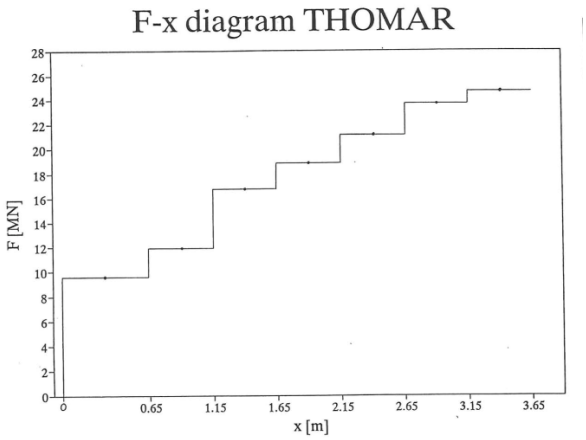

Figure 2.18: Force-Displacement diagram for CEMT IV Ship from study of Joustra and Pater [35]

The area under the graph is equal to the distortion energy, the energy which is required to crumple the ships bow to that point. Therefore, by setting the integral of the F-x diagram equal to the kinetic energy, a direct relationship is established between the failure load (impact force) and the kinetic energy of the colliding ship.

To validate the hand calculations, and create more (accurate) data, a computer-simulation is carried out. This is done using finite element software by MSC, MSC Dytran. This is an explicit finite element analysis (FEA) software program, a widely-used method to simulate such a collision. Different simulation situations are treated with varying conditions. The mesh size is not specifically described in the report, but from the figures, a global mesh size of 250 mm is estimated. Furthermore, from the time-step calculation, a minimum size of 100 mm is read.

A stress-strain diagram is obtained from experiments. One linear part elastic, and a second linear part plastic, shown in figure 2.19.

This stress-strain diagram is based on Fe 430 steel, which is now called S275 steel. The elastic part is defined with a Young's modulus of 210 GPa and a yield strength of 270 MPa. Ultimate strength is set on 430 MPa. The plastic part is schematised to a linear stress-strain relationship with a modulus of 800 MPa. At an assumed failure strain of 20%, the failure stress is considered to be reached, and the steel has failed. This failure strain

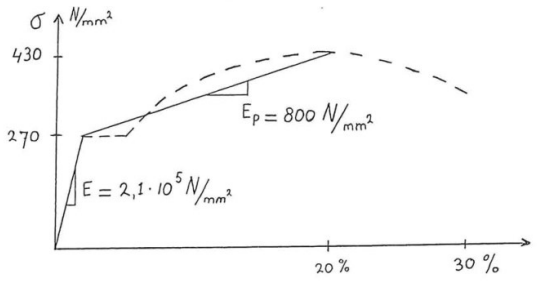

Figure 2.19: Schematised stress-strain diagram from background study of ROK [35]

is lower than followed from the experimental tests, to include failure of connections. The elements that have reached this failure strain will be deleted in the analysis and are not regarded in the following time steps.

Figure 2.20 shows the results of the hand calculation and computer calculation. The hand calculation results are shifted on the x-axis in such way that both curves correspond correctly in terms of location in the ship's bow.

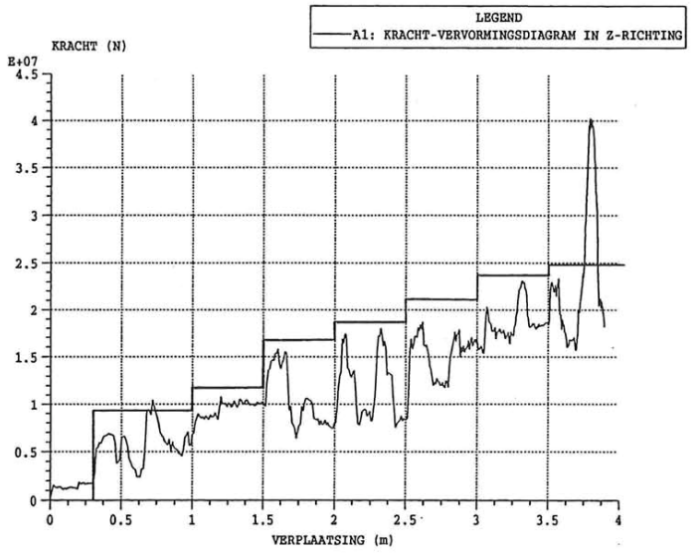

Figure 2.20: Force-displacement diagram for CEMT class IV ship Thomar (computer simulation and hand calculation (stepped curve)) [35]

At first glance, it can be noticed that both results generally follow the same trend. The FEM results are more detailed than the hand calculation results. The hand calculations indicate the upper limits, whereas the FEM force results only exceed those limits on a few locations. For every frame transition within the ship's bow, the maximum forces are almost equal for both the FEA and hand calculations.

Both calculations are applicable to the Thomar, a CEMT class IV class ship. For this ship, quantitative judgement can be made about the distortion behaviour at a collision onto a rigid wall and the impact force corresponding to that. In the study, two linear expressions are determined to describe the force-displacement. One for the peak forces and one for the mean forces, with equal tangent. The peak force is fitted with a non-zero value as starting point. The curves are converted to force-energy curves and a general formula is determined which gives the maximum impact force at a frontal collision of the Thomar onto a rigid wall at a certain energy level. This curve is described with eq. 2.14 which is adopted in the guideline of Rijkswaterstaat on ship collision forces on bridge piers.

Eq. 2.14 shows a multiplication of a root dependence by 3.3 and an upward shift of 5.6 which is the consequence of the non-zero starting point of the peak force curve.

An important note is added regarding the application for Dutch ships: Because the formula is derived from the simulation and hand calculation of this certain ship, the formula is valid until an energy level up to about 50 MNm and deformation up to about 4 m. With that as maximum, a maximum impact force of 29 MN is valid for this formula.

One of the recommendations of Joustra and Pater is that for a precise knowledge about the impact force of different sizes of ships, more computational calculations are necessary for each normative ship size per inland waterway. Moreover, the hand calculations should be validated by failure tests on steel plates or (a part of) the ship's bow.

3

Methodology

This chapter contains an explanation of the methodology framework that was used to conduct this study, followed by an explanation of the verification and validation to evaluate the results of the utilised method.

The diagram in figure 3.1 shows the process, which is explained in this chapter.

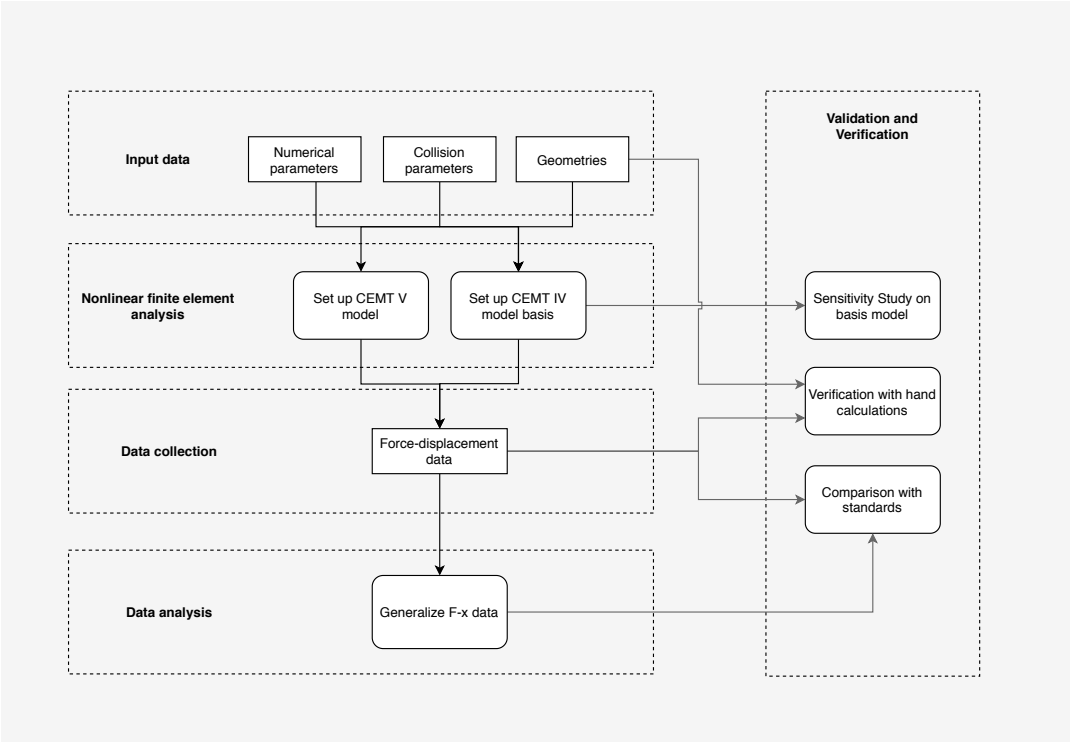

Figure 3.1: The analysis methodology of this thesis.

The analysis of structural crushing and the resulting forces is conducted using a dynamic dynamic finite element simulation (NLFEA). Three different ships of various sizes are analysed with the proposed NLFEA.

3.1. Nonlinear Finite Element Analysis Approach

In the case of a ship collision simulation, a finite element code must be capable of robustly representing nonlinear inelastic material behaviour (with failure), a part-to-part and self contact algorithm, and large displacements compatibility. Comparable studies are generally done in the commercial codes LS-DYNA or ABAQUS/Explicit. Storheim, Notaro, Johansen and Amdahl did a comparative study between the two software packages on a simulation of ship collision and concluded that both packages had equivalent results [69]. ABAQUS/Explicit [62] is used in this study to numerically simulate the collision of a ship onto a bridge pier with an explicit, dynamic analysis. This type of analysis is computationally efficient for the analysis of large models with relatively short dynamic response times and also for the analysis of extremely discontinuous events or processes. Moreover, this analysis allows for the definition of very general contact conditions and uses a consistent, large-deformation theory.

With this finite element analysis, the inherent nonlinearity of a collision incident is taken into account. This nonlinearity is both a physical and geometrical nonlinearity: Physical nonlinearity consists of the nonlinearity of the material model. This means that the material is not merely described by Hooke's law but also by a law for plasticity and fracture. Geometric nonlinearity is related to large structural displacements: when a structure is believed to suffer a small deformation under a given load, a series of simplifications may be used without a greater loss of accuracy. This is, however, not the case in ship collision scenarios as the large deformations imposed on the structures require nonlinear formulations.

Two methods have been previously used when simulating ship impacts: quasi-static simulations and dynamic simulations. The usage of both of the methods on ship on ship or ship on bridge pier impacts produces results in good accordance with experiments [21]. Quasi-static simulations use a statics nonlinear finite element formulation, which accurately calculates large displacements but does not take into account the dynamic effects inherent to an impact. A dynamic analysis takes into account the dynamic effects of the impact and delivers more detailed results, such as the time-history of the impact force, stresses and strains, displacements, and energy in the system. These detailed results are necessary for a qualitative judgement of the analysis output. Therefore, a dynamic analysis is performed for the present study on ship-bridge collision forces. The procedure of computational modelling using the FEM broadly consists of four steps:

1. Modelling the geometry
2. Meshing (discretisation)
3. Specification of material property
4. Specification of boundary, initial and loading conditions

The first step of this process is presented in appendix B. The subsequent steps are fully presented through the application of ship impact to a rigid wall in chapter 4.

Structural data of the to be analysed ships is provided as digital 2D drawings by the ship design company "Concordia-Damen", or is provided by a colleague student who performed an internship on the same subject. The current guideline on ship impact forces on bridge piers by Rijkswaterstaat is established with a study performed on a CEMT class IV ship [35]. It is found valuable to perform a new study on a comparable ship size to have a good comparison with the current guideline and results of the previous study (shown in appendix G). Therefore, a CEMT Class IV ship will be investigated. Moreover, to gain insight into the ship size dependency of the impact force, other ship sizes are investigated. A large class V ship (5130 t) and a smaller class V (3500 t) are studied. Structural information about the smaller class V ship is found in the study which led to the current guideline from Rijkswaterstaat. Ji Fan Chan conducted a study on this ship before and provided the 3D geometry model [14]. Concordia-Damen provided structural drawings for the other ships. From these drawings, a 3D geometry model is set-up in the present study using Rhino/Grasshopper CAD software (explained in appendix B).

The structural geometries are drawn with the CAD software Rhino with visual programming tool Grasshopper. Afterwards, the geometries are separated in groups of equal thickness and exported as .igs file to ABAQUS/CAE, where the geometry is processed and prepared for the finite element analysis.

Most of the necessary input data for the NLFEA is obtained from, or based on, previous research on the particular input subject.

3.1.1. Short characteristics of dynamic algorithm

The selected nonlinear dynamic analysis is performed using the ABAQUS/Explicit code [62]. In this section, the algorithm implemented in this code is described.

The main equation to be solved is the dynamic equilibrium equation of the system:

$$M\ddot{u}(t) + f(t) - p(t) = 0 \tag{3.1}$$

Where:

u = State vector (displacements or rotation parameters)
M = Mass matrix
f = Internal force vector
p = External load vector
t = time

The time integration procedure implemented in the code is based upon the implementation of an explicit integration rule together with the use of the diagonal or "lumped" element mass matrices. The time step from t_n to t_{n+1} is performed as follows. From eq. 3.1, the acceleration is computed for time t_n:

$$\ddot{u}_n = M^{-1}\left[p_n - f(u_n)\right] \tag{3.2}$$

Where the mass matrix is lumped for greater efficiency. Then, the equations of motion for the body are integrated using the explicit central difference integration rule:

$$\dot{u}^{(i+\frac{1}{2})} = \dot{u}^{(i-\frac{1}{2})} + \frac{\triangle t^{(i+1)} + \triangle t^{(i)}}{2}\ddot{u}^{(i)} \tag{3.3}$$

$$u^{(i+1)} = u^{(i)} + \triangle t^{(i+1)} + \dot{u}^{(i+\frac{1}{2})} \tag{3.4}$$

Velocity $\dot{u}_{n+\frac{1}{2}}$ of the system is computed using eq. 3.3, and the displacement u_{n+1} from eq. 3.4. It can be noticed that the solution process was advanced in time using values known from the previous step. This scheme is only conditionally stable, the size of the time increment is therefore limited. Details about this step size in the code is written in paragraph 4.6.5.

This explicit solver is very efficient for the reason that the stiffness matrix does not need to be formulated and factorised, and the procedure requires no iterations. Moreover, it is well suited to define general contact conditions and accommodate large rotations and large strains.

3.2. Verification and Validation Approach

For the present study, a computer simulation model is utilised to model the collision process with the goal to produce accurate and credible results. To evaluate this goal, verification and validation of the simulation (NLFEA) model is necessary. This is performed by using different methods, explained in the following sections.

3.2.1. Sensitivity Analysis

A sensitivity analysis is performed in which input parameters of the simulation model are changed one by one to find the effects and magnitude of the influence for each parameter. The sensitivity analysis will be involved in the iterative process of defining the parameters for the final simulations. Moreover, the sensitivity of the NLFEA model is investigated by changing different parameters and singularities could be observed.

3.2.2. Validation with calculation methods from literature

Results of the NLFEA calculations are compared to results from already established and validated calculation methods found in the literature. These simplified analytical methods, in general, use the concepts of structural crashworthiness. Individual damage processes of elements within the structure are analysed and idealised with theoretical models, after which these models are combined to create global damage models with formulae for individual structural components.

3.2.3. Subsystem Validity

Since the crushing of a ship bow is very complex as it consists of many elements with a different kind of failure mechanism, it is not possible to use basic, well-known and widely-used theories to calculate forces generated by the complete ship bow. Therefore, one element will be considered separately and is compared with theories, both qualitatively and quantitatively.

3.3. Result interpretation

The obtained results from the finite element simulations will be interpreted to eventually establish a general expression to estimate impact forces for different ship sizes. This will be done by curve fitting a general expression using the least-squares fitting technique. The fitted expression is applied to generate impact force estimations for CEMT class ships.

4

Nonlinear Finite Element Analysis

Dynamic nonlinear finite element analyses are performed to answer the research question of this thesis. Simulations are carried out in order to emulate a ship impact on a rigid wall. The simulations are executed using ABAQUS finite element software, with an explicit dynamic analysis. In this chapter, the input parameters are elaborated on and presented.

The model assembly which is analysed consists of both a model of the ship, and a model of the collided structure. The model and boundary conditions are configured to model a ship-bridge collision the moment before contact, as can be seen in figure 4.1.

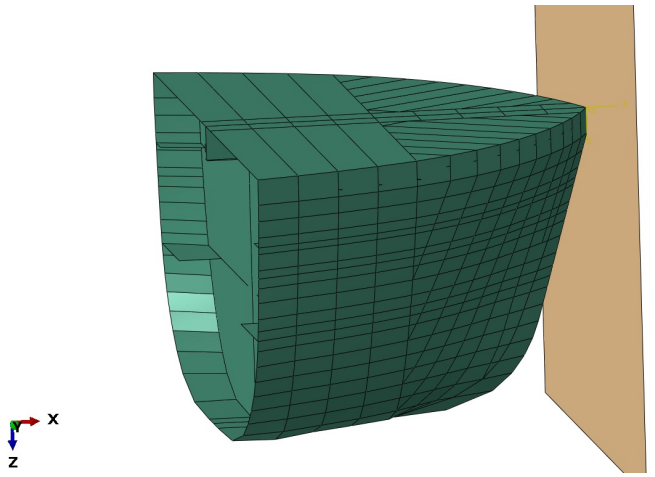

Figure 4.1: The assembly of the ship collision simulation with a rigid wall.

4.1. General configuration

The CAD model is imported into ABAQUS/CAE, where the simulation is configured. In this software package, the model is meshed (discretised) into elements to accomplish an accurate calculation. A flat geometry is added to the model to simulate the rigid wall. This object is configured with rigid properties and displacements are fixed in all directions. The size of the wall is chosen such that it is larger than the cross-sectional dimensions of the ship models. An initial distance of 10 mm between the objects is defined to prevent singularities. With the provided initial velocity, the ship's bow will move toward the wall. The steel structure is crushed until the kinetic energy of the system is dissipated, and the ship is stalled.
A material model and thicknesses properties are assigned to the elements of the ship's bow. Interface properties are added to configure the behaviour between the ship and the rigid wall. The ship is given an initial velocity and extra mass to simulate the complete ship mass. With this, the ship is configured with the kinetic energy defined before impact. The extra mass is inserted at the end of the ship's bow (lowest x-coordinates),

on a rigid flat element which is connected to the outer ends of the bow. In this way, the mass is evenly spread over the cross-section of the bow. Output parameters are defined for visualisations and force analyses afterwards.

4.2. Material properties

4.2.1. General

An accurate description of the material hardening is a prerequisite for evaluating where and how strains will concentrate, thus providing the basis for accurate predictions of plastic energy dissipation and fracture [68]. A complete stress-strain relationship of the steel material is necessary for nonlinear finite element simulation of ship collisions (with plastic deformations), whereas only the steel grade is known in the design phase.

For inland waterway ships in the Netherlands, Grade A steel is used. This material is similar to the S235 steel used in constructions and generally includes the following nominal values:

σ_y [MPa]	σ_u [MPa]	ϵ_f [-]	E [MPa]	ν [-]	$\rho[kg/m^3]$
235	430	0.2	210000	0.3	7800

Table 4.1: Nominal values for Grade A steel

Note that these values are nominal values for the steel grade in general and not the exact values which are used in the analysis of this study. The precise values are determined from a test database. This procedure is described in appendix D.

Ship-bridge collisions generally involve high plastic deformation, since high energy levels occur which are dissipated into the structure. This asks for a nonlinear approach. In linear analysis, the initial structure is recovered at the end of the collision. This is not the case for the collisions analysed in this study. This nonlinear approach requires stress-strain information of the material for the total strain range, from elastic up to fracture, which is to be defined by more information than only the nominal values. Namely, properties describing the elastic strain, yielding strain, strain (or work) hardening, necking and fracture are necessary to know. A typical stress-strain curve for low carbon steels is depicted in figure 4.2, where these different phases are shown.

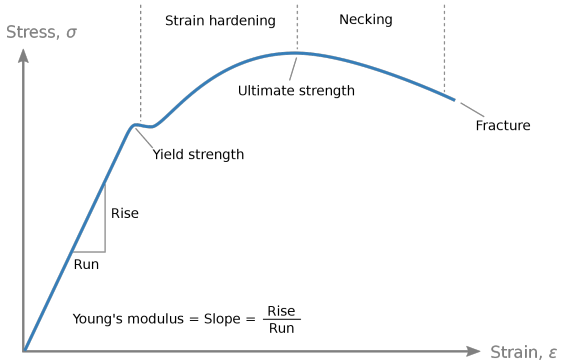

Figure 4.2: Typical engineering stress-strain relationship for steel [24]

Hogström et al.[30] and Hogström and Ringsberg [29] studied the effects of differences in strain hardening properties on the damage in a ship collision, concluding that the strain hardening significantly influences the force-displacement relation and the predicted damage in a given impact scenario. Moreover, Paik [50] recognised that the stress-strain relationship of material models used for the finite element modelling significantly affects the resulting simulations of structural crashworthiness.

The ship structure is subjected to dynamic (impact) loads during the ship-bridge collision. The mechanical properties of structural materials are significantly affected by the involved loading speed (strain rate). The strain rate is defined as a ratio which describes the loading speed of structural displacement between two

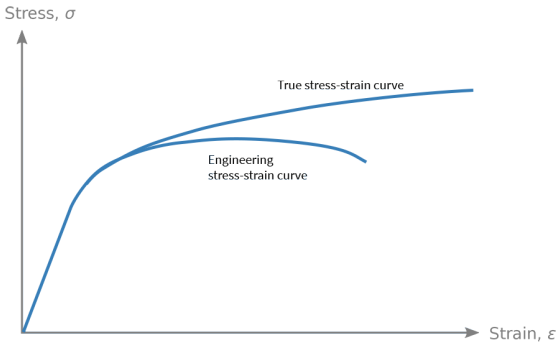

Figure 4.3: True vs. Engineering stress-strain relation

reference points, formulated as:

$$\dot{\epsilon} = \frac{d\epsilon}{dt} \tag{4.1}$$

Where ϵ is strain, and t is time.

Mainly three major differences considered between static/quasi-static and dynamic/impact loading cases [55]. First, the stress field differs since tensile stresses can occur locally, even under compressive loading conditions. Stress concentrations can happen even without notches under impact loading conditions. Second, the material response under impact varies as a function of the strain rate. Generally, the material could respond in a stiffer and stronger way. Therefore, the global structural response varies as a function of the impact load. These two aspects always interact. The third difference concerns failure strain. Materials under impact loading conditions tend to become more brittle, decreasing the strain value for material failure, the failure strain. This is due to the fact that the energy absorption capacity is decreased at higher strain rates. This is a result of the increases yield strength. Given these differences, strain rate properties are considered to be a primary factor affecting collision mechanics and structural crashworthiness. The strain rate involved in a ship-bridge collision is mainly determined by the impact speed of the ship. However, on the local level, higher values can be observed. Mechanisms responding to the impact could cause a higher speed in elements than the global velocity. Ko et al.[39] developed an empirical relation for strain rate as a function of collision velocity for ship-ship collisions:

$$\dot{\epsilon} = 2.970 V_0 - 0.686 \text{ for } V_0 \geq 0.231 \text{ m/s} \tag{4.2}$$

This could be different for a ship-bridge collision but gives an indicative value. Accurate values are calculated during the finite element analysis calculation.

The (material) temperature does also have a significant influence on the mechanical properties of materials [56]. However, as the ship-bridge collisions considered in this study occur under 'normal' conditions, without extreme temperature conditions, this factor is neglected.

4.2.2. Material properties for NLFEA

The response of ductile metals in collisions can be described in several stages: elastic behaviour up to yielding (yield strength), a yield plateau without significant hardening, a plastic hardening until the maximum tensile strength is reached, and strength decreases due to necking/softening [68]. In a uniaxial tension test, maximum strength occurs at the point of diffuse necking, in which localised contractions in the width direction occur which balance the increased strength due to strain hardening. A local neck will then form, and the specimen rapidly becomes thinner without large contractions in the width direction. Eventually, fracture occurs in the local neck. From these tests, engineering stress-strain relationships can be obtained.

Stress-strain curve

Usually finite element packages need a *true* stress-strain relationship of the material instead of the *engineering* stress-strain relationship which is determined with uniaxial tension tests. The true stress versus strain relationship characteristics of a material can generally be obtained by the transformation of engineering stress versus strain relationship as follows [1]:

$$\sigma_t \approx \sigma_e(1+\epsilon_e) \tag{4.3a}$$
$$\epsilon_t = \ln(1+\epsilon_e) \tag{4.3b}$$

Where:

σ_t = true stress
ϵ_t = true strain (integral of change in length over instantaneous length)
σ_e = engineering stress (force divided by unstressed area)
ϵ_e = engineering strain (change in length divided by initial length)

With test data from tensile tests on a specimen, this engineering stress versus strain relationship can be transformed to data valid for the numerical analysis. Traditionally, the engineering stress-strain curve is used up to the ultimate tensile stress only, since equation 4.3 does not account for the softening behaviour beyond the ultimate tensile stress.

To account for the material behaviour after necking, the true stress-strain curve up to the ultimate tensile stress can be extrapolated. The plastic behaviour can be described by the following power law as proposed by Hollomon [31]:

$$\sigma = K \cdot \epsilon^n \tag{4.4}$$

Where:

K = strength coefficient
n = strain hardening exponent

With true stress-strain data up to the ultimate tensile stress, a curve fit can be obtained to extrapolate for the behaviour after necking.

Strain-rate dependency
The strain rate effect on the material properties is considered using the Cowper-Symonds equations [16]:

$$\sigma_{Yd} = \left(1 + \left(\frac{\dot{\epsilon}}{C}\right)^{\frac{1}{q}}\right)\sigma_y \tag{4.5a}$$
$$\epsilon_{fd} = \left(1 + \left(\frac{\dot{\epsilon}}{C}\right)^{\frac{1}{q}}\right)^{-1}\epsilon_{fc} \tag{4.5b}$$

Where:

σ_y = static yield stress [MPa]
σ_{Yd} = dynamic yield stress [MPa]
ϵ_{fc} = static fracture strain [-]
ϵ_{fd} = dynamic fracture strain [-]
$\dot{\epsilon}$ = strain rate [1/sec]
C and q = test constants [-]

The Cowper-Symonds equations for strain-rate dependent behaviour (eqs. 4.5) is combined with the Power-Law formulation (eq. 4.4) to define the material tensile behaviour, including strain-rate dependency and work hardening:

$$\sigma_d = \left(1 + \left(\frac{\dot{\epsilon}}{C}\right)^{\frac{1}{q}}\right) \cdot \max\left(\sigma_y, K \cdot \epsilon^n\right) \tag{4.6}$$

Where C, q, K and n are variables dependent on the material.

Grade A steel
In 2017, Paik et al.[56] created a test database on material properties for marine applications of Grade A mild steel, focusing on the effects of temperature and strain-rate. Dr. Carey Walters, one of the supervisors of this thesis, advised this database for the use of simulations of modern ships where strain-rate dependency is included. The common engineering tensile test standards of ASTM-E8 [7] formed the basic set up of the experiments. Different test set ups were prepared, including impact tests. The engineering stress–strain curve was constructed from the impact test measurements for different strain rates. ABAQUS requires the true stress–strain curve, where the stress and strain becomes nonlinear as a function of the true cross-sectional area of the specimen. Therefore, the data is converted using equations 4.3a and 4.3b and fitted on the combined Cowper-Symonds strain-rate equation and power law (eq. 4.6). This process is described in appendix D. Analysing this data resulted in the following values which determine the material behaviour with equation 4.6:

σ_y **[MPa]**	**C** $[s^{-1}]$	**q**	**K**	**n**
300.7	74.4	2.4	722.0	0.19

Table 4.2: Values fitted from experimental data [56] which define the NLFEA material behaviour.

In commercial FE codes, including ABAQUS, the strain and strain-rate hardening can often be included in the material model by using an implemented material model or by defining the flow curve in tabular form [64]. If a tabular model is used, the data can be taken either directly from measurements or calculated from a theoretical model. The latter option is used in this study. Stress is calculated for a range of strains using the formula in equation 4.6. Data points after yielding are extracted and inserted in the plastic material parameters. Elastic material parameters are defined by the E-Modulus, which is equal for all strain-rates, and the yield strength which is extracted from the data points. The strain hardening was described up to 70 % plastic strain, and in the dynamic model the strain hardening was described at five different strain rates: 0.0001 s^{-1}, 1 s^{-1}, 10 s^{-1}, 100 s^{-1} and 1000 s^{-1}.

4.3. Failure criterion

Assessment of structural failure in ship collision events is a very complex process influenced by diverse factors. This is mainly about the mechanical properties of the ship structure; among others materials, geometry of the various ship components, loading and boundary conditions and manufacturing defects [12]. In numerical simulations of ship collision events, these factors are simplified to algorithms with input parameters which require the adoption of a correctly established failure criterion. This is important because of its presumed strong influence on the global structural energy absorption. Nowadays, where increasing computational power increases the availability for a more accurate numerical calculation, the numerical modelling of rupture and tearing is still the most challenging task in the naval structural collision analysis [12].

The formulation of the true-stress strain curve established in appendix D does not include an indication whether the initial rupture of the tensile piece has occurred or not, since this expression is only based on actual measurements of the cross-sectional area. The rupture and eventual fracture cannot be easily captured in a tensile test since the initial failure starts in a micro-scale at the central axis of the specimen, which propagates perpendicularly to the surfaces of the specimen until a full fracture occurs. For nonlinear finite element analysis, the input needed is the true strain at rupture, which is called the critical failure strain. With this definition, at first, only a few elements will fail in a FEM tensile test, while fracture occurs when all elements of the section have failed. Generally, it is considered that rupture occurs when the following failure criterion is met [92]:

$$\epsilon_{eq} \geq \epsilon_f \tag{4.7}$$

Where:

ϵ_{eq} = Maximum equivalent strain at a deformed finite element
ϵ_f = Critical failure strain defined in the input for the calculations

Defined by the equation for isotropic von Mises plasticity, the equivalent plastic strain ϵ_{eq} is the integral over

time of the equivalent plastic strain rate $\dot{\epsilon}_{eq}$:

$$\epsilon_{eq} = \int_0^t \dot{\epsilon}_{eq} dt \tag{4.8}$$

The critical failure strain is highly affected by the size of the elements (explained in section 4.3.1), and therefore the failure criteria are often defined to be mesh-dependent. Different failure criteria (generally formulations which define the fracture strain ϵ_f dependent on some variables) are defined in literature. In nonlinear finite element simulations, the elements that reach the defined maximum equivalent strain are removed from the structure at a next incremental time step. Most often, given the relatively large structural size of the ship compared to the thickness of the structural elements, the shell elements composing the ship structure have a large size compared to their thickness. Therefore, when removing an element once a failure criterion is met, this could result in considerable consequences in the numerical calculation. In other words, using a 100 per cent accurate failure criterion is not possible for the given size of the naval collision analysis, but a reliable criterion will be used, taking computational time into consideration.

The most common failure criterion used in ship collision numerical modelling is the equivalent plastic strain criterion [12]. Local material rupture is assumed to occur when the equivalent plastic strain reaches a given critical value. Usually, the maximum plastic strain is obtained from uniaxial tensile tests on a material specimen. A wide range of maximum plastic strain values for shipbuilding steel has been reported, resulting in maximum equivalent plastic strain ranges from 10% to 70% [12]. In the study of Joustra and Pater, this failure criterion is used with a plastic failure strain of 0.2 [35]. Itamura [38] also used a plastic failure strain of 0.2 in a well-known study in the field of FEM simulation of collision and grounding damage of naval structures from. This is lower than the value obtained of experimental tests, 0.3. This lower value is substantiated by an aim to cope with geometrical stress concentration which is not well captured by the adopted coarse mesh sizes. Wu et al.[88] calibrated a rupture plastic strain based on experimental collision data. An optimal rupture strain value followed for better reproduction of the overall structural response of the experimental tests.

Important to mention is that both the study of Kitamura and Wu et al. is conducted considering a ship-ship collision where a colliding ship impacts a struck ship at the side-hull. The failure modes in the side hull from the struck ship are different from the failure modes in the colliding ship. Where tearing and rupture dominates the failure modes in the side hull of the struck ship, buckling and folding are the main failure modes in the structure of the striking ship. In the struck ship, most of the collided area will be in tension, whereas in the bow of the striking ship, only areas where bending occurs are in tension and are exposed to highly plastic behaviour. As mainly compression occurs in the striking ship, the fracture strain is less relevant, especially for the maximum load determination of this study. The plastic failure strain however, is relevant for the mean crushing force and consequently, the energy dissipation of the system. A study on the influence on the failure strain is performed and explained in section 6.1.

4.3.1. Element size-dependent failure strain

In uniaxial tensile tests, where the rupture strain of a material specimen is determined, the measurement of this strain depends on the gauge length. Figure 4.4 shows this behaviour. Since necking occurs locally, with high local strains, a large gauge length will generate lower values for the failure strain because the severe local elongation near failure is averaged within the specimen length. On the contrary, with shorter gauge lengths, this local severe elongation effect is emphasised, resulting in high strain values.

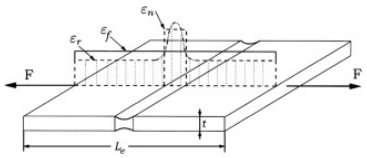

Figure 4.4: Failure strains evaluation using a gauge length L_e [12]

In 1880, Barba [10] presented a description to this non-uniform strain distribution in specimen. Barba's law states that failure strains, obtained from a uniaxial tensile test, can be expressed as a function of the gauge length in an asymptotic relation according to:

$$\epsilon_f = \epsilon_u + c\frac{\sqrt{WT}}{L} \tag{4.9}$$

Where:

ϵ_f = engineering strain at rupture
ϵ_u = uniform engineering strain
c = Barba constant
L = gauge length (or the equivalent element size in finite element modelling)
W = width the tensile specimen
T = thickness of the tensile specimen

The first term of eq. 4.9 refers to the uniform strain along the length of the specimen, and the second term the localised strain due to necking.

More recently, material failure criteria are created based on Barba's law. In 2006, Yamada conducted research where a Barba's law based formula is provided to convert failure strain to true failure strain [89]. In 2012, Högstrom performed tests on shipbuilding steel for material characterisation both numerically as experimentally and defined a formula for failure strain dependence on element size, based on Barba's law [28]. A common conclusion found in literature is that the failure strain is strongly dependent on the element size. Figure 4.5 shows the result of experimental tests on different steel specimen and the dependency of element size on plastic strain at rupture. It can be seen that for small element sizes, the equivalent plastic strain at rupture increases exponentially. Moreover, some researchers stated that the strong influence of the element size effect is even more important than the failure criterion formulation itself [19].

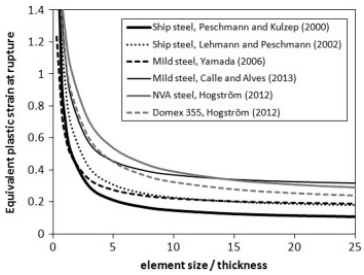

Figure 4.5: Failure strain versus ratio between element size and thickness [12]

When disregarding the width of the specimen, a through-thickness strain criterion can be used to determine the failure strain. This was initially proposed by Germanischer Lloyd AG [79] and is based on the experimental measurement of the through thickness strain of damaged plates in actual ship structures subjected to ship collision and grounding accidents. The following failure value for thinning strain (strain in the thickness direction) is proposed:

$$\epsilon_f = \epsilon_g + \epsilon_e(\frac{T}{l_e}) \tag{4.10}$$

4.3.2. Applied fracture criterion

Fracture of stiffened panel structures, such as a ship's bow, is a complex process. The following aspects need to be taken into consideration when analysing such a structure with FE modelling [70]:

1. Fracture is dependent on the strain state (triaxiality) and the deformation history of the material.
2. The process of strain localisation is highly dependent on plastic material behaviour.
3. The ability to capture the correct strain concentration is highly dependent on the mesh size, i.e. the FE discretisation.
4. Statistical variability is inherent to the above aspects.
5. The assumed load conditions will not cover all possible scenarios. Therefore, conservative simplifications are made.

Numerous criteria are defined to incorporate the fracture strain into a FE analysis. Well-established criteria are the RP-C208 criterion, RTCL damage criterion, BWH instability criterion, GL criterion, Peschmann criterion and the constant plastic strain criterion [68]. The most recent criterion is from DNVGL-RP-C208

[18]. This document is provided by international organisation DNV GL, the Nordic classification society and accredited registrar. This organisation is established in 2013 as a result of a merge between two leading organisations in the field, Det Norske Veritas and Germanischer Lloyd, and has become the world's largest classification society. The DNVGL-RP-C208 document provides rules and standards for the determination of structural capacity by nonlinear finite element analysis methods for the design of ships. One of the defined rules is the failure criterion RP-C208, which is a simple and widely known and used fracture criteria. A distinction is made between the favourable capacity; low capacity as a conservative option for the design of ships, and high capacity for collision analysis. The RP-C208 criterion is well applicable for the present study. Moreover, it is widely used and accepted. Therefore, this failure criterion used in this study.

The most important part of this criterion is stated in the local membrane strain check ϵ_{crl} (major principal strain), where the gross failure strain is scaled as:

$$\epsilon_{crl} = \epsilon_{crg}\left(1 + \frac{5t}{3l}\right) \tag{4.11}$$

Where:

ϵ_{crl} = critical local strain
ϵ_{crg} = critical gross failure strain
t = element thickness
l = element length

The critical gross failure strain ϵ_{crg} needs to be determined according to Calibration Case CC01 from DNVGL-RP-C208 document. This is performed for the material defined in section 4.2.2. The calculation of the critical gross failure strain is presented in appendix E. This results in a critical gross failure strain of $\epsilon_{crg} = 0.18$. The element length is dependent on the finite element model, but for this calculation example, $l = 50$ mm is used. The element thickness in the regarded ship bow structures generally ranges from 8 to 16 mm, a weighted average of 11 mm is used. The critical local strain is than becomes

$$\epsilon_{crl} = 0.18\left(1 + \frac{5 \cdot 11}{3 \cdot 50}\right) = 0.24 \tag{4.12}$$

This means that for an element size of 50 mm and a thickness of 11 mm, the element is considered as failed at a strain of 0.24, and will consequently be removed. For a mesh of 25 mm, this is at a strain of 0.31.

Stress triaxiality is not regarded, and failure strain is taken as constant over stress triaxiality range 0.0-0.7. Moreover, failure strain is assumed constant for different strain rates. Mainly due to a lack of experimental data on the material. Assumed is that this will not have a significant effect on the desired output (maximum collision load and energy dissipation). This assumption is based on the sensitivity study written in section 6.1. The damage evolution algorithm of ABAQUS is disregarded since it will mainly have an effect on a local scale, not on the scale of ship-bridge pier collisions.

4.4. Mesh discretization

4.4.1. Mesh elements

Four-noded quadrilateral, stress/displacement shell elements with reduced integration and a large-strain formulation (S4R) are utilised to model the steel plates with five integration points through the thickness, default hourglass control (relax stiffness) and drilling stiffness (default). The S4R element uses a reduced integration rule with one integration point that makes this element computationally less expensive than S4. By using this reduced integration element, attention should be paid to artificial energy. More about this is written in section 4.6.2. The shell formulation considered in S4R is that of finite-membrane strain; therefore, these elements can be used to perform large strain analyses. This type of elements are widely used for industrial applications because they are suitable for both thin

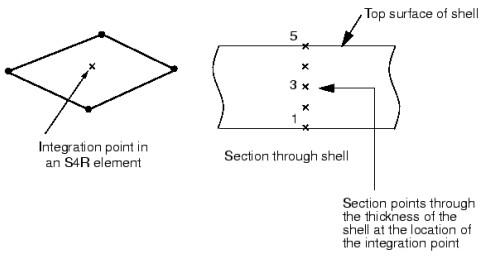

Figure 4.6: Four-noded shell element with five integration point through thickness [62]

and thick shells [41]. Moreover, the four-noded elements are usually
preferred for collision simulations due to the large number of structural details required for a proper discretisation of the structural members involved and are known to be more appropriate than triangular elements [54]. Figure 4.6 shows the configuration of section points in a numerically integrated shell element.

4.4.2. Mesh size

In finite element analysis, mesh size is a critical issue. It closely relates to the accuracy, computing time and efforts required for meshing of finite element models, which determines their complexity level. The mesh size determines the size of the elements and thus, the distance between the nodes. Elements should be sufficiently small to capture the major local deformations, such as folding and buckling. For large structures such as ships, as a general principle, a least fine mesh should be used in the collision zone to reduce the computational effort [52, 18]. The mesh size can not be excessively small due to constrains of computational time and resources. Alsos, Storheim, Amdahl and Toernqvist [4, 67, 73] concluded that when an element length-to-thickness ratio is in the range of 5 to 10, the local stress and strain fields are sufficiently accurate. This meshing range was later applied in collision simulations, and comparison with empirical and analytical methods proved a successful result [25, 8]. In a study from Sha and Hao a mesh convergence test is conducted on a barge [61] with mesh sizes of 200 mm, 100 mm and 50 mm. In this study, a mesh size of 200 mm predicted a smaller impact force predicted than 100 mm and 50 mm elements, the mesh size of 50 mm and 100 mm resulted in very similar numerical results. In 1995, Lehman and Yu conducted research on progressive folding on bulbous bows, where these authors stated that the mesh size should be chosen between 9 and 15 times the thickness of the plate [42].

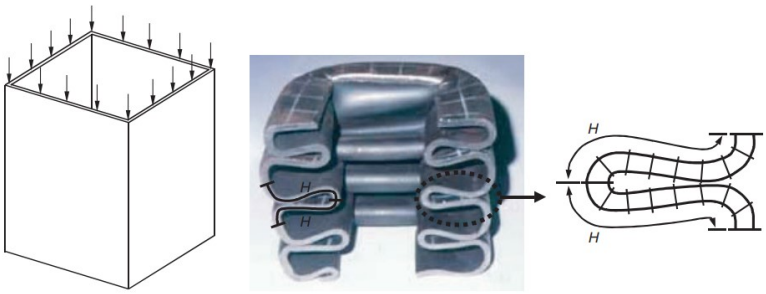

Figure 4.7: A thin-walled structure crushed under predominantly axial compressive loads and cut at its mid-section [51]

Nevertheless, simplified analytical equations and recommendations are useful to define 'optimum mesh size', because costly convergence studies are not necessary [52, 51]. A preliminary estimation of a proper mesh size can be readily determined analytically. In collisions, major failure modes are crushing, fracture (tearing or cutting), and plate tension. Among them, the crushing mechanism requires a relatively fine mesh size to reflect folded configuration. Figure 4.7 shows a typical crushing pattern of thin-walled structures under compressive loads. From this figure, it is found that a minimum of eight finite elements is necessary to capture this folding pattern, for half-length H of one structural fold [50]. Therefore, the relevant mesh size to properly capture the crushing behaviour of a thin-walled structure, such as a ship's bow, can be determined depending on the expected half-length of one structural fold.

A number of analytical equations are available to predict the expected length of one structural fold. A well-known example is proposed by Wierzbicki and Abrahamowicz [85]. According to their conclusions, the following formula can be used to predict the half-fold length for thin-walled structures under crushing load:

$$H = 0.983 b^{2/3} t^{1/3} \tag{4.13}$$

Where b is the breadth of plating between stringers or support members, t the plate thickness and H a half-fold length. Equation 4.13 can be roughly applied to different types of sections. To establish a preliminary estimation for the proper mesh size, this equation is applied to the to be analysed geometry. The graph in figure 4.8 shows approximations for different thicknesses over changing width. Since the geometry of a ship bow consists of many plates with different shapes and dimensions, a lower bound value is estimated. Assumed is that the plates of this geometry are not narrower than 100 mm, which is very likely giving an often used

frame spacing of 500 mm. The smallest half-folding length is determined by the smallest thickness; therefore, a small thickness of 8 mm is considered. Following eq. 4.13, the smallest half-fold length is estimated at 42 mm. According to this approximation, the maximum mesh size should be 42/8 = 5.25 mm, in order to capture all possible folding mechanisms within the considered geometry. This is an unrealistically small mesh size for the size of the analysed structures, which would cause enormous computational costs. To prevent these high computational costs and make sure the analyses could be run within a reasonable time frame, a larger mesh size should be applied.

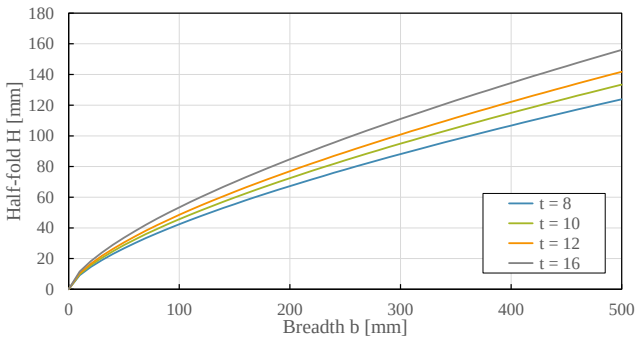

Figure 4.8: Half-fold lengths for different element thicknesses according to eq. 4.13

Remarkable is the disagreement about the mesh size determination in literature, where some recommend an aspect ratio between 5-10 [4, 67, 73], Paik recommends a much smaller mesh size which should be calculated with the half fold length divided by eight, or an aspect ratio near unity [50]. To determine the optimal mesh size for this study – in terms of accuracy and computational costs – a mesh convergence study is performed. The results are presented in section 6.1.1.

The convergence study shows for a mesh size of 25 mm convergence for the collision force during about the first quarter of the simulation time. This means that a mesh size of 25 mm is not yet optimal in terms of accuracy. However, since computational costs will increase drastically when decreasing the mesh size further, this mesh size is considered optimal in terms of both computational costs and accuracy. Moreover, the fold lengths are measured in the visual results of the simulations and a fold length of about 300-350 mm is found for the deck plates, with different mesh size simulations. This is substantially larger than the estimated fold length using eq. 4.13. When considering the strict recommendation from Paik on the mesh size, this should be around 20 mm – given this half-fold length. This is in a better agreement with the 25 mm mesh size than the previously calculated 5.25 mm.

Moreover, a mesh size of 25 mm is still very precise given the recommended aspect ratios of 5-10 [4, 67, 73] – confirmed by Haris and Bae [25, 8] – or 9-15 [42] times the element thickness, since the element thicknesses in the considered structures are 8-16 mm. Given these ratios, a larger mesh size could be appropriate if the structural size is increased, to decrease the computational costs and balance the computational costs with the accuracy. A 50 mm mesh is applied for the substantially larger structure of the class V ships, where a 25 mm mesh is not feasible.

Note that this size is configured as global mesh size, local elements can be smaller according to the best fit of the mesh algorithm in ABAQUS. Minimum size control is kept on the default as a fraction of the global mesh size, which is set at 0.1. This means that the smallest elements in the mesh model could be as small as 10% of the global mesh size.

According to recommendations about the contact algorithm, explained in section 4.6.1, the rigid wall (master surface) should have a mesh size not finer than used for the ship bow (slave surface) to avoid significant penetration for hard contact. Therefore, a relatively coarse mesh size of 400 mm is chosen for the collided object, which is equal to the automatically proposed mesh size by ABAQUS/CAE.

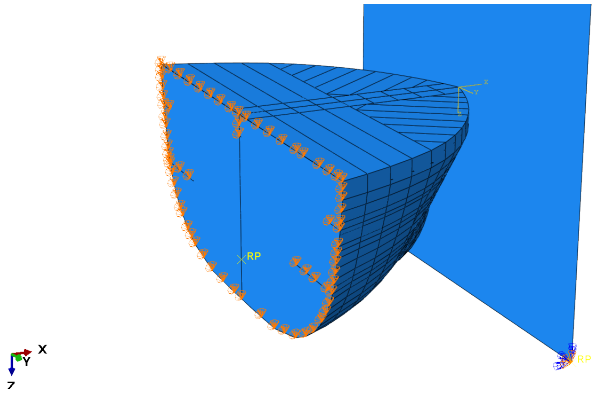

Figure 4.9: Support conditions of CEMT Class IV simulation.

4.5. Initial conditions

4.5.1. Impact velocity

The object emulating the ship in the analysis is provided with an impact velocity. It is necessary to incorporate this on the complete object at $t = 0$, to avoid local singularities. This is included in the NLFEA as a predefined variable. For all nodes of the moving object, the impact velocity is configured, so that all nodes move parallel towards the rigid wall and inertia effects will be avoided (see section 4.6). By defining this predefined variable, it is made sure that the kinetic energy of the ship is included in all nodes of the object together. The value of the impact velocity is dependent on the simulation and is therefore not quantified here.

4.5.2. Boundary conditions

A rigid body in a three-dimensional space has six degrees of freedom (6DoF): translational and rotational and both in three dimensions. These degrees of freedom in the NLFEA are configured to agree with the boundary conditions of the simulation. The rigid object emulating the bridge pier is fixed in all directions. This is done by setting all six degrees of freedom to zero. Since the object is rigid, this is only necessary for one node within the object. The outer ends of the ship model are connected to a rigid surface on which the extra mass of the rest of the ship is defined. The connection is rigid in translational directions but free in rotational directions. Therefore, the outer ends of the ship bow can bend independently from the rigid surface, which is in agreement with reality. Support conditions for the ship are configured on the nodes at the outer end the ship bow, where the structure is continuing into the remaining structure of the ship (which is not modelled). Only translational directions are fixed, except for the direction of the velocity vector. In this way the end nodes can rotate freely, however, globally. The ship bow is clamped at the end since the supports work together to create globally a fixed connection. In this way, rotation (and thus sliding) of the ship's bow during the collision is prevented, and conservative 'worst case' results are obtained. Nevertheless, it is not an unrealistic assumption, since the high inertia of the long part of the ship behind the ship's bow will prevent this movement. The support conditions of the simulation objects are shown in figure 4.9.

A more accurate description of the boundary conditions can be obtained by either fixing the bow at the end with a spring stiffness depending on the global ship inertia. Or define the inertia centre of mass of the remaining non-modelled part of the ship, add this point to the model and rigidly connect this point to the nodes at the outer end of the modelled part of the ship. However, this will increase the complexity since the full structure of the ship needs to be known, including mass and cargo distribution. Besides, it will only add little extra accuracy to the simulation. The chosen boundary conditions in the present study are conservative and will result in an upper limit, which is desirable. Note that for non-frontal collisions, where the centre line of the ship is not parallel to the centre line of the bridge pier, the boundary conditions of the ship bow are much more important because of a higher impact on the results.

4.6. Other numerical analysis parameters

4.6.1. Contact formulation

At a structure-structure collision such as the ship-bridge collision, interaction occurs between the structures. A contact formulation is determined to avoid penetration of elements. ABAQUS/Explicit offers a general con-

tact algorithm which includes contact surface weighing, surface polarity and a sliding formulation. Generally, contact constraints in a finite element model are applied in a discrete manner, meaning that for 'hard' contact a node on one surface is constrained to not penetrate the other surface. Among the contact formulation, the master and slave surfaces need to be characterised. The surface which is more coarsely meshed should be chosen as the master surface, or when using slide surface with rigid materials, the rigid material should be chosen as the master surface. Since the rigid wall is defined as a rigid analytical surface, ABAQUS/Explicit will automatically consider this surface as master surface. This is also preferred because of the coarser mesh of the rigid wall. The surfaces of the ship's bow are defined as slave surface.

During the simulation, the elements between the bow and wall move to each other, and the algorithm calculates if a slave element has passed a master element. If this is the case, a penalty force is applied to the contact interaction. In general, ABAQUS/Explicit uses a balanced master-slave formulation for all surfaces. Balanced master-slave contact minimises the penetration of the contacting bodies and, thus, provides better enforcement of contact constraints and more accurate results in most cases. In pure-master slave contact, less accuracy is ensured since master surfaces can penetrate the slave surface unhindered (see figure 4.10). The default balanced master-slave contact algorithm is utilised for the simulations of the present study.

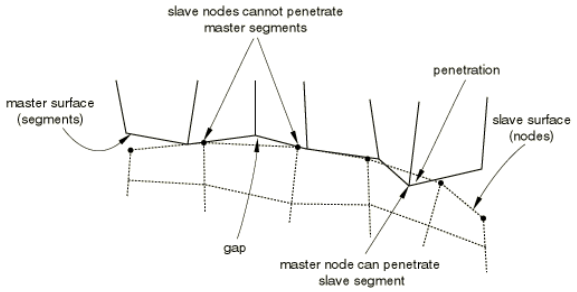

Figure 4.10: Master surface penetrations into the slave surface with pure-master slave contact and coarse discretization [62]

By default, the contact property model in ABAQUS assumes 'hard' contact in the normal direction, no friction, no thermal interactions, etc. However, the collision between the ship and a bridge pier is an interaction between materials; friction will occur. This interaction is modelled by setting a friction penalty property. Friction is considered during computation, and the friction coefficient set on 0.3, which is generally assumed for steel-concrete contact and ship-bridge pier collision simulations (for example by Consolazio and Cowan [15], Abubakar and Dow [3] and Sha and Hao [61]). Joustra and Pater concluded that the friction coefficient does not have a significant influence on the impact force at a head-on collision [35], which is also expected since the ship will collide with the bridge pier with centre-lines overlapping. This should prevent sliding. Moreover, sliding is also prevented by the defined boundary conditions. Possibly, friction could occur on a local scale due to bending or folding. When sliding is involved, either global sliding of the structure along the bridge pier or local sliding due to the pier geometry, this coefficient will be significantly more important. Yet, this is not the case for the present study.

4.6.2. Artificial energy

For a collision simulation, the structural response from the numerical analysis is affected by the artificial strain energy associated with the constraints to remove singular modes, such as hourglass deformation mode. For maritime crashworthiness simulations, which involve severe deformations of large structures, the result is usually acceptable if the artificial energy is less than 10 % [63]. If the artificial energy exceeds this 10 % significantly, full integration elements (S4 in this case) can be considered to prevent hourglass deformation. However, these elements are computationally more expensive than reduced integration elements. Mesh refinements can also result in a decrease in artificial strain energy, with a similar side effect.

Hourglass control is typically necessary for reduced integration elements, since trapezoidal deformation of the element is possible without physical meaning. Artificial stiffness has to be added to prevent deformation in this mode. This stiffness is added up into artificial energy.

Drilling stiffness is an artificial stiffness which is introduced to restrain the local nodal rotation about the normal to the element plane. This stiffness yields increased strain energy, however, is not part of the five degrees of freedom shell theory [34] and is therefore required to solve the system of equations in an implicit calcu-

lation, while it is not required in an explicit calculation. Nevertheless, ABAQUS recommends that drilling stiffness is turned on if not calibrated towards experiments. Accordingly, ABAQUS is programmed that the drill constraint is always active for finite-strain conventional shell elements such as S4R, which is used in this simulation. This default setting is kept in all simulations.

4.6.3. Initial imperfections

Initial imperfections in the form of initial plate deflections and residual stresses have an influence on the structural behaviour of a plated structure, such as ships, and are primarily caused by the welding process of the structure. Because such fabrication-related initial imperfections may have an effect on the structural properties and load-carrying capacities of the structure, they must be treated as parameters of influence in structural design and strength assessment. Moreover, initial imperfections can significantly reduce ultimate strength and thus must be taken into account in ultimate limit state assessment. However, they do not play a significant role in structural crashworthiness that is related to such accidental phenomena as collision, grounding, fire and gas explosions in which structural consequences are more likely to be governed by large strains [33]. Therefore, the effects of initial imperfections are neglected in this case of a ship collision as accidental limit state assessment. Moreover, this is assumed as a conservative approach since such fabrication-related imperfections of degradation phenomena will generally lower the global stiffness of the ship structure.

4.6.4. Inertia effects

In some cases for impact response simulations of thin-walled structures, it may be necessary to take inertia effects into consideration [58, 26, 36]. Strain distributions during impact simulations could be non-homogeneous at any moment in time, as a result of inertia effects and stress wave propagation phenomena. It is typically considered that the inertia effects become more important with increasing strain rate, starting at 0.1 s^{-1}. To investigate this effect, Paik and Chung [53] carried out experiments on the crushing of square steel tubes. Concluded is that the inertia effects can be neglected for strain rates less than 50 s^{-1}. With the considered impact velocities, it is very likely that this limit is not being reached somewhere in the structure during the collision. Therefore, the inertia effects are neglected. This assumption is confirmed by the results of the first simulations.

4.6.5. Time step and range

The time step in ABAQUS/Explicit is automatically estimated by the solver in terms of the stable time increment and is dependent on the mesh size and material. The stable time increment size is an approximation to the stability limit and is often written as the shortest transit time of a dilatational wave across any of the elements in the mesh. In general, the thickness of the elements is not considered in the process of determining the smallest element dimension for conventional shells. The stability limit is determined by the mid-plane. The time increment chosen by ABAQUS/Explicit accounts for any stiffness behaviour in a model associated with penalty contact.

The time increment used in the analysis must be smaller than the stability limit of the central-difference operator. If the time increment is not small enough, it will result in an unstable solution. When the solution becomes unstable, the time-history response of solution variables such as displacements will usually oscillate with increasing amplitudes. The total energy balance will also change significantly. The stable time increment is calculated as follows:

$$\Delta t \approx \frac{L_{min}}{c_d} \tag{4.14}$$

Where:

L_{min} = smallest element dimension in the mesh
c_d = dilatational wave speed, dependent of material properties

It is desirable to have an time increment step as large as possible since a small time step causes a higher amount of increments and thus a longer calculation duration. However, this time step needs to be smaller than the maximum stable time increment. Given eq. 4.14, it is observed that the time step is dependent

on the minimum element length (mesh size) and the dilatational wave speed. This speed is calculated with values of the material from table 4.1 by the following expression:

$$\begin{aligned} c_d &= \sqrt{\frac{E}{\rho}} \\ c_d &= \sqrt{\frac{210000}{7800}} \\ c_d &= 5189 \text{ m/s} = 5.19\text{e}^6 \text{ mm/s} \end{aligned} \tag{4.15}$$

For a global element size of 50 mm, an approximation of the stable time increment is made. Using eq. 4.14, a stable time increment step of 9.6×10^{-6} seconds is calculated. Note that this is calculated with a global mesh size, local mesh sizes could be as small is 10% of this size as defined in section 4.4.2. This means that a stable increment step as small as 9.6×10^{-7} seconds can occur.

The time duration of the collision simulation needs to be sufficiently long to provide results for the whole crushing process until the kinetic energy is fully dissipated. This could be determined depending on the simulation input parameters, of which the mass and velocity will have the largest influence. The time range will be roughly around 1.0 second. With the approximated time increment steps, this results in a total amount of increments between around 100×10^3 and 1000×10^3.

4.6.6. Double precision

Since the simulation will consist probably of a high number of increments (>300×10^3 time steps), numerical accuracy is important to avoid round-off errors. Therefore, the double-precision executable (with 64-bit word lengths) of ABAQUS/Explicit is enabled. This increases the computational costs but is necessary for sufficient accuracy.

4.6.7. Output

Relevant output is generated during the analysis, to evaluate the results. At 1000 points evenly divided over the simulation time, data is generated and saved into an output file. This output file could be analysed in ABAQUS/CAE. Most importantly, time-history data on the reaction force of the ship supports is recorded. This can be combined with displacement-history data to create a time-displacement graph. Energy levels within the system such as total energy, kinetic energy, internal energy, frictional dissipation energy, plastic dissipation energy and artificial strain energy are recorded.

During the analysis, the stress levels and spatial displacements of all elements are recorded at 100 points over the simulation time. Afterwards, this data is used to visualise the collision and gain insight into the failure mechanisms.

5

Simplified Analytical Calculation Methods

This chapter provides understanding about already established simplified calculation methods which are used to verify the comprehensive calculations used to answer the research question of this thesis. Moreover, first approximations are obtained in the form of crushing strength of cross-sections.

Simplified analytical methods generally capture the characteristics of a damage process, and employ theoretical formulae for structural components [84]. The simplified analytical methods, in general, use the concepts of structural crashworthiness, which is a proven practice in the automobile industry. Individual damage processes of elements within the structure are analysed and idealised with theoretical models, after which these models are combined to create global damage models with formulae for individual structural components. They provide insight into both global and local levels, and are more advanced tools which designers can use for analyses. With these tools, energy dissipation or mean crushing force can be calculated with the input of geometric and material properties of the ship. These methods have already been applied to a widespread of accident situations for ships, including head-on collision on rigid wall. The analytic expressions are used in the present study to provide a first estimation of collision forces on different geometries, gain insight into the collision process which lead to the collision forces, and to verify the results of the numerical analysis both quantitatively and qualitatively.

Several analysis models have been established for the estimation of the global loads and deformation energies involved in ship collisions. A well-known analysis model was published by Minorsky in 1959 [46]. Hereafter, some based on the analysis of Minorsky came Woisin [86], Gerard [23], Amdahl [6] and Yang and Caldwell [90], which proposed specific procedures for predicting the crushing loads of structures and are, although their age, still of importance. Most of the models have variables which depend on the cross-section geometry of the structure, where geometric characteristics are quantitatively implemented by the summation of basic crush elements, shown in figure 5.1.

5.1. Folding mechanism theory

Most of these simplified analytical approaches are based on the folding mechanism described by Wierzbicki and Abramowicz [85], where the hinge line theory is adopted to a folding element.

The basics of this theory are obtained from lecture notes of Dr. C. Walters of the TU Delft Strength of Ships course, and shortly explained here. For the crushing of a box column, the theory is applied as follows. Since the cross-section of a column box is double symmetric, one flange is considered. The external work is defined by the integral of the crushing strength:

$$\begin{aligned} W_{ext} &= \int_0^{t_1} P\dot{\Delta} dt \\ &= \int_0^{\Delta_{max}} P d\delta \\ &= \Big[\frac{1}{\Delta_{max}} \int_0^{\Delta_{max}} P d\Delta \Big] \Delta_{max} \end{aligned} \tag{5.1}$$

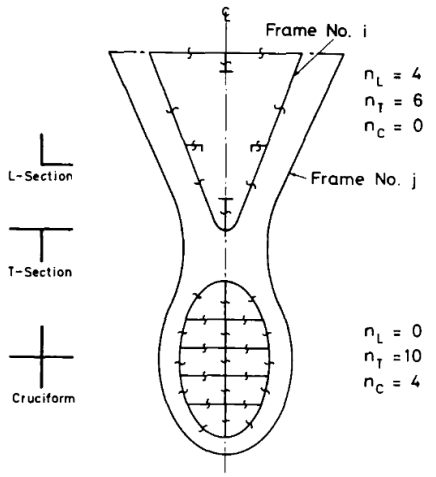

Figure 5.1: Method of cutting cross-sections of a (bulbous) bow in order to determine the number of basic crushing elements [57]

Where P is the unknown crushing strength, t element thickness, Δ the indentation and W_{ext} is the external work. We assume that the fold crushes completely closed:

$$\Delta_{max} = 2H \tag{5.2}$$

Where H is half the length of the fold, the so-called half-fold length. Then, the mean crushing force states:

$$P_m = \frac{1}{\Delta_{max}} \int_0^{\Delta_{max}} P d\Delta \tag{5.3}$$

And the external work becomes:

$$W_{ext} = \int_0^{t_1} P\dot{\Delta} dt = P_m 2H \tag{5.4}$$

For bending of the flange, the deformation is defined by:

$$\begin{aligned} \Delta &= 2H(1-\cos\theta) \\ \dot{\Delta} &= 2H\dot{\theta}\cdot\sin\theta \end{aligned} \tag{5.5}$$

The internal energy dissipation due to folding is found:

$$\begin{aligned} \dot{E}_b &= \sum M_0 \dot{\theta}_i b_i = 4M_0\dot{\theta}b \\ E_b &= \int_0^{t_1} \dot{E}_b dt \\ &= 4M_0 b\frac{\pi}{2} \end{aligned} \tag{5.6}$$

b is the width of the flange. For membrane action of the flange, the energy dissipation is given by:

$$\dot{E}_m = \int_S N_{\alpha\beta}\dot{\epsilon}_{\alpha\beta} dS \tag{5.7}$$

Where $N_0 = \sigma_0 t$, the stress per length.

Wierzbicki adds to this that the instantaneous crushing force P is defined by the requirement that the rate of internal dissipated energy, by different mechanisms, is equal to the external dissipated energy [85]: $\dot{E}_{ext} = \dot{E}_1 + \dot{E}_2 + \dot{E}_3$. This is in agreement with assuming a global equilibrium in the shell. An expression for the force-shortening characteristics of the compression member is developed. This expression involves two unknown geometrical parameters H and b. These values can be determined using the mean crushing force P_m. The general form of the formula for P_m follows from analytical expressions on the change in geometry:

$$\frac{P_m}{M_0} = A_1\frac{b}{h} + A_2\frac{C}{H} + A_3\frac{H}{b} \tag{5.8}$$

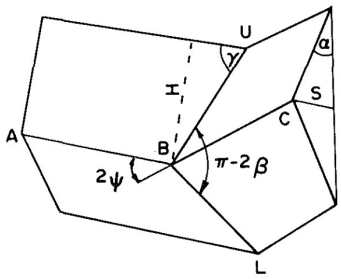

(a) Global geometry of basic folding mechanism [85]

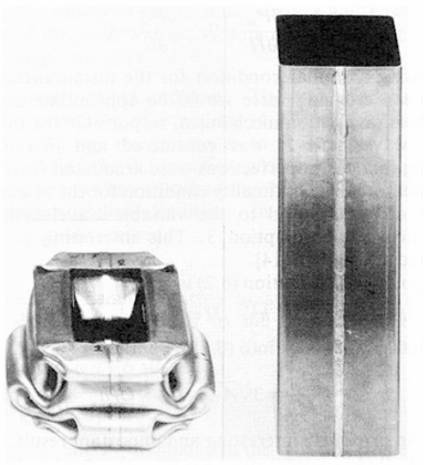

(b) Typical view of a fully crushed rectangular box column [85]

Where numerical values of the parameters A_i are known and depend on the type of problem.

Applying this theory to the crushing of a box column yields the following conditions: since a cross-section of a rectangular tube is composed of four basic folding elements, all energies within the $\dot{E}_{ext}$ equation should be multiplied by four. Moreover, because of clamped boundary conditions at the horizontal edges, energy level E_2 should be doubled. The energy balance equation yields:

$$2HP_m = M_0\left\{64I_1\frac{bH}{h} + \pi C + 16I_3\frac{H^2}{b}\right\} \tag{5.9}$$

Where $C = \frac{1}{2}(c+d)$ c and d are the cross-section dimensions, h the wall thickness.

The solution for H and b is calculated for the box column:

$$\begin{aligned} H =& 0.983\sqrt[3]{hC^2}, \\ b =& 0.687\sqrt[3]{h^2C} \end{aligned} \tag{5.10}$$

And the mean crushing force becomes:

$$\frac{P_m}{M_0} = 38.27\sqrt[3]{\frac{C}{h}} \tag{5.11}$$

This formula could be applied for box column. Different formulas for other structural elements are established; some of them are used in the next section.

5.2. Semi-emprical applications

5.2.1. Minorsky

One of the first studies in the area of ship collision damage assessment was carried out by Minorsky [46] in 1959, who developed an empirical relationship of the damaged material volume and the amount of energy absorbed, based on a number of real collisions reported to the U.S. Coast Guard. The formula is very simple but is unreliable for minor impacts.

It is assumed that most of the energy is absorbed plastically. Fundamental principles of impact mechanics are applied to develop a relationship between strain energy absorbed during a collision and the kinetic energy of the ship. A linear relationship was found to exist between the energy absorbed, E_a, and resistance factor, R_t, which defines the volume of damaged material in the ships.

$$E_a = C_1 R_T + C_2 \tag{5.12}$$

For the damaged material volume, the members having a depth in the direction of penetration are to be used, such as decks and a longitudinal component of the shell of the ship (which is assumed as 70% of the

shell area). Important to note is that the investigated collisions involved ships probably built between 1940 and 1955. A number of changes in ship design have emerged since then, probably resulting in a softer bow structure.

5.2.2. Gerard's method

Gerard's semi-empirical crushing formula has been established on the basis of the correlation against results of a series of panel test with various stiffener types [23]. This formula is outside of the field of marine structures a well-known model for estimating the crushing load of structures. It was originally developed for aircraft structures but has later found application in automobile and ship engineering. According to Gerard, the maximum crushing strength can be estimated by:

$$\sigma_c = \sigma_0 \mu \left[\left(\frac{nt^2}{A} \right) \sqrt{\frac{E}{\sigma_y}} \right]^m \tag{5.13}$$

The total crushing load is then given by

$$P_m = \sigma_c A \tag{5.14}$$

Where:

σ_y = yield stress
σ_0 = compressive flow stress
E = Young's modulus of steel
μ, m = coefficients depend on edge restraint
n = sum of cuts and flanges determined by the cross-section
t = average thickness for considered cross-section
A = Area of considered cross-section

The method states that the maximum strength is a function of the plate slenderness ratio defined as:

$$\beta = \frac{b}{h} \frac{\sqrt{\sigma_y}}{E} \tag{5.15}$$

With:

$$\frac{\sigma_{max}}{\sigma_y} = \mu \left(\frac{1}{\beta} \right)^m \tag{5.16}$$

Where h and b are width and thickness of the considered element. The constants μ and m are subject to fitting with experimental data. Gerard made a clear distinction within these constants for unloaded edges which remain straight of which warp during postbuckling. For distorted edges, which are mostly found in the regarded ship's bow structure, a best fit was obtained with: $\mu = 0.56$ and $m = 0.85$.

The formula given in eq. 5.16 is recalculated to the generalised formula in eq. 5.13, which is created to predict the maximum crushing load of considered plated structures within ± 10% of the experimental results of these structures. One of the major drawbacks with this model is that it has been derived from the crushing of relatively simple and regular plate constructions, where the variation of parameters has been limited [57]. Normal bow structures consist of a combination of plate panels of different dimensions and stiffener sizes. Using the simplified method from Gerard by adding up the maximum crushing load of individual panels to determine the maximum load for the completer structure is expected to produce conservative results. However, even with its existing shortcomings, this model has been found suitable for particularly accidental design load assessments in the aviation and ship design industry [57].

5.2.3. Amdahl's Method

Amdahl's method [6] is established on the basis of theoretical consideration on plastic deformation hinge lines shown by Wierzbicki [85], combining with correlation against model test results. From the theory of Wierzbicki, the total energy dissipated is a summation of the plastic deformation energy necessary for the folding of each structural intersection such as angles, T-sections and cruciforms, see figure 5.1. The total crushing load of a specific structure is determined by adding up the contributions from all basic elements of a considered cross-section. For each element, the folding length and crushing load are determined by a

minimisation of the deformation energy absorbed during the folding process, according to the theory of hinge lines. This procedure from Amdahl leads to the following formula to predict the average crushing strength:

$$\sigma_c = 2.42\sigma_0 \left[n_{AT} t^2 / A \right]^{0.67} \left[0.87 + 1.27 \frac{n_c + 0.31 n_T}{n_{AT}} \left(\frac{A}{(n_c + 0.31 n_t) t^2} \right)^{0.25} \right]^{0.67} \tag{5.17}$$

Similar as for the total crushing load in the model of Gerard, the total crushing load according to Amdahl is found by multiplying with the associated cross-sectional area of the deformed steel material:

$$P_c = \sigma_c A \tag{5.18}$$

Here:

σ_c = average crushing strength of the cross-section under consideration
σ_0 = flow stress of steel
t = average thickness for cross-section
A = Area of cross-section
n_c = number of cruciforms in the cross-section
n_T = number of T-sections in the cross-section
n_{AT} = number of angle- and T-sections in the cross-section

Equation 5.17 is established by a satisfactory correlation obtained between experiments and theory. The vessel in consideration is a supply vessel of 5000 t displacement. The structural arrangement is shown in figure 5.3. For calculating the correlation with the formula, mild steel properties are used: $\sigma_y = 240\ N/mm^2$ and $\sigma_u = 450\ N/mm^2$.

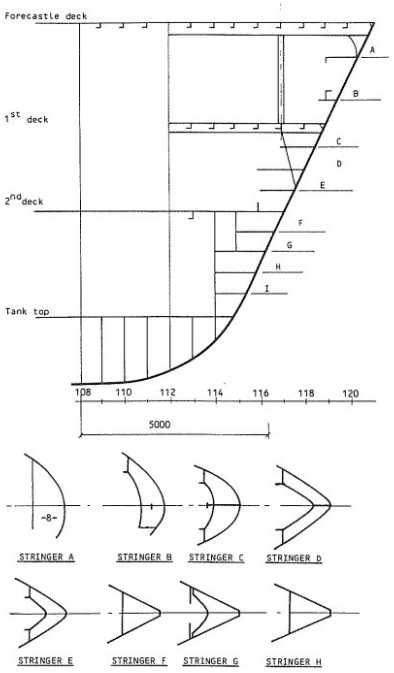

Figure 5.3: Structural arrangement supply vessel as case model for Amdahl formula [6]

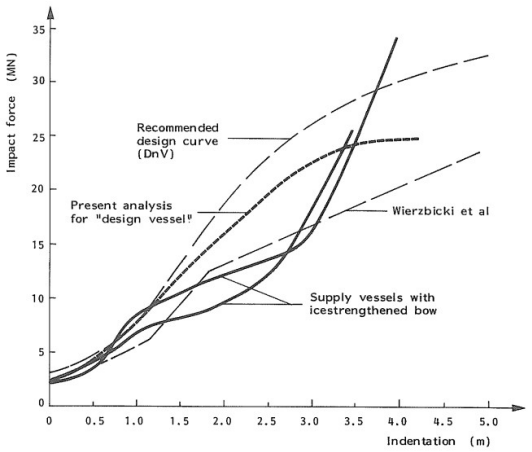

Figure 5.4: Load indentation curve for bow impact from Amdahl [6]

Both the structure, mass and material properties are comparable to Dutch inland waterway ships. Therefore, the simplified formula from Amdahl, eq. 5.17 could be promising. Expected is that impact forces from Dutch inland waterway ships are comparable to the design vessel curve in figure 5.4.

5.2.4. Yang and Caldwell's Method

Yang and Caldwell [90] proposed a slightly similar crushing model as Amdahl [6], but assume a different energy dissipation. Moreover, Amdahl determines the folding length by a minimisation of the deformation energy absorbed during the folding process, where Yang and Caldwell propose taking the folding length H equal to the spacing between transverse frames, provided that the frame spacing is less than the theoretical folding length [57]. Thereby suggest Yang and Caldwell that longitudinal stiffeners in the structure may be included through an equivalent thickness of the shell plating so that the plastic bending moment of the equivalent plating equals the plastic bending moment of the shell plating with longitudinal stiffeners. By using these assumptions, Yang and Caldwell propose the following formula for estimating the crushing load of a section of a complex bow structure [90]:

$$P_m = \sigma_0 \Bigg[1.178/H \sum^{n_f} b_i t_i^2 + 0.215H \sum^{n_{AT}} t_i + 6.935 \sum^{n_{AT}} t_i^2 + 0.265H \sum^{n_T} t_i + 0.589 \sum^{n_T} t_i^2 + 0.75H \sum^{n_c} \sum^{4} t_i + 0.375 \sum^{n_c} \sum^{4} t_i^2 \Bigg] \tag{5.19}$$

Where:

P_m = mean crushing load of structure
σ_0 = flow stress based on the mean value of the yield and the ultimate strength of the steel
b_i = width of the i-th plate flange
t_i = thickness of the i-th plate flange
H = folding length of the distorted plate flanges
n_c = number of cruciforms in the cross-section under consideration
n_T = number of T-sections in the cross-section
n_{AT} = number of angle- and T-sections in the cross-section
n_f = total number of flanges of angles, T-sections and cruciforms

The two last terms of eq. 5.19 refer to dissipated energy in cruciforms where the plate thickness is summed up for the four flanges of the cruciforms.

5.2.5. Validation of simplified models by Pedersen

Pedersen et al.[57] presented in 1993 a method to derive the crushing load as functions of penetrations. Concluded is with an empirical expression for bow collision forces for merchant vessels between 500 DWT and 300 000 DWT, depending on the length, mass and velocity of a considered ship. This formula, however, is based on bulbous bow ships and will be unrealistically conservative for the conventional bows of Dutch inland waterways regarded in this study since a bulbous bow has an increased steel volume at the front. Nonetheless, Pedersen et al. investigated the simplified models explained in section 5.2 and executed a comparison of the different models as validation. A modified Amdahl formula is introduced to better fit with experimental crushing results of the regarded small scale bow models. Results from experimental tests are employed as validation data. It is found that the modified Amdahl formula predicts reasonable crushing loads compared with test results for transversely-stiffened bow structures. For longitudinal-stiffened bows, the application of the modified Amdahl formula may load to somewhat conservative estimates of the crushing loads, while on the other hand corresponding estimates of the Yang and Caldwell method are somewhat low, see figure 5.5. In all cases considered, Gerard's load predictions are significantly higher than the experimental results. The crushing load results of the studied bow structure, which corresponds visually best with the regarded structures of Dutch inland waterway ships, is presented in figure 5.5.

The total collision load is estimated as the sum of the crushing load of the deformed part of the bow. This applied procedure of adding up the load contributions of the elements in the bow will not always be a correct method. For example, for a relatively stiff frontal part of the bow followed by a weaker rear part, the deformations may start in the rear part of the structure. This will result in a lower crushing load of the bow than that is predicted by the presented methods. Moreover, one has to keep in my by applying these methods for actual cases of collisions that the results are only validated for experiments under static conditions (low strain rates)[57]. During a ship-bridge collision, dynamic effects need to be considered in order to determine more realistically the appropriate magnitude of the collision force.

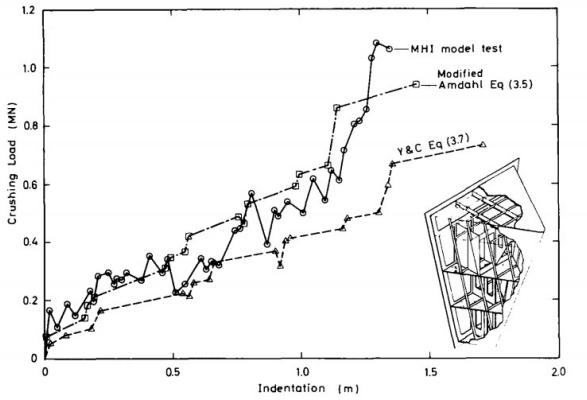

Figure 5.5: Comparison between numerical predictions with experimental results [57]

5.3. Application of semi-empirical expressions

The three simplified methods explained in section 5.2 are validated with experiments and could generate the first estimations of the crushing load for the ships investigated in the present study. Therefore, cross-sections of the class IV ship are considered, and the crushing load is calculated.

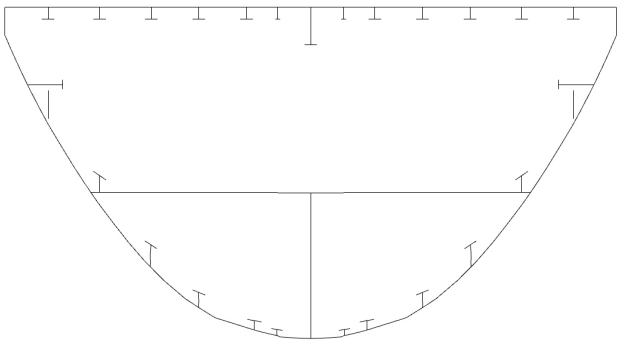

Figure 5.6: Cross-section of CEMT IV ship at depth $x = 2.4$m

The analytical models explained above can be a valuable verification step for the numerical analysis of the simulation done in this chapter. Attention should be paid to the failure mechanisms observed in the simulation, which should be comparable to the mechanisms assumed in the analytical models if the verification is being done on these theories.

The geometrical model is combined with thickness data of the elements. With Rhino/Grasshopper software, used for the geometry, an algorithm is programmed which shows the cross-section, calculates the average thickness and calculates the cross-sectional area for a specific location along the longitudinal direction of the geometry. A loop is added to generate this information for cross-sections on 200 mm distance intervals. This distance interval has shown to be precise enough with satisfactory results. From the cross-sections, the intersection elements are counted manually and used with the extracted data for the average thickness and cross-sectional area. Important to note is that the diagonal stiffeners at the frontal part of the bow are excluded in this calculation. The theory of these semi-empirical is obtained for members with their longitudinal direction parallel to the global longitudinal direction. This is not the case for the diagonal stiffeners and should therefore be excluded. Calculation data for the class IV ship calculation using the Amdahl method is presented in table 5.1.

The data is used in equation 5.17 to calculate the mean crushing force based on Amdahl's method. Results

d mm	$\mathbf{n}_c$ -	$\mathbf{n}_t$ -	$\mathbf{n}_a$ -	$\mathbf{n}_{at}$ -	$\mathbf{n}_{sum}$ -	$\mathbf{t}_{avg}$ mm	**A** mm^2	σ_c MPa	$\mathbf{P}_c$ MN
0	0	0	0	0	0	0.0	0.00E+00	0.00	0.00
200	1	4	4	8	9	11.8	5.37E+04	115.24	6.18
400	2	6	4	10	12	11.5	1.01E+05	98.00	9.94
600	2	12	4	16	18	11.6	1.45E+05	102.76	14.94
800	1	16	4	20	21	12.0	1.66E+05	105.39	17.47
1000	0	10	4	14	14	11.8	2.04E+05	68.66	14.00
1200	0	10	4	14	14	12.0	2.04E+05	69.86	14.23
1400	0	10	4	14	14	11.9	2.11E+05	68.21	14.39
1600	0	10	4	14	14	11.9	2.25E+05	65.61	14.73
1800	0	10	4	14	14	11.9	2.47E+05	62.00	15.32
2000	0	10	4	14	14	11.7	2.69E+05	58.11	15.62
2200	0	10	4	14	14	11.8	2.61E+05	59.83	15.59
2400	0	10	4	14	14	11.8	2.80E+05	57.35	16.07
2600	0	10	4	14	14	11.8	2.90E+05	56.12	16.28
2800	0	10	4	14	14	11.7	2.89E+05	56.14	16.23
3000	0	10	2	12	12	9.8	1.07E+06	21.42	22.96
3200	0	8	2	10	10	11.8	2.90E+05	48.30	14.00
3400	0	8	2	10	10	11.8	2.97E+05	47.57	14.14
3600	0	8	2	10	10	11.8	3.04E+05	46.91	14.26
3800	0	8	2	10	10	11.8	3.10E+05	46.33	14.38

Table 5.1: Calculation data for Class IV ship, which is used for hand calculation with Amdahl's method [6].

are shown in the last two columns of table 5.1.

By using the obtained data, calculations are done with Gerard's method and Yang and Caldwell method as well. For the Gerard's method, the following values are used: Flow stress σ_0 = 380 MPa, Yield strength σ_y = 300 MPa and Young's modulus E = 194000 MPa, which are extracted from the material model established in appendix D. Coefficients β = 0.56 and m = 0.85 are used which values are recommended for ship structures. For the Yang and Caldwell calculation, a half-fold length H of 250 mm is assumed, which is equal to half the frame distance, and b_t = 50 mm.

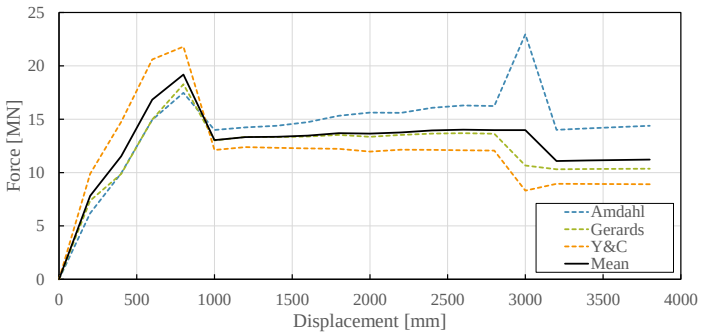

Figure 5.7: Hand calculation results by using semi-empirical approaches.

Results of the hand calculations are depicted in figure 5.7. A mean curve is added to show the result of a quick meta-analysis on the three approaches. The three results of the methods show good agreement, which is also seen in the validation of Pedersen in figure 5.5. Remarkable is an increase up to the highest (mean) peak at 800 mm, after which the force decreases to an almost constant force until the furthers regarded cross-section. This corresponds directly to the amount of counted intersections, which clearly has a high impact on the calculated collision force. A distinct difference between the calculation methods of Amdahl with the other two methods is observed at a distance of 3000 mm. At this point, a sudden peak in the cross-sectional area

found with a decrease in intersecting elements. The Amdahl method responds stronger on the increase in area than the decrease in intersecting elements and shows a higher collision force. For the other two methods, this is the other way around.

5.4. Conclusion

This chapter shows some general knowledge about the development and origination of the collision impact force. Moreover, the main factors contributing to the magnitude of the collision force are found by studying the theories on experimental results. The global agreement is found that the cross-sectional properties and material properties are the main contributors.

From experimental tests and plastic deformation theories, expressions are obtained to evaluate the crushing force of thin-walled structural elements (the basics are explained here in section 5.1). These structural elements are considered main contributors on the average crushing strength and are used in theories about the crushing strength of thin-walled structures [23, 6, 90]. These theories combine the amount of structural elements and their thicknesses with material properties to estimate the average crushing strength, which is multiplied with the cross-sectional area to eventually find the crushing force of a particular cross-section. The material properties are defined with the Young's Modulus, yield strength and flow stress. The flow stress is an approximate to simplify the strain dependency of the strength of the material and shows the highest influence in the crushing force expressions, in comparison the the Young's Modulus and yield strength.

Note that the simplified expressions are based on general thin-walled structures, such as a box column, and not on complex structures such as a ship's bow. A significant difference is found in the depth of these structures. Where a general thin-walled structure is constant in depth, the ship's bow does not only increase in dimensions in depth, but could also show a change in structural elements. This could result in significant crushing force differences if discontinuities are present in the depth of the structure. For example, for a relatively stiff frontal part of the bow followed by a weaker rear part, the deformations may start in the rear part of the structure. This will result in a lower crushing load of the bow than that is predicted by the presented methods. Moreover, one has to keep in my by applying these methods for actual cases of collisions that the results are only validated for experiments under static conditions (low strain rates). During a ship-bridge collision, dynamic effects need to be considered in order to determine more realistically the appropriate magnitude of the collision force.

A study performed by Pederson [57] shows good agreement between the simplified expressions and experimental results on ship's bows with different geometries. This gains confidence for the application of the expressions on ship collision analyses. The expressions are applied to one of the investigated ship's bows and results are analysed in section 5.3. These results are compared thoroughly with the results from the nonlinear finite element analysis further in this report in section 6.2. But by looking at the hand calculations separately, the results show realistic values. The global behaviour shows an steep increasing trend at the start, with a more constant curve from 1000 mm displacement. Since the cross-sectional dimensions are increasing at this considered part of the ship's bow, a logical expectation is that the crushing force increases simultaneously. However, this is not observed in the results of the hand calculations. This is caused by the ratio of the stiff structural elements and cross-sectional area. The amount of structural elements – or intersections – is about constant from a depth of 1000 mm, and the cross-sectional area is still increasing. From this phenomenon, a decreasing average crushing strength follows with the calculation expressions, which is multiplied with the increasing cross-sectional area. Together, this results in a roughly constant crushing force.

6

Verification and Validation

For the present study, a computer simulation model is utilised to simulate the collision process with the goal to produce accurate and credible results. Verification and validation techniques are applied to evaluate this goal. In the context of computer simulation, verification of a model is the process of confirming that it is correctly implemented with respect to the conceptual model[9]. It should match with specifications and assumptions regarded acceptable for the given purpose of the application. Validation checks the accuracy of the model's representation of the real system. Model validation is defined to mean "substantiation that a computerised model within its domain of applicability possesses a satisfactory range of accuracy consistent with the intended application of the model"[60].

The validation and verification is performed using three techniques:

- A Sensitivity Analysis, where the influence of different input parameters is investigated.
- Validation with calculation methods which are already established in the literature, where validated semi-empirical expressions are used to compare with NLFEA results.
- A Subsystem Validity check, where one element of the complete model is validated with already validated theories.

The NLFEA model described in chapter 4 is verified and validated here for the class IV ship model. It is considered that after verification for this specific model, the analysis applied to other (similar type) ship's bows is verified as well.

Results from first calculations are analysed and presented in appendix G. A quick verification is performed in this appendix by comparing the deformation of the ship's bow visually with a real case, comparing maximum collision forces with the standards and the force-displacement data with a reference study. In this chapter, a more comprehensive verification and validation is obtained.

6.1. Sensitivity Analysis

This section reports a system for quantifying and comparing the sensitivity of the nonlinear finite element analysis of the collision of a ship on a bridge pier to variations of different input parameters. Using the modelling techniques described in chapter 4, a sensitivity analysis was conducted to investigate the effect of various collision affecting parameters on structural damage characteristics. A sensitivity analysis provides information about the influence of each parameter, and with that, the sensitive parameter in the system which needs more attention.

A basis model is obtained, which is different from the final model defined in chapter 4 since the final model is set up through an iterative process starting from this basis model. Conclusions from this sensitivity analysis are used to set up the final properties for the eventual simulation of the present study on ship-bridge collisions. The basis model is configured with the (final) geometric model of the class IV ship bow structure, described in chapter B. Material properties are equal to the determined properties from a previous Dutch study on inland waterway collisions on bridge piers, the background study for the current ROK guideline

[35]. This study is described in section 2.4. This basis model will be further on referred to as reference model, or A0.

From the basis model, one parameter at a time is changed and consequences in the results are observed. The number of parameters in the numerical model makes it impractical to investigate all of them, so the investigations were restricted to the parameters that define the mesh size, material model, failure strain and assembly of the model. Moreover, a study is performed on the effect of changing the element thicknesses. Input parameters determining the initial kinetic energy, the mass and the velocity, are not analysed. This is because it is already confirmed that for ship-bridge pier collisions with lower kinetic energy, the same force trajectory is found [35].

Force-time data is combined to establish force-displacement curves which are plotted to compare the responses of different parameters. By observing force-displacement curves, a better comparison is obtained since the stiffness per cross-section over the length of the ship bow is equal. Force-time curves could be stretched out or compressed for different simulations since the dissipation in velocity could be different.

6.1.1. Mesh size

The mesh size plays an important role in the accuracy of the finite element models. Elements should be sufficiently small to capture the major local deformations, such as folding and buckling. On the other hand, mesh size can not be excessively small due to constrains of computational time and resources. More about the mesh size is written in section 4.4.2.

Three different mesh global mesh sizes are defined to find the variance and convergence in the results with changing mesh sizes. In the reference model, a mesh size of 50 mm is defined with a minimum size control of 10% of the global mesh size. Two other analyses are performed with global mesh sizes of 100 mm and 25 mm. A larger mesh size than 100 mm is regarded as too coarse, and a smaller mesh size than 25 mm will result in too many computational costs. One predictor of the model accuracy is the artificial energy which is used to compensate computational singularities; it is recommended that the artificial energy may be 10% of the total energy at maximum [63]. More about artificial energy is written in section 4.6.2. Furthermore, force-displacement data is compared for the different mesh sizes since this is the main output of the final simulations. And local differences are observed.

Global comparison

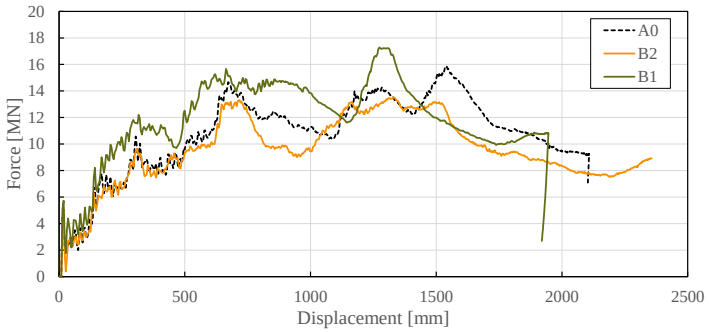

Figure 6.1: Reaction forces of simulations with mesh sizes 25 mm (B2), 50 mm (A0) and 100 mm (B1).

Globally, the results of a 50 mm mesh and 100 mm mesh are in good agreement. However, the 100 mm mesh gives higher forces and therefore a lower penetration depth. The maximum force is for the 100 mm mesh about 10% higher.

Expected is a more accurate outcome with a smaller mesh size. The result is until 0.5 meters penetration almost equal between 50 and 25 mm, that means a convergence of the results for the collision process up to 0.5 meters. However, after this point, clear differences can be seen. The peaks are a bit lower for the 25 mm mesh, which results in a higher penetration depth which will be reached after the simulation time has ended.

Since the artificial strain energy is considered a good predictor for the accuracy, the values are compared. Figure 6.2 shows the contribution in each simulation. The artificial strain energy is divided by the total en-

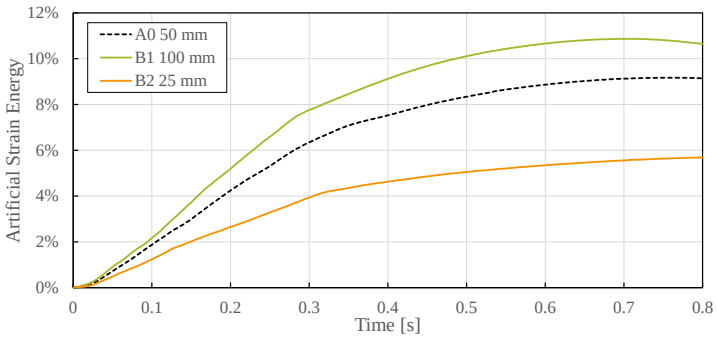

Figure 6.2: Artificial Strain Energy contribution to total energy dissipation in simulations with mesh sizes 25 mm (B2), 50 mm (A0) and 100 mm (B1).

ergy to find its contribution ratio. As stated in section 4.6.2, the total artificial strain energy decreases with reducing global mesh size. Less energy is needed for computational singularities with a smaller mesh size. All three total strain energies are close together, however, only mesh sizes 50 mm and 25 mm are within the requirement of a maximum of 10% of the total energy.

Local comparison

Since the mesh sizes influences the local behaviour directly, and global behaviour only indirectly, it is useful to compare the results of the mesh sizes locally. Moreover, it is expected that the mesh sizes show significant differences at folds which occur in the structure due to compression of thin plates.

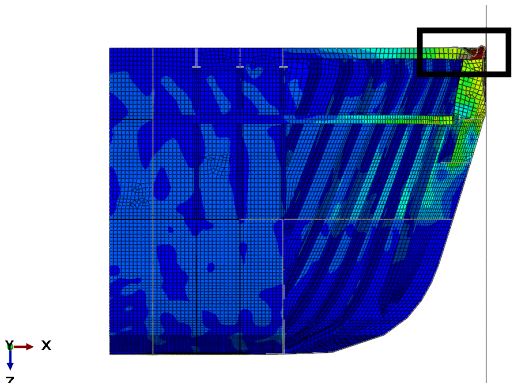

Figure 6.3: Location of analysed fold at 50 mm mesh

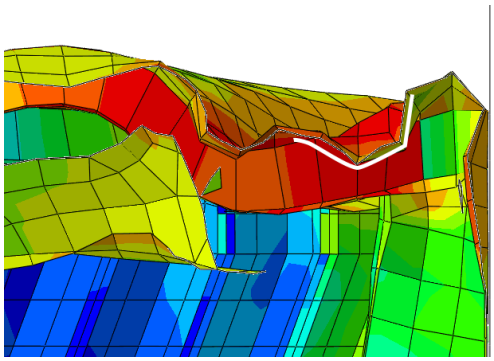

Figure 6.4: Frontal fold at mesh size = 100 mm

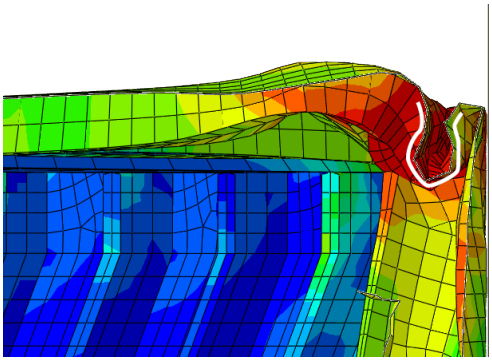

Figure 6.5: Frontal fold at mesh size = 50 mm

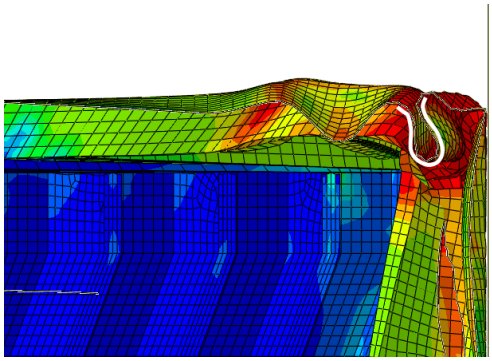

Figure 6.6: Frontal fold at mesh size = 25 mm

One folding section is selected to compare the visual results of the strains and stresses at that location. The location of the regarded section is indicated in figure 6.3. This section represents a deck plate at the far most

front end of the structure. Since this part is the first section which deforms during the simulated collision, the choice of this particular section will prevent that substantial deformation surrounding the analysed location will have a high influence on the folding mechanism. The folds are compared at $t = 0.08$ seconds. At this time, the folding mechanism is not influenced by a highly deformed surrounding structure. Moreover, the differences in global results are smaller at the beginning of the collision simulation. With that, a fair comparison is provided because, for example, the penetration depths differ not yet significantly between the different simulations. And most importantly, the regarded section shows a clear fold which could be analysed.

Figures 6.4 to 6.6 show the different responses with different mesh sizes. The fold is highlighted with a white line. Note that the scale of the pictures does not change, the element sizes do change. The observed folds show the same behaviour as was expected for a plated structure which is explained in section 2.2.2. However, generally, the local responses show large differences. The progression of the fold is at a different stage for the different mesh sizes, where the fold angle is at its highest for the smallest mesh. With this, the surrounding of the fold shows different behaviour as well. The length of the fold is a good factor for comparison and potential convergence. The length is calculated by counting the mesh elements in the length of the fold. The results are presented in table 6.1. The fold lengths are in good agreement. The fold length of the fold with a 100 mm mesh size is different because the fold could not end halfway of an element.

Mesh size	**2H fold length**	**2H fold length**
25 mm	14 elements	350 mm
50 mm	7 elements	350 mm
100 mm	3 elements	300 mm

Table 6.1: Fold lengths for different mesh sizes.

With the measured fold lengths of 350 mm, the half-fold length is determined and compared to the proposed equation of Wierzbicki and Abrahamowicz to estimate the half-fold length given the breadth of the plating and plate thickness. With a given deck plate thickness of 12 mm and breadth of 500 mm, the half-fold length according to the proposed eq. 4.13 is 142 mm. This gives a fold length of 282 mm which is relatively close to the 350 mm, but underestimates the length. Consequently, this shows an overestimation in the necessary preciseness of the mesh recommended by Paik, explained in section 4.4.2.

Another recommendation from Paik on the mesh size is to have at least eighth elements to represent one half-fold length [50]. This requirement is not met by any of the applied mesh sizes. However, the fold in the structure with a 25 mm mesh size shows a typical fold geometry found in experiments (see figure 2.15 in section 2.2.2). The fold with a 50 mm mesh shows the same geometry, but different behaviour outside of the considered fold. Where the considered section at the 25 mm mesh shows a propagating folding pattern, this area is flatter for the 50 mm mesh. This could be a result of different behaviour of the surrounding structure as well. The 100 mm mesh fold shows a propagating pattern, but far less smooth than for the 25 mm mesh.

The differences are quantified using the force-displacement data of the simulations. The data is extracted from the same time step (n) as for the fold visualisations. Since local peaks could be spread around a particular time step for the different simulations, the peaks are neutralised by averaging the data of time step n-1, n and n+1 for a fair comparison. Results are presented in table 6.2.

	A0 (50 mm)		**B1 (100 mm)**		**B2 (25 mm)**	
Displacement [mm]	436.92	100%	433.79	99%	437.46	100%
Force [MN]	9.00	100%	10.45	116%	8.74	97%

Table 6.2: Force and displacement results of simulations with different mesh sizes at $t = 0.08$ s.

The table shows that whereas local deformation differences are clearly observed, the global results on displacement and force are not equally different. A 100 mm and 25 mm mesh show a difference of +16% and -3% in force, respectively, in comparison to a 50 mm mesh. The displacements are not significantly different.

Conclusion
Convergence within this mesh variance results is only found for the mesh sizes of 25 mm and 50 mm up to 0.5 meters penetration depth. One could conclude that a 50 mm mesh is sufficient for simulating the first part of the collision process. However, further into the process, the convergence is not found. More simulations should be conducted with smaller mesh sizes to find full convergence. For example, a mesh size of 12.5 mm could result in convergence. But by taking half the length and width of an element, the number of elements increases exponentially. Consequently, the computational costs will rise rapidly. Hence, simulations with a smaller mesh size of 25 mm are considered not possible in the present study.

Final simulations for the present study are preferably conducted with a mesh size of 25 mm since it is generally acknowledged for finite element analyses that a smaller mesh size will increase the accuracy of the simulation. It is concluded that 25 mm is in good agreement in the general trade-off between computational costs and accuracy of the analysis. Since different geometric models are investigated in this research, which differ in total size, the mesh size determination will have to be done on a case-by-case basis. Computational costs could change enormously in absolute terms, given the size of the general problem.

Important to note is that only one parameter has been changed during these sensitivity analyses. Else, the results are not to be considered directly related to a particular parameter. This means for the mesh sensitivity analysis, the mesh size has been changed, but the failure strain is kept constant. This is in contrast with the remarks written in section 4.3 about the relation between the mesh size and failure strain. According to the applied failure criterion, the failure strain should increase with a decrease in mesh element size. This failure criterion is not implemented in the used nonlinear finite element software ABAQUS, but outcome values are inserted. The inserted values defining the failure strain represent the average of all involved elements, in terms of thickness and size. Within this mesh sensitivity analysis, it is chosen to keep the failure strain equal to form a better judgement about the mesh size on its own. However, valuable information about the convergence could be extracted if the failure strain is recalculated for the different mesh sizes. This is not done in the present study but is advised to incorporate in further research.

6.1.2. Simulation assembly

In the reference model of this study, the assembly is set up such that the bridge pier is moving towards the modelled ship bow. With this, the bridge pier is assigned the initial kinetic energy which is found in a real ship-bridge pier collision and will therefore penetrate the ship bow until this kinetic energy is dissipated. This assumption simplifies the model build-up, and a more comprehensive output could be extracted as reaction forces of separate structural elements are obtained. However, as the ship construction is not equal stiff over length, results may differ as the collision is a fast dynamic problem where material wave speeds can be of influence.

Simulation in the reference model (A0) is done with the rigid wall assigned with an initial velocity, and the ship is supported as immovable. Both initial velocity and support conditions need to be changed to turn this around. This is done in simulation A1. Since not the whole ship is regarded in the model, a mass reference point is added. This added mass represents the mass of the midship and stern, the mass of the bow structure is already incorporated in the material of the bow. A rigid frame is added to the back of the bow structure to divide this mass evenly over the section. This rigid frame consists of an infinitely stiff plate with a reference point on which the mass is added. The plate is tied to all edges at the back of the bow with three degrees freedom (u_x, u_y, u_z). At these edges, the bow is supported in both y- and z-direction ($u_y = 0$, $u_z = 0$). The sum of the masses of the bow and the added mass is equal to the total displacement tonnage of the regarded ship. The rigid wall is supported and clamped in all three directions, to schematise a rigid, immovable bridge pier. This model assembly is equal to the assembly defined in chapter 4.

Results
Up to 1.5 meters of penetration depth in the collision, both simulations show almost equal results in the support reactions. The simulation with the ship moving shows a less oscillating reaction force, however. In this case, support reactions are extracted from the rigid wall, which show a more balanced reaction force, especially in the beginning phase of the collision. Since the NLFEA is programmed to initiate damage at a strain of 0.2, this is a phase where a lot of damage is created. The damage initiation can cause local stress differences which propagate through the construction, but will not change stresses in contact with other structures as no significant deformation occurs, which influences the contact area.

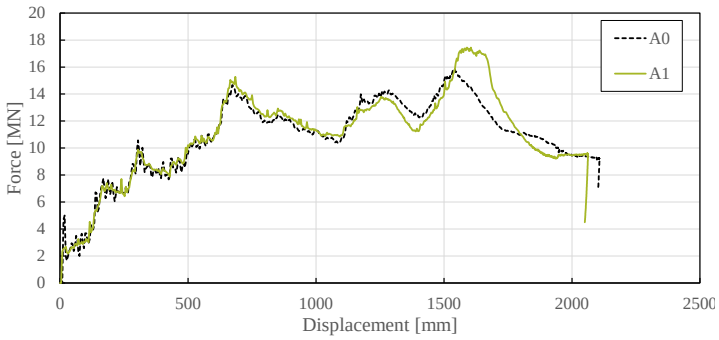

Figure 6.7: Reaction forces of simulations with ship moving + wall immovable (A1), and wall moving+ship immovable (A0).

The peak force of simulation A1 is about 10% higher than the peak force in the reference model. This is a result of a difference in deformation within the structure, which can be a consequence of the location of the applied force. In figure 6.8 is the deformation of the bow shown at $t = 0.36$ seconds for both simulations. This is the moment of the highest peak in both reaction forces. Remarkable is the difference in deformation of the longitudinal deck girder at the centre of the bow. For simulation A1, this girder is higher and pushes therefore onto a bigger part of the girder further back. This causes a higher peak force.

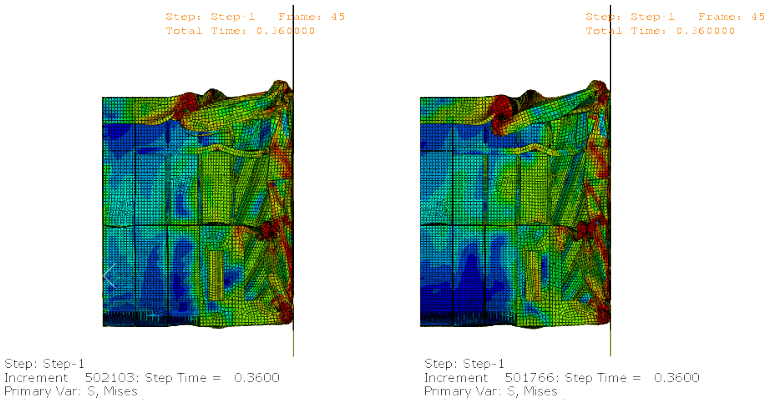

Figure 6.8: Deformation at t=0.36s in simulation A0 (right) and A1 (left)

As simulation A1 simulates reality best and gives the highest (most conservative) peak force, the model defined in chapter 4 is build up with the assembly of this simulation, where the ship bow 'moves' towards the bridge pier.

6.1.3. Material model

The material model obtained for the reference model is created with parameters found in the study of Joustra and Pater [35]. This is a bi-linear model, linear elastic followed by linear plastic behaviour. Since the material parameters could have a significant impact in the crushing force, multiple models are regarded and observed:

- A0 Bilinear (reference)
- C1 Elastoplastic-hardening
- C3 Elastoviscoplastic-hardening
- C4 Elastic-perfectly plastic

Bilinear model

The values for this model are established from parameters from the reference study [35]. The bilinear material model is widely used in numerical analyses and simple to set up. Work hardening is included by a linear plastic part. Mechanical properties are presented in table 6.3.

Stress-strain diagram is shown in 6.9. In ABAQUS, elastic behaviour is defined by the E-modulus and Poisson's

Bilinear					
$E_{elastic}$	$E_{plastic}$	σ_y	σ_u	ϵ_f	nu
210.0 GPa	800.0 MPa	270.0 MPa	430.0 MPa	0.2	0.3

Table 6.3: Mechanical properties of bilinear material model

ratio. Plastic behaviour is defined by the given stress and their strain of points on the plastic part of the stress-strain curve.

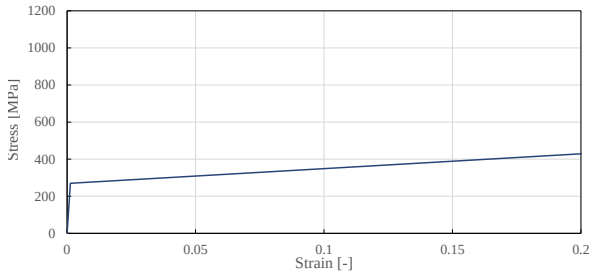

Figure 6.9: A0 Bilinear stress-strain diagram

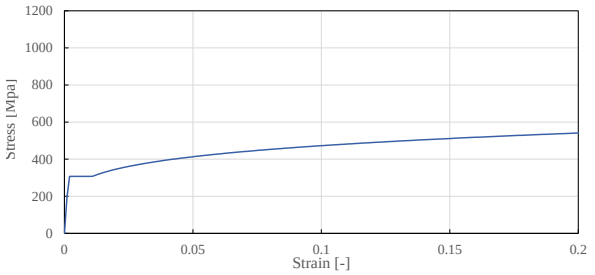

Figure 6.10: C1 Elastoplastic-hardening stress-strain diagram

More about this material model is explained in chapter 2, where the background study is described. The results from the simulation with this material model (A0) is used as a reference for comparison with the other material models.

Elastoplastic-hardening model
In simulation C1 elastoplastic-hardening material behaviour is provided. This material model is obtained from data generated by experimental tests of Paik et al. [56]. The process of obtaining the material properties from the experimental tests is explained in D. Different load rates are used in the experimental tests, resulting in stress-strain curves which are strain-rate dependent. The material model of simulation C1 does not include strain-rate dependent properties. Therefore, the test results of the lowest strain-rate ($\dot{\epsilon} = 0.001\ s^{-1}$) are used to simulate the (standard) static material properties. Stress-strain diagram is shown in figure 6.10 and mechanical properties are presented in table 6.4.

Elastoplastic-hardening				
$E_{elastic}$	σ_y	σ_u	ϵ_f	ν
194.0 GPa	300.6 MPa	463.9 MPa	0.43	0.3

Table 6.4: Mechanical properties of elastoplastic-hardening material model

In comparison with the reference model, this material model contains a lower Youngs' Modulus. Elastic behaviour is, therefore, less stiff, which can result in lower force peaks at elastic deformation of the structure. Since buckling strength is dependent on the elastic stiffness, a lower Youngs' Modulus will result in a lower critical buckling load. However, the higher yield strength (+11%) can compensate for this since it will take more force to cause yielding of the material especially if the plates structures are defined as stocky, where failure is governed by yielding of the plate. Because for yield failure, the strength is linearly dependent on the yield strength. Moreover, the ultimate strength is higher for the material in simulation C1. This could result in higher peak forces when plastic deformation is present in the structure. The failure strain is especially significantly higher (+115%). This difference is explained by an assumption made in the reference study to lower the failure strain to incorporate the lower strength of welded connections. Since elements fail with a higher strain, more plastic capacity is provided in the material, and occurring stresses can be higher.

The reaction forces are depicted in figure 6.11. The elastoplastic-hardening material model results in globally stiffer behaviour. Higher yield stress could be a governing factor for stiffer behaviour. Moreover, since plastic

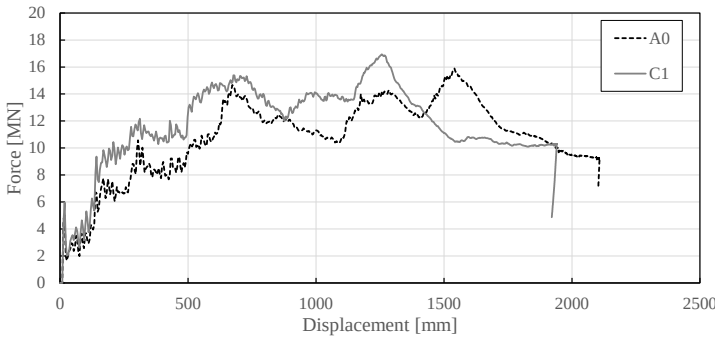

Figure 6.11: Reaction forces for elastoplastic-hardening material (C1) w.r.t. reference model (A0)

deformation is broadly present during the crushing process, a higher fracture strain could be another reason for the higher forces after the first (mainly) elastic part of the crushing process. Although the average reaction forces of simulation C1 are generally higher during the crushing process than in simulation A0, the maximum peak force is not very significantly higher (<10%).

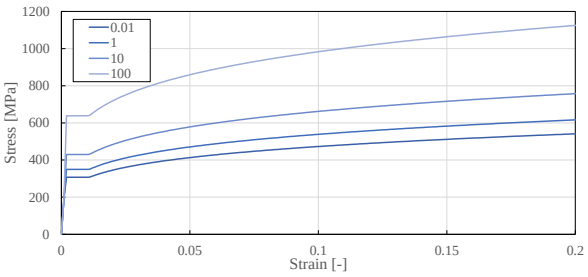

Figure 6.12: C3 Elastoviscoplastic-hardening stress-strain diagram. Strain rates are given in the diagram legend.

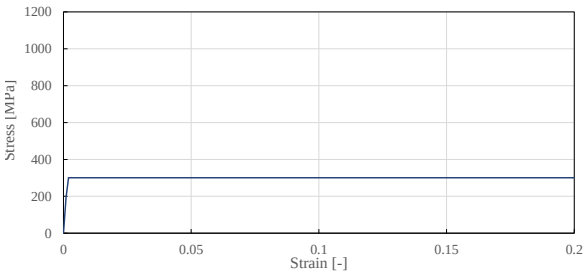

Figure 6.13: C4 Elasto-perfectlyplastic stress-strain diagram.

Elastoviscoplastic-hardening model

The elastoviscoplastic-hardening material model is assumed to represent the real material the best. It is the most comprehensive model. Difference between the elastoplastic and this model is the addition of strain rate dependency. The material occurs to respond differently when strain is acting quicker on the material; this is implemented in this model. The data is established from a database built by Paik [51]. With this data, the elastoviscoplastic-hardening material is established. This process is explained in appendix D. Generally, the material responds stiffer with a higher strain rate (see figure 6.12). Nevertheless, the Young's Modulus stays constant.

Since relatively increased strain rates are observed in the collision process of the present study, the increased stiffness for higher strain rates is expected to be utilised. Consequently, the global stiffness will be increased, and reaction forces are higher as the movement is stopped faster. This is most significant at the beginning of the collision process, where the colliding velocity is the highest.

To find a strain-rate sensitivity, this model is compared with the elastoplastic-hardening material model. Force-displacement results are depicted in figure 6.14.

The figure shows what is expected, a stiffer response globally. Both curves show exactly the same behaviour and oscillation, but with a different amplitude. The strain rate dependency is especially visible in the first peak of the curves. At this point, the velocity is equal for both simulations. The simulation with strain rate dependency reacts significantly stiffer here as relatively high strain rates occur at the moment of the first contact. From a displacement of about 0.3 to 0.5 meter, the simulation including strain rate dependency shows a higher force, which could be caused by the fact that a lot of material is acting in this area which has an increases yield strength. This could also be the cause of the high peak at a later stage of the process, where both

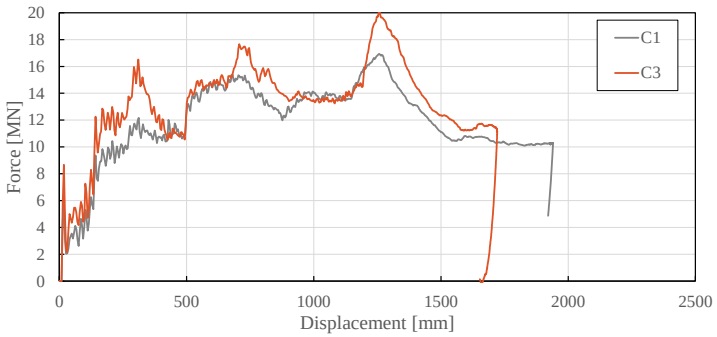

Figure 6.14: Reaction forces for elastoviscoplastic-hardening material (C3) w.r.t. elastoplastic-hardening (C1).

curves reach their maximum. The velocity, thus strain rate, is decreased here, but still, a significant difference in reaction force is observed. This is probably since a lot of extra material is included in the crushing process at this point.

Elasto-perfectlyplastic model

A very simple material model is applied here. The simplicity of this model allows for good comparison with hand calculations, which is done further on in this study. The stress-strain diagram is depicted in figure 6.13. This model is established with the yield strength of the obtained material model, σ_y = 300 MPa. In comparison to the reference model, the yield strength is 30 MPa higher, but the ultimate strength is 130 MPa lower since this is equal to the yield strength for this material model.

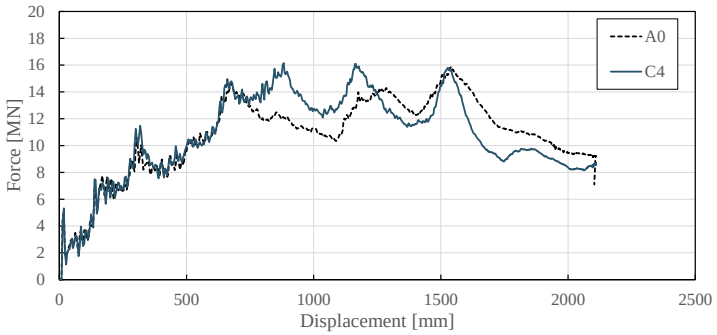

Figure 6.15: Reaction forces for elasto-perfectlyplastic material (C4) w.r.t. the reference model (A0).

Figure 6.15 shows a comparison between the reaction force. Remarkable is the similarity in the local peaks up to a displacement of 600 mm. The behaviour up to this point is almost exactly equal, but with minor differences in the height of the peaks. The increase in yield strength is not very clearly visible in the results. The difference is only visible after 600 mm. Nevertheless, the maximum collision force is very similar for both simulations, although the location of the peak is different.

General conclusion on material model

Concluding remarks are made about the total envelope of all curves of different material models. All curves of the study on this parameter are depicted in figure 6.16.

The average maximum force of the simulation from the sensitivity analysis is $F_{p,avg}$ = 17.21 MN and an average maximum displacement of x = 1981 mm. The final simulation results from the simulation established in chapter 4 is inserted in the plot of fig. 6.16 for comparison. The curve of the final simulation fits almost everywhere in between the other curves. Remarkable is that the maximum force of the final simulation is almost equal to the mean peak force, with F_p = 17.15 MN.

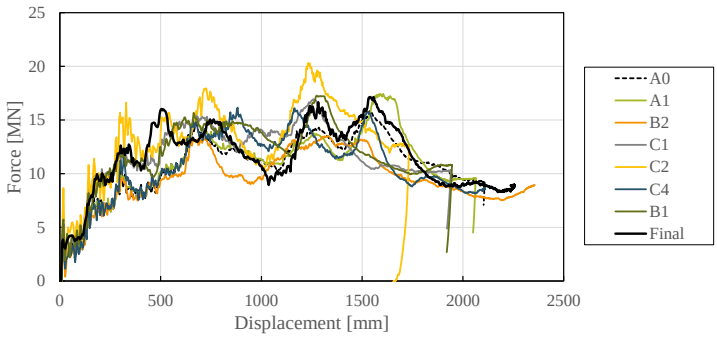

Figure 6.16: Reaction forces for all studied material models in the sensitivity study, including the final material model from chapter 4.

6.1.4. Plate thicknesses

Simulations are performed with different thicknesses to gain some insight into the influence of the structural properties on the result. Thicknesses in a range of 80% up to 120% of the reference model (A0) plate thicknesses are used. The results are shown in figure 6.17.

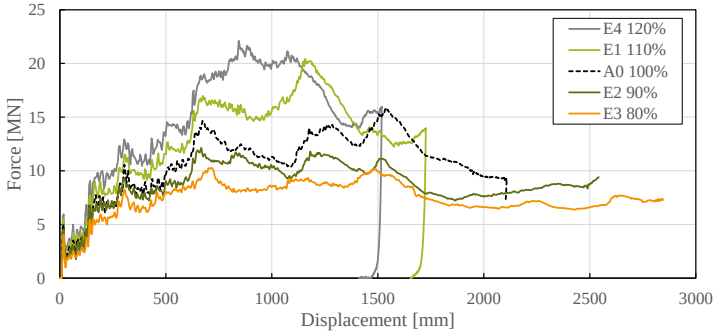

Figure 6.17: Reaction forces for collision with 80-120% of ship structure element thickness.

The trivial expectation that a higher thickness gives higher reaction forces is confirmed. With an increase in thickness, plates are more stocky and will have, for example, a higher critical buckling force since the slenderness ratio is decreased. Some elements of intersections might fail through yielding as the thickness is increased such that buckling is prevented. Moreover, the out-of-plane bending stiffness (with moment of inertia I) of a plate increases drastically by increasing the thickness: $I = \frac{1}{12}bt^3$, as well as the section modulus: $W = \frac{1}{6}bt^2$. This causes a higher increase of the global stiffness than with a linear relationship.

Thickness	**Peak force [MN]**	**Peak force**	**Average relative force**	**I(t^3)**	**Area(t)**	**W(t^2)**
80%	10.27	65%	73%	51%	80%	64%
90%	12.14	76%	86%	73%	90%	81%
100%	15.89	100%	100%	100%	100%	100%
110%	20.41	128%	125%	133%	110%	121%
120%	22.11	139%	138%	173%	120%	144%

Table 6.5: Relative result by changing thickness of structural elements in simulation.

This is confirmed by the data presented in table 6.5. With a decrease of 20% in thickness, the peak force decreases with 35%. As a reference, structural parameters are added, which are depending on the thickness to the power of 1 up to 3. The peak force increase is in most cases in between the values for the increase in section modulus and moment of inertia. This corresponds to the thickness dependency defined in the simplified expressions explained in chapter 5, where the plate thickness is squared in the expressions to calculate the crushing strength.

6.1.5. Failure strain

The failure strain determines the strain in an element at which the element is considered as failed. Generally, the failure strain is determined by a failure criterion. In section 4.3, more is explained about the failure criterion. In this section, the influence of the failure criterion in terms of failure strain is tested. As mentioned before, the mesh size determines the to be used critical failure strain as an input for the finite element calculation, since the most simple definition to estimate the strain depends on the length and the thickness of the element. This mesh size dependence is important for elements failing in tension, such as the outer and inner shell at a sideways struck ship. However, this seems less relevant for crushing and folding failure mechanism since strains will not develop to very high levels on global scale.

As is defined in section 4.3, the DNVGL C208 criteria is used in the present study. This criterion determines the critical failure strain with a given element length and element thickness. Assumed is that global values could be used for both the length and thickness, since the failure criterion is expected to have no significant impact on the collision force of the studied geometries. A test is done with two different critical failure strain values, to confirm this assumption. Damage Evolution is incorporated in these simulations to activate deletion of elements, although the value for 'Displacement at Failure' is set to zero to disregard the main application of Damage Evolution; to 'soften' the stress decrease at failure strain.

A reference finite element simulation (H3) is performed with a global mesh size of 50 mm. Given this mesh size and the average thickness of structural elements, the critical failure strain should be $\epsilon_f = 0.24$, established in section 4.3. A second simulation (H5) is done using a critical failure strain twice as high to judge the variance in the results by changing this parameter: $\epsilon_f = 0.48$. The results of the simulations are compared in terms of force-displacement, and contribution of the damage dissipation energy.

A higher failure strain (H5) is expected to increase the overall strength of the ship bow. And since less material is degraded to zero stiffness, the overall stiffness is expected to be higher as well. Consequently, the penetration depth of simulation H5 is expected to be shorter as the kinetic energy is dissipated more quickly with higher forces. What might be expected is a more oscillating graph for simulation H3 since more elements will be deleted, which in their turn result in local force drops. This is, however, a local phenomenon which could be neutralised over the whole structure.

Reaction forces and damage dissipation energy of the simulations are shown in figure 6.18 and 6.19, respectively.

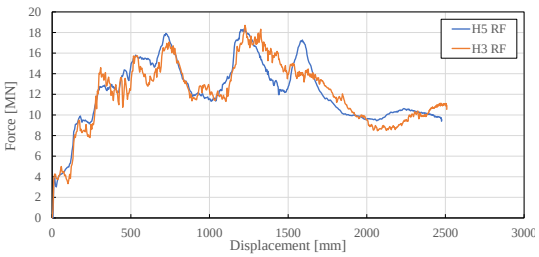

Figure 6.18: Forces from simulations with neutral failure strain (H3) and 200% failure strain (H5).

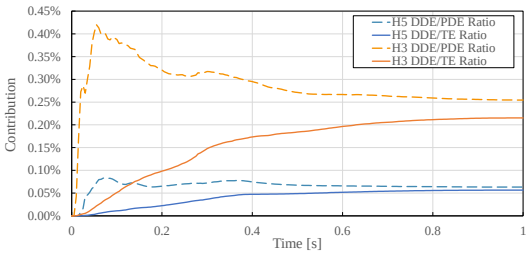

Figure 6.19: Damage dissipation energy (DDE) contribution in comparison with plastic dissipation (PDE) and total energy (TE) for simulation H3 and H5.

The reaction forces of both simulations are very similar. This means that the higher failure strain does not contribute significantly to a higher stiffness, as was expected. Moreover, the maximum displacement is for both simulations around 2500 mm. A clear difference is observed on local level, where the simulation with a lower failure strain shows a more oscillating behaviour as more elements are being deleted from the simulation. An interesting insight is obtained by comparing the damage dissipation energy with the plastic dissipation energy and total energy within the simulations, shown in figure 6.19. Generally, for both simulations, relatively many elements are damaged at the beginning of the collision process in comparison to the amount of plastically deformed elements. This is probably caused by the fact that only a little amount of elements are present at the frontal part causing that forces could not be redistributed to other elements with remaining plastic capacity. Nonetheless, a large difference is found in the overall contribution of the damage dissipation energy between the simulations with a failure strain of 0.24 and 0.48. For a failure strain of 0.24, the total

damage dissipation contribution is four times higher than for a failure strain of 0.48, with 0.22% of the total energy in comparison to 0.06%. That means that a difference in failure strain has a great impact on the damage of the elements in the simulation. However, since the damage dissipation energy is only a fraction of the total energy involved, the influence of the failure strain on the simulation results is negligible. This confirms the assumption that the failure strain does not have a significant impact on a (frontal) ship-bridge pier collision simulation. And concluded is that simplifying the failure criterion by using average values for the input variables will show no significant effect on the collision force.

6.1.6. Conclusion of Sensitivity Analysis

A sensitivity study is performed by changing the following parameters: mesh size, the simulation assembly, material model, plate thicknesses and the failure strain.

- From the mesh size analysis, it is concluded that the artificial energy requirement will be met for a mesh size of 50 mm or smaller. Full convergence in the force-displacement results is not found. It is recommended to use a mesh size of 25 mm or smaller.
- By changing the assembly of the simulation (either the ship bow or the bridge pier as moving object), the force-displacement results are not significantly different. However, the realistic case with a moving ship is preferred.
- The material model can cause significant effects on the force-displacement results. Therefore, the most comprehensive and realistic material model is recommended.
- The plate thicknesses do have an important effect on the force-displacement results, which was expected. This analysis gave some insight into the failure modes which are present in the collision process.
- The failure strain analysis shows that a change in this parameter does have a large effect on the damage process, in relative terms. However, in absolute terms, the effect is very marginal, which leads to the conclusion that the failure strain is not of high importance for (frontal) ship-bridge pier collision simulations.

More generally, it is found that the simulation model behaves in response to changes as is expected. No singularities are found, and the model is considered as stable. Furthermore, some insights into the simulation process and the crushing process are obtained. This could be useful for the overall judgement of the results.

6.2. Validation with existing calculation methods

In literature, some semi-empirical expressions are obtained for the crushing of a ship bow. This is done by analysing failure mechanisms, employing theoretical formulas and fitting parameters on experimental data. In chapter 5, three well-known semi-empirical formulas are explained. Since these methods are already validated on experimental data, these methods are used to validate the results from the NLFEA used in the present study. The input values for the methods consist of geometrical and material data, by which mean crushing force is calculated.

The semi-empirical calculation methods are applied to the class IV ship, according to the application explained in section 5.3. Mean crushing forces per considered cross-section are obtained. These forces are compared with results from the NLFEA to find a correspondence. Simulation C1 with elasto-plastic material, reported in section 6.1, is used for this comparison since the material model of this simulation is in best agreement with the assumptions and parameters used for the semi-empirical expressions. Since strain-rate dependency is not considered in the expressions and material properties of the material model from simulation C1 are inserted.

Figure 6.20 shows the calculated forces obtained by hand calculations and the reaction forces of simulation C1. A mean curve is added, which represents the average of the hand calculations. Remarkable similarities are found. The rapid increase in the first 500 mm is equally steep for both the mean hand calculations as the NLFEA calculation. This means that an equal stiffness is found for the bow up to 500 mm with both methods. The hand calculation curve increases with almost the same gradient after this point up to a maximum (mean) force of 19.2 MN, where the NLFEA curve increases more gradually up to its peak of 16.9 MN. The difference in peak forces is noteworthy since the hand calculations represent a mean peak force, but the mean peak is

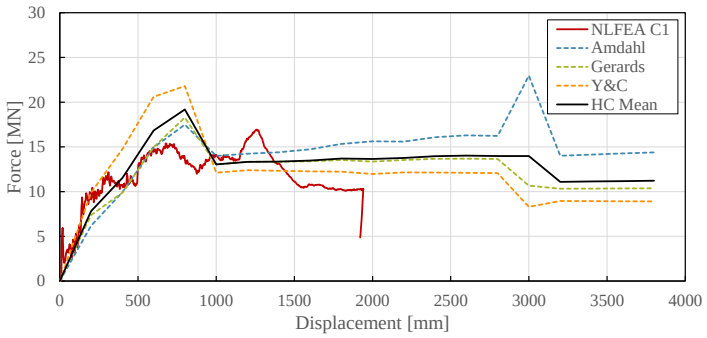

Figure 6.20: Reaction forces of simulation C1 and hand calculations performed with semi-empirical expressions.

still 14% higher than the NLFEA peak force. This could confirm the statement by Pedersen that the semi-empirical expressions from Amdahl and Gerards are on the conservative side [57]. However, this is not in full agreement with the separate results, since the Yang and Caldwell method specifically shows the largest force.

A clear difference is observed at the very beginning of the curves. A relatively high peak is observed at the start of the NLFEA curve, which is not found in the hand calculations. This is because of the nature of the hand calculations, where mean forces are considered with variables for the cross-sectional area and amount of stiff elements (intersections) in the cross-sections. Since both values are zero at $x = 0$ mm (with x as displacement), the force is zero, which is true with reality. However, the next interval is at $x = 200$ mm, where a linear line between the intervals is assumed. This linear assumption corresponds to conclusions drawn by visual inspection of the geometry and the values for the cross-sectional area, where both the number of stiff elements and the area increases linearly, in general. Moreover, the calculated forces by hand calculation represent the mean crushing force; this means that local peaks are not regarded in these calculation methods.

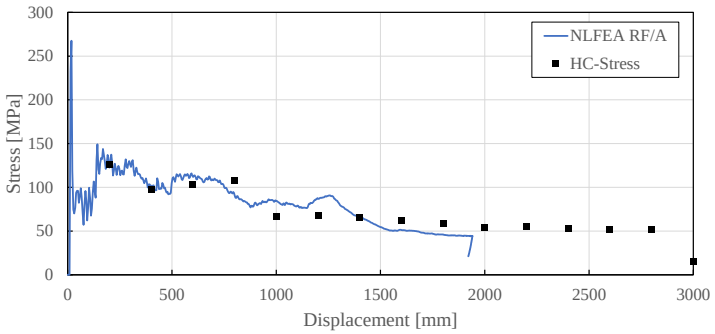

Figure 6.21: Stress levels calculated by simulation C1 (NLFEA RF/A) and hand calculations (Amdahl & Gerard, HC-Stress)

Both Amdahl's [6] and Gerard's [23] method with the principle of calculating a stress level which is multiplied with the cross-sectional area to obtain the mean crushing force for a particular cross-section. Given this, the force-displacement curve from the hand calculations and NLFEA calculations can be presented both as average stress level in the cross-sections. The collision forces following from simulation C1 are divided by the cross-sectional area data which is obtained for the hand calculations. This results are shown in figure 6.21. The presented stresses obtained by hand calculations are the averages of calculation with Amdahl's method and Gerard's method.

Overall, these results of both calculation methods correspond very well. A decreasing cross-sectional stress is observed with both methods, which is mainly caused by the increasing cross-sectional area. The stress results of simulation C1 show a high peak at a very low displacement, this is caused by the fact that the cross-sectional area is very small at that point, and the force is relatively high. The peak corresponds to the first local peak shown in the simulation results in figure 6.20, but is emphasised by the dividing the curve with the cross sectional area.

Energy dissipation is not considered in the hand calculations. Consequently, no endpoint is defined for the hand calculation curve. Therefore, the maximum displacement is not compared. However, by comparing the stress levels of both calculation methods, a valuable conclusion can be drawn about the location of the maximum impact force peak. A decreasing trend in average stress level over displacement is observed in figure 6.21. The hand calculations show extra information about the continuation of the collision force for the area after the point that the velocity of the ship is zero in the simulations, at about $x = 2000$ mm. At this point, the width of the ship's bow is about 7.2 m, which is 75% of the maximum width of the complete ship. With this extra information, it can be concluded the collision force will not be increased if, for example, the impact velocity is higher, resulting in an increased kinetic energy level which should be dissipated and therefore higher displacement. But this conclusion is only valid if the cross-sectional properties will not be very different from the calculated part of the bow.

The semi-empirical expressions of the hand calculations explained in chapter 5 are already validated, and generally accepted [57] for the application on thin-walled structures. The impact force results of the NLFEA simulation showed good agreement with these hand calculations. Moreover, the calculated stresses with semi-empirical expressions, presented in figure 6.21, show an average difference of about 15% with the stresses following from the NLFEA at the same displacements. This is remarkably low given the completely different approach of the calculations.

6.3. Subsystem validity

Since a ship's bow is a complex steel structure, a great number of assumptions is necessary for determining the forces of the full structure. This causes a need to pay close attention to its validity. In order to verify the finite element model, it is possible to find a governing failure mechanism of a single structural element, at which it is possible to determine the forces by an analytical expression. A failure mechanism of a structural element can be analytically described and compared to the finite element model. Therefore, the problem size is decreased to element level, for which validated theories are present.

On element level, well-known analytical models are established, which formulate the basis of many calculations on steel structures. One of the models which is widely used is the thin plates theory of Timoshenko [72], where analytical solutions are determined assuming a deflection surface of the buckled plate which can be represented by sinusoidal waves.

In this section, verification of the NLFEA model is done analytically, to compare the numerical results of the NLFEA model with results obtained by analytical solutions. As the whole model is too complex to do proper hand calculations on, one element is taken. It is found that a deck plate is a convenient element for the verification.

The process is visualised in figure 6.22. First, material properties are simplified for an analytical verification, and the simulation is run with this material. The reaction forces of the support at the end of the deck structure are read. Then, the deck structure is analysed separately, and the outcome is compared mainly qualitatively with the reference model results. Ultimately, a deck plate is analysed both with hand calculations and an eigenvalue analysis. The results of the deck plate are compared with the deck structure analysis, both qualitatively as quantitatively.

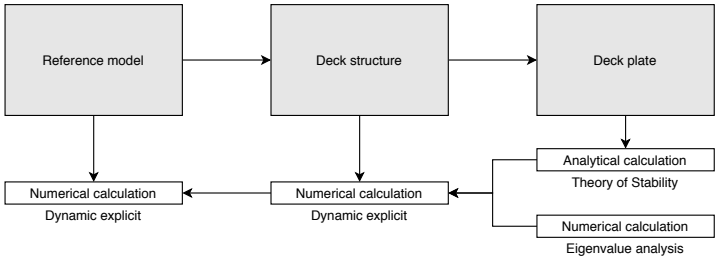

Figure 6.22: Verification process

6.3.1. Failure of plates

The ship's bow consists of a number of different members, mainly plates and stiffeners, in different directions and with different dimensions. Therefore, it is a complex structure to model and verify the results by simple hand calculations. To be able to verify the numerical model using analytical solutions, a clear failure mode of a typical element is taken.

An analysis of the failure modes during a simulated collision is done and reported in G. It is found that the deck structure behind the frontal bow structure shows a clear failure mode during the collision and this part of the deck is constructed with a relatively simple geometry since it is flat and does not have longitudinal stiffeners. As shown in figure 6.23, after about 0.18 seconds, the frontal part of the deck is deformed after which this part pushes onto the part of the deck plate behind the first frame. With the front part of the deck pushing onto this plate, the plate is compressed until it fails. It buckles with two half-sine waves in both longitudinal and transverse direction. As we take half of the plate in the width of the deck and the part between two frames, a typical buckling mode with one half-wave in both directions can be observed. That part is simplified and analysed with analytical solutions.

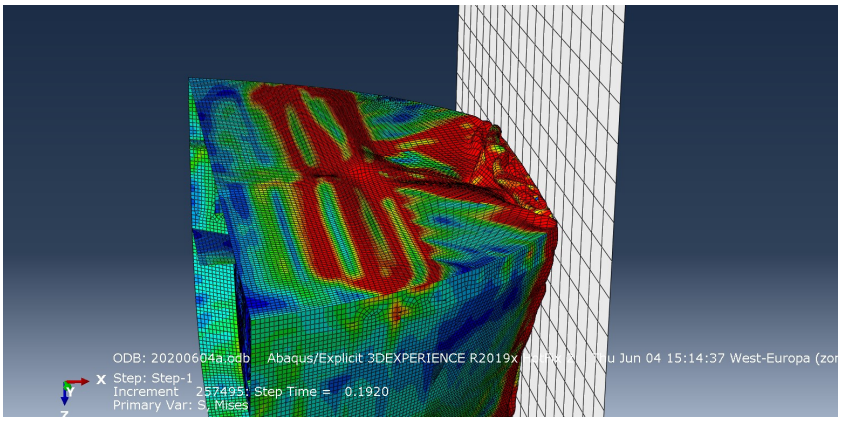

Figure 6.23: Buckling of deck at t = 0.192 s

6.3.2. Numerical solution

Model

The deck is analysed separately in the NLFEA model to find a force which could be compared to the analytical solution. As this comparison is generalised for whole the model, this separate model should as much as possible represent the same part within the complete model. Therefore, only the geometry and boundary conditions are changed, and other properties of the simulation are unchanged.

The geometry is changed to merely the deck structure (including transverse stiffener). The rigid wall is kept similar. Geometric connections are in general schematised with boundary conditions, as shown in figures 6.25 and 6.26.

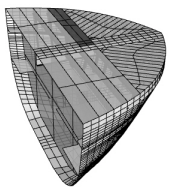

Figure 6.24: Highlighted (dark) deck plate in analytical verification

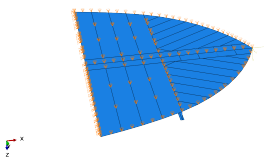

Figure 6.25: Deck structure with schematised boundary conditions

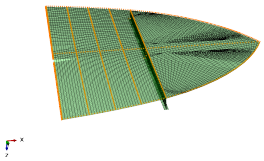

Figure 6.26: Meshed deck structure with schematised boundary conditions

All the supports are free in the y-direction, and only the support at the inner end of the structure supports the structure in the x-direction. This support will therefore provide rigidity at this simulation where the rigid wall is moving towards the front of the bow.

The elasto-perfectly plastic material model (C4 from sensitivity study on material) is used for this simulation. This is a simplified material model which makes the comparison with analytical solutions easier. Only elastic properties are incorporated into this material model. The properties presented in table 6.6 are applied.

Elasto-perfectly plastic		
$E_{elastic}$	σ_y	ν
194.0 GPa	300.6 MPa	0.3

Table 6.6: Mechanical properties of elasto-perfectly plastic material model

Mesh size is configured at 50 mm globally.

The frontal part of the deck is highly schematic. In the original model, the deck is stiffened with some steel stiffeners connected to the deck. These stiffeners provide stiffness to the deck during a frontal collision. In the results from chapter G, it can be seen that this part of the deck is folding around the stiffeners, which create a complex failure mode. After the folding and crushing of this part, the part behind is getting compressed. That is the part considered for the analytical verification, referred to as deck plate. The frontal part of the deck is increased in thickness up to a thickness of 16 mm, which causes a similar failure process for the regarded part to force this behaviour without adding stiffeners. Moreover, as it is unknown which magnitude of the total mass of the ship is resisted by the deck during a collision, the total mass is unchanged. The rigid wall is configured with the total mass of the ship and is moving towards the deck structure. As the deck structure separately will have less stiffness than the whole bow structure and the mass is taken as equal, the initial velocity of the rigid wall will decrease less rapidly and will have therefore a higher impact velocity the moment of buckling of the deck plate. However, as only buckling forces are considered, it is assumed that this difference will have no significant influence on the outcome.

A simulation is done with the full bow geometry and material properties as used in this simulation to compare the deck model as a valid verification model for the full model. This is simulation C4, which is done for the sensitivity study on material properties.

Results

Figure 6.27 shows the deck failure mode at the moment the deck behind the first frame buckles. A comparable failure mode can be seen, with two half-sine waves in both directions. The time duration up to this failure mode is different in both simulation, that is mainly due to the difference in stiffness in the frontal part of the deck.

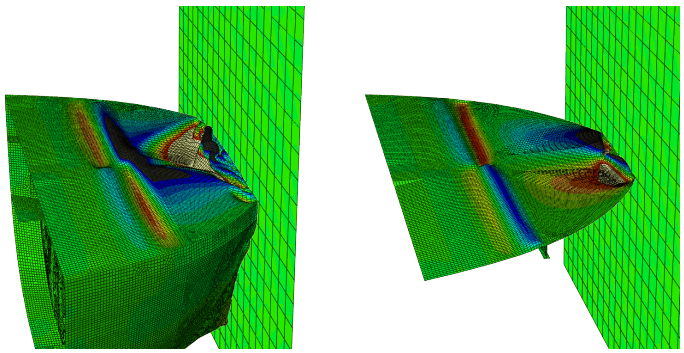

Figure 6.27: Simulation C4 (left) shows a comparable failure mode with the numerical simulation of the deck (right)

Forces are extracted from the history output files. At first, the deck model is regarded, simulation F1. Secondly, the results are compared to simulation C4 with the complete structure.

Figure 6.28 shows the reaction forces of the horizontal end support during the deck collision with a rigid wall. Oscillating behaviour is observed in the first part of the graph. This could be a result of the small history output data time step (0.0003 s), where the steel wave propagation speed becomes significant (5940 m/s), i.e. 1.8 meters per time step. Moreover, the contact algorithm could be another cause of the impulsing forces. Nonetheless, one could determine the failure load for the regarded part of the structure from this data. Up to

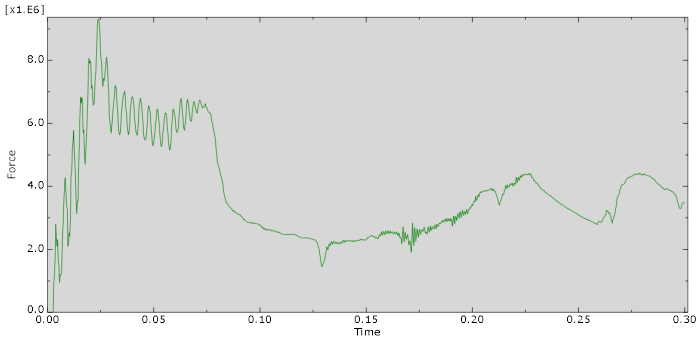

Figure 6.28: Reaction forces simulation F1, deck structure

0.024 seconds, the frontal part of the deck is being crushed and fails at about 9.2 MN due to buckling (figure 6.29b). Directly hereafter, the deck structure behind the first frame is stressed up to a point where it fails due to buckling. When this part is buckled at 0.072 seconds, the force drops as the total deck structure has lost its stability.

The force which is to be verified by analytical solutions is the reaction force at t = 0.072 seconds, where the deck fails due to plate buckling. It is clear from the simulation that the frontal part 'pushes' onto the part behind which causes a (non-uniform) stress on that part. The reaction force at that moment is 6.8 MN. The buckled part is tapered with an average width of 6891 mm and a thickness of 12 mm. The average stress during buckling is:

$$\sigma_x = \frac{F}{A} = \frac{6.8 \times 10^6}{(6891 \cdot 12)} = 82.2 \text{ MPa} \tag{6.1}$$

This is the average stress, as the force occurred due to the collision of the frontal bow, the force is acting at the central part of the deck. Therefore, at the moment before buckling, the forces are at its highest at the central part of the deck. The consequence of this is that the central part of the deck could fail before the more outward part, because of stress concentrations. This means that the onset of buckling at the central part happens at a lower total reaction force, whereas the load increases up to the moment the whole part buckles (at t = 0.072 seconds). At a uniform load, the onset of buckling results directly in buckling of the complete considered plate in transversal direction with a high maximum peak load. Since this happens in this case due to the non-uniform load in a more gradual process, the peak load is flattened, and the (buckling) load is lowered. Therefore, the 82.2 MPa will be higher in a case where the load is uniform over the width of the plate.

For comparison, the reaction forces of the separate deck simulation are presented together with the reaction forces on the deck support of simulation C4, where the full bow structure is simulated with the elastic-perfectly plastic material. This is shown in figure 6.30. Important to note is that the forces in the deck structure in simulation C4 are spread over the whole structure and are not 1:1 supported by the deck structure. The peak of the crushing of the frontal part of the bow is therefore not clear to see in the curve of simulation C4, because these forces are spread over different supports. Moreover, as the stiffness of the frontal bow in both simulations, the moment of buckling of the regarded deck structure is different in both simulations (as can bee seen in figure 6.27). Besides these differences, a valuable statement can be made about the magnitude of the reaction forces at the moment before buckling occurs at the regarded deck plate. This moment lies for simulation F1 at t = 0.072s with a force of 6.8 MN. For the deck support of simulation C4 this is at time and force of t = 0.17s and 5.5 MN, respectively. In other words, the buckling load of the deck structure is in the separate simulation 6.8 MN, and for the complete structure 5.5 MN. The difference in maximum load is explained by the stress distribution over the elements connected to the deck in simulation C4, especially with the longitudinal girder in the middle of the deck, which is supported in x-direction but not included in the reaction forces of the deck.

The reaction force of 6.8 MN is noted as the buckling load of the deck plate, which is equal to a critical buckling stress of 82.2 MPa. For further verification, this force is compared with results from an analytical solution in the following section.

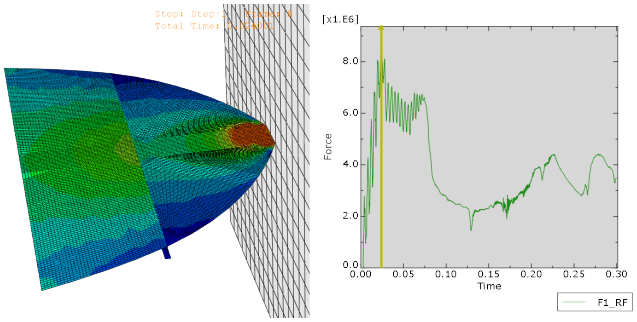

(a) Simulation F1 with reaction forces over time at t = 0.024s

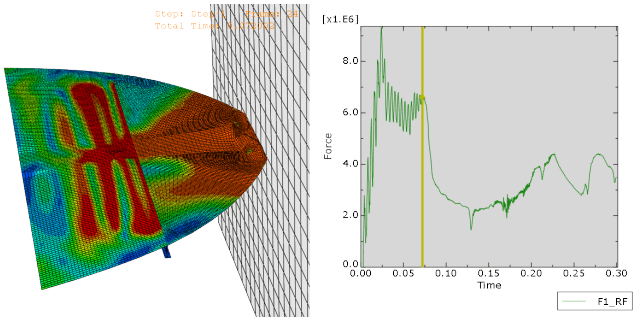

(b) Simulation F1 with reaction forces over time at t = 0.072s

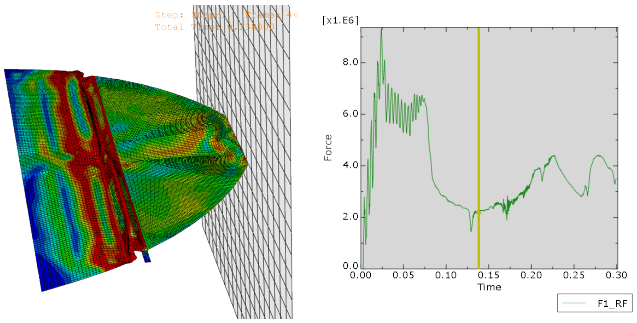

(c) Simulation F1 with reaction forces over time at t = 0.14s

6.3.3. Analytical solution

With analytical solutions, the buckling load could be estimated with some simplifications. The results of this calculation are used to verify simulation F1, conducted in section 6.3.2. And wen simulation F1 is considered verified, the full model explained in chapter 4 is considered verified as well. In this section, Timoshenko Theory of Elasticity [72] is utilised for determination of the critical buckling load, since this is a widely used and well-known theory for plates and acts as the basis for plate verification in the Eurocode. To simplify the problem, the following assumptions are made:

- Thin flat plate without stiffeners,
- Uniaxial stress along two plate edges,
- Plates are rectangular, see figure 6.32,
- Elements have a uniform cross-section,
- No residual stresses,
- No imperfections in material of structure,
- Isotropic material.

Failure of plates can occur by buckling, folding or yielding of the plate. The failure mode of the plate is among others dependent on the boundary conditions of the plate, especially those of the supports. Most of the plates in the bow of a ship are at two-, three-, or four edges simply supported. For almost all plates in the ship structure, the side frames form two boundaries for the plates in between.

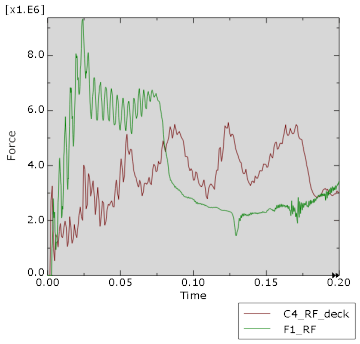

Figure 6.30: Reaction forces [N] of simulations F1 vs the deck support of C4

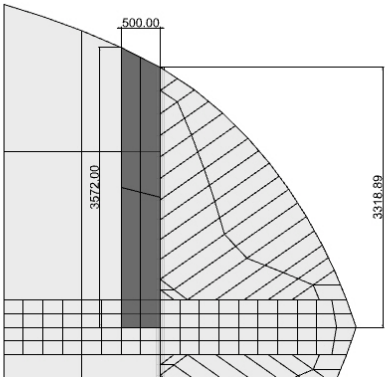

Figure 6.31: Deck plate dimensions

The general work equation for plates is the basis for the failure calculation:

$$U = \int_A \frac{1}{2}\left\{\frac{EI}{1-\nu^2}(w_{xx}^2 + w_{xx}w_{yy} + w_{yy}^2 + \sigma_x t w_x^2\right\} dA \tag{6.2}$$

Where:

U = Work
E = Youngs' Modulus
I = Moment of inertia (Plates: $I = \frac{1}{12}h^3$)
ν = Poisson ratio
w_x = First derivative to x of displacement w
w_{xx} = Second derivative to x of displacement w
w_{yy} = Second derivative to y of displacement w
σ_x = Compressive stress in x-direction
t = Thickness of the plate
A = Area of the plate

With $D = \frac{EI}{1-\nu^2}$ and $h = t$, from eq. 6.2 follows the differential equation:

$$D\left[w_{xxxx} + 2w_{xxyy} + w_{yyyy}\right] = t\sigma_x w_{xx} \tag{6.3}$$

Where w_{xxxx} is the fourth derivative with respect to x of displacement w.

Equation 6.3 is used to calculate the buckling load of the deck plate in case of a uniform and non-uniform compressive load since it is assumed that the real value will lie in between these loads.

Uniform compressive load

From buckling theory it is known that the deflection surface of the buckled plate can be represented by the double sine equation, in the case of simply supported edges:

$$w = a_{mn} \sin\left(\frac{n\pi x}{a}\right) \sin\left(\frac{m\pi x}{b}\right) \tag{6.4}$$

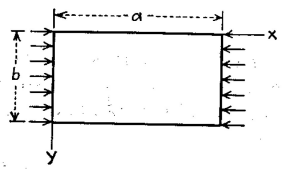

Figure 6.32: Plate uniformly compressed in one direction [72]

Theoretically, the displacement in x-, and y-direction can develop in n, and m half waves into which the plate buckles. Moreover, if a is smaller than b, the minimum critical load is obtained by taking $m = 1$ and $m = 1$ [72], i.e, by assuming that the plate buckles in one half-wave and that the deflection surface is in the form of:

$$w = a_{11} \sin\left(\frac{\pi x}{a}\right) \sin\left(\frac{\pi x}{b}\right) \tag{6.5}$$

Substitution of eq. 6.3 and 6.5 gives:

$$N_{x,cr} = \frac{\pi^2 D}{b^2}\left(\frac{b}{a} + \frac{a}{b}\right)^2 \tag{6.6}$$

If the width of the plate is taken constant, and we gradually change the length a, the factor before the parentheses changes with the change of the ratio a/b. It can be seen that this factor is at its minimum when $a = b$. Which means that for a plate with a given width, the critical value of the load is the smallest if the plate is square. In this case:

$$N_{x,cr} = \frac{4\pi^2 D}{b^2} \tag{6.7}$$

For other proportions of the plate, the expression 6.6 can be represented in the form:

$$N_{x,cr} = k\frac{\pi^2 D}{b^2} \tag{6.8}$$

In which k is a numerical factor, the magnitude of which depends on the ratio a/b.

The regarded deck plate has the following dimensions:

a = 500 mm
b = $\frac{(3572+3319)}{2}$ = 3446 mm
t = 12 mm
$a/b = \frac{500}{3446} = 0.145$

Magnitude k becomes:

$$k = \left(\frac{b}{a} + \frac{a}{b}\right)^2 = 49.52 \tag{6.9}$$

This is a relatively high number, which could be expected from wide a plate. Parameter D is determined from the material parameters and thickness:

$$D = \frac{Eh^3}{12(1-\nu^2)} = \frac{194000 \cdot 12^3}{12(1-0.3^2)} = 30.7 \times 10^6 \text{Nmm} \tag{6.10}$$

With equations 6.8, 6.9 and 6.10, the critical buckling load per millimetre width is calculated:

$$N_{x,cr} = 49.52 \cdot \frac{\pi^2 \cdot 30.7 \times 10^6}{3446^2} = 1263.5N \tag{6.11}$$

Which is equal to a critical buckling stress of:

$$\sigma_{x,cr} = \frac{N_{x,cr}}{t} = \frac{1263}{12} = 105.3\text{MPa} \tag{6.12}$$

According to the Timoshenko plate theory, the plate will buckle at uniform stress of 105.3 MPa.

Non-uniform compressive load

By using a more advanced derivation from Timoshenko [72], plates with a non-uniform compressive stress can be calculated. A simply supported rectangular plate is considered, with along its side edges at $x = 0$ and $x = 1$ distributed forces acting in the middle plane of the plate. The magnitude of the distributed forces is in the form of following equation:

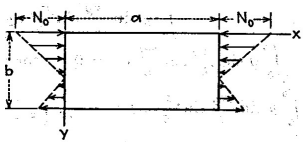

Figure 6.33: Plate non-uniformly compressed in one direction [72]

$$N_x = N_0\left(1 - \alpha\frac{y}{b}\right) \tag{6.13}$$

Where N_0 is the intensity of compressive forces at the edge $y = 0$ and α is a numerical factor defining the stress distribution. For example, by taking $\alpha = 0$, the case of a uniformly distributed compressive force is obtained. A case of $\alpha = 2$ defines by pure bending. The deflection of the buckled plate is again taken is the double trigonometric series:

$$w = \sum_{m=1}^{w} a_{mn}\, sin\frac{m\pi x}{a} sin\frac{n\pi x}{b} \tag{6.14}$$

Using the energy method, the critical value of the compressive force N_0 can be obtained. Again, it is assumed that $m = 1$ and $n = 1$ will give the lowest critical value. For cases where $\alpha < 2$, the following equation is used for calculating σ_{cr} [72]:

$$\frac{{\sigma_{cr}}^2 a^4 h^2}{\pi^4 D^2}\left(\left(1-\frac{\alpha}{2}\right)^2 - \frac{256\,\alpha^2}{81\,\pi^4}\right) - \frac{\sigma_{cr}\, a^2 h}{\pi^2 D}\left(1-\frac{\alpha}{2}\right)\left(\left(1+\frac{a^2}{b^2}\right)^2 + \left(1+4\frac{a^2}{b^2}\right)^2\right) + \left(1+\frac{a^2}{b^2}\right)^2\left(1+4\frac{a^2}{b^2}\right)^2 = 0 \tag{6.15}$$

This is simplified to a similar equation as eq. 6.8 from the calculation for a uniform load:

$$\sigma_{x,cr} = k\frac{\pi^2 D}{b^2 h} \tag{6.16}$$

Where k is defined not only by geometric conditions a and b, but also load condition α. Magnitude k is evaluated from eq. 6.15 and eq. 6.16 and plotted with different values of α in figure 6.34. The curve where $\alpha = 0$ can also be established with the theory for uniform compressive load, and therefore, with eq. 6.9.

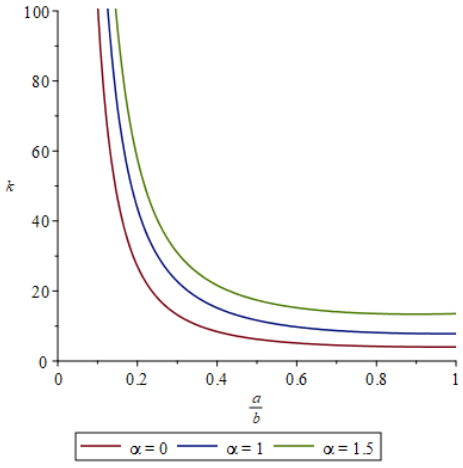

Figure 6.34: Magnitude k for different load conditions α

To find a value for α, the load conditions on the regarded deck plate of fig. 6.31 are schematised. Assumed is a linearly decreasing compressive stress with a maximum in the centre of the bow ($y = 0$) to zero at the outer edge ($y = b$). This stress distribution coincides with the observed stress distribution of the deck in the numerical simulation. This, load condition is defined by a factor $\alpha = 1$. Geometric conditions are unchanged ($a = 500$, $b = 3440$) and defined by a ratio of $\frac{a}{b} = 0.145$. With these parameters, k magnitude in eq. 6.16

becomes: $k = 77.0$. And the critical stress: $\sigma_{x,cr} = 163.6$ MPa. As the critical stress intensity is defined by the same equation as for the load distribution from eq 6.13, the distribution of the critical stress is:

$$\sigma_{x,cr}(y) = 163.6(1 - \frac{y}{3440}) \tag{6.17}$$

Which results in an average critical stress over the width of the plate:

$$\sigma_{x,cr,avg} = \frac{163.6}{2} = 81.8 \text{ MPa}. \tag{6.18}$$

This means that buckling of the plate is initiated at an average stress of magnitude 81.8 MPa if the load is non-uniformly applied. If the applied load is uniformly distributed, the plate buckling is initiated at a stress of 105.3 MPa. The difference is caused by stress concentrations which occur at applying a non-uniform load.

6.3.4. Eigenvalue analysis

An extra verification step has been performed with a buckling analysis, conducted with ABAQUS/Standard. In this software package, the exact plate dimensions are computed with material and mesh properties as in the deck simulation F1. This is the simulation where only the deck is analysed with elastic-perfectly plastic material properties. With the eigenvalue analysis as an extra verification step, the schematising and assumptions of the analytical verification with Timoshenko Plate theory are verified.

Uniform load

The highlighted plate of figure 6.31 is set up in ABAQUS/Standard, simply supported at all four edges. At the longer edge in the width direction, the plate is supported in the normal and transverse direction. And at the shorter edge, a uniform unit load is provided in the normal direction of the plate. The results are in the form of eigenmodes with their corresponding eigenvalues. As identified in the analytical verification, the lowest critical buckling load occurs with one half-wave in both directions. This eigenmode is shown in figure 6.35, which represents the buckling mode calculated in section 6.3.3.

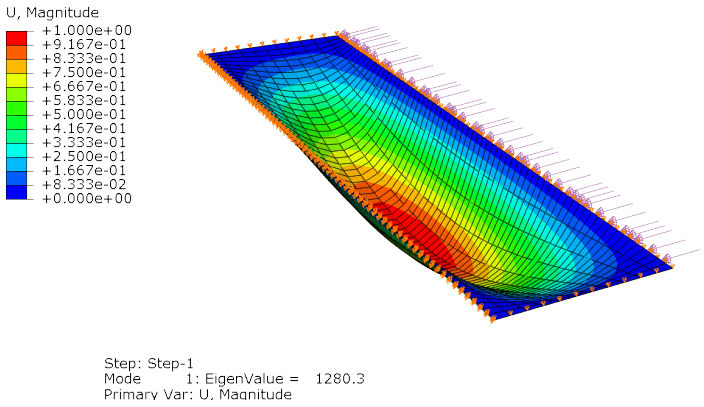

Figure 6.35: Eigenmode 1 from ABAQUS/Standard buckling analysis with uniform load

An eigenvalue of $\lambda = 1280.3$ is found for the first eigenmode. The critical buckling stress obtained in the eigenvalue analysis is therefore:

$$\sigma_{x,cr,ba} = \frac{\text{unit load} \cdot \lambda}{t} = \frac{1 \cdot 1280.3}{12} = 106.7\text{MPa} \tag{6.19}$$

Non-uniform load

The same analysis is performed for a non-uniform compressive load. The model is exactly the same, except for the load distribution. A unit load is added with the distribution defined as equation 6.13, which is from the centre of the bow linearly decreasing to zero. The result of eigenmode 1 is presented in figure 6.36. This eigenmode corresponds to the buckling initiation found in the analysis of the deck. When compressed further, the undeformed part of the deck will buckle also. Moreover, during the initiation of buckling, stress is

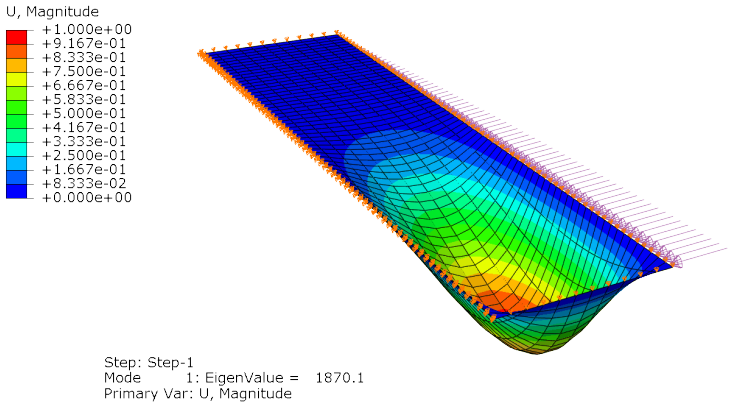

Figure 6.36: Eigenmode 1 from ABAQUS/Standard buckling analysis with non-uniform load

distributed to the undeformed parts of the plate until the complete plate is buckled. This process has also been found in the deck analysis.

The eigenvalue corresponding to the first eigenmode with a non-uniform load distribution is $\lambda = 1870.4$, hence:

$$\sigma_{x,cr,ba,avg} = \frac{0.5 \cdot 1870.4}{12} = 77.9\text{MPa} \tag{6.20}$$

6.3.5. Conclusion of analytical verification of subsystem

With the complete reference model, a simulation is performed with an elastic-perfectly plastic material model. It is found that a plate from the deck structure is the best structural element for a useful analytical verification. A separate model is created with only the deck structure, and boundary conditions are defined in such a way that the failure process is comparable to the full model. The failure process of the deck plate is qualitatively equal for both simulations; therefore, forces could be compared. Reaction forces are extracted, and the buckling load in the numerical simulation is determined. The buckling load of the regarded plate is noted as $\sigma_{x,cr,n} = 82.2$ MPa.

Using the Timoshenko Theory of Elasticity[72], hand calculations are conducted on the regarded deck plate. The plate is simplified to a rectangular plate simply supported at four edges, uniformly loaded. From the hand calculations, the critical buckling stress is estimated at $\sigma_{x,cr,hc} = 105.3$ MPa. Verification on the schematising and assumptions of the hand calculations is done using an eigenvalue analysis on the regarded plate. Eigenmode 1 with a buckling mode similar to the assumed buckling mode in the hand calculations corresponds to a critical buckling stress of $\sigma_{x,cr,ba} = 106.7$ MPa. This is considered highly comparable to the result from the hand calculations and assumptions are therefore verified. The minor difference can originate from the rectangular plate assumption in the hand calculations, whereas the considered deck plate in the eigenvalue analysis is in the shape of a trapezoidal, which corresponds to the shape of the plate in the complete model.

The obtained difference between critical buckling stresses of the numerical model and the hand calculations is about 20%. This difference is mainly due to the assumption used in the hand calculation that the stresses are uniformly distributed along the width of the plate. The part of the plate at the centre of the bow structure is stressed at first and reaches the critical buckling stress, therefore, earlier than the more outward part of the plate. The buckling onset is thus started prematurely, with a lower average buckling load on the total width, which lowers the buckling load of the complete plate. With this remark, the hand calculations result in a comparable outcome with simulation F1, on the deck separately, both qualitatively and quantitatively. Therefore, it is concluded that the hand calculations do match the output of the complete model.

6.4. Conclusion

The sensitivity analysis showed the influence of different parameters on the force-displacement results of the simulated ship collision. It is found that the simulation model behaves in response to changes as is expected. No singularities are found, and the model is considered as stable. Furthermore, some insights into the simulation process and the crushing process are obtained. This could be useful for the overall judgement of the

results.

The force-displacement results from the NLFEA simulation show good agreement with crushing strengths calculated with simplified calculation methods based on the cross-sections of the ship's bow structure. This provides confidence in the magnitude and development of the force results.

A subsystem of the complete model is verified by comparing results about the force with widely accepted theories. A deck plate is calculating using an elasticity theory and eigenvalue analysis, which showed force results highly comparable to the results from the NLFEA.

With this, it is demonstrated that the configured nonlinear finite element model according to the set-up which is described in chapter 4 shows no singularities, good agreement with existing simplified calculation methods and results which are substantiated by well-known theories. Concluded is that the NLFEA could be applied with sufficient confidence in the results.

7

Results

In this chapter, the results of the nonlinear finite element analysis calculations are presented. The calculations are done for one class IV ship, referred to as class IV ship since the specific name is not known by the author. Additionally, two class V ships are analysed, both different in size.

First, an analysis of the general properties of the ship and its bow structure is presented to gain some general insights and thereafter, results of the NLFEA are shown. Energy levels are analysed, and most importantly, the force-displacement curve is investigated. For each ship analysis, a comparison with hand calculations is performed, which is described at the end of each of the ship sections.

Visualisations of the final deformation and stresses of the analyses are shown in appendix I.

7.1. Class IV Ship

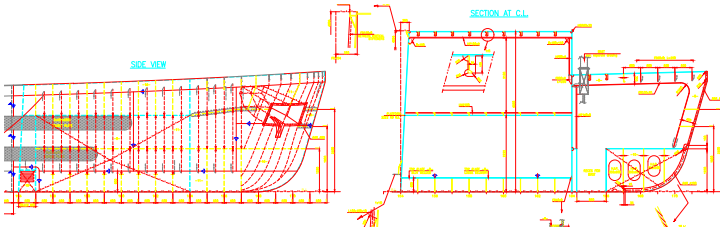

Figure 7.1: Side view of Class IV ship's bow from Concordia-Damen

The Class IV ship investigated in this study is a ship from shipbuilder Concordia-Damen and is constructed in China. It can ship a deadweight tonnage of 1600 t and is 85.0 m long, with an approximate mass of 2136 t. The investigated class IV ship can be characterised as an average ship compared to other Dutch inland waterway ship. From comparison with ships found in the binnenvaart.nl data, which is shown in figure 7.2. A velocity of 5.3 m/s is considered in calculations since this is the recommended collision speed according to the ROK [59]. The ship is constructed with a conventional bow, which is modelled symmetrically through the longitudinal plane.

CEMT IV	
Mass	2136 t
Velocity	5.3 m/s
Length	85.0 m
Width	9.6 m
Draft	3.0 m
E_{kin}	30.2 MNm

Table 7.1: General characteristics of considered Class IV ship

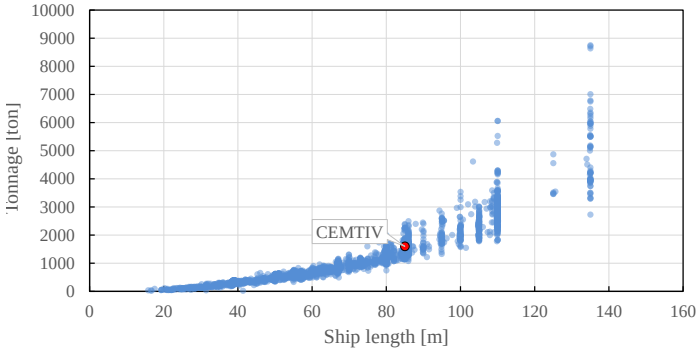

Figure 7.2: Length-tonnage ratio comparison of class IV ship.[78]

7.1.1. Ship's Bow Structure

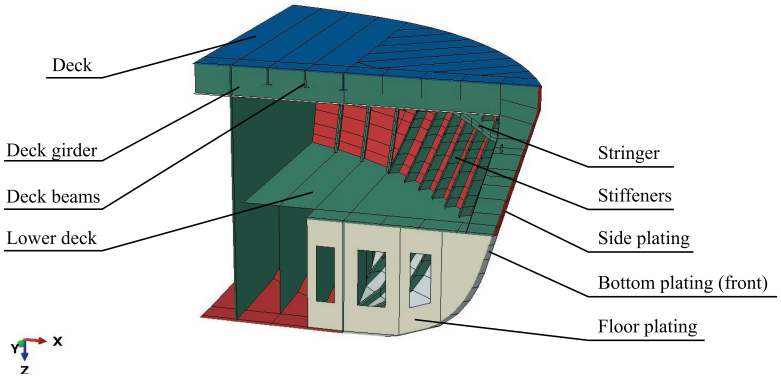

Figure 7.3: View-cut of Class IV ship's bow in ABAQUS/CAE. Element thicknesses are coloured: red = 11 mm, green = 8 mm, blue = 12 mm, grey = 16 mm, antiquewhite = 10 mm.

The geometry is modelled up to the bulkhead (depth of 4500 mm). A panting stringer is placed which provides stiffness to the hull, at the height of 2400 mm. Transverse side frames are equally distributed at a distance of 500 mm. Around middle height, a lower deck is constructed. The main deck is centrally supported by a deck girder and transverse beams. What stands out in this structure are diagonal stiffeners at the frontal part of the bow. Since these stiffeners are 'rotated' in the direction of the moving direction, they offer high stiffness in this direction, which is very relevant for a frontal collision. However, a structural discontinuity is observed at the end of the floor plating (antiquewhite in figure 7.3). This plate is not supported directly in longitudinal direction. This could decrease the global stiffness in the this direction significantly.

At the lower frontal bow structure, the outer plates are thicker than the side plates, shows with grey colour in figure 7.3. This can be a design consideration for accidental states as grounding. The side plates are 11 mm thick, and most of the internal stiffeners are 8 mm thick. An average thickness of the modelled structure is calculated on t_{avg} = 11.2 mm. Figures of the structure and their corresponding thicknesses are provided in appendix C.

7.1.2. NLFEA Calculation results

The constructed CAD model is meshed with a global mesh size of 25 mm, resulting in about 290,000 elements. The generated mesh is verified using the verify tool from ABAQUS, which resulted in no errors, and only 0.6% of the elements showed warnings. The mesh model is shown in figure 7.4. The simulation is run up to t = 1.0 s. Mass scaling is utilised to increase the stable time increment up to around 1E-6. The total augmented nodal masses as a percentage of total model mass is 9.93E-02 per cent. A total of 1050×10^3 time increments is calculated, which took about 28 hours on 24 cores.

Elements	Thickness [mm]
Bottom plating (front)	16
Deck	12
Deck beams	8
Deck girder	8
Floor plating	10
Lower deck	8
Side plating	11
Stiffeners	8

Table 7.2: Element thicknesses of class IV ship structure

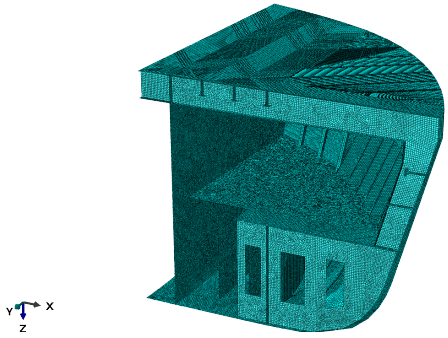

Figure 7.4: View-cut of Class IV ship's bow model with a mesh of 25 mm.

Energy balance

The development of the energy levels over time are through in figure 7.5, which shows decreasing kinetic energy until it is almost fully dissipated at $t = 1.4$ s (1.1% kinetic energy left). This is considered the end of the collision process. The internal energy is the sum of the recoverable (elastic) strain energy, the energy dissipated through inelastic processes such as plasticity (plastic dissipation), the energy dissipated through viscoelasticity or creep (viscous dissipation) and the artificial strain energy.

The dissipation distribution is shown in table 7.3. Plastic dissipation is the main contributor to the dissipation of kinetic energy, which can be confirmed by the visualisation of the strains and stresses. The total energy is constant during the simulation, as is expected from a closed system. And the artificial strain energy is well below the 10% limit as discussed in chapter 4, which is a very good score for this type of structural mesh. The frictional energy is 6.7% with this head-on collision, which is probably mainly caused by upward forces of the front part of the bow, explained in section 7.1.2.

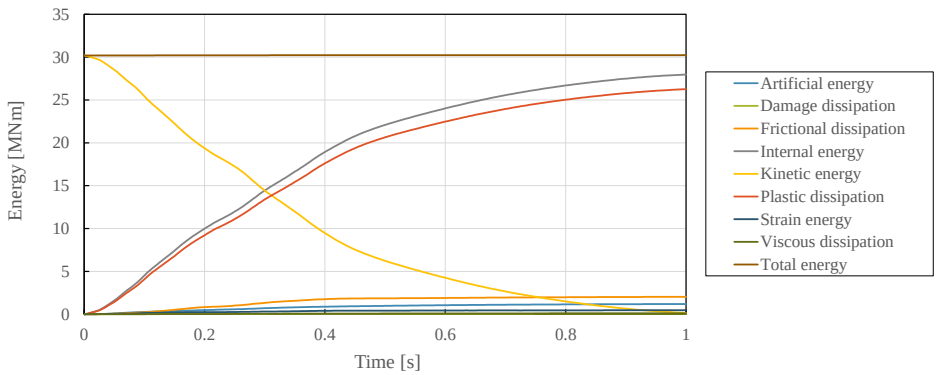

Figure 7.5: Energy levels during class IV ship collision simulation.

Artificial energy	3.9%
Damage dissipation	0.2%
Frictional dissipation	6.7%
Plastic dissipation	87.0%
Strain energy	1.5%
Viscous dissipation	0.4%

Table 7.3: Energy dissipation distribution of Class IV collision simulation at $t = 1.0$ s.

Force results

The x-directional forces from the support of the rigid wall depicted in figure 7.6a. Since this is the force which is acting on the rigid wall, this is the collision impact force we are looking for.

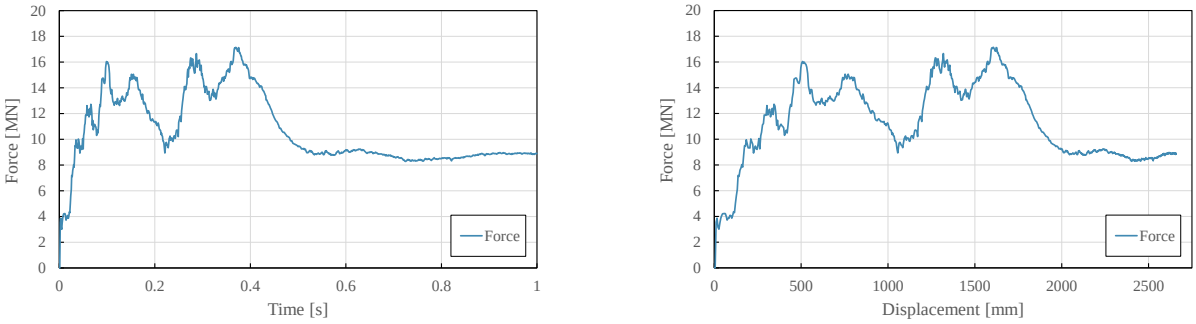

(a) Force-time history of class IV ship collision simulation.

(b) Force-displacement of class IV ship collision simulation.

Figure 7.6: Collision force data for class IV ship from the NLFEA.

It can be seen that the impact force-time history could be divided into three periods: the initial stage during which the impact force increases rapidly, the second stage during which the impact force fluctuates and the third stage during which the force is constant. Still, little kinetic energy is left at the end of the simulation (0.5%). Therefore, force is still acting on the bridge pier. Once the kinetic energy is fully dissipated, the force depicted in figure 7.6b will drop to zero. Since not all kinetic energy is dissipated into plastic deformation but also in elastic deformation, this elastic energy will be released once the kinetic energy is zero and the structure will push itself backwards. The amount of elastic energy is, however, insignificant. This phenomenon is found in a previous simulation, explained in appendix G where an elaborate interpretation is performed on the first full simulation for this ship model, but with the preliminary input parameters.

The force-time history curve is combined with displacement data to create the force-displacement curve presented in figure 7.6b. The displacement is obtained from a reference point on the rigid surface at the end of the ship's bow geometry. This displacement is considered as equal to the penetration depth of the bridge pier into the ship's bow. From this curve, information is obtained about forces from different cross-sections as the force is directly correlated to a location in the structure.

The curve has many local ups and downs, which may be caused not only by the complexity of the deformation process but also by numerical effects such as removal of the finite elements in which the ultimate plastic strain (failure strain) is exceeded in the integration points, and the contact algorithm, which exploits only a set of discrete points of the ship on which contact forces are applied. This is explained in section 4.6.1.

Almost exactly at a displacement, or penetration depth, of 500 mm, a local peak force is observed. This is mainly caused by achieving the buckling load of the deck structure, after which the force decreases as the deck is folding. The maximum peak force is at about 1600 mm penetration depth. At this point, many stiffeners are utilised to provide stiffness together with the side plating. The stringer distributes the force over the depth of the structure where the transverse side frames distribute this force again from the stringer to the higher and lower areas of the side plates. The frontal stiffeners bend and provide stiffness directly onto the side plates which are in contact with the bridge pier. The force decreases eventually at the moment the stringer is buckled. At the end phase, where the force stabilises, the middle segment of the bow is crushed.

Therefore, the frontal part of the bow crushes into the end part of the bow. The middle segment serves here as the weakest link in the structure at that moment.

By observing the deformed structure at the end of the simulation, an approximation can be made about the consequences of the not yet completely dissipated kinetic energy. The ship is still moving into the bridge pier, however, with very low velocity ($v = 0.36$ m/s). Moreover, the structure still contains some deformation capacity, where folded elements are still able to continue their folding process. Therefore, it is expected that given the deformed structure, and given the low remaining velocity, the force will not reach a higher force than the force at the end of the simulation and will decrease quickly hereafter. This is also found in the hand calculation results shown in chapter 5, where the curve continues further than the NLFEA curve.

Given the force-displacement data, the maximum impact force during the collision and the maximum penetration depth are extracted. The maximum force acting on the bridge pier during the collision process is equal to a value of 17.14 MN. And the ship's bow is as a consequence of all involved forces crushed up to 2.66 meters.

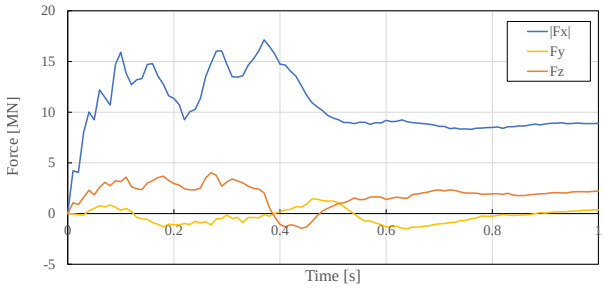

Figure 7.7: Force-time history for three support directions of the rigid wall. (Absolute values of force in x direction are shown for clarity)

Figure 7.7 shows the reaction forces in all three directions of the bridge pier support. Logically, the forces in the x-direction are the largest since the velocity vector of the involved kinetic energy is in this direction as well. Remarkable is a relatively high force in the z-direction, which shows a force of about 3-4 MN downwards up to 0.4 seconds in the collision. This is explained by the global geometry of the ship's bow, where the highest point of the bow, at the front of the deck, will have the first contact with the bridge pier. In this way, the moving mass of the lower structure 'pushes' the structure towards the pier, which eventually leads to the upper point at the front of the deck. Since the structure here is under an angle with the collision direction, the acting force is also under an angle. According to this angle, force is generated at the zone of contact, and this force is resolved into perpendicular forces compensated by the support.

The reaction forces of the bridge pier in the y- and z-direction are taken up by the supports on the ship's bow, and will not result in large movements in these directions since the ship's bow is supported in both y- and z-direction (showed in section 4.5). Only bending of the bow could result in sliding in y- and z-direction, but this is restricted by the boundary conditions. Hence, the forces in y- and z-direction will not contribute to the overall dissipation of the initial kinetic energy. The total area under the force-displacement curve depicted in figure 7.6b is equal to the amount of dissipated energy (since: $W = Fu$) This is at the end of the collision equal to the amount of initial kinetic energy, disregarding leftover elastic distortion which releases into kinetic energy.

7.1.3. Comparison with hand calculations

The force-displacement curve from the NLFEA calculation has been compared with the hand calculations explained in chapter 5. Note that this comparison is about the comparison of forces, partly disregarding the displacement location of this force as both calculation methods have a different definition of the displacement. For the NLFEA, a realistic collision process is simulated. This is not the case for the hand calculations. The force-displacement curves are generated by calculating a particular cross-section at the point of 'displacement', which disregards previous crushed steel material.

The results of an NLFEA calculation on this ship type has been compared before with hand calculations, presented in chapter 5. To provide a fair comparison, the material model of the simulation is chosen such that

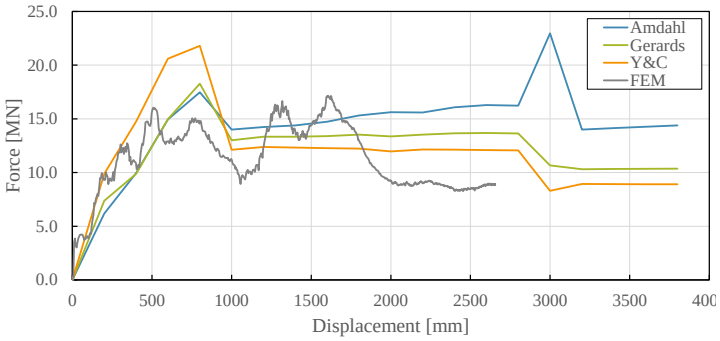

Figure 7.8: Force-displacement graph for class IV ship from NLFEA and hand calculations

it is comparable with the assumptions made for the hand calculations (no strain rate hardening for example). This showed good agreement. This is also found for the final simulation presented in this section. The average curve of the hand calculations confirm that the maximum found impact force is within the simulated part of the ship's bow, and that the impact force will not increase when the crushing length is extended for about one meter.

7.2. Class V Ship - Sietske

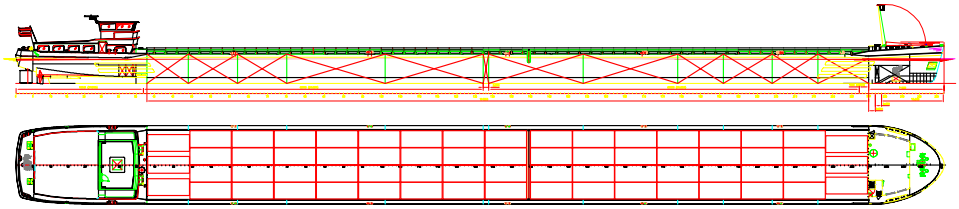

Figure 7.9: Side and top view of Sietske (Class V) from Concordia-Damen

The Sietske is a Class V ship designed by Concordia-Damen. It can ship a deadweight tonnage of 5130 t, and 135 m long. A velocity of 5.5 m/s is considered as this is the recommended moving speed according to the ROK. The ship is constructed with a conventional bow, which is modelled symmetrically through the longitudinal plane.

CEMT V	
Mass	5130 t
Velocity	5.5 m/s
Length	135.0 m
Width	11.45 m
Draft	3.6 m
E_{kin}	77.6 MNm

Table 7.4: General characteristics of Class V ship Sietkse

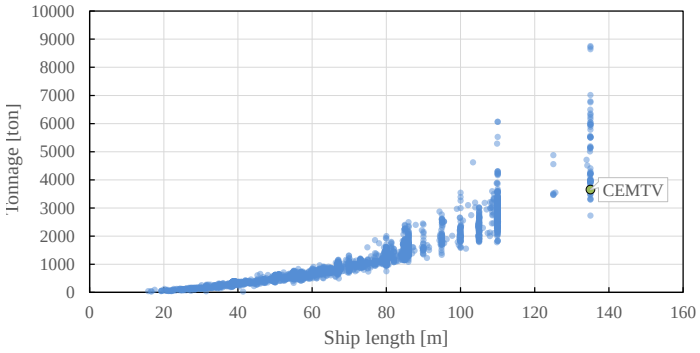

Figure 7.10: Length-tonnage ratio of class V ship.[78]

7.2.1. Ship's Bow Structure

The geometry is modelled up to 6500 mm depth, partly including the lower part of the deckhouse. The total height is around 4400 mm. Two panting stringers are constructed at the height of 2650 mm and 1600 mm. All side frames are constructed transversely, equally distributed with a distance of 500 mm in between. In

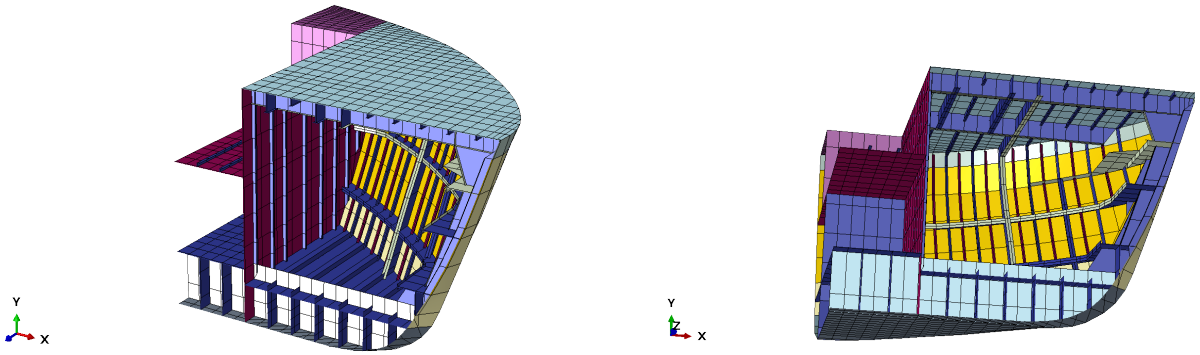

(a) Upper cut-view

(b) Lower cut-view

Figure 7.11: Class V ship Sietske structure. Element thicknesses are coloured: red = 7 mm, blue = 8 mm, lightgreen = 10 mm, yellow = 11 mm, white/lightblue = 12 mm darkgrey = 13 mm, pink = 15 mm, blue-green = 25 mm.

the centre between these side frames, intermediate stiffeners are placed with lower thickness of 7 mm. At the frontal part of the bow, a row of four longitudinal stiffeners are constructed at both sides of the centre, their webs are in parallel to the collision direction. The deck is supported by a central longitudinal girder and two longitudinal side girders, with transverse beams for local load-bearing capacity. A structural discontinuity is observed at the bulkhead, at the beginning of the deckhouse. The longitudinal deck girders are weakly supported in collision direction here. The deck structure distributes the longitudinal forces in the transverse deck beams. Side plates are 11 mm thick, and the bottom plating is constructed with an increased thickness of 13 mm. An average thickness of the complete modelled structure is calculated on t_{avg} = 11.15 mm. Table 7.5 shows the different thicknesses per structural element.

Elements	**Thickness [mm]**
Bottom plating (front)	13
Upper plating (front)	25
Deck	12
Deck beams	8
Deck girder	8
Floor plating	12
Side plating	11
Side frame Stiffeners	8
Intermediate Stiffeners	7

Table 7.5: Element thicknesses of class V ship structure

7.2.2. NLFEA Calculation results

The constructed model is meshed with a global mesh size of 50 mm, resulting in about 542,000 elements. The mesh is verified using the verify tool from ABAQUS, which resulted in no errors, and only 0.5% of the elements showed warnings. The mesh model is shown in figure 7.12. The simulation is run up to t = 1.4 s. Mass scaling is utilised to increase the stable time increment up to around 5E-6, which resulted in an artificial change in mass of 2.0E-02 per cent. A total amount of 335.6×10^3 time increments is calculated, which took about 2 hours on 20 cores.

Energy balance

The energy levels over time are depicted in figure 7.13. The kinetic energy is almost completely dissipated at at t = 1.4 s (1.1% kinetic energy left), which is considered the end of the collision process. The energy dissipation distribution is shown in table 7.6. Artificial strain energy is well below the 10% limit, as discussed in chapter 4. This is not as low as for the class IV ship simulation, which was expected since a larger mesh size is configured.

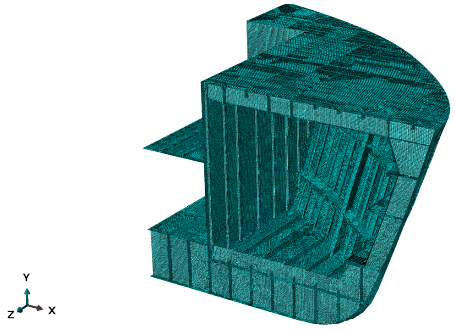

Figure 7.12: View-cut of Class V ship's bow model with a mesh of 50 mm.

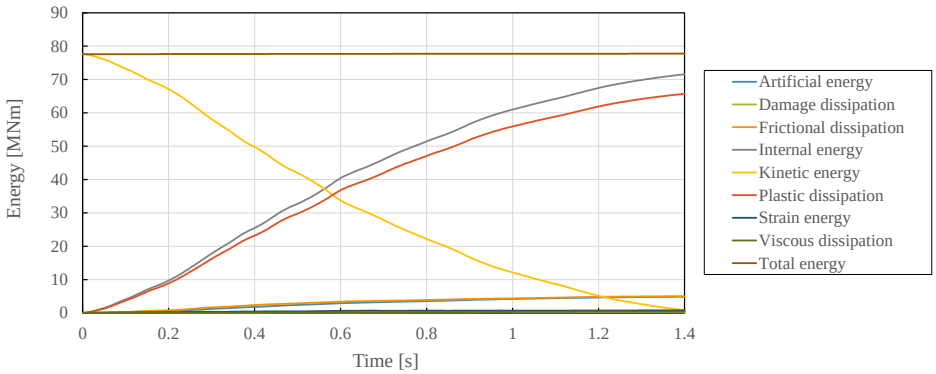

Figure 7.13: Energy levels during class V ship collision simulation.

Force results

The forces are extracted from the support of the rigid wall, in the x-direction, shown in figure 7.14a. This force is considered equal to the collision force on a bridge pier.

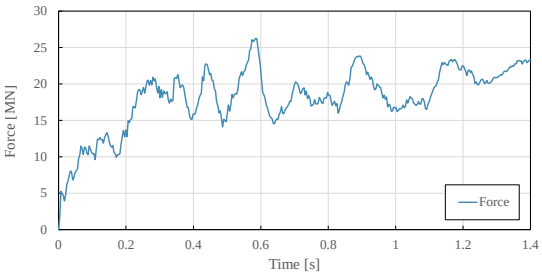

(a) Force-time history of class V ship collision simulation.

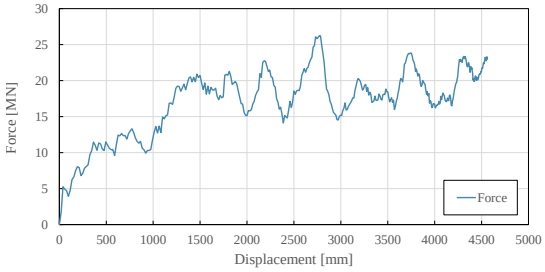

(b) Force-displacement of class V ship collision simulation.

Figure 7.14: Collision force data for Sietske from the NLFEA.

A rapid increase is shown at the beginning of the collision, up to 0.3 seconds, following with a fluctuating curve with a roughly constant average force. The curve continues up to 1.4 seconds, where it ends as the end of the simulation time range is reached. By observing the deformed structure, and given the low remaining velocity, it is expected that the force will not reach a higher force than the force at the end of the simulation and will decrease quickly hereafter.

The force-time history curve is combined with displacement data to create the force-displacement curve from figure 7.6b. Remarkable is that local peaks fluctuate a period of 500 mm, which corresponds to the frame spacing of the ship. The transverse side frames are spaced at a equal distance of 500 mm. The force peaks appear around the centre between the frames. Opposed as for force-displacement curve of the Class IV ship simulation, this trend is apparent. This can have different causes, but the clear repetition within the

Artificial energy	6.3%
Damage dissipation	0.3%
Frictional dissipation	6.4%
Plastic dissipation	84.7%
Strain energy	1.0%
Viscous dissipation	0.5%

Table 7.6: Energy dissipation distribution of Class V collision simulation at $t = 1.4$ s.

structure is probably an important factor. After a penetration depth of 1500 mm, the frontal bow is almost completely crushed. Therefore, the part behind 1500 mm from the first contact point is not significantly influenced by the frontal part of the bow. In this way, a more apparent response from that part is visible. This is in contrary to the collision process of the Class IV ship, where the frontal bow consists of multiple stiffeners in the diagonal direction. For the class IV ship's bow, the side frame construction starts only after 3000 mm. Before this point, diagonal stiffeners are applied.

The force curve increases rapidly at a depth of 2400 mm up to 2750 mm. During this increase, a large proportion of the side plates are activated by the two stringers together and a relatively large side frame stiffener which is pushed by the crushed steel at a depth of 3000 mm. Due to this increase in stiffness by activating extra elements, the amount of impact force the ship can produce on the bridge pier increases. The peak decreases once one of the stringers has been buckled.

During the last phase of the collision process, the ship's bow is deformed hugely and acts as a rigid block in between the bridge pier and the remaining part of the ship. Consequently, both sides next to the deckhouse are activated and the connection between the ship's bow and this part is crushed.

The maximum impact force which acts on the bridge pier is 27.2 MN. And the maximum (known) penetration depth is 4.56 m. It is expected that a maximum penetration of 4.60 m is reached eventually through a quick analysis on the kinetic energy dissipation behaviour.

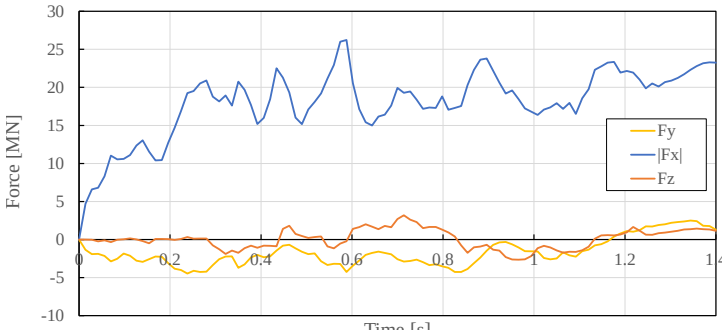

Figure 7.15: Force-time history for three support directions of the rigid wall.

Figure 7.15 shows the reaction forces in all three directions of the bridge pier support. The force in x-direction is definitely dominating. The force in the y-direction is in the direction of the height of the ship and is relatively high. Note that the applied coordinate system is rotated in this analysis in comparison to the class IV ship analysis. The high force in y-direction is caused by the same phenomenon as for the class IV ship, the asymmetry in the height of the ship's bow where the upper elements have contact with the bridge pier at first. The force in the z-direction, which is the direction over the width of the ship, is not that significant. The forces of the ship's bow support and the bridge pier support in y- and z-direction are in balance.

7.2.3. Comparison with hand calculation

The force-displacement curve from the NLFEA calculation is compared with the hand calculations as explained in chapter 5. A similar trend is found in both the results of both calculation methods. Only the Yang and Campbell calculation method shows a big difference in crushing force up to 2000 mm penetration depth. This is caused by a high sensitivity on cruciform intersection elements of this calculation method and is assumed as overly sensitive, given the results of the other hand calculation methods and NLFEA result. The

collision progress starting from 2000 mm shows a good agreement between all the calculation results. And the results of the hand calculations from after 4500 mm confirm the expectation that the found maximum impact force from the NLFEA will not increase substantially if the crushing distance is increased.

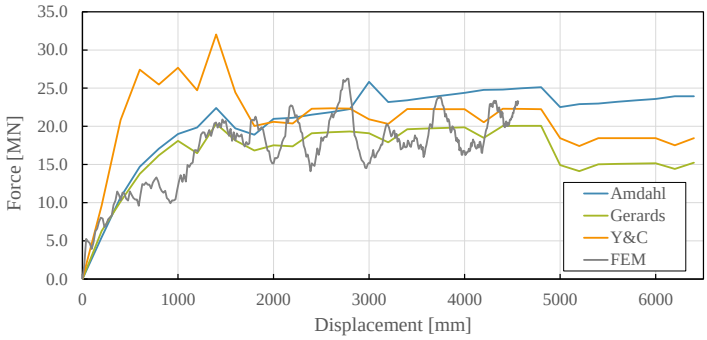

Figure 7.16: Force-displacement graph for Sietske from NLFEA and hand calculations.

7.3. Class V Ship - Berdina

The Berdina (CEMT V) is studied by Joustra and Pater on ship collision forces in 1993 [35]. During this study, an approximate collision force is established using hand calculations. No finite element analysis is done, however. Ji Fan Chan from the Structural Engineering dept. of the TU Delft followed an internship at Nobleo Bouw & Infra and performed an FEA on the Berdina. The report of his study [14] is published internally. Chan used geometrical information from Joustra and Pater's paper. From the geometrical information, a 3D model is created. The FEM input parameters of the study of Chan differ such that the results could not be compared fairly. However, the 3D model is shared with the author of this research to perform an NLFEA study on. This geometrical model is established from information used hand calculations of Joustra and Pater and is significantly less detailed compared to the models for the Sietske and CEMT IV ship. Moreover, it is found that the modelled bow is too short for dissipating all initial kinetic energy. Therefore, at the end of the collision, the reaction forces are unrealistically high due to the strong influence of the support conditions. This part of the results is disregarded, and a maximum impact force is extrapolated.

The Berdina is classified as CEMT Class V ship, with a tonnage of 2500 DWT and approximated mass of 3500 t [35]. The ship lies in terms of weight, length and width in between the class IV and class V ship investigated in the present study. Table 7.7 shows the general figures of the Berdina. In the plot of figure 7.17, the Berdina is presented with tonnages and lengths of the ships from the binnenvaart.nl data. The Berdina fits within the larger ships in terms of length and tonnage but is just under the mean tonnage for ships of equal lengths.

Berdina	
Mass	3500 t
Velocity	5.5 m/s
Length	110.0 m
Width	10.5 m
Draft	3.2 m
$\mathbf{E}_{kin}$	52.9 MNm

Table 7.7: General characteristics class V ship Berdina.

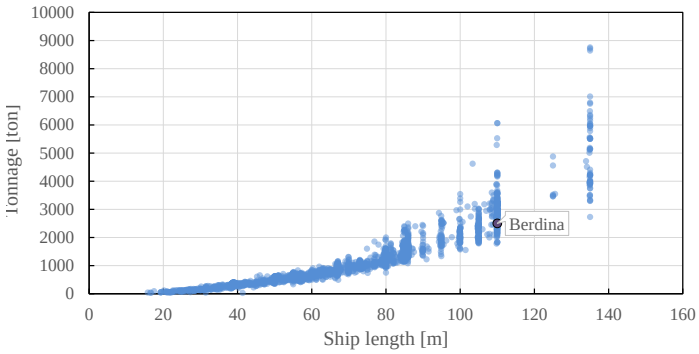

Figure 7.17: Length-tonnage ratio comparison of class V ship. (data source: debinnenvaart.nl

7.3.1. Ship's Bow Structure

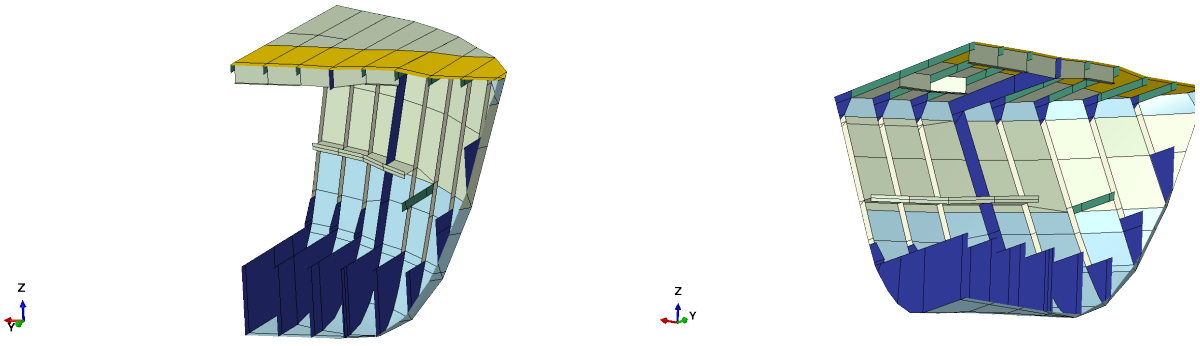

(a) Upper cut-view

(b) Lower cut-view

Figure 7.18: Class V ship Berdina structure. Element thicknesses are coloured: darkblue & green = 8 mm, lightgreen = 10 mm, orange = 14 mm, lightblue = 15 mm.

The geometry is modelled up to d = 4300 mm, only up to this part of the structure information about the structure is provided. The total height is around 3950 mm. The internal structure of the ship's bow is very different in comparison to the other ships presented in this chapter. The frontal part of the bow does not have any stiffeners in longitudinal direction. Only side frames are present which provide stiffness to the side

panels. A stringer is constructed to the side panels at about half the height of the bow. The stringer does not continue into the frontal part of the bow, but is only constructed up to about two meters before the front end. The same applies to three deck girders. Most of the out of plane stiffness of the side plates is provided by the side frames, which are repeatedly placed every 500 mm.

The discontinuities of very important longitudinal elements is remarkable. The structure hence has very little stiffness at the frontal part. This seems unrealistic, and impression rises that structural information is missing in the 3D model. On the other hand, relatively thick elements are found, with an average of t_{avg} = 12.21 mm. Table 7.8 shows the different thicknesses per structural element.

Elements	**Thickness [mm]**
Bottom plating (front)	15
Upper plating (front)	15
Deck (middle)	14
Deck (sides)	10
Deck beams	8
Deck girder	10
Floor plating	8
Side plating	10
Side frame Stiffeners	10

Table 7.8: Element thicknesses of Berdina bow structure

7.3.2. NLFEA Calculation results

The constructed model is meshed with a global mesh size of 25 mm, resulting in 166646 elements. The mesh is verified using the verify tool from ABAQUS, which resulted in no errors, and only 0.03% of the elements showed warnings. The mesh model is shown in figure 7.19. The simulation is run up to t = 1.0 s. Mass scaling is utilised to increase the stable time increment up to around 1E-6, which resulted in an artificial change in mass of 5.8E-06 per cent. A total of 104.2×10^3 time increments is calculated, which took about 5 hours on 24 cores.

It is found that the modelled 3D model of the bow is too short for dissipating all initial kinetic energy. Consequently, at the end of the collision, the reaction forces are unrealistically high due to the strong influence of the support conditions. This part of the results is disregarded, and the results are only presented up to 0.5 seconds. From observing the visualisation of the deformed model with stresses, it is found that up to this point, the support condition effect is not significant, in contrary to the results after 0.5 seconds. Extending the 3D model of the ship's bow is not possible since information about the structure is not available. The calculation results are analysed up to t = 0.5 s to find an approximation of the maximum impact force. This analysis is presented in appendix H. Because of the inaccuracy as a consequence of extrapolating the data, and the unrealistic structural discontinuities, the development of the regarded force data over time is omitted further in the present study. However, the determined maximum impact force given the ship size is considered as valuable information which is obtained with sufficient accuracy.

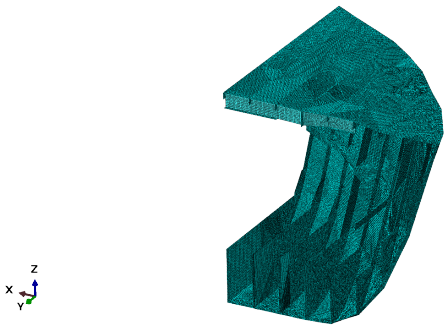

Figure 7.19: View-cut of Berdina ship's bow model with a mesh of 25 mm.

Energy balance

The energy levels over time are depicted in figure 7.20. Data is used up to $t = 0.5$ s, with a remaining of 72.4 per cent of the initial kinetic energy. The dissipation distribution at $t = 0.5$ seconds is shown in table 7.9. While these values are extracted at a very different moment during the collision process compared to the class IV and the Sietske, the values are comparable. Only frictional dissipation deviates significantly from previous results, which is probably caused by the fact that only the beginning phase is considered, the phase where the colliding elements have a greater collision angle with the bridge pier compared to further into the collision process. An extrapolation on the kinetic energy and plastic dissipation energy is performed, explained in appendix H.

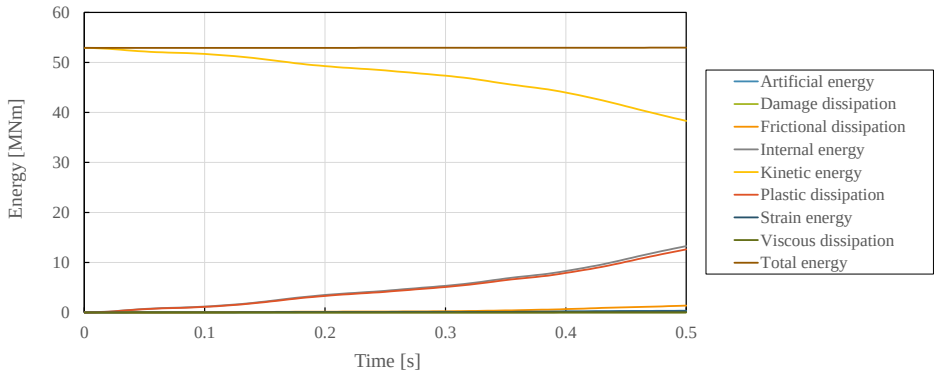

Figure 7.20: Energy levels during Berdina collision simulation.

Artificial energy	2.5%
Damage dissipation	0.2%
Frictional dissipation	9.4%
Plastic dissipation	86.2%
Strain energy	1.8%
Viscous dissipation	0.3%

Table 7.9: Energy dissipation distribution of Berdina collision simulation at $t = 0.5$ s.

Force results

Force-time history data and force-displacement data are depicted in figure 7.21a and 7.21b, respectively. The curves are truncated at $t = 0.5$ seconds, where original curves are depicted transparent. Remarkable is a very different character than the curves from the class IV ship and the Sietske. The steep increase in force at the very beginning of the collision process is not present in the Berdina simulation. The curve shows a more linear character. This is clearly substantiated by observing the structure. As mentioned before about the structure, the frontal part of the bow is considered relatively weak with the lack of longitudinal stiffeners.

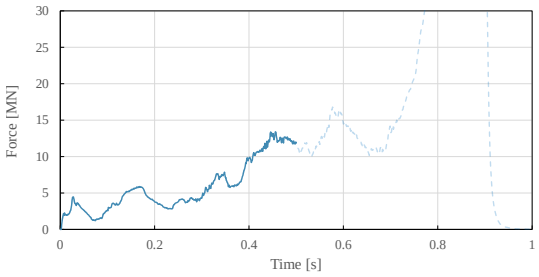

(a) Force-time history of Berdina ship collision simulation.

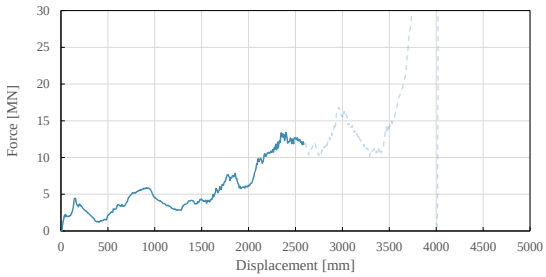

(b) Force-displacement of Berdina ship collision simulation.

Figure 7.21: Collision force data for Berdina from the NLFEA. The dotted part of the curves is disregarded in the data analysis.

The maximum impact force obtained from the observed data is 13.3 MN. This value is not the maximum impact force of the Berdina, since only part of the kinetic energy is dissipated within this observed data.

The maximum impact force of a collision of the Berdina with a bridge pier is determined to be 27.15 MN, calculated using regression analysis and extrapolation (see appendix H). This value is used further in this study. The force development data is considered incomplete and therefore not usable.

Collision forces in x-, y- and z-direction are depicted in figure 7.22. Forces in y- and z-direction are relatively stable around zero. Perhaps this is caused by the relatively weak front part of the bow, with also less stiffness the direction in the height of the bow. Fewer forces are 'pushing' into the bridge pier in that direction, with lower stiffness.

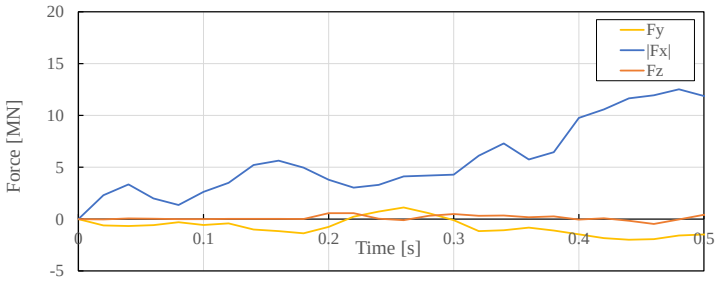

Figure 7.22: Force-time history for three support directions of the rigid wall.

7.3.3. Comparison with hand calculation

The force-displacement curve from the NLFEA calculation is compared with the hand calculations explained in chapter 5. Equal global behaviour is found with in the results of the hand calculations; lower forces up to a displacement of 1500 mm and then increasing with the structural stiffness. Amdahl's method shows zero force up to about 1500 mm, which is unrealistic of course. This is caused by the sensitivity on the amount of t-shaped intersections and cruciforms in the cross-sections. For this part, these intersections are not present since only angular intersections are found, which results in zero crushing force.

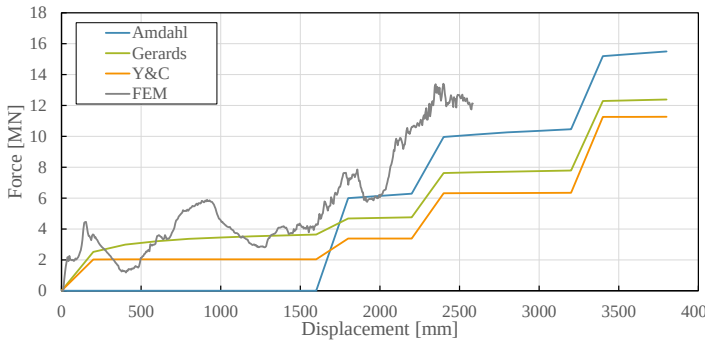

Figure 7.23: Force-displacement graph for Berdina from NLFEA and hand calculations.

7.4. Result interpretation

In this section, the NLFEA calculation results are discussed and analysed. Force-displacement results from the calculations on the class IV ship and Sietske are thoroughly analysed to eventually come to a conclusion on the impact force depending on a ship size. The calculation results from the Berdina are only regarded partly, since not all data is considered valid. From this calculation, only the maximum collision force is considered valid and used in the interpretation of the results.

7.4.1. Comparison between class IV and Sietske results

The characteristics of the class IV ship and Sietske differ in a way that they provide good samples for the analysis on collision forces for different ship sizes, with initial kinetic energy's of about 30 and 78 MNm.

	Class IV	Sietske
Mass	2136 t	5130 t
Velocity	5.3 m/s	5.5 m/s
Length	85.0 m	135 m
Width	9.6 m	11.45 m
Draft	3.0 m	3.6 m
$\mathbf{E}_{kin}$	30.2 MNm	77.6 MNm

Table 7.10: Characteristics of regarded ships.

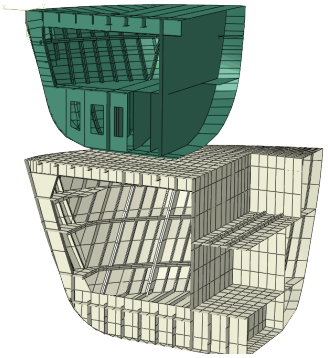

Figure 7.24: Structural geometries of the ship's bows.

The amount of kinetic energy of the Sietske is more than double the energy of the class IV ship. Where the bow geometries might look equal from the outside, the structural properties in the bow are very different. Mainly because the stringers and stiffeners are located differently. In the class IV ship's bow, the stiffeners are connected to the hull at a diagonal angle from the longitudinal central line (and the collision angle) at a relatively long frontal part. For the Sietske this is only for a small frontal part, where four rows of stiffeners are connected parallel to the collision angle. Behind these four rows, all stiffeners at the hull are at a perpendicular angle to the collision angle. Therefore, with more stiffeners in a relatively low angle to the collision angle, the class IV ship's bow was expected to react stiffer at this part of the bow. However, with increasing penetration depth, the dimensions of the Sietske increase even more than for the class IV ship. With this increasing cross-sectional area, higher resistance to compression was expected and therefore a higher collision force. Both of these expectations are confirmed by the NLFEA calculation result. Note that the collision object, a schematic bridge pier as a rigid wall, is greater than the cross-section dimensions of both ships. This means that this size does not have any influence on the difference of the results.

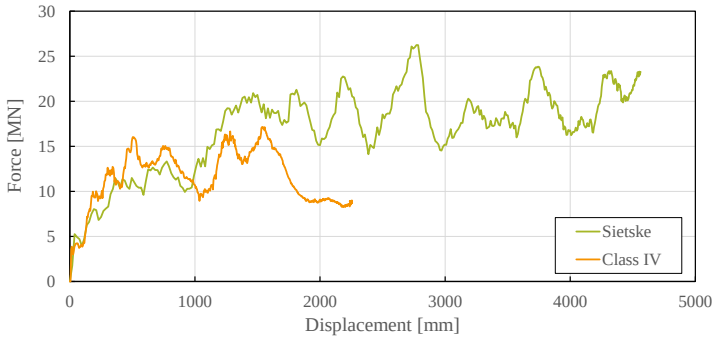

Figure 7.25: Force-displacement NLFEA results for class IV ship and Sietske

Figure 7.25 shows the force-displacement curves for the class IV ship and the Sietske. At the first part of the deformation of the bows, up to 1000 mm, the collision forces are comparable. This is the part where the dimensions of both ship's bows are proportionate. The first minor peak is for the class IV ship higher, which could be explained by the stiffeners located at the very beginning of the bow connected to the hull at a parallel angle to the collision angle. After this part, the collision forces for the class IV ship are higher up

to a displacement of 1000 mm, when the diagonal stiffeners are still active. Hereafter, the extra structural elements of the Sietske are activated increasing the stiffness and therefore, causing higher impact forces.

The collision of the class four-ship stops at around 2250 mm displacement, as the velocity is almost zero and the kinetic energy is – considered – fully dissipated. The Sietske contains more than double the amount of kinetic energy and is therefore still moving towards the pier. The high difference in initial kinetic energy is confirmed by the curves. Both curves end at the moment the initial kinetic energy is almost fully dissipated. The dissipated energy can be obtained by calculating the area under the force-displacement curve ($W = Fu$). Since the force curve from the Sietske becomes higher and ends at a displacement of about two times the value for the class IV ship, this large difference in initial kinetic energy is confirmed.

7.4.2. Analysis of general behaviour

The eventual goal is to review the current guideline of Rijkswaterstaat (ROK) on collision forces and form advice of the collision forces for a wide range of Dutch inland waterway ships. Therefore, a quick comparison is made with the guideline and the study of Joustra and Pater, which is the base for the guideline.

Comparison with Richtlijnen Ontwerp Kunstwerken guideline

The guideline of Rijkswaterstaat gives eq. 2.14 to estimate the impact force based on the initial kinetic energy of the ship (explained in chapter 1, Introduction)

In table 7.11, the energy levels are shown for the studied ships, their maximum collision force from the finite element analysis and the advised collision force from the guideline of Rijkswaterstaat. The Thomar is included as a reference, which is studied in the background study of the guideline.

	Class -	**Mass** [t]	**Velocity** [m/s]	**Kinetic energy** [MNm]	**Collision force**[1] [MN]	**ROK force**[2] [MN]	**Difference** [%]
CEMTIV	IV	2140	5.3	30.1	17.4	23.7	-28%
Thomar	IV	3080	5.6	48.3	-	28.5	-
Berdina	V	3500	5.5	52.9	27.2	29.6	-8%
Sietske	V	5130	5.5	77.6	26.2	34.7	-24%

Table 7.11: General values of regarded ships and their calculated collision force.

[1] As is calculated in the present study
[2] As calculated according to the guideline of Rijkswaterstaat on collision forces on bridge piers, disregarding the factor 1.1 on the kinetic energy for added mass to make a fair comparison.

It is observed that the collision force is increasing with an increase in initial kinetic energy (higher mass and/or velocity). Moreover, the established maximum collision forces from the analyses of this study are all lower than the forces calculated by the guideline of Rijkswaterstaat

In the study of Joustra and Pater [35], the equation for the maximum collision force depending on the energy level is determined by a visual fit on the force-displacement curve. The force-displacement curve 'behind' eq. 2.14 is presented as follows:

$$F_{peak} = 5.6 + 5.97x \tag{7.1a}$$

$$F_{mean} = 5.97x \tag{7.1b}$$

Equation 7.1a is fitted on the peaks of the results of three simulations on the Thomar, equation 7.1b is a linear interpolation of the complete curve. The curves of these equations are depicted over the F-x data from the present study to obtain judgement about the comparability (see figure 7.26).

The linearisation of the F-x curves does not fit the behaviour of Sietske and the class IV ship, which follow a more asymptotic behaviour.

Force-energy relationship

The calculated values are depicted with the standards as a reference to gain insight into the relation of the initial kinetic energy and the collision force. The treated standards are explained in chapter 2. All calculation results of the present study fall in between the curves of the standards. The Thomar is added as a reference;

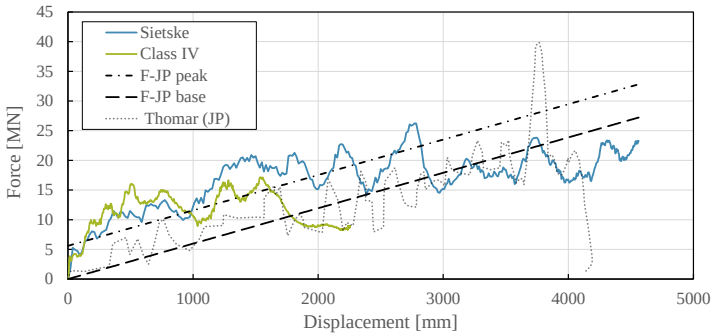

Figure 7.26: Force-displacement comparison with expression from background study ROK guideline [35].

the data from this point comes from the study of Joustra and Pater [35]. The data point from the Thomar lies almost exactly on the curve of the ROK which is to be expected since the curve is created from data of the Thomar. The other data points lie under the ROK curve; this could be an indication of conservatism in the guideline of Rijkswaterstaat. The data points "Class IV" and "Sietske" are considered validated. The data from the Berdina is considered less precise since this data is extrapolated with rough approximations.

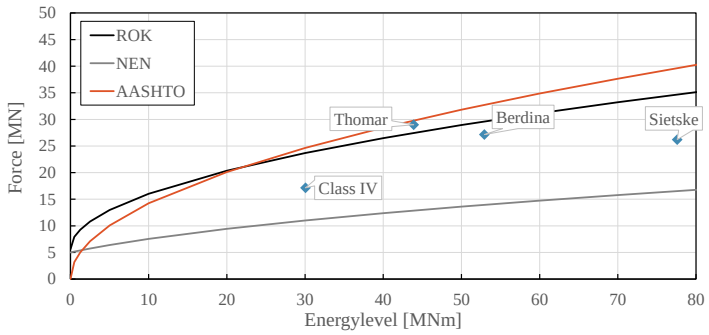

Figure 7.27: Result comparison with guidelines on ship collision forces with variable energy level.

The eventual goal of this study is to find a relation between the ship size and the collision impact force. In the graph of figure 7.27, the ship sizes are quantified into the initial kinetic energy. Therefore, this graph should be observed precisely. However, it is not very precise to find a relation with only these four data points from which even only two are considered completely valid. Nonetheless, since a lot of collision data is known behind these data points, the background of the data points is a better base for finding the relation.

For example, force-displacement data is easily converted to force-energy data, which could be very informative. With this information, the force can be read with a given initial kinetic energy level. Energy dissipation-time data is combined with displacement-time data to find the dissipated amount of energy for a given displacement. This is combined with force-displacement data to eventually find a force-energy relationship. This procedure can be performed analytically by integrating the force-displacement curve with the trapezoidal rule, but in that way, not all energy dissipation processes are incorporated. Therefore, data of the displacement, time, kinetic energy and reaction forces are combined to convert to force-energy ratios. The converted curves of the data from the Sietske and class IV ship are depicted in figure 7.28.

To use these curve to estimate the force for a given initial kinetic energy level, we assume similar force development when kinetic energy levels are different. This assumption is confirmed valid by tests from Joustra and Pater [35]. This means that, if the energy level is for example 20 MNm, the maximum force can be read from the part of the curves before the 20 MNm is reached.

Except for the Eurocode guideline, a proper alignment of the curves is found with the standards, especially for the Rijkswaterstaat guideline. However, by observing the very beginning of the curves, up to 10 MNm, forces of the class IV ship exceed the force estimation by the ROK. This means that by following this curve, the collision forces should be higher for these energy levels. A larger discrepancy is found for energy levels above

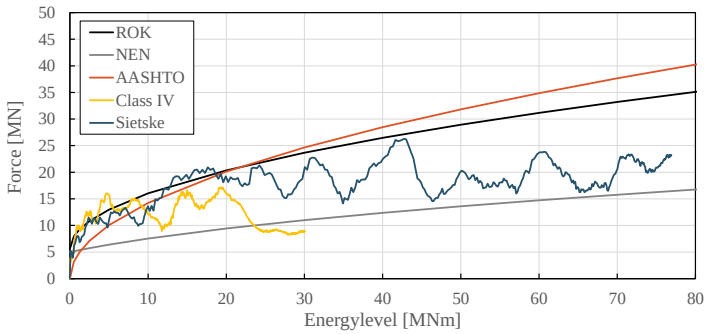

Figure 7.28: Result comparison as energy-curves with guidelines on ship collision forces with variable energy level.

20 MNm. Both the AAHSTO and ROK estimate substantially higher collision forces for this amount of energy levels. This corresponds to the aforementioned asymptotic behaviour of the found curves.

7.4.3. Numerical interpretation of results

As mentioned before, the force-displacement data is considered as good basis to find the relationship between the initial kinetic energy level and collision impact force. Data regression is utilised to find a function which approximates the behaviour.

With simple equations, the force-displacement curve is converted to a force-energy curve. First, two functions are defined which represent the mean force over displacement (F_m) and the peak forces over displacement (F_p). The area under mean force-displacement curve F_m is equal to amount of dissipated energy, which is calculated with eq. 7.3:

$$E_{diss}(x) = \int F_m dx \tag{7.2}$$

Where:

E_{diss} = Dissipated energy,
F_m = mean force function,
x = displacement.

The total amount of energy is assumed to be conserved, therefore, the energy balance can be used:

$$E_{diss}(x_{max}) - E_{kin} = 0 \tag{7.3}$$

By equating the dissipation energy E_{diss} with the initial kinetic energy E_{kin}, and substituting eq. 7.2 into eq. 7.3 the maximum penetration depth x_{max} can be determined.

If the initial kinetic energy is known, the unknown is the force function. Three methods are proposed here to find the force function the ship collision, which will be fitted on the data:

- Analytical approach
- Empirical approach - root function
- Empirical approach - asymptotic function

The first step of this procedure to find a relationship between the collision impact force and the kinetic energy is to find functions which describe the force-displacement behaviour. One function which describes the mean force over displacement to adopt the energy dissipation behaviour, and another function which describes the maximum force given a displacement value. It is assumed that both curves follow the same behaviour, but are scaled. A general form is defined where fit-variables are implemented which are fitted to the obtained data.

The general form is established from analysing the data and studying factors influencing the data.

Analytical approach
Analytical equations are utilised to find a (qualitative) relationship between the force and displacement, or penetration depth, to find the expression form in which we should find the eventual solution from the data.

Note that the only relevant output from this analysis is the form in which the displacement ends in an expression for the force. The quantitative values are not relevant. This applies to multipliers and constants in the expressions but does not apply completely for values as exponents or roots since these values determine the form of the function.

As starting point, we already have obtained the following equations. An element thickness formula (eq. 2.1) is found in the DNVGL recommendations on plate thicknesses (for side plates), see chapter 2. A relationship between the ship length and the dead weight tonnage is obtained from the data of Dutch inland waterway ships in chapter 2, eq. 2.2. The ROK guidelines writes a rule of thumb on the relationship between deadweight tonnage and ship mass: $M = 1.4$DWT.

Equation 2.2 is multiplied by 1.4 and inverted to find a relationship between the length and the mass of the ships:

$$L = 2.46M^{0.463} \tag{7.4}$$

By assuming material factor $k = 1$ and stiffener spacing $s = 0.5$ m for eq. 2.1, and substituting eq. 7.4, a relation between the recommended thickness and ship mass is found:

$$t = 3.48 + 0.05M^{0.463} \tag{7.5}$$

Using the kinetic energy function $E_{kin} = 0.5Mv^2$ and assuming a velocity $v = 5.5$ m/s, this expression is formed with dependency on the energy level:

$$t = 3.48 + 0.014E^{0.463} \tag{7.6}$$

The expression of eq. 7.6 determines the minimum element thickness for side plating as recommended by DNVGL from a given kinetic energy level.

From this point, the semi-empirical formulas from literature provide useful information. In these studies, analyses are performed where a relation is established between geometric factors and the mean collision force. Three semi-empirical formulations are treated in chapter 6 which are used to verify the NLFEA results. These formulas share a similar approach, but differ in used variables and complexity yet generate comparable results. Since the results do not differ significantly, the most simple approach is used since this simplifies the process.

Gerard [23] provides a simple formula to establish a mean stress level, where it is clearly observed how each variable influences the result in eqs. 5.13 and 5.16 described in chapter 6. Note that variable m is a important coefficient as it influences the relation between element thickness and area with the collision force. $m = 0.85$ is recommended for ship structures, and is used in this approach.

All variables except area A and number of cuts and flanges n in equation 5.13 are considered constant over depth. These constant values are inserted, to eliminate the variables over depth. The following values are inserted: $\sigma_0 = 380$ MPa, $\mu = 0.56$, $t = 11$ mm, $E = 194000$ MPa, $\sigma_y = 300$ and $m = 0.85$. In this way, a relation is found of the force over depth or, force over displacement. The average thickness t could vary over depth, however, but it is found in the data of the regarded ships from the present study that this value is only varying with around 10% of the mean value. The elimination provides the following function:

$$F = 0.19\left(\frac{n}{A}\right)^{\frac{17}{20}} A \tag{7.7}$$

From the data of the Sietske, functions which describe the cross-sectional area and the number of cuts and flanges is obtained:

$$A = 170 \times 10^3\, x^{0.563} \tag{7.8a}$$

$$n = 5.5\, x^{0.18} \tag{7.8b}$$

With depth x in meters. Substituting these functions in the function from Gerard, eq. 5.13 and eq. 5.16, the following expression is acquired:

$$F = 15\,x^{0.24} \tag{7.9}$$

This is the eventual form which should describe the relationship between the collision force F and penetration depth x based on analytical expressions. The function could be approached by a fourth root. With that, is concluded that the force-displacement solution could to be found in the form of:

$$F = C\sqrt[4]{x} \tag{7.10}$$

This as based on analytical relations. C is a to be fitted multiplication constant.

This shows a root function to describe the force development, which was already expected from the plate thickness analysis based on design rules in chapter 2.

Data regression analysis Constant C from the force function in eq. 7.10 is determined using data regression with the least-squares method on force-displacement data obtained in the nonlinear finite element analysis. Two functions are necessary to describe the curves: a mean force function to determine the energy dissipation and a peak force function to determine the maximum force with a given displacement.

The mean force curve is established using all obtained force-displacement data points from the class IV ship and the Sietske. The peak force function is determined by a selected set of data points which represent local peaks in the NLFEA data, indicated in figure. 7.29.

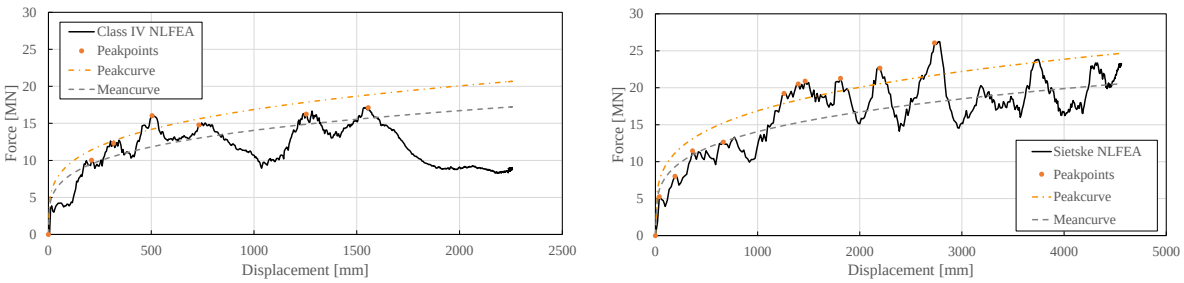

(a) Force-displacement regression fit on curve and peak points for Class IV ship.

(b) Force-displacement regression fit on curve and peak points for Sietske.

Figure 7.29: Force-displacement regression fit using least squares method on semi-empirical approach.

Figure 7.29 shows a graphical comparison of the found curves with the force data from the NLFEA. The following functions are established as best fit for both Sietske data and class IV ship data:

$$F_{peak} = 1.1 \times 3.07\sqrt[4]{x} = 3.38\sqrt[4]{x} \tag{7.11a}$$

$$F_{mean} = 2.49\sqrt[4]{x} \tag{7.11b}$$

The mean curve shows a good fit globally as it runs through the average between local highs and lows. The fitting of the peak curve creates a good fit on the peak data points. However, the fit is obtained to find a good fit for all peak data points. This means that the curve represents an average of the peak points. Yet, since this curve should represent the maximum forces for a given displacement, it should cover the highest peak forces. An increase of 10% is implemented to raise the curve in a way it covers the peak force data points.

The force of the simulations on the Class IV ship and Sietske are now defined by a function dependent on the penetration depth. To establish a formula which fulfils the goal of finding a design collision force for a given ship size, the force function should be dependent on the initial kinetic energy level. The energy balance described in equations 7.2 and 7.3 are used to convert this function.

$$E_{diss} = \int F_{mean}\,dx = \int 2.49x^{\frac{1}{4}} = \frac{4}{5}2.49x^{\frac{5}{4}} = 1.99x^{\frac{5}{4}} \tag{7.12}$$

The maximum penetration depth is reached once the kinetic energy is completely dissipated, since velocity is zero at that moment. In practice, at this point, some energy is stored in the structure as potential (elastic)

energy. Since some structural elements are elastically loaded and will unload when the force is zero, which causes a negative velocity. However, this is of no significant importance for the maximum collision force and is therefore neglected. The energy balance is then formulated as follows:

$$E_{kin} - E_{diss}\,(x_{max}) = 0 \rightarrow\ E_{kin} = E_{diss} \rightarrow E_{kin} = 1.99(x_{max})^{\frac{5}{4}} \tag{7.13}$$

With a given maximum displacement (mm), the initial kinetic energy (MNmm) can be calculated. By rearranging this equation, the maximum displacement can be found with a given initial kinetic energy. For practical reasons, the kinetic energy is multiplied by a factor 1000.

$$x_{max} = \left(\frac{1}{1.99}\right)^{\frac{5}{4}} (E_{kin} * 1000)^{\frac{5}{4}} = 144.85(E_{kin})^{\frac{4}{5}} \tag{7.14}$$

With kinetic energy in MNm. By substituting this equation in equation 7.11a for the peak force, the general formula for determining the peak force based on a given kinetic energy level is found:

$$F_{peak} = 3.38\sqrt[4]{x} = 3.38\left(144.85(E_{kin})^{\frac{4}{5}}\right) = 11.72\sqrt[5]{E_{kin}} \tag{7.15}$$

Algebraically, the energy dependency of the collision force is found in the form of a 5th root function. This shows a steep curve at low energy levels, but the gradient decreases rapidly to a more flat curve.

Empirical approach - root function

Another approach to find a trend within the results and conclude with a general method for calculating the collision forces for different ships is by finding the relationship empirically. The form-finding of the used expression is not limited by known theories, but only limited by the assumption that the force should increase with an increasing initial energy level. The freedom of this yields the possibility of a better fit with the results.

Similar as for the semi-empirical approach, the starting point is the energy balance defined with eq. 7.3 from section 7.4.3. The kinetic energy is presumed as known, which makes the force function the only unknown. Therefore, a general force function is investigated to fit ships of different sizes.

By observing the F-x data closely, and trying different types of functions, an expression is found which is presumed to result in the best fit. Equal to the function of the analytical approach and formulas given in standards, this expression is found in the form of a root function:

$$F(x) = Ax^{\frac{1}{n}} + B \tag{7.16}$$

Where A, B and n are fitting constants which scale, move the function and determine the root coefficient, respectively. Where coefficient n is generally assumed as a positive (real) integer, here, a positive (real) non-integer is assumed to find a precise fit. This could eventually be simplified for practical engineering purposes.

Constant B is determined by establishing the initial condition that the force is zero at $x = 0$: $F(0) = 0$ which results in $B = 0$.

Coefficients A and n are now remaining to fit on the data. This is done in a similar manner as with the analytical approach. However, least-square regression is applied to two constants instead of one in this approach. The regression is applied to establish a mean curve and a peak curve. Both curves are defined to differ in multiplication factor A but to have an equal root coefficient n to make sure the curves show the same behaviour. Therefore, the curve functions are established in the form:

$$F_p = A_p x^{\frac{1}{n}} \tag{7.17a}$$

$$F_m = A_m x^{\frac{1}{n}} \tag{7.17b}$$

The regression is performed on the force-displacement data of the class IV ship and the Sietske simultaneously to find a general best fit. The least-square fitting method is applied on the functions of eq. 7.17. The best fit is found with $n = 2.76$, $A_p = 1.40$ and $A_m = 1.05$. Consequently, the curve fit functions following from the empirical approach are:

$$F_p = 1.40x^{\frac{1}{2.76}} \tag{7.18a}$$

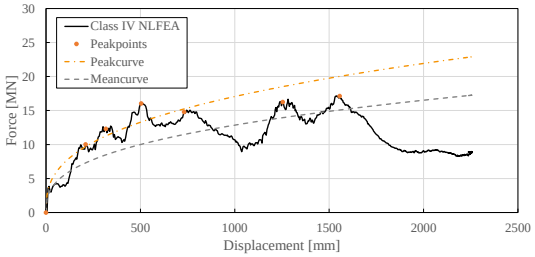

(a) Force-displacement regression fit on curve and peak points for Class IV ship.

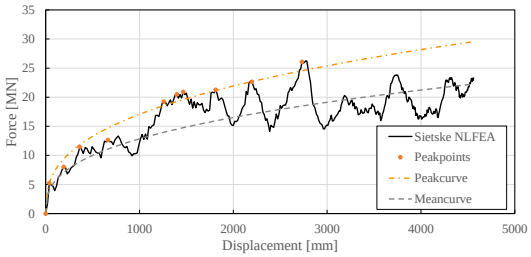

(b) Force-displacement regression fit on curve and peak points for Sietske.

Figure 7.30: Force-displacement regression fit using least squares method on empirical approach.

$$F_m = 1.05x^{\frac{1}{2.76}} \tag{7.18b}$$

Figure 7.30 shows a graphical comparison of the established curves with the reference data. The established functions are treated similarly as is done with the analytical approach. The mean function is substituted in equation 7.2 to calculate the dissipation energy and eventually find a function for the maximum displacement using the energy balance. This maximum displacement function is substituted into the peak force functions to form an expression for the peak force dependent on the kinetic energy, which follows as:

$$F_p = 9.41\,E_{kin}{}^{\frac{1}{3.76}} \tag{7.19}$$

This function shows similar behaviour as the function established with the analytical approach. However, this function shows a root value of 3.76 instead of 5 and a higher scale value.

Empirical approach - asymptotic function

From the analytical expression, it is found that a root function describes the force function. But given the curves presented in figure 7.25, asymptotic behaviour is observed. The hand calculation results from the simplified analytical methods showed this behaviour as well.

Therefore, an asymptotic function is used as trial solution. The hyperbolic tangent is found to show comparable behaviour as what is found in the force-displacement data, and will be utilised to fit the data on.

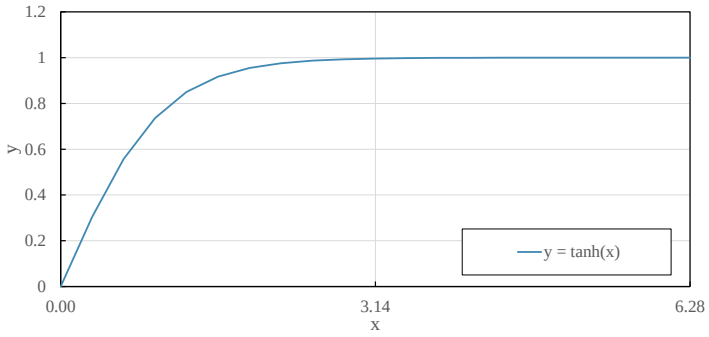

Figure 7.31: Hyperbolic Tangent function

The typical hyperbolic tangent behaviour is depicted in figure 7.31. The function approaches the asymptote with a height of $y = 1$ at $x = \pi$. By adding fitting parameters, the hyperbolic tangent function can be scaled with respect to the x and y-axis to create a proper fit.

$$y = a\tanh(b \cdot x) \tag{7.20}$$

This function is to be fitted on the force-displacement data of the Sietske and the class IV ship. Parameters a and b are to be determined using the least-squares data regression method. However, since the asymptotic heights of the two curves differ, a good fit cannot be established directly. The data needs to be normalised

first, to ensure the curves to overlap. When this is done, one expression could describe both curves but should be scaled afterwards for each case.

The height of the curves is normalised using general geometric information of the ships. Intuitively, the curve height could be normalised using the total frontal area. The total frontal area, draught d times beam b, is a simplified factor of the cross-sectional area and is assumed to represent the difference in cross-sectional areas between ships. With this, it is assumed that the ratio between the total frontal area and the (average) cross-sectional area is equal for different ships. Therefore, a proper factor to normalise the curves with could be the total frontal area.

However, physically, the ratio between the beam and the width of the collided structure is an important factor which determines the impact force. If the beam is broader than the width of the structure, the ship structure will show more bending instead of compression failure modes since part of the ship structure will not directly hit the collided structure.

This factor is not investigated in this study. Therefore, beam b is eliminated for normalising the curves. Draught d is hence used as the the normalising factor..

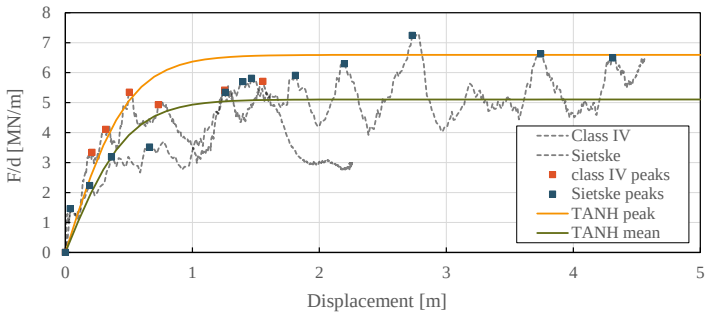

Figure 7.32: Normalised force-displacement curves with tanh(x) fit function

Figure 7.32 shows the normalised curves and the hyperbolic tangent which showed the best fit on the data. Through the normalisation variable, the curves show good overlap. Peaks of the class IV ship simulation results are determining in the first stage, where the longer simulation of the Sietske determines forces of the later stage.

The mean hyperbolic tangent function is fitted on the complete data set. The expression which describes the local peaks is fitted on the indicated peaks and multiplied by 1.1 to cover the higher peaks and describe the upper limit.

$$F_{peak} = 1.15.99 \tanh(2.03x) = 6.59 \tanh(2.03x) \tag{7.21a}$$

$$F_{mean} = 5.01 \tanh(2.03x) \tag{7.21b}$$

Eventually, these curves are re-scaled with d to find the actual force. From the obtained curves, it is already determined that with sufficient kinetic energy to penetrate deep enough to reach the asymptote, the maximum force is found by $6.59d$. And the peak forces are $6.59/5.01 = 32\%$ higher than the mean forces.

The fitted eqs. 7.21a and 7.21b are treated in a similar manner as the previous paragraph – integrating the mean function and equalling with the energy balance. However, these equations are eventually re-scaled by multiplying the equation with variable d. The impact force formula depending on the energy level describing asymptotic behaviour is found as follows:

$$E_{dissipation} = \left(\frac{5.01}{2.03}\right)\ln(\text{abs}(\cosh(2.03x))) \tag{7.22a}$$

$$F_{peak} = 6.59d \tanh(\text{arcosh}(e^{0.404E_{kin}})) \tag{7.22b}$$

Where eq. 7.22a represents the mean energy dissipation during collision, and eq. 7.22b the maximum impact force given an energy level.

7.4.4. Review on proposed force functions

In the previous sections, force-energy curves are established with three different methods. The results are depicted in the figures 7.33 and reviewed in this section.

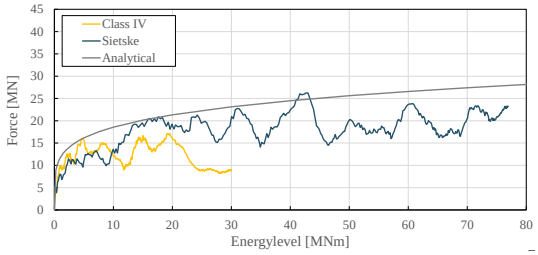

(a) Fit with analytical approach.

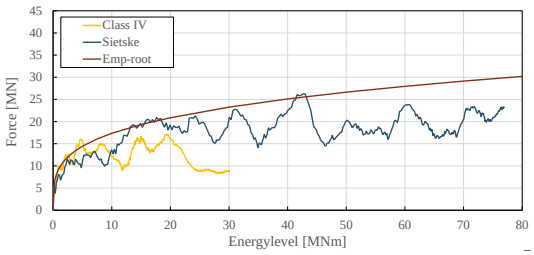

(b) Fit with empirical approach - root.

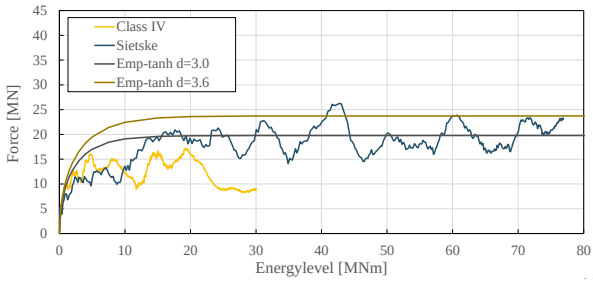

(c) Fit with empirical approach - asymptotic.

Figure 7.33: Force-energy curves following from data regression with different approaches, plotted with converted force-energy curves from the simulation results.

Figure 7.33a shows the curve which is found using the analytical approach. The root function shows both a good fit on the steep beginning stage of the collision simulation of the class IV ship, and on the higher peak forces of the simulation of the Sietske. However, as a consequence of fitting on the combination of these curves, the curve overestimates the forces for the for the higher energy levels in results of the class IV ship and Sietske.

The root curve in figure 7.33b, which is obtained empirically, shows a less steep first stage but ends with a higher force at an energy level of 80 MNm since the gradient decrease is lower in the complete curve. The curve underestimates some peaks from the class IV ship simulation data, but shows good agreement with the local peaks from the data of the Sietske. However, the curve overestimates the forces at the end stage.

The opposite is true for the hyperbolic tangent function, depicted in figure 7.33c. The curve shows a behaviour which increases to a relatively high value at the beginning, but the gradient decreases quickly to a flat line. With that, the curve overestimates forces at the beginning stage of each ship. Especially around 10 MNm. However, this curve shows better agreement with the end stage of the result curves.

The maximum collision impact force is estimated with the obtained functions by putting the initial kinetic energy level into the formula, but could be extracted graphically as well by intersecting the curves with a given kinetic energy level. This means that for the performed simulations, the estimated impact force is found by finding the force on the obtained functions which corresponds to the maximum energy level.

Table 7.12 shows the analysed ships and corresponding estimated forces compared to the calculated force. The Thomar is added since this ship is studied in a previous study where the current ROK formula is originating from.

Figure 7.34 shows the estimated forces for different ship classes, including the analysed ships and their calculated impact force. The ships are ordered on kinetic energy level.

From table 7.12 and figure 7.34 the different estimation techniques are judged. The ROK is added for comparison. Globally, the analytical, empirical root and the ROK estimations show the same character which is originated by their root function. The gradient of the functions differ which is caused by the difference in root values.

Name	L [m]	W [m]	D [m]	E_{kin} [MNm]	Empirical - Root [MN]	Analytical [MN]	Empirical - Asymptotic [MN]	ROK [MN]	Calculated [MN]
Class IV ship	85	9.6	3.0	30.1	23.3	23.1	19.8	23.7	17.1
Thomar[1]	103	9.5	3.2	42.4	25.5	24.8	21.1	27.1	29.0
Berdina	110	10.5	3.2	54.9	27.3	26.1	21.1	30.0	27.2
Sietske	135	11.5	3.6	77.6	29.9	28.0	23.7	34.7	26.2

Table 7.12: Analysed ship data and estimated and calculated forces. [1]Calculation from previous study [35].

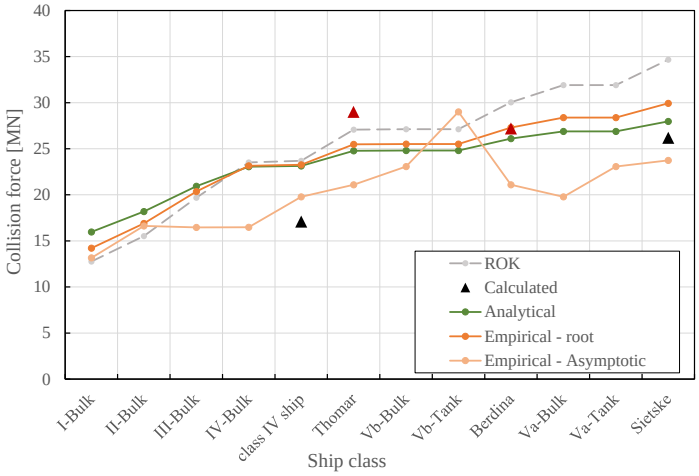

Figure 7.34: Estimated forces for different ship classes with different methods, including calculated forces. The black triangles are thoroughly calculated forces established in this study.

A clearly deviating character is found in the asymptotic function, this is predominantly caused by the ship draught dependency on the estimated impact force. Because of this deviating character, the lack of substantiation on this draught dependency and therefore substantiation of this character, it is advised to not apply this function until further research shows its accuracy. Most importantly, the draught dependency should be confirmed before application, and the function should by judged with the results of further analyses.

The differences between the estimation functions are quantitatively evaluated by calculated the ratio between the calculated value and the estimated value. This is presented in table 7.13.

Name	Empirical - root	Analytical	Empirical - Asymptotic	ROK
Class IV ship	136%	135%	116%	139%
Thomar	88%	85%	73%	93%
Berdina	100%	96%	78%	110%
Sietske	114%	107%	91%	132%
Average	110%	106%	89%	119%

Table 7.13: Difference between estimated value and calculated value for different methods.

The ROK deviates the most from the calculated values, the analytically obtained formula shows the best agreement. However, still, this formula overestimates the force for the class IV ship significantly (+35%). This is caused by the fact that this ship response relatively stiff at the frontal part of the ship's bow, where a high amount of kinetic energy is dissipated. The part behind this stiff part shows not a such stiff character and the kinetic energy is already dissipated significantly, therefore the potential for a high impact force given the large cross-sectional dimensions are not reflected in the results. This is also confirmed by the fact that the asymptotic function shows the best fit for this ship.

The obtained force estimation functions show about 10% difference with the calculation result for the Sietske. The ROK shows a big difference here. Ultimately, this is caused by the linear relationship between force and displacement assumed to obtain this formula, which causes a low root value (cubic) in the force-energy formula.

7.4.5. Concluding force estimation proposal

Given the results of the different functions, one function is chosen to form an answer to the research question of this study.

The asymptotic function is considered unfounded. Most importantly since the draught dependence is not substantiated thoroughly, but shows high impact. Both the analytically obtained and empirically obtained functions show good agreement with the global behaviour of the force-displacement curves from the simulations. Moreover, the relationship between force and displacement and therefore, force and energy, in the form of a root function was expected given the underlying factors determining the impact force of a ship structure. With that, the analytically obtained root function shows the best agreement with the calculated maximum impact forces and is intuitively substantiated by previous found relationships.

Therefore, it is recommended to use the formula of eq. 7.15 to determine the impact force on bridge piers in the event of ship collision, on Dutch waterways. Given this equation, the recommended values for the impact force per ship type are calculated and presented in table 8.1 in chapter 8.

A comparison is made with the current standards, which is shown in figure 7.35. The advised equation shows higher force estimates for smaller ships than class IV ships, and lower estimates for larger ships. This is clearly observed in a relatively flat curve following from the presented equation. The Eurocode guideline shows significantly lower force estimates, but shows a remarkably comparable gradient.

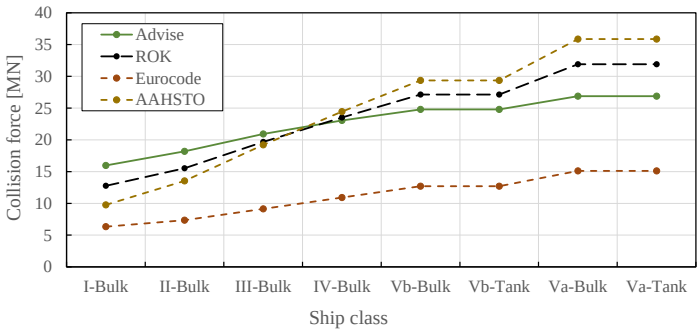

Figure 7.35: Advised impact force values compared to current standards

The increased force estimations for smaller ships is a consequence of the relatively high stiffness of the frontal part of the analysed ship's bows, which resulted in a steep start of the force-displacement curve. This is distinctly observed in figure 7.26, where force-displacement curves obtained in the current study are compared with the force-displacement curves of the study which led to the current ROK guideline. Moreover, in figure 7.27 the force-energy results curves from the simulations of this study are plotted with the current standards where both result curves show higher impact forces up to 20 MNm compared to the standards. With that, the forces are lower at a later stage of the collision, which is a reason for the lower force estimates for larger ships.

This phenomenon of high estimates for the impact force of smaller ships is not only a result of the obtained data, it is founded by the origination of the impact forces as well. In section 7.4.3, acquired knowledge is combined to derive the form for the expression which led to the eventual advised equation to estimate the collision forces (eq. 7.15). An important factor for this derivation is the rule on element thicknesses in ship's bow structures, defined by DNVGL. This rule shows a relationship between plate thickness and ship size where the thickness does not show a high difference for different ship sizes, see figure 2.9. The plate thickness starts at a non-zero value for zero-kinetic energy and develops with behaviour similar to a root function.

It is found that the impact force shows a strong relationship with the plate thickness (presented in table 6.4) from the plate thickness study performed in the sensitivity study of the calculation model. The obtained peak forces showed a higher relative increase than the relative increase in plate thickness (or cross-sectional

area). This is also confirmed by the plate thickness dependency of the crushing strength defined by simplified calculation methods explained in chapter 5, where the thickness is squared in the expressions.

Now we have showed that the plates thickness increases in a root function with increasing ship size, and the impact force increases exponentially with an increasing thickness. These two relations balance out to an approximately linear relationship between the ship size and the impact force, which starts at a non-zero value and continues with a low gradient.

This confirms the validity of the relatively low gradient of the advised collision force estimation of eq. 7.15, in comparison to the ROK and American standard. Moreover, this is in agreement with the gradient of the Eurocode guideline.

8

Conclusion and Discussion

8.1. Conclusion

The purpose of this thesis was to propose a simple technique for the estimation of the maximum impact forces acting on bridge piers in the event of ship collisions. This technique was determined for Dutch commercial inland waterway ships (CEMT classes) and set up to be applied by bridge engineers to determine the required bridge pier strength.

The background of the collision event was explained to provide basic knowledge and understanding of the origination of the impact forces. A dynamic nonlinear finite element model was created using ABAQUS/Explicit to simulate the ship-bridge pier collision event. The bridge pier is assumed to be rigid and fixed, while the ship structure is assumed to dissipate all initial kinetic energy through plastic deformation (crushing). The material properties have been obtained from a test database and include rate effects. An optimal mesh size of 25 mm is found by doing tests and analytical calculations. Tests have shown that the value for the fracture strain has only little effect on the results and is therefore incorporated in a simplified manner. The output of the simulations is presented in the form of impact force versus penetration depth.

Existing analytical calculation methods on the crushing strength of a ship's bow structure are presented and studied for the verification of the numerical finite element model. A sensitivity analysis is performed on the simulation, and showed expected behaviour with no singularities. The correlation between the results of numerical simulations and analytical calculation methods showed good agreement. Moreover, analyses of the behaviour of an isolated deckplate of the structure showed satisfactory agreement with existing plate theories and its behaviour in the complete structure. It is concluded that the numerical calculation model is verified as stable and results are in agreement with existing calculation methods.

Numerical simulations are performed on one class IV and two class V ship's bow structures. The deformation process resulting from these simulations showed visually comparable failure behaviour with a real case. Moreover, a thorough analysis of the reaction forces per structural element of the ship's bow is performed where local forces are compared with deformation processes. This showed good correlation.

A relationship between initial kinetic energy levels and maximum impact force is developed based on the results of the numerical calculations. The global form of the relationship is determined by analysing the results and using found relationships. This form is fitted on the obtained result data through curve fitting techniques. With the established expression, the estimated maximum impact force can be calculated for the event of a ship collision, given an initial kinetic energy level involved in the collision event.

This equation gives for Dutch inland waterway ships the estimated impact forces as presented in table 8.1.

The impact force values presented in table 8.1 differ from the current Dutch standard on this topic. For ships smaller than a medium-sized ship (CEMT IV), the impact force values are higher than is found in the current Dutch guideline. However, lower impact forces are estimated for ships larger than this medium-sized ship. This difference mainly originate from the relatively stiff response of the frontal part of the analysed ship's bows, compared to the ship's bow structure that led to the current Dutch guideline. This shows the impact of

Class-Type	**Length**[1] [m]	**Width**[1] [m]	**Draught**[1] [m]	**DWT**[1] [t]	**Mass**[2] [t]	**V**[3] [m/s]	**Kinetic Energy**[4] [MNm]	**Impact force** [MN]
I-Bulk	38.5	4.1	2.2	400	560	4.1	4.7	16.0
II-Bulk	55.0	6.6	2.6	560	784	4.8	9.0	18.2
III-Bulk	67.0	8.2	2.5	1000	1400	5.1	18.2	20.9
IV-Bulk	85.0	9.5	2.5	1500	2100	5.3	29.5	23.1
Vb-Bulk	135.0	11.4	3.5	3000	4200	4.5	42.5	24.8
Vb-Tank	135.0	21.8	4.4	3000	4200	4.5	42.5	24.8
Va-Bulk	110.0	11.4	3.0	3000	4200	5.5	63.5	26.9
Va-Tank	110.0	11.4	3.5	3000	4200	5.5	63.5	26.9

Table 8.1: Impact force calculated with eq. 7.15 for different ship types.

[1] From bureauvoorlichtingbinnenvaart.nl (see appendix A)
[2] Calculated with 1.4 DWT according to the recommendation by Rijkswaterstaat [59].
[3] Recommended impact speed according to Rijkswaterstaat [59].
[4] Calculated with eq. 1.1, without added mass.

the type of ship structure that is considered. Therefore, it is strongly advised to perform more analyses on a range of different ship types to find out more about the general behaviour.

With the proposed impact force expression, the maximum impact force on bridge piers in the event of ship collisions could be estimated with increased accuracy.

It should be noted that eq. 7.15 and, with that, the values in table 8.1, should be handled as the upper limit for estimating the impact forces on bridge piers in the event of ship collisions, since conservative assumptions are made where appropriate. Moreover, limitations described in section 8.2 need to be taken into consideration when applying eq. 7.15 or table 8.1. The estimated force, or energy input value, could be lowered according to specific cases, which should be incorporated by the bridge design engineer, mainly considering the probability of the collision event and the load angle.

8.2. Limitations

In the process of finding the results for the problem of determining collision forces for inland waterway ship on bridge piers, a couple of assumptions are incorporated to simplify the problem. This comes with some limitations of the outcome, which are explained here.

8.2.1. Conditions

The conditions of the considered ship-bridge pier collision are somewhat simplified to decrease the problem size.

A real situation of a ship colliding with a bridge involves all kinds of factors influencing the impact force on the bridge. Think of the cause of the collision; this could be stormy weather, a stalled ship engine or maybe a drunk skipper. All these situations come with their own specific conditions which could evolve in a high or low impact force. These factors are all incorporated into the external dynamics of the ship-bridge collision problem, which is not included in the scope of the present study. This is all simplified to a given initial kinetic energy level, which includes the mass and velocity of the ship. Surrounding water which moves together with the ship is also neglected but could be incorporated into the kinetic energy as added mass.

Apart from the initial kinetic energy consequences of different collision causes, the angle and location of impact on the bridge pier could also vary substantially for different collisions. The probability that a ship will collide with a bridge pier with both centre-lines exactly aligned is small, given all situations where such collision events can occur. A ship could slide or rotate if the angle of location is different from the assumed frontal collision. These phenomena will contribute to the dissipation of kinetic energy and possibly to a lower collision impact force.

Furthermore, a river flow velocity or stalled engine could have an impact on the energy balance which is assumed in the solution since these factors will add energy into the closed system. This is not included in the research.

The response of the bridge pier during a collision is not regarded in this research. Most possibly, the impact force is decreased since the structure of the bridge pier could damp some of the forces. However, when the collision forces initiate transverse oscillation of the bridge pier, which is not very likely with high structural damping present, the oscillating motion could amplify the impact force.

8.2.2. Structural Geometry

Both the structure of the ship as the structure of the bridge are simplified in the approach of the problem.

The ship's structure is modelled with 3D software where a high amount of structural information is included. However, not every element within the ship hull is exactly on the location as presented in the drawings. This is mainly caused by the fact that all elements should coincide with the defined nodes to be compatible with the finite element simulation. This means that some of the elements are shifted up to 50 mm. Nonetheless, since an eventual generalisation is necessary, such minor differences will not have a significant impact in the solution since these minor differences will be found when observing different kinds of ship structures.

The modelled bow structures of the class IV ship and Sietske consist only of a part of the ship structure, up to a point where is assumed that boundary conditions do not have a significant influence in the impact force. These boundary conditions define the connection to the remaining ship structure and are defined as pinned. This means that local bending is possible, but displacement is prevented. Because of these simplified conditions, global inertia of the investigated ship is not considered. When it is desired to implement rotational freedom of the bow with respect to the bridge pier, either the complete ship should be modelled, or the boundary conditions should be defined more comprehensively with for example supports with some spring stiffness. From the support data of the bridge pier, it is observed that significant forces are acting in other directions than the initial moving direction of the ship as well, concluded from this is that the prevention of rotation does have some influence here. However, without this prevention, the forces are probably lower since other dissipation mechanisms are acting.

Besides, only structural elements which are considered to have significant contribution in the resistance to a frontal collision are included in the structural model. For example, the chain locker and plate stem are neglected. If these elements are included, little more material is present in the ship's bow and collision forces could be increased.

Connections between the elements are modelled as rigid, whereas in reality, these connections are established by welding of the material. Welds are often weak spots of a structure. This is because of a heat-affected zone surrounding the weld which is exposed to high temperatures during welding has changed material properties. This can lead to residual stresses, reduced material strength, increased brittleness, and decreased resistance to corrosion and/or cracking within the material. Moreover, the weld itself has a relatively low resistance to fatigue. When a ship is getting older and such connections have undergone many load cycles, the weld is getting weaker. As a consequence of these effects, the chances are high that the connections between steel plates will fail first during a collision. This has not been taken into account since incorporating such weaker spot increases the complexity of the simulation model considerably. Moreover, high computational power is necessary to allow small mesh elements for the simulation of connections. Some studies on ship collisions lower the failure strain value to implement this implicitly. However, it is found in chapter 6 that this change will have no significant influence in the calculated maximum collision force. Moreover, from chapter 5 it is concluded that the collision force is mainly influenced by cross-sectional area and geometric intersections which act as stiff element. Typical weak weld failures modes as tension failure and bending failure are not very likely to occur within the crushing modes explained in the studies of the simplified expressions.

Local or global imperfections could also have an influence in the maximum collision force or energy dissipation. These phenomena are not incorporated in the geometrical model as explained in chapter 4 since it is expected that it will not have a significant impact, and it could only lower the maximum force (which is not considered as a conservative assumption). But for a more accurate model, this should be looked into.

8.2.3. NLFEA Parameters

Within the input parameters of the analyses, some assumptions or simplifications have been made, which could have an effect on the validity of the results.

Material

The considered material in the present study could differ from the actual material used in the shipbuilding industry for Dutch inland waterway ships. The shipyard of the class IV ship and Sietske is located in China. Due to different steel producers globally, the steel which is used for such ships could have different properties than the properties obtained for the present study. However, the adopted material model could be judged to be in the upper limit of the nominal properties for grade A steel, the steel class which is used for the considered ships. Stiffer behaviour due to material differences is, therefore, not very likely.

Material temperatures could have a significant effect on its behaviour [51]; this factor is not incorporated in the material model. The material properties adopted in the present study are for a temperature of 20°C, although the water temperature involved could be substantially lower. And with that, the temperature of the structural elements within the bow structure. The lower temperature could cause a more brittle behaviour of the material.

Mesh size

The utilised mesh size in the finite element calculation is verified theoretically. However, to establish a final confirmation for the accuracy of this mesh size, convergence should be found within the result of different mesh sizes. This is not completely the case in the present study since the computational power is limited, and a calculation with a smaller mesh size to confirm convergence was not possible.

Failure strain

The failure strain is assumed to be equal for all the elements, whereas the elements have various sizes and thicknesses. Furthermore, failure strain is dependent on strain rate [51], which is not implemented in the present study. The failure criterion should be implemented in the calculation to calculate the failure strain for each element independently, with a dependence on strain rate to obtain extra accuracy in the numerical model. Nevertheless, the sensitivity study showed that the failure strain does not have a significant impact on the impact force (see chapter 6).

8.2.4. Generalisation of force-energy dependency

The generalisation from two data points to a full force curve dependent on energy level could be judged as inaccurate. However, the process behind the data points is investigated thoroughly and used to generate this force curve with a high amount of data to find an accurate solution.

The eventual force-energy force equation (eq. 7.15) is completely based on the geometry of a conventional bow. This is done since most of the inland waterway ships are constructed with a conventional bow. However, many ships on the Dutch waterways carry cargo by barges, which consist of a very different frontal structure. It is expected that barge ships show a different response on a bridge pier collision and should therefore not be calculated with the force formula presented in the conclusion of this study.

8.3. Recommendations

8.3.1. Conditions

A collision event is always about an interaction of multiple bodies. This is simplified into one rigid and one deformable structure. But in reality, both structures are deformable and movable, but in different magnitudes. Therefore, the bodies will interact and will act differently than in the simplified event. The interaction is neglected in this study because this should create a conservative solution and simplifies the problem substantially. Moreover, this is recommended in literature [81] and this behaviour is observed in a real case. However, this is not substantiated by research and should be confirmed by experiments.

Moreover, attention should be paid to the impact impulse when considering the collision interaction. A very large force applied for a very short time duration could be an insignificantly small impulse for the global response of a bridge pier. This phenomenon is considered when analysing the interaction.

8.3.2. Structural Geometry

The employed ship models are set-up by interpreting 2D drawings of the ships. Simplifications are applied in these models by using knowledge about steel structures, but without expertise in ship building. To obtain a completely valid 3D model, the model should be created with the consult of ship design engineers. Even more desirable is the use of a 3D model provided by ship design engineers, or a real design of a to be build ship. This could not be provided by the ship design companies consulted for this research.

Structural deficiencies in the form of welds and imperfections are neglected in this research to obtain sufficiently conservative results. However, the amount of conservatism could not be determined since the structural deficiencies are not investigated. A study on the influence of incorporating welds – notably the heat-affected zone – and imperfections (caused by the manufacturing process) is necessary to judge the conservatism of the results. With enough certainty, the estimations on maximum collision impact forces could be decreased.

8.3.3. NLFEA Parameters

The material properties used in the analyses are obtained from a general database of properties of ship building steel. The precise material properties of Dutch inland waterway ships could differ from the found properties. Experimental tests are necessary on the particular steel specimen from the same steel which is found in Dutch inland waterways ships to provide more certainty in the correctness of the applied material properties.

Moreover, mesh convergence tests should be performed for the type of analyses performed in this study. Convergence should be found within the results of the tests. With this, the optimal mesh size could be determined for dynamic simulations on the regarded ship types with sufficient confidence in the accuracy.

8.3.4. Generalisation of force-energy dependency

The conclusions of this study are mainly based on the behaviour of two ship's structures. The increased estimated impact force for relatively small ships is primarily a result of the analysed ship's bow structures. Nonetheless, this conclusion could have a big impact on the design of new bridges and more research is therefore strongly advised.

More ship samples should be investigated to provide certainty in the generalisation of the results of this study. These samples could be observed visually to make a qualitative judgement about the differences in the structure with the investigated ships. with that, a judgement can be made about the generalisation of the results to other ships. More comprehensively, other ship samples could be used for the nonlinear finite element analysis. Most input parameters could be kept similar as is applied in the performed analyses in this study, only the geometry, mass and plate thicknesses are to be changed. If a substantial amount of analyses are conducted on similar ship types, the maximum collision impact force for other ships could be found by data analyses instead of the force development during the collision – which is done in this study. Then, more certainty is

provided about the generalisation of the collision force results to ships with unknown collision force.

A

Dutch Inland Waterway Ship Classes

Scheepstypen

Bureau Voorlichting Binnenvaart

Klasse		
I	 Spits Lengte 38,5 meter - breedte 5,05 meter - diepgang 2,20 meter - laadvermogen 350 ton	 14 x
II	 Kempenaar Lengte 55 meter - breedte 6,60 meter - diepgang 2,59 meter - laadvermogen 655 ton	 22 x
III	 Dortmund-Eemskanaalschip (Dortmunder) Lengte 67 meter - breedte 8,20 meter - diepgang 2,50 meter - laadvermogen 1.000 ton	 40 x
IV	 Rijn-Hernekanaalschip (Europaschip) Lengte 85 meter - breedte 9,50 meter - diepgang 2,50 meter - laadvermogen 1.350 ton	 54 x
Va	 Groot Rijnschip Lengte 110 meter - breedte 11,40 meter - diepgang 3,00 meter - laadvermogen 2.750 ton	 120 x
Vb	 Groot Rijnschip Lengte 135 meter - breedte 11,40 meter - diepgang 3,5 meter - laadvermogen 4.000 ton	 160 x
Vla	 Tweebaksduwstel Lengte 172 meter - breedte 11,40 meter - diepgang 4 meter - laadvermogen 5.500 ton	 220 x
Vlb Vlc	 Vier- of zesbaksduwstel Lengte 193 meter - breedte 22,80 / 34,20 meter - diepgang 4 meter - laadvermogen 11.000 / 16.500 ton	 440 / 660 x
Va	 Standaard tanker Lengte 110 meter - breedte 11,40 meter - diepgang 3,50 meter - laadvermogen 3.000 ton	 120 x

Klasse		
Vb		 380 x
	Grote tanker Lengte 135 meter - breedte 21,80 meter - diepgang 4,40 meter - laadvermogen 9.500 ton	
Va		 60 x
	Autoschip Lengte 110 meter - breedte 11,40 meter - diepgang 2,00 meter - laadvermogen 530 auto's	
III		 16 x
	Containerschip Kempenaarsklasse Lengte 63 meter - breedte 7 meter - diepgang 2,50 meter - laadvermogen 32 TEU	
Va		 100 x
	Standaard containerschip Lengte 110 meter - breedte 11,40 meter - diepgang 3,00 meter - laadvermogen 200 TEU	
Vb	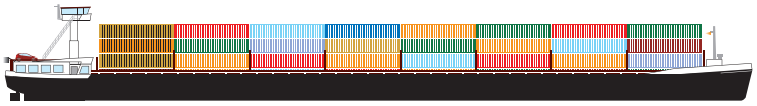	 250 x
	Groot containerschip Lengte 135 meter - breedte 17 meter - diepgang 3,50 meter - laadvermogen 500 TEU	
Va		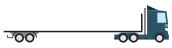 72 x
	Ro-roschip Lengte 110 meter - breedte 11,40 meter - diepgang 2,50 meter	
Vlb		 240 x
	Koppelverband (schip met duwbak) Lengte gemiddeld 185 meter - breedte 11,40 meter - diepgang 3,50 meter - laadvermogen 6.000 ton	
Vlb		 240 x
	Koppelverband (schip met schip) Lengte gemiddeld 185 meter - breedte 11,40 meter - diepgang 3,50 meter - laadvermogen 6.000 ton	

the Blue Road
duurzaam vervoer over water

B

Modelling of a Bow Geometry

For numerical analysis, hand calculations and practical understanding of the structure, a virtual 3D ship's bow model is drawn digitally. Original drawings of the structure from Concordia-Damen are used to create a (schematic) 3D structure, consisting of a hull, decks, frames and stiffeners. For the modelling of the ship's bow, commercial 3D CAD drawing software, Rhino, is used. Since geometry in this software is based on the NURBS mathematical model, complex double-curved structures can be modelled. With the Grasshopper3D (graphical algorithm editor) add-on, the geometry can be built by visual programming, which makes modifying the model easier. Afterwards, this complex double-curved geometry is simplified to nodes and four-point surfaces to use it in the NLFEA software ABAQUS/CAE. In this chapter, the process to establish a 3D FEA model is explained for one of the analysed ship's bows.

Ship Geometry The regarded ship is classified as CEMT class IV ship with dimensions LxB 85.95x9.6 m and a draught of 3.0 m. The bow of this ship is modelled until 0.5 m behind the bulkhead. Estimated is that a front part of 4.5 meters should be enough to model the collision onto a bridge pier, where this part will dissipate all kinetic energy involved.

The bow of this class IV ship is not modelled up to detail level. At some places, the model is a simplification of reality. For example, the hawse pipe and anchor are not included in the model as these elements will not contribute significantly to the overall stiffness of the bow of the ship. At this place, a global estimation is made for a replacement geometry which is structurally comparable to reality. Furthermore, the chain locker is simplified. In order to reduce computational time and to allow the use of a larger shell element mesh, the so-called 'Holland-Profielen (HP)' are smeared into plate panels. Their moment of inertia and cross-sectional area are calculated and reformed into plates consisting of a web and a flange. All simplifications that have been made are considered with an engineering approximation on their consequences to the overall stiffness of the hull with regard to the reality, by finding a balance between the accuracy of the schematic stiffness compared to the real stiffness and the simplicity of schematising.

The bow of the ship consists mainly of the hull, decks, frames and stiffeners. During the modelling process, these elements are created in the order of big to small to start off simple and add more complexity throughout the process. Globally, the complexity is reduced by dividing the double-curved hull into smaller flat elements to simplify the meshing and mainly, to simplify the addition of other elements connected to the hull.

At first, relevant parts of the drawings from Concordia-Damen are copied to a Rhino model and combined to create the double curved surface of the hull, see figures B.1 and B.2. At this point, the hull consists of four curved surfaces which are then mirrored to a full bow model. Hereafter, based on the locations of important sections, a 3D grid is defined. At intersections from the hull with the grid, points, or nodes, are created. After this step, a point cloud is defined with points that will define the final model. In this way, the schematic hull can be defined as four-point surfaces where other structural elements can be added easily, without gaps between the elements and the hull. This was a time-costly procedure since the geometry needs to be fully correct in terms of connection of elements, no overlapping and errors to import the file into the NLFEA software. Figures B.3 and B.4 show the CAD model. In appendix C, plots of the complete model can be found.

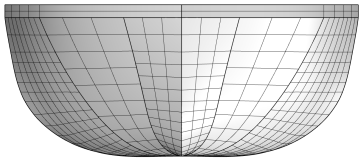

Figure B.1: Front view double curved base CAD model

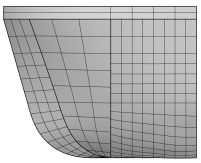

Figure B.2: Side view double curved base CAD model

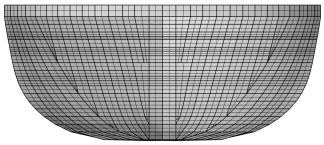

Figure B.3: Front view surfaces CAD model

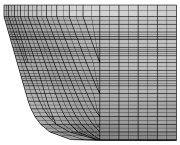

Figure B.4: Side view surfaces CAD model

Dimensions of members

The geometry in Rhino is created without thickness definition; this property is defined in ABAQUS. Therefore, all elements with the same thicknesses are grouped together and exported separately to ABAQUS. In this way, the definition of thickness can be done at a group at once. After the thickness property assignment, the parts are merged into one geometry and meshed. Thicknesses of the elements are shown in appendix C.

A simulation is run on this geometry, which is presented in chapter 7.

C

Geometries

C.1. Class IV ship - Complete CAD model

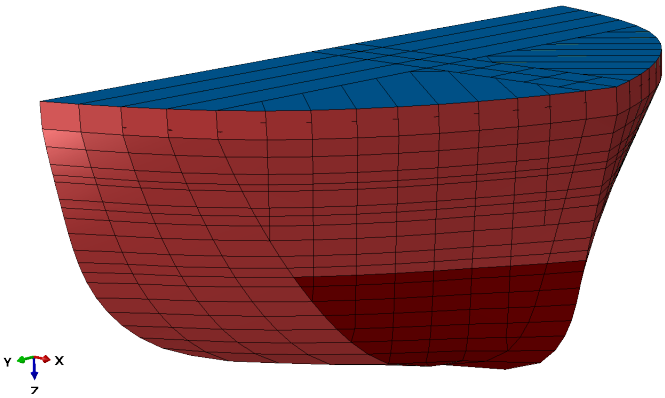

Figure C.1: Front 3D view CAD model

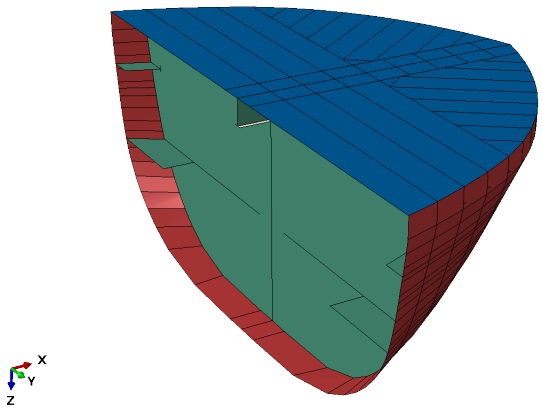

Figure C.2: Back 3D view CAD model

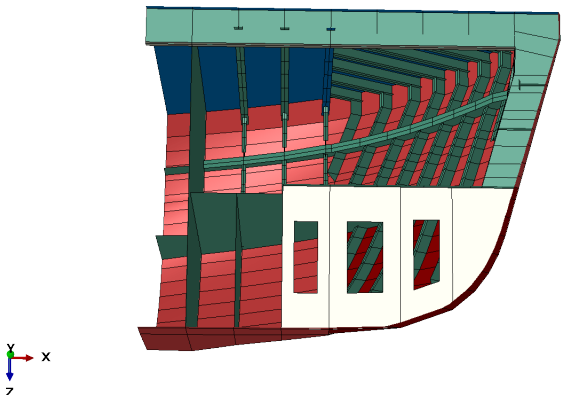

Figure C.3: Cut view CAD model

C.2. Class IV ship - Separate parts CAD model

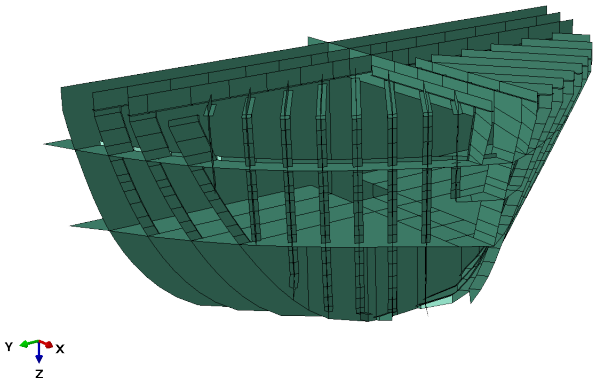

Figure C.4: Structure with thickness 8 mm

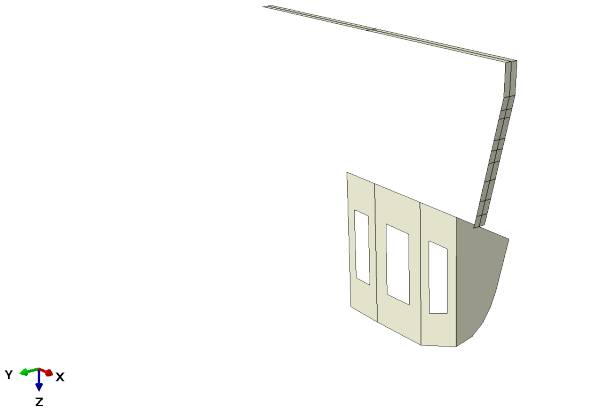

Figure C.5: Structure with thickness 10 mm

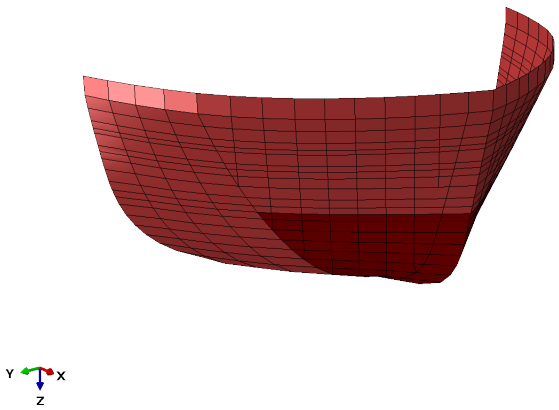

Figure C.6: Structure with thickness 11 mm (light red) and 16 mm (dark red)

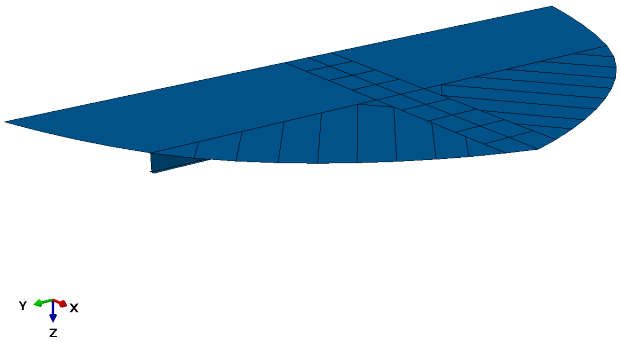

Figure C.7: Structure with thickness 12 mm

C.3. Class IV ship - Mesh model numerical analysis

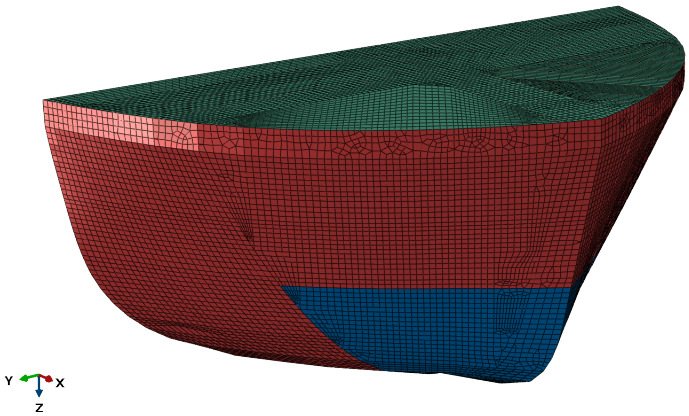

Figure C.8: Mesh 3D front view

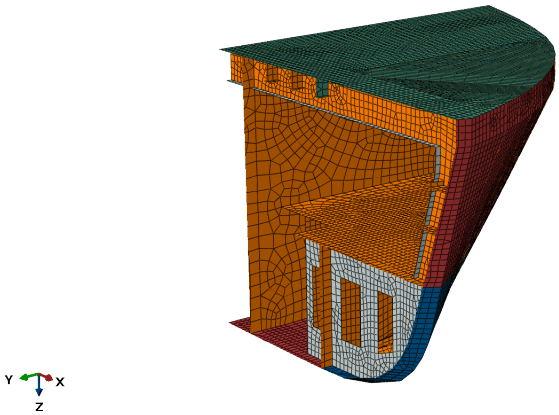

Figure C.9: Mesh 3D front cut view

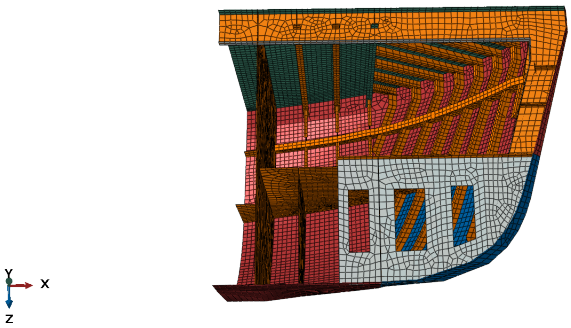

Figure C.10: Mesh 3D front cut lower view

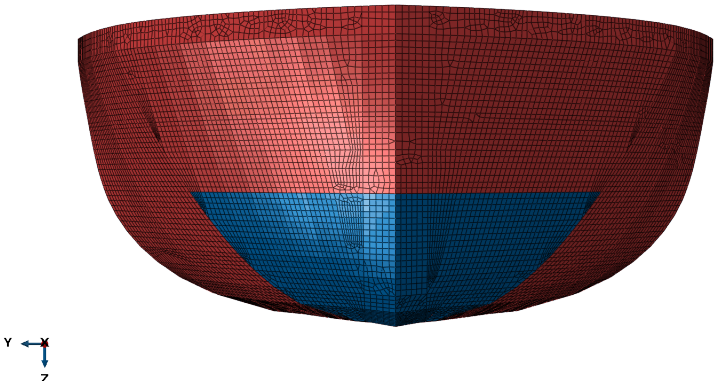

Figure C.11: Mesh front view

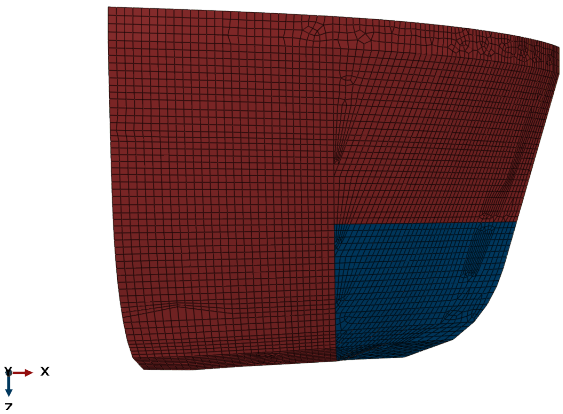

Figure C.12: Mesh side view

C.4. Sietske - Complete CAD model

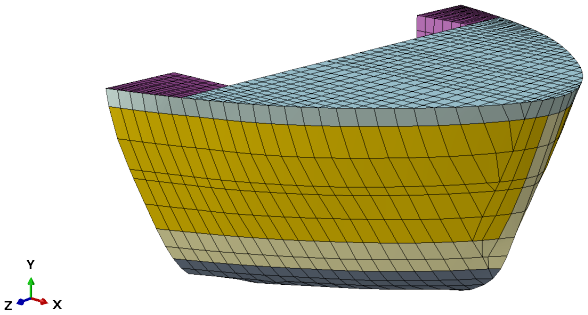

Figure C.13: Front 3D view CAD model

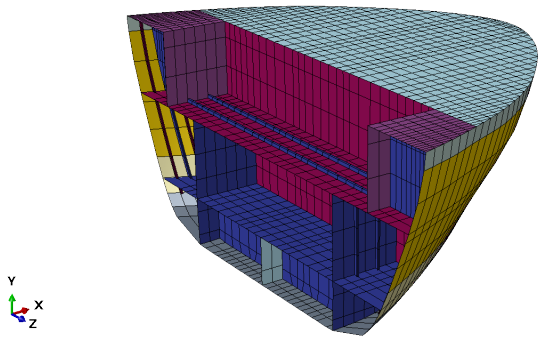

Figure C.14: Back 3D view CAD model

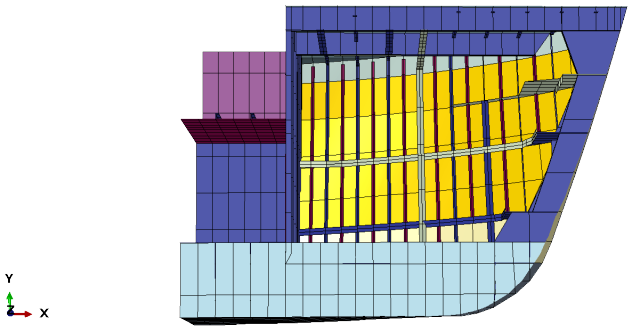

Figure C.15: Cut view CAD model

C.5. Sietske - Separate parts CAD model

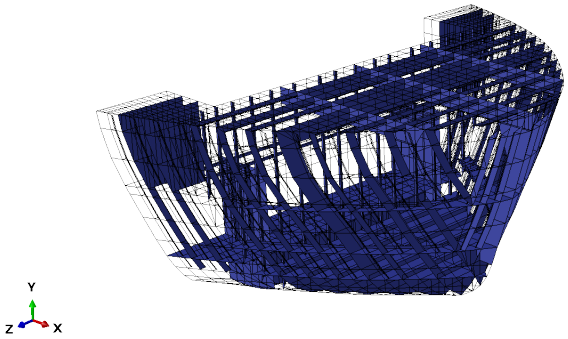

Figure C.16: Structure with thickness 8 mm

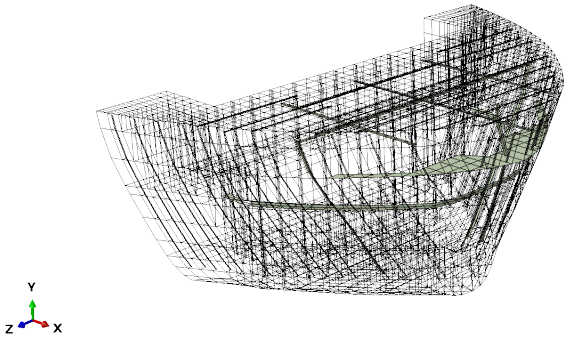

Figure C.17: Structure with thickness 10 mm

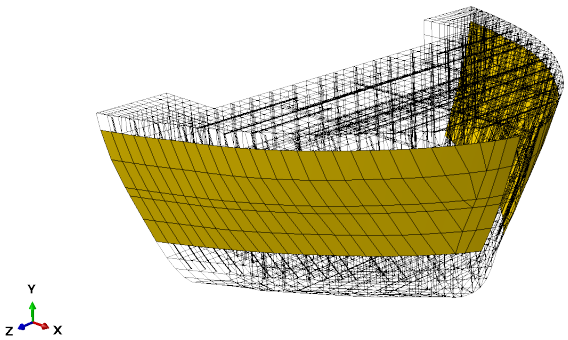

Figure C.18: Structure with thickness 11 mm

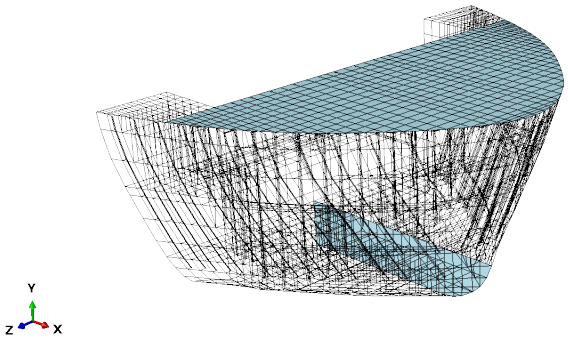

Figure C.19: Structure with thickness 12 mm

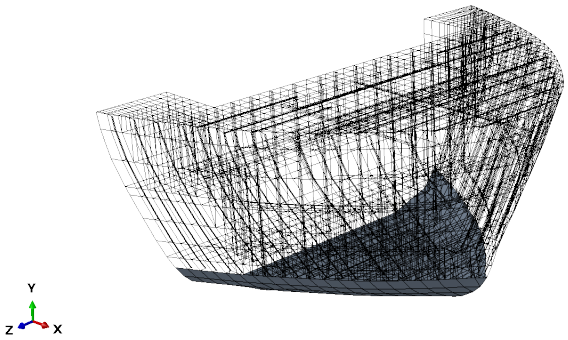

Figure C.20: Structure with thickness 13 mm

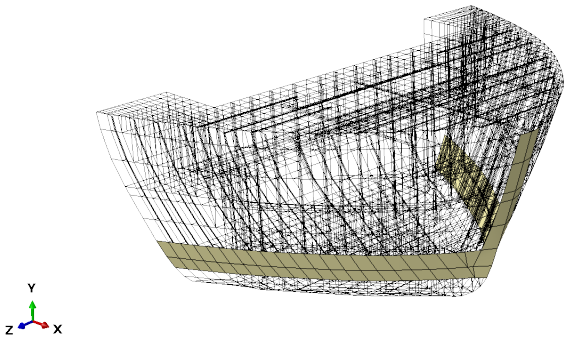

Figure C.21: Structure with thickness 16 mm

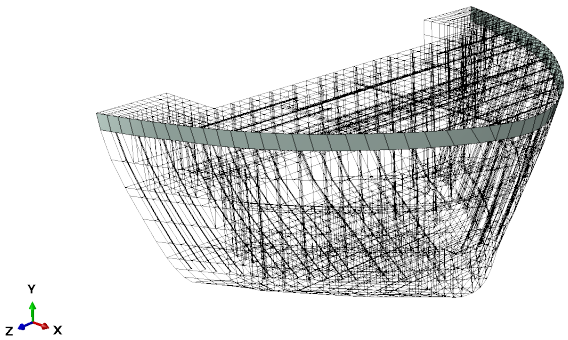

Figure C.22: Structure with thickness 25 mm

C.6. Sietske - Mesh model numerical analysis

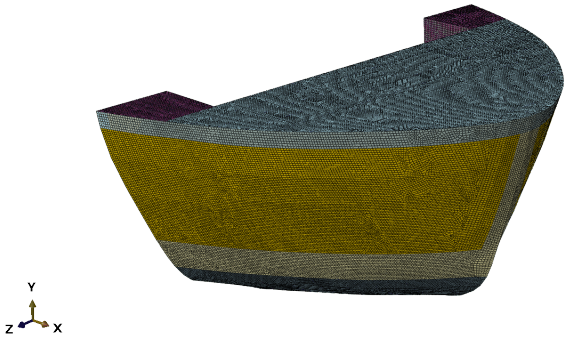

Figure C.23: Mesh 3D front view

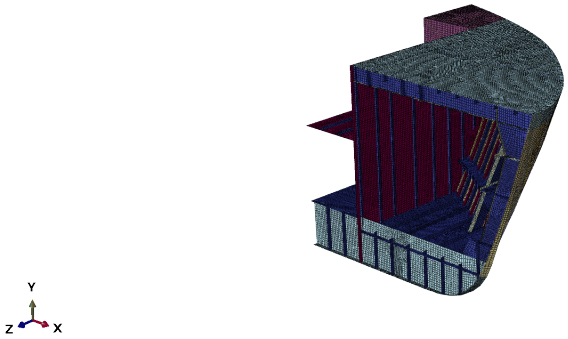

Figure C.24: Mesh 3D front cut view

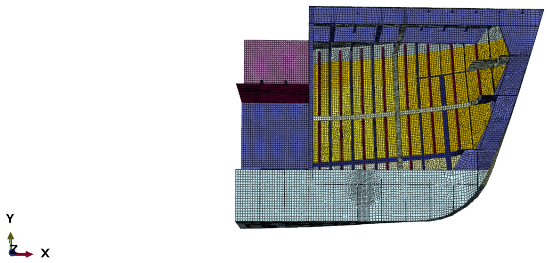

Figure C.25: Mesh 3D front cut lower view

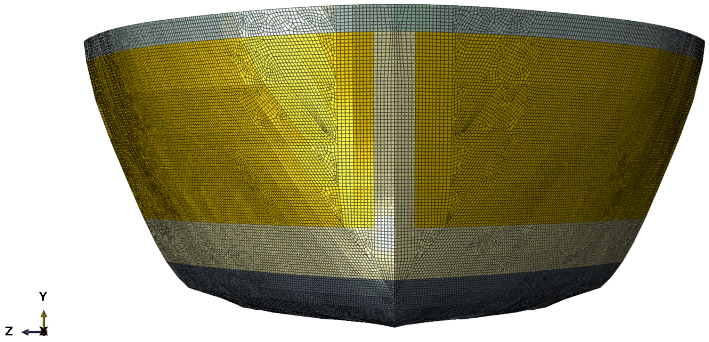

Figure C.26: Mesh front view

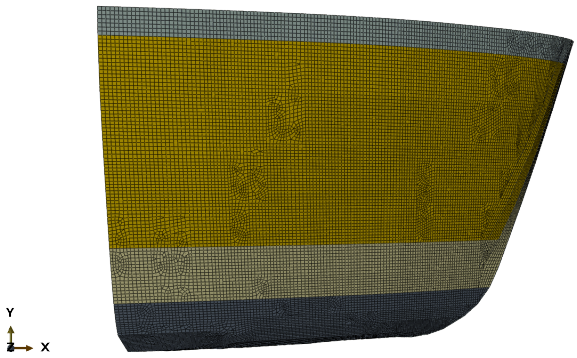

Figure C.27: Mesh side view

D

Material stress-strain relationship

Grade A steel test data is obtained by the study Paik et al.[56], where different uniaxial tensile tests are conducted to account for strain-rate dependency. This data is used to determine the material behaviour of the Grade A steel in the analyses of this work. The applied method is explained in section 4.2.

Tests with different dynamic modes are conducted (table D.1) according to rules of the ASTM [7]. At first glance, the impact mode seems to be the most interesting test for this work. However, during a collision, many different strain rates can occur, especially at buckling behaviour of plated structures. Therefore, the whole range of dynamic modes will be treated. Nonetheless, creep, and hypervelocity impact probably not occur in the simulations of this study.

Strain rate (1/s)	$< 10^{-5}$	$10^{-5} - 10^{-1}$	$10^{-1} - 10^{1.5}$	$10^{1.5} - 10^{4}$	$> 10^{4}$
Dynamic mode	Creep	Quasi-static	Dynamic	Impact	Hyper velocity impact

Table D.1: Dynamic modes of loading versus the strain rate [83]

D.1. Test data

The averaged test data for typical mechanical properties from quasi-static loading is presented in table D.2. These values are used in the simulations of this study. It is noted that the yield strength of the mild steel is not necessarily 235 MPa, which is a minimum requirement for mild steel, but is almost 300 MPa at room temperature.

	E[GPa]	σ_y[MPa]	σ_t [MPa]	ϵ_F	ν
Grade A	194.0	299.6	463.9	0.425	0.3

Table D.2: Mechanical properties of mild steel (grade A) at 20°C [56]

E is the Young's Modulus (or modulus of elasticity), σ_y the yield strength, σ_t the ultimate tensile strength, ϵ_f the fracture (total breaking) strain and ν the Poisson's ratio.

Figure D.1 presents the details of the test results. The figure presents the stress-strain relationships of the material for different loading speeds. Generally, it is observed that the yield and ultimate tensile strengths tend to increase with increasing loading speed, while the fracture strain tends to decrease. Moreover, it is found that the work hardening decreases with an increase in the strain rate.

D.2. Curve fitting

Some steps need to be undertaken to obtain true stress-strain relationships for different strain rates.

1. Digitise graph data

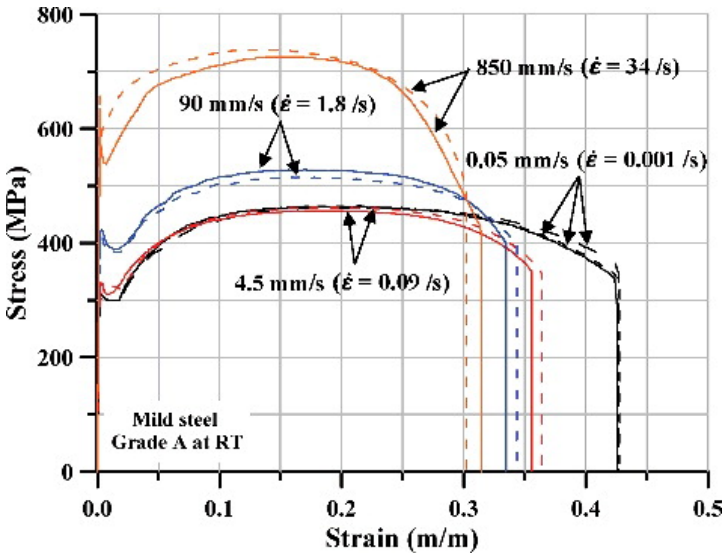

Figure D.1: Engineering stress-engineering strain curves for mild steel Grade A at 20°C for different strain rates[56]

2. Convert engineering stress-strain data to true strain and true stress data
3. Fit true stress-strain data on an equation for extrapolation

Step 1 At first, data is generated from the test results. The graph is digitised and the data is extracted. Table D.3 shows the extracted values.

Step 2 To convert engineering stress-strain to true stress-strain, traditional conversion equations are used, see eq. 4.3 in section 4.2. These equations are only valid up to the strain of ultimate tensile strength. Therefore, the data is cut off at the maximum engineering stress level.

Step 3 Up to this point, the true stress-strain relationships for different strain rates are known. Since the material behaviour after necking is necessary to be known, an extrapolation is made. This extrapolation is conducted by fitting the data on functions describing the material behaviour to calculate extra data points afterwards. The plastic behaviour can be described by the power law as proposed by Hollomon, eq. 4.4 presented in section 4.2.

However, since strain-rate dependency needs to be incorporated (described in chapter 4), extra variables are needed to fit the data. The Cowper-Symonds model is utilised, also known as the Plastic Kinematic Hardening model which is described in section 4.2. This model is combined with the power law to eventually form eq. 4.6 where the data is fitted on.

First, estimations are done to start iterations and compare for validity. Cowper-Symonds variables C and q are often taken as $C = 40.4\ s^{-1}$ and $q = 5$. K and n are the power law variables. In the Hollomon's expression, the strain-hardening exponent measures the ability of a metal to strain-harden, larger magnitudes indicate larger degrees of strain hardening. For most metals, the strain-hardening exponent falls between 0.10-0.50. Table D.4 shows typical power-law hardening parameters for steel alloys. These values provide a first approximation. From the data fit generated in this study, the values should be comparable. The $\dot{\epsilon}$ in eq. 4.6 followed from the test speed used for the uniaxial tension tests.

To find the best-fit parameters of eq. 4.6, the least-squares curve fitting method is used with initial values: $C = 40.4\ s^{-1}$, $q = 5$, $K = 700$ MPa and $n = 0.2$. The best-fit is found using Excels' solver. Found parameters are shown in table D.5.

The obtained values which describe the true stress-strain relation in terms of strain hardening of the material are closely related to the initial values which provides confidence. The values which describe the strain-rate hardening differ by around a factor 2. This is still within realistic limits.

$\dot{\epsilon} = 0.001s^{-1}$		$\dot{\epsilon} = 0.09s^{-1}$		$\dot{\epsilon} = 1.8s^{-1}$		$\dot{\epsilon} = 34s^{-1}$	
ϵ_e[-]	σ_e[MPa]	ϵ_e[-]	σ_e[MPa]	ϵ_e[-]	σ_e[MPa]	ϵ_e[-]	σ_e[MPa]
0.003731	309.1946	0.003288	327.5607	0.001774	390.771	0.000341	543.3391
0.008495	300.0248	0.008993	310.2303	0.015621	390.69	0.006548	541.255
0.019012	299.0351	0.025324	349.0535	0.0309	415.174	0.022306	598.5007
0.030096	343.9653	0.044526	388.9054	0.045703	452.9713	0.039973	658.8069
0.042588	375.6344	0.063218	412.4293	0.06337	483.5847	0.065757	689.3728
0.063689	408.349	0.087645	433.929	0.085812	505.979	0.099181	710.6789
0.08573	432.903	0.107742	442.1509	0.115894	519.1136	0.129741	722.7868
0.101044	440.0906	0.139319	452.447	0.143588	524.071	0.149795	725.7411
0.123541	452.401	0.171365	457.6425	0.18131	526.9219	0.168417	725.6322
0.150803	456.5622	0.20149	458.7507	0.209482	526.7571	0.199932	718.2806
0.176632	461.7395	0.229699	457.8126	0.238131	519.4223	0.222851	701.7642
0.201018	461.8106	0.251205	452.7732	0.26296	510.062	0.242428	677.0763
0.229226	460.8724	0.278446	445.7098	0.286357	492.5189	0.253888	654.4837
0.251215	457.8753	0.300895	433.5304	0.308799	465.7665	0.268213	612.4203
0.273684	455.9	0.329525	403.0016	0.324079	429.8409	0.280628	564.2248
0.300925	448.8366	0.350977	369.3907	0.333629	399.0683	0.292087	516.0349
0.328151	434.6302	0.35525	353.0766			0.304502	465.7916
0.351559	423.474					0.313097	423.7618
0.378292	401.1029						
0.400716	375.6581						
0.414541	354.2698						
0.424071	336.9507						

Table D.3: Obtained engineering stress-strain data

The material model is described with the following equation:

$$\sigma_d = (1 + (\frac{\dot{\epsilon}}{74.4})^{\frac{1}{2.4}}) \cdot \max(300.7; 722.0 \cdot \epsilon^{0.19}) \tag{D.1}$$

Material	n	K [MPa]
Low-carbon steel (annealed)	0.26	530
4340 steel alloy (tempered @ 315 °C)	0.15	640
304 stainless steel (annealed)	0.450	1275

Table D.4: Tabulation of n and K Values for several steel alloys [13]

σ_y [MPa]	C [s^{-1}]	q	K	n
300.7	74.4	2.4	722.0	0.19

Table D.5: Values fitted from experimental data[56], determining the regarded material behaviour

E

DNVGL-RP-C208 Failure criterion - critical gross failure strain

Determination of critical gross failure strain is done using Calibration Case CC01 of the document DNVGL-RP-C208 [18]. It is found by making a calibration analysis with the actual element type and with an element size relative to thickness t x t and 5t x 5t. The gross yielding strain limit is determined using given deformation limits. The deformation limits of section 5.1.6. are used for this study as values in this section are given for cases where low capacity is unfavourable, such as collision analysis. For different steel strengths, different deformation limits are provided. In this study S235 is used, which gives a deformation limit of 80 mm. The calibration is obtained using ABAQUS. Results are shown in figures E.1 and E.2.

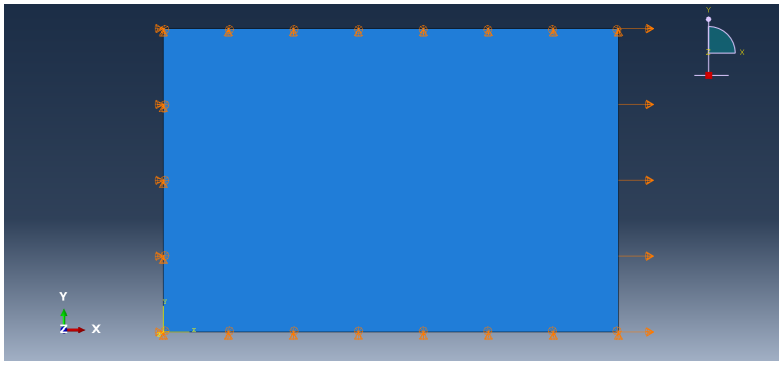

Figure E.1: ABAQUS CC01 quasi static test model. Displacement on one edge is increased from 0 mm to 80 mm linearly at time=0 s to 1 at time=1 s.

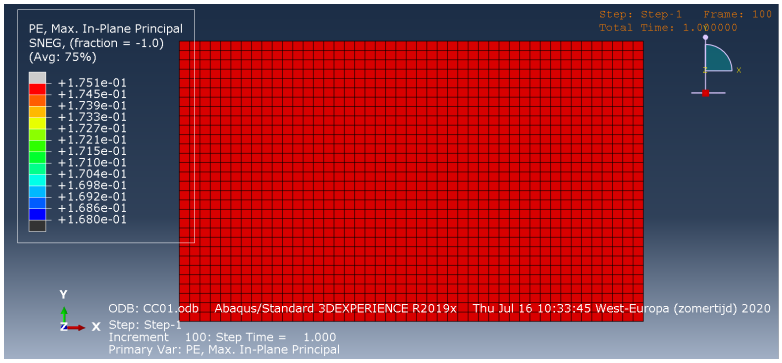

Figure E.2: PE principal strain at last increment where deformation is 80 mm.

A gross failure strain is found of $\epsilon_{crg} = 0.1778$

F

Visual Results of First Class IV Analysis

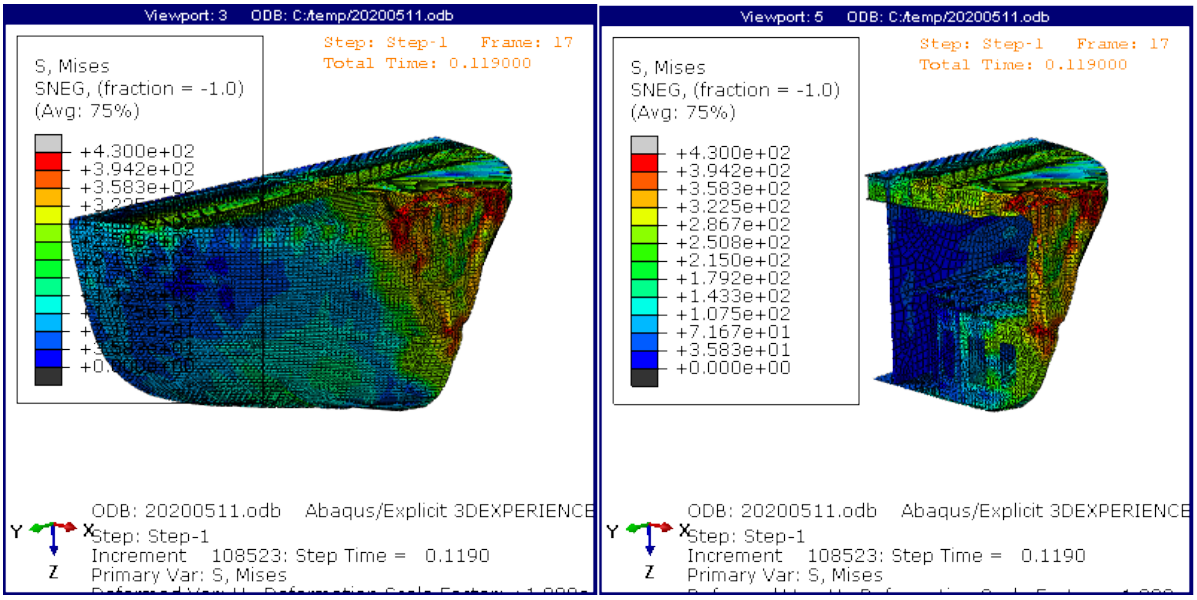

Figure F.1: CEMT IV simulation t = 0.119 s

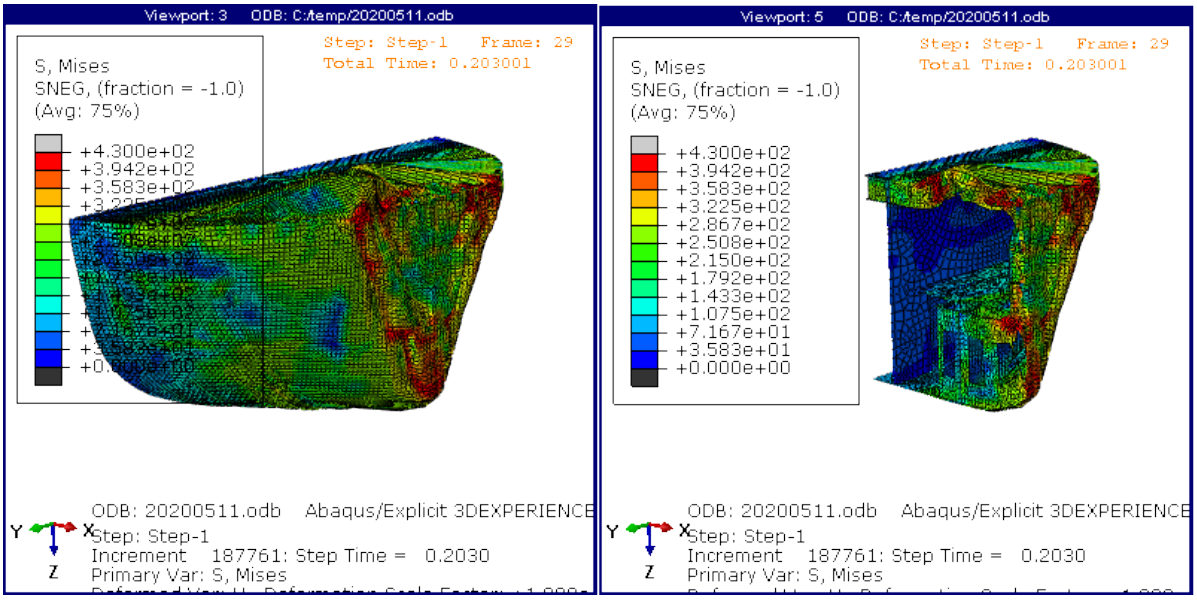

Figure F.2: CEMT IV simulation t = 0.203 s

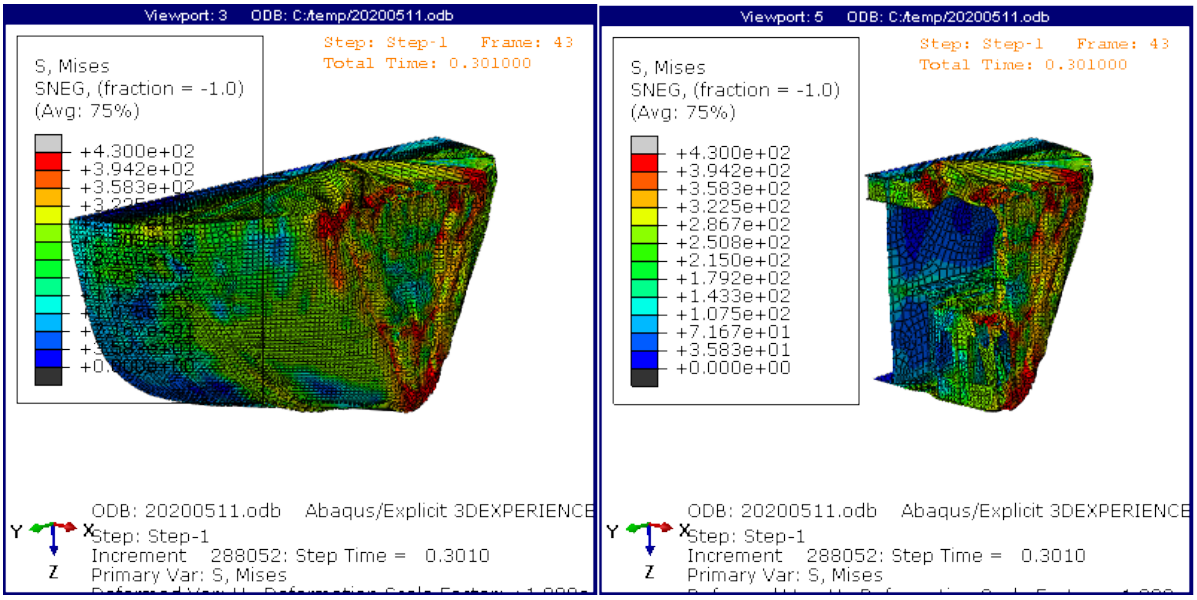

Figure F.3: CEMT IV simulation t = 0.301 s

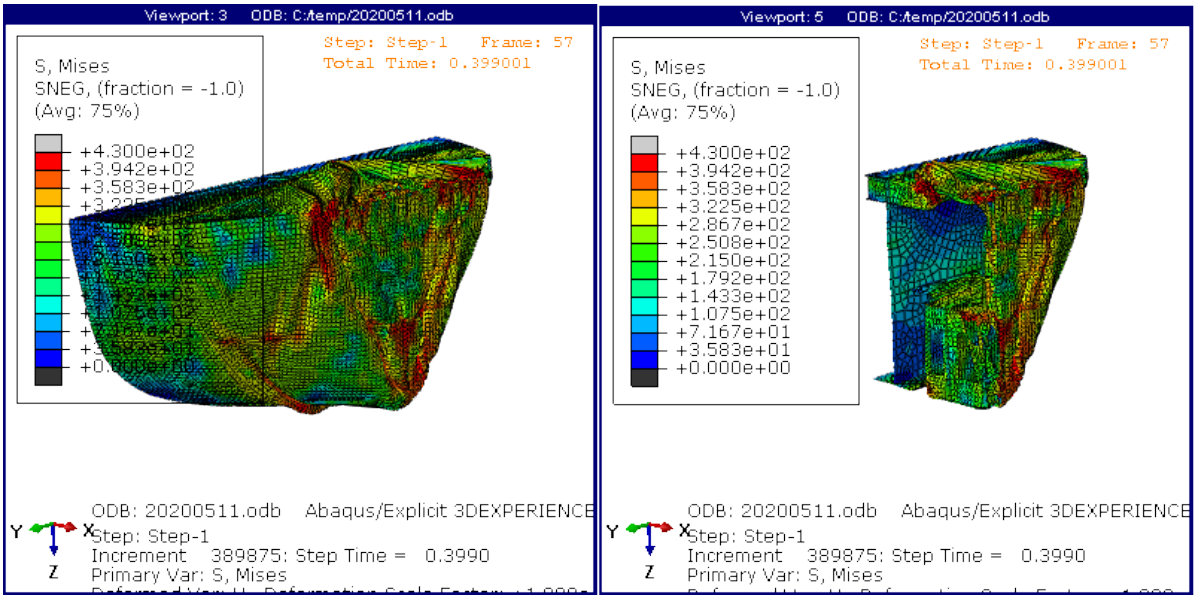

Figure F.4: CEMT IV simulation t = 0.399 s

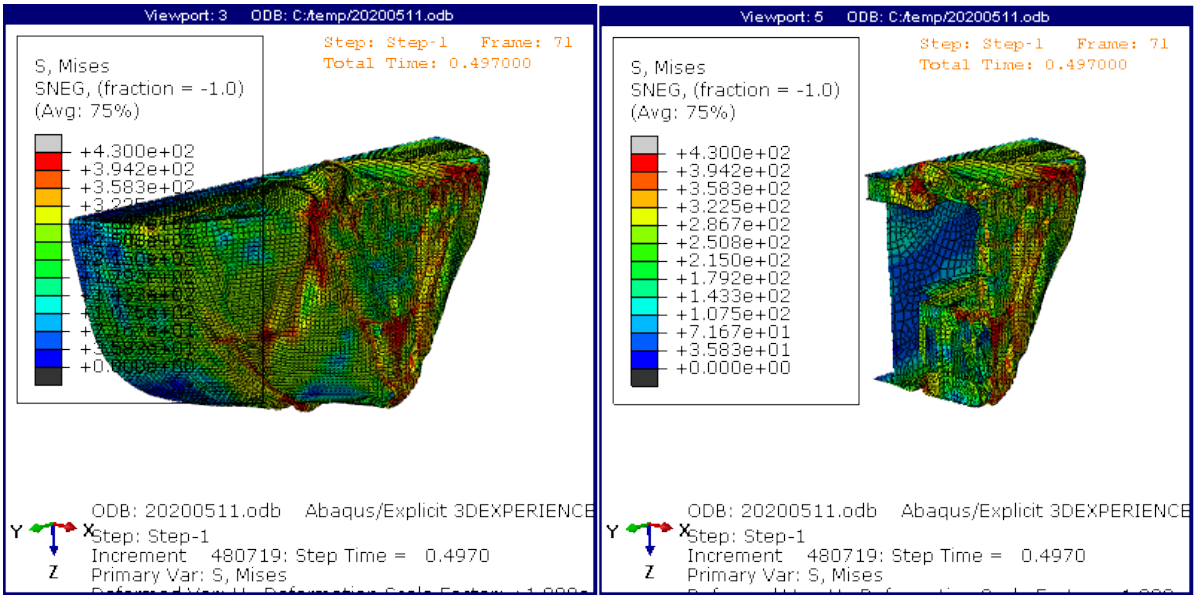

Figure F.5: CEMT IV simulation t = 0.497 s

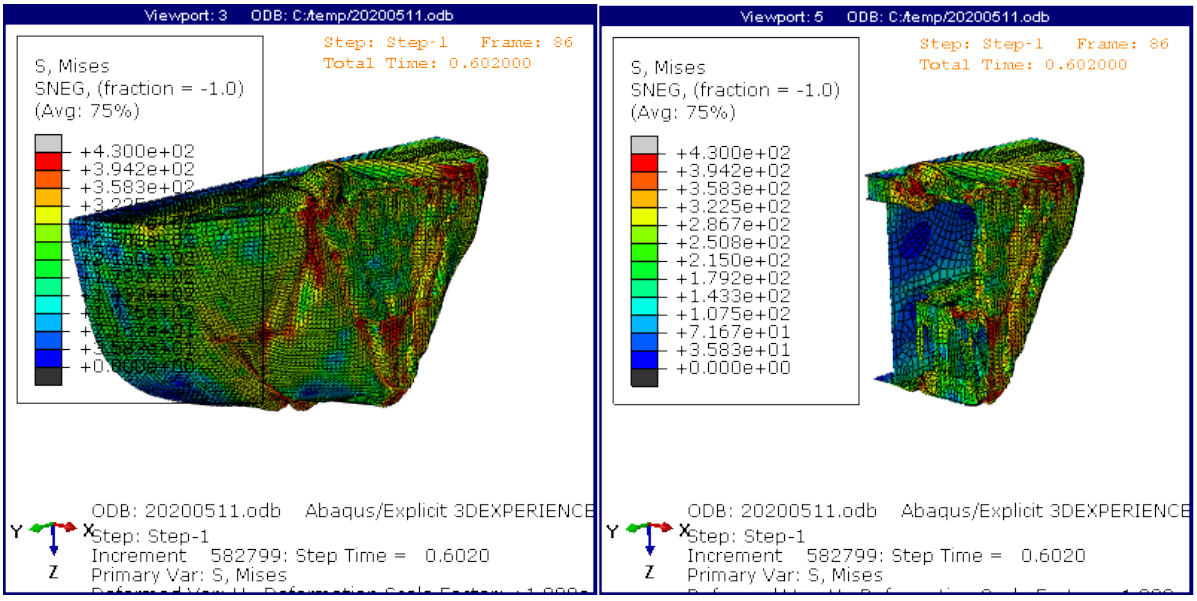

Figure F.6: CEMT IV simulation t = 0.602 s

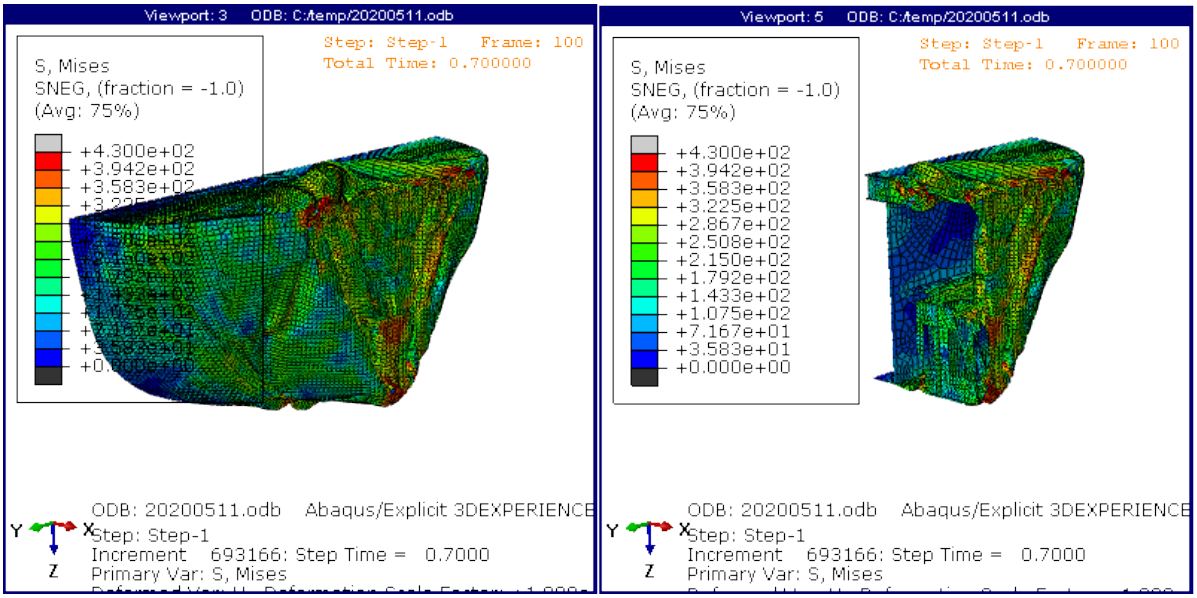

Figure F.7: CEMT IV simulation t = 0.700 s

G

Interpretation of First Results

A first explicit dynamic finite element analysis was conducted for the class IV ship bow. This simulation is performed using different parameters than for the final simulations which are described in 4, since the final parameters are the outcome of an iterative process of which this simulation was part of. Appendix F shows screenshots of the visualisations of the Mises-stresses on the deformed structure during the collision process.

The crush depth (in terms of displacement), reaction force on supports and energy levels were extracted from the finite element simulation data. Force results obtained from the simulation are presented in figure G.1. Visualisations of the stresses and strains are shown in appendix F. It is noticed that the impact force-time-history could be divided into four periods: the initial stage during which the impact force increases rapidly; the second stage during which the impact force fluctuates, the third stage during which the force is constant, and the final stage during which the impact force decreases rapidly as the kinetic energy is dissipated. Remarkable are two locations where almost equal peak forces are presented, at a depth of around 0.7 meters and around 1.3 meters, these are marked as the maximum impact force.

The curve shows many local ups and downs, which may be caused not only by the complexity of the deformation process but also by numerical effects. This could be caused by removal of the finite elements in which the ultimate plastic strain is exceeded in the integration points, and by the contact algorithm, which exploits only a set of discrete points of the ship. The local fluctuation decreases gradually together with decreasing velocity.

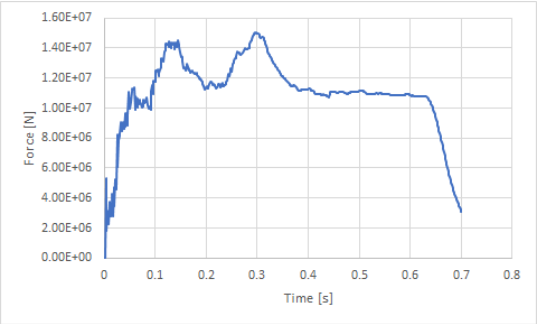

Figure G.1: Force over time CEMT IV ship

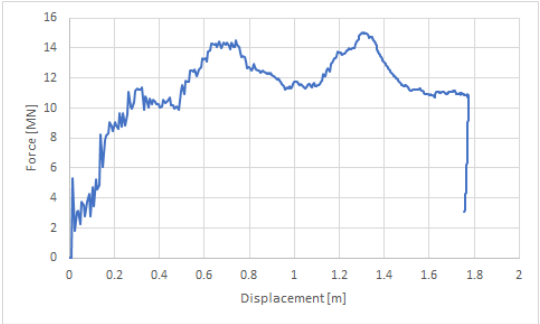

Figure G.2: Force over displacement CEMT IV ship

Maximum impact force is of this simulation is 15 MN. Maximum crushing depth is about 1.8 meters.

The energy levels plotted in figure G.3 show the decreasing kinetic energy until fully dissipated, followed by a slight increase as strains are released. Plastic dissipation is the main contributor to the dissipation of kinetic energy, which can be confirmed by the visualisation of the strains and stresses where high stress levels are reached. The total energy is constant during the simulation, as is expected from a closed system. And the artificial strain energy is about 10% which is acceptable, as discussed in paragraph 4.6.2. The frictional energy is only 2.5% with this head-on collision.

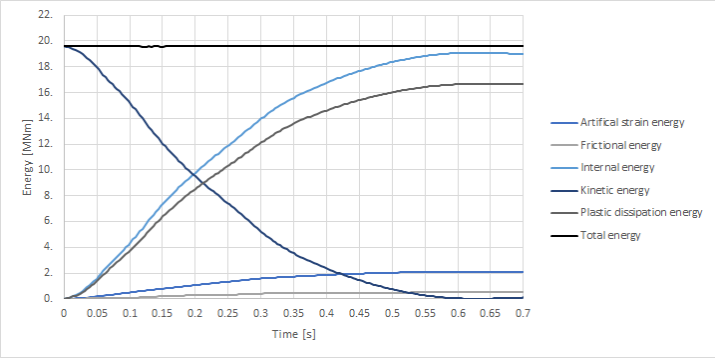

Figure G.3: Energy levels during collision simulation

G.1. Failure analysis

The forces are extracted separately per supported structural element and then compared to the visualisation of the stresses and deformation to gain understanding about the complex deformation process. Since the forces are generated at the unsupported end of the structure, and elements within the structure are connected, the extracted support forces do not correspond one to one with the actual forces within each element. However, it gains some extra insight into the distribution of forces. Important to note is that support forces per mesh element are combined and summed per structural element, this results in the forces shown at figure G.4. Characteristic points are noted, and (failure) events within the crushing process are described in table G.1.

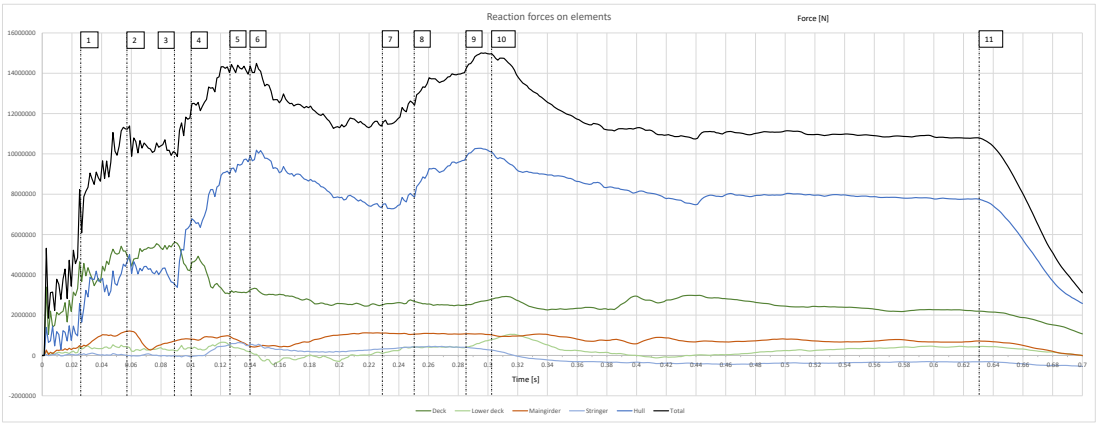

Figure G.4: Reaction force over time on different elements

G.2. Visual validation

The deformation process of results from the NLFEA are compared to a collision event presented in chapter 1, of the Eemshorn. This ship hit the structure with an initial energy level of 22 MNm. From the vessel tracking system AIS it is found that this collision happened at a right angle, which is equal to the frontal collisions of the present study. Therefore, a good comparison could be made. A visualisation of the moment where the deformation development is on the same level as the eventual deformation from the Eemshorn is shown in figure G.5. This is not the ultimate deformation from the class IV ship since the class IV ship contains more kinetic energy which consequently ensures a deeper penetration.

Globally, the structures are deformed in a similar manner. The main difference is caused by the fact that the collided structure did not cover the entire frontal area of the ship's bow for the Eemshorn collision. This was a part of the *Oosterscheldekering* (see figure 1.4) which spanned above the water level. The collided structure of the class IV ship is set-up in such way that its area covers the full frontal area of the ship's bow. This difference

Nr.	Event
1	Stringer activation by failure of frontal elements
2	Front girder failure and maingirder buckling → more force to deck
3	Collision of lower deck, force distribution to hull
4	Deck buckling followed by activation of radial stiffeners, increase in hull force because of stiffness stringer and lower deck
5	Stringer support buckling, introduction of bending moment on main girder
6	Buckling of lower hull followed by main girder+deck folding
7	Frontal bow part completely crushed → lowerdeck activation
8	Buckling of lower side hull behind stiff section
9	Lowerdeck buckling
10	Folding of front structure into back structure
11	Kinetic energy is equal to zero and fully dissipated into the structure

Table G.1: Failure events during the collision

Figure G.5: Deformation of class IV ship during collision process at t=0.27 s.

Figure G.6: Deformation of the ship Eemshorn after collision with bridge pier.

is clearly seen. The bottom of the Eemshorn ship's bow which is not directly hit by the structure is relatively undeformed.

Remarkable is the tearing of the frontal side plating of the Eemshorn; this is not observed in the deformed structure of the class IV ship. This could be caused by a difference in internal structure, which is unknown for the Eemshorn. This could also be the cause that the Eemshorn is only deformed in the frontal part of the structure, where the class IV ship shows already deformation deeper in the structure. It is noted that in the 'mid-bow' part of the class IV ship, a structural discontinuity is observed, it is possible that this is not the case for the structure of the Eemshorn.

G.3. Comparison with standards

With information about the DWT, initial velocity and kinetic energy, a comparison can be made with codes. The Dutch code for Rijkswaterstaat bridges (ROK)[59], the Eurocode[47] and the American code for bridge design (AASHTO)[2] are studied to calculate impact force for the considered ship. The different codes are treated more comprehensive in section [follows later].

DWT	1263 tonnes
Velocity	5.6 m/s
Kinetic energy	$0.5 * DWT * v^2 = 19.8$ MNm

Table G.2: Energy CEMT IV ship

Figure G.7 shows the results obtained with various formulas from codes. The ROK the largest estimate of the collision force, but coincides with the AASHTO for this energy level. The Eurocode seems to underestimate impact force but is equally distant from the numerical analysis results as the ROK and AASHTO are.

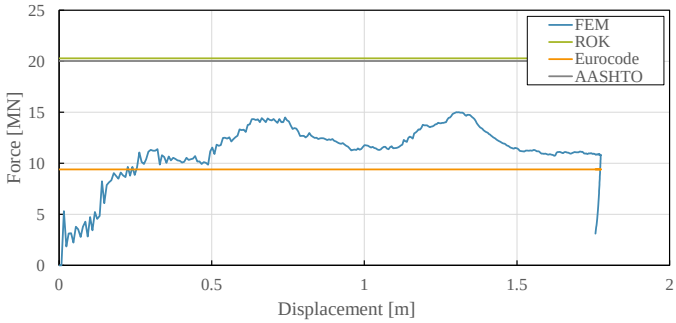

Figure G.7: Force-displacement curve and maximum forces according to standards.

G.4. Comparison with previous studies

Joustra and Pater First, a comparison is made with the underlying study for the ROK guidelines on collision forces, shown in figure G.8. Parameters of the finite element analysis are chosen equal if possible, in a way that results can be compared fairly.

	class IV ship	Simulation JP-A1	Simulation JP-A5
DWT	1263 tonnes	3000 tonnes	1500 tonnes
Velocity	5.6 m/s	5.6 m/s	5.6 m/s
Kinetic energy	19.8 MNm	47.8 MNm	23.9 MNm

Table G.3: Kinetic energy level of conducted simulation in comparison to simulations conducted by Joustra and Pater(JP)[35].

Simulation JP-A1 is a frontal collision with the Thomar, the ship regarded in the background study of the ROK guideline on ship collision forces. Simulation JP-A5 is a comparative analysis with the same model but provided with a lower mass, and therefore, lower energy level. The kinetic energy level of simulation JP-A5 is more comparable to the energy level obtained from the class IV ship in this study. In both graphical comparisons, it can be seen that the energy levels are greater than the regarded ship in the conducted simulation since the area under the force-displacement curves is larger. As a consequence of the higher initial energy level, the simulations JP-A1 and JP-A5 resulted in larger crushing depth. Remarkable is that simulations JP-A1 and JP-A5 of Joustra and Pater show a linear character globally, with a line starting from the origin, while the class IV ship simulation shows a relatively steep force-displacement curve from the start, followed by a fluctuating curve around a flat line.

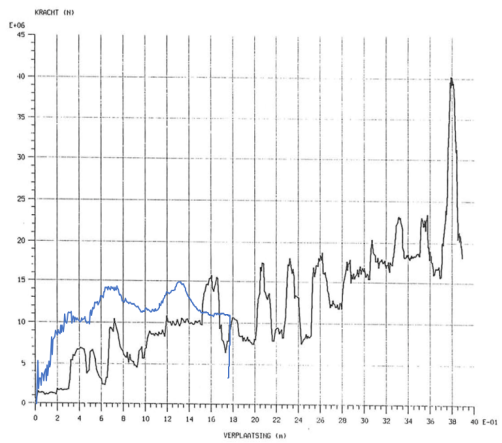

Figure G.8: Force-displacement curve of simulation on class IV ship (blue line), and simulation JP-A1 (black line).

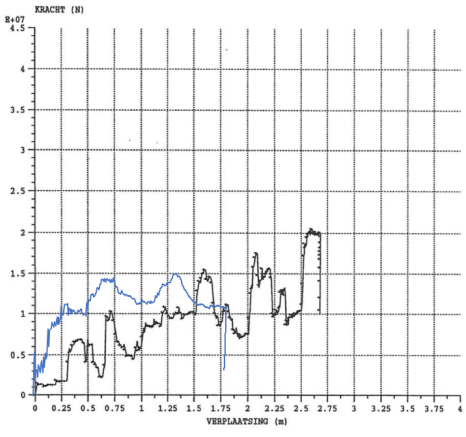

Figure G.9: Graphical comparison of output with Joustra and Pater study simulation A5 (black line) [35] and finite element analysis force history of CEMT IV ship(blue line).

One can say that the class IV ship simulations show a more stiff character of the ships' bow, especially at the first 0.4 meters of the crushing zone as the curve is constantly well above the simulations of Joustra and Pater. From the structural information of the ship bow model, the same conclusion can be drawn. Whereas the bow of the regarded class IV ship in this study is formed with a line of stiffeners in a low angle to the collision direction, these stiffeners are not present in the model of Joustra and Pater where only stiffeners are present perpendicular to the collision direction (frames). Moreover, the thickness of the elements is generally 1 mm less in the model of the Joustra and Pater study. Both differences should result in a variation in stiffness between the regarded models. Besides numerical analysis differences in the simulations, these geometrical differences can an explanation for the difference in stiffness characteristics between the simulations.

Despite these differences in curve development over the crushing depth, the maximum impact force is comparable, considering the crushing depth. Over 1.8 meters depth, the maximum impact force of all simulations is around 15 MN.

H

Berdina Result Extrapolation

As mentioned in chapter 7, the modelled geometry of the Berdina is too short for dissipating all initial kinetic energy. After $t = 0.5$ seconds, the support conditions at the end of the ship bow have too much impact on the results and will therefore not be used. However, the result data up to $t = 0.5$ seconds is considered as valuable data for an estimation of the collision force for the Berdina.

The goal of this analysis is to determine the maximum collision impact force for the Berdina. Data about the kinetic energy, plastic dissipation energy, displacement and force are used up to $t = 0.5$ s. This data is analysed and extrapolated to find approximations for the total time duration of the collision process, the maximum displacement (or penetration depth) of the ship. With this information, the estimation of collision force is determined for the Berdina. This is all done under the main assumption that the collision process after $t = 0.5$ s behaves similarly as before this time, in terms of force, energy and displacement.

Mainly the kinetic energy(KE) curve is determining for the total collision duration as the collision is considered as ended as the kinetic energy is zero. The main contributing factor of the kinetic energy dissipation is the plastic dissipation energy(PDE). From the simulation of the class IV ship and the Sietske, a mean contribution factor of the PDE of 0.86 is found. This means that 86% of the initial kinetic energy is dissipated by plastic deformation in the structure.

An extrapolation of both the kinetic energy and the plastic dissipation energy is performed (see figure H.1a and H.1b) to find the moment at which the kinetic energy is zero. The curve of the kinetic energy over time curve is considered as (negative) second-order polynomial curve ($KE(t) = -At^2 - Bt + C$), starting at the value of initial kinetic energy. The development of the PDE is considered equal to the inverse of the kinetic energy function and starting at zero and is multiplied by 86% to take its contribution into account. ($PDE(t) = 0.86 \times (At^2 + Bt + 0)$). Parameters A and B are taken as equal for both functions, to emulate an equal development.

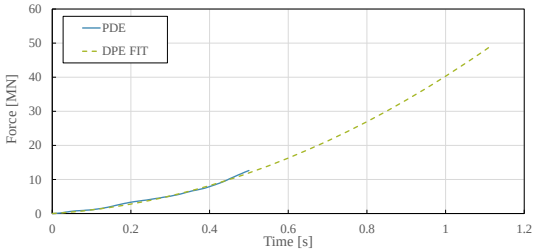

(a) Plastic dissipation energy (PDE) during simulation for Berdina.

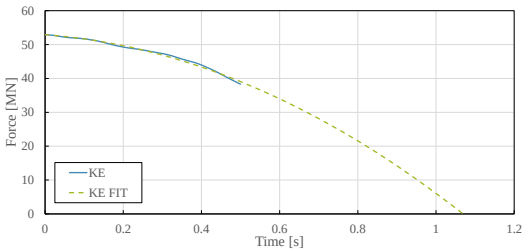

(b) Kinetic energy (KE) during simulation for Berdina.

Figure H.1: Polynomial curve fit on Berdina KE and PDE development over time.

Least squares multiple regression is performed to fit both curves at the same time for a combined fit. The obtained curve performs very well with the reference data ($R^2 = 0.994$ for PDE and $R^2 = 0.992$ for KE). Thereafter,

the function of the kinetic energy is solved to find its intersection with zero:

$$KE(t) = -38.30\,t^2 - 8.56\,t + 52.90 \tag{H.1}$$

The intersection is found at $t = 1.07$ seconds. At this point, the kinetic energy should be completely dissipated.

Linear regression is applied to the force-time curve. This is an arbitrary decision which is based on estimates about the force development and structural information of this particular ship model. A linear function to evaluate the mean force over time is established with all force-time data up to $t = 0.5$ seconds and is defined to start at zero. Another linear function is obtained to form a peak force function. This function is fitted on (arbitrary) defined local peaks within the reference data. In figure H.2 the curves are plotted. Four data points are highlighted, which are used as reference data for the regression of the peak force. Note that the shown functions are in units of seconds and newtons. When calculating with meganewtons, this function states:

$$F(t) = 22.9\,t + 2.67 \tag{H.2}$$

The intersection point of kinetic energy equal to zero is filled in in eq. H.2 to calculate the eventual maximum collision force of 27.15 MN.

A short analysis is done with previous information in combination to displacement-time and force-displacement data. By taking the integral of the linearly regressed force-displacement function (the area under the curve for $W = Fu$), the maximum displacement can be obtained by setting this equal to the initial kinetic energy. The maximum displacement is then estimated at around 5000 mm. This is in agreement with a short analysis of the force-displacement curve. At $t = 1.07$ seconds, a displacement of about 5000 mm is approximated. This is considered a quick check on the validity of the maximum collision force calculation.

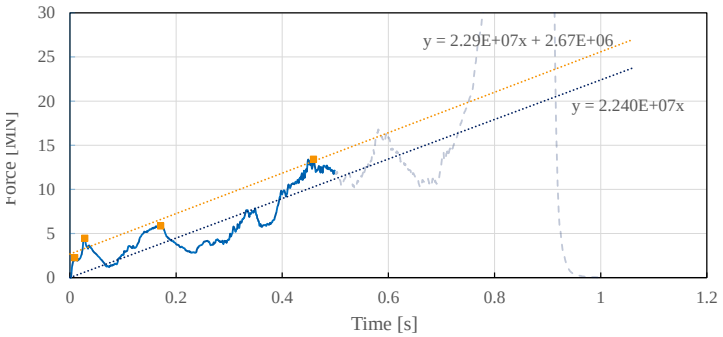

Figure H.2: Berdina force over time curve with linear regression curves for mean(blue) and peak(orange) forces. Reference peak data points are highlighted.

I

Numerical Analysis Final Simulation Visualisations

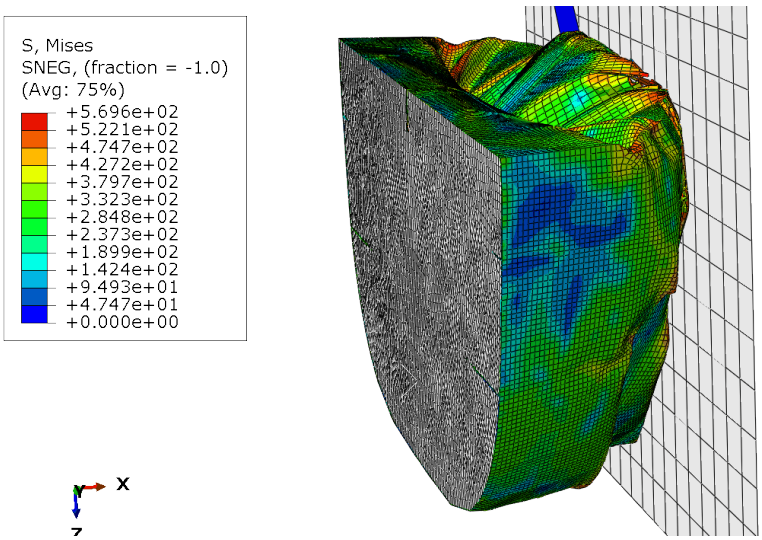

Figure I.1: class IV simulation t = 1.0 s

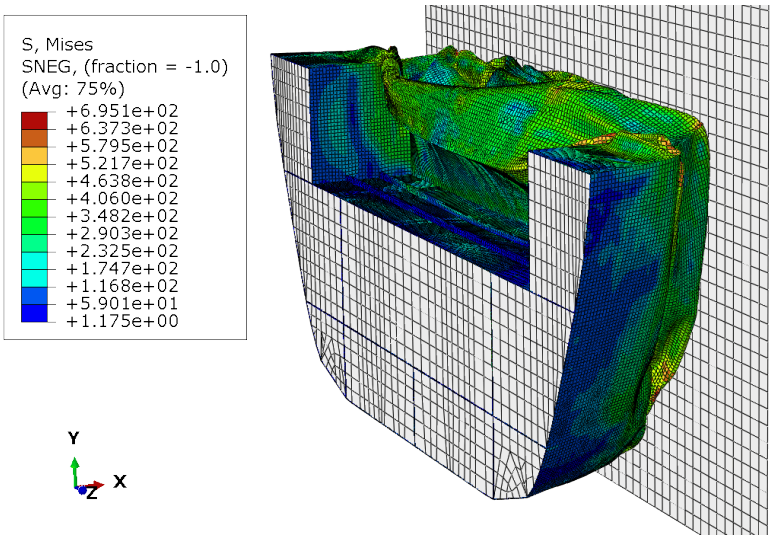

Figure I.2: Sietske simulation t = 1.4 s

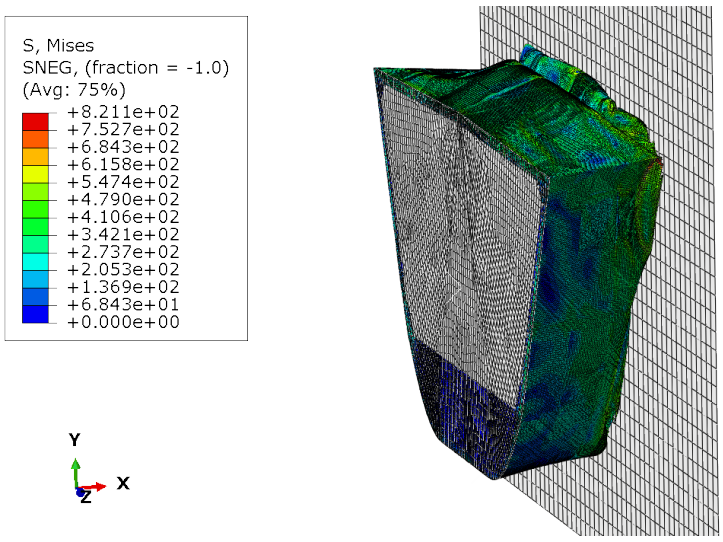

Figure I.3: Berdina simulation t = 0.5 s

Bibliography

[1] InCom Working Group 19. *Ship Collisions due to the Presence of Bridges*. Pianc, 2001.

[2] AASHTO. *Guide Specifications and Commentary for Vessel Collision Design of Highway Bridges*. American Association of State Highway and Transportation Official, 2009.

[3] A AbuBakar and R S Dow. The impact analysis characteristics of a ship's bow during collisions. *Engineering failure analysis*, 100, 2019.

[4] H S Alsos and J Amdahl. On the resistance of tanker bottom structures during stranding. *Marine Structures*, 20(4), 2007.

[5] J Amdahl and E Eberg. Ship collision with offshore structures. In *Structural Dynamics EURODYN*, volume 93, 1993.

[6] J Amdahl and T Soreide. Energy absorption in ship-platform impacts. In *Reports of the Working Commissions (International Association for Bridge and Structural Engineering 42*. The Norwegian Institute of Technology, Trondheim, 1983.

[7] ASTM International. *Standard test methods for tension testing of metallic materials*. ASTM international, 2012.

[8] D M Bae, A R Prabowo, B Cao, A F Zakki, and G D Haryadi. Study on collision between two ships using selected parameters in collision simulation. *Journal of Marine Science and Application*, 15(1), 2016.

[9] J Banks. *Discrete event system simulation*. Pearson Education India, 2005.

[10] M J Barba. Mémoires de la Société des Ingénieurs Civils. *Memoirs of the Society of Civil Engineers*, 1880.

[11] A Bela, H Le Sourne, L Buldgen, and P Rigo. Ship collision analysis on offshore wind turbine monopile foundations. *Marine Structures*, 51, 2017.

[12] M A G Calle and M Alves. A review-analysis on material failure modeling in ship collision. *Ocean Engineering*, 106, 2015.

[13] W D Jr. Callister. *Fundamentals of Materials Science and Engineering*. John Wiley & Sons, 2nd edition, 2005. ISBN 978-0-471-47014-4.

[14] J F Chan. *Technical Report Internship at Nobleo*. TU Delft, 2020.

[15] G R Consolazio and D R Cowan. Nonlinear analysis of barge crush behavior and its relationship to impact resistant bridge design. *Computers and Structures*, 81(8-11), may 2003. ISSN 00457949. doi: 10.1016/S0045-7949(02)00474-1.

[16] G R Cowper and P S Symonds. Strain-hardening and strain-rate effects in the impact loading of cantilever beams. Technical report, Brown Univ Providence Ri, 1957.

[17] DNVGL. *Part 3 Structures, equipment, Chapter 5 Other structures*. DNV-GL, 2015.

[18] DNVGL. DNVGL-RP-C208: Determination of structural capacity by non-linear finite element analysis methods. *Det Norske Veritas*, 2016.

[19] S Ehlers, J Broekhuijsen, H S Alsos, F Biehl, and K Tabri. Simulating the collision response of ship side structures: a failure criteria benchmark study. *International Shipbuilding Progress*, 55(1-2), 2008.

[20] D J Eyres and G J Bruce. *Ship Construction (Seventh Edition)*. Butterworth-Heinemann, 2012.

[21] A Farinha, L Sousa, and L Reis. Evaluating lock gates' strength due to ship collisions: A douro waterway lock gates case study. *Marine Structures*, 60, 2018.

[22] C Gabrielle. An aerial photo from may 9, 1980, shows the freighter summit venture after it collided with the sunshine skyway bridge. the bridge collapse killed 35 people., 1980. URL https://www.tampabay.com/news/florida/2020/05/08/the-skyway-bridge-collapsed-40-years-ago-heres-how-were-remembering-the-tragedy/.

[23] G Gerard. Handbook of structural stability part V: compressive strength of flat stiffened panels. 1957.

[24] Nicolás Guarín-Zapata. Stress vs. strain diagram for a ductile material, 2020. URL https://commons.wikimedia.org/wiki/File:Stress_strain_ductile.svg.

[25] S Haris and J Amdahl. Analysis of ship–ship collision damage accounting for bow and side deformation interaction. *Marine Structures*, 32, 2013.

[26] J J Harrigan, S R Reid, and C Peng. Inertia effects in impact energy absorbing materials and structures. *International Journal of Impact Engineering*, 22(9-10), 1999.

[27] M de Hertog. *Aanvaarbelasting op starre constructies volgens ROK 1.3*. 2019.

[28] P Hogstrom. RoPax Ship Collision–a Methodology for Survivability Analysis, 2012.

[29] P Hogstrom and J W Ringsberg. An extensive study of a ship's survivability after collision - a parameter study of material characteristics, non-linear FEA and damage stability analyses. *Marine structures*, 27 (1), 2012.

[30] P Hogstrom, J W Ringsberg, and E Johnson. Survivability analysis of a struck ship with damage opening - influence from model and material properties uncertainties. *Ships and Offshore Structures*, 6(4), 2011.

[31] J H Hollomon. Tensile deformation. *Trans. AIME*, 12(4), 1945.

[32] H Huang. College physics i. *Department of Applied Physics, Hong Kong PolyU*, 2020.

[33] O F Hughes, B Dominique, and J K Paik. *Ship structural analysis and design*. Society of Naval Architects and Marine Engineers, 2010.

[34] T J R Hughes. *The Finite Element Method: Linear Static and Dynamic Finite Element Analysis*. Prentice-Hall, 1987. ISBN 9780133170252.

[35] N D Joustra and R P N Pater. Aanvaarbelasting door schepen op starre constructies. 1993.

[36] D Karagiozova, M Alves, and N Jones. Inertia effects in axisymmetrically deformed cylindrical shells under axial impact. *International Journal of Impact Engineering*, 24(10), 2000.

[37] S Khasnabis. Types of Bow Designs Used For Ships, 2020. URL https://www.marineinsight.com/naval-architecture/types-of-bow-designs-used-for-ships/.

[38] O Kitamura. FEM approach to the simulation of collision and grounding damage. *Marine Structures*, 15 (4-5), 2002.

[39] Y G Ko, S J Kim, J M Sohn, and J K Paik. A practical method to determine the dynamic fracture strain for the nonlinear finite element analysis of structural crashworthiness in ship–ship collisions. *Ships and Offshore Structures*, 13(4), 2018.

[40] O D Larsen. *Ship collision with bridges: The interaction between vessel traffic and bridge structures*, volume 4. IABSE, 1993.

[41] A Laulusa, O A Bauchau, J Y Choi, V B C Tan, and L Li. Evaluation of some shear deformable shell elements. *International Journal of Solids and Structures*, 43(17), 2006.

[42] E Lehmann and X Yu. Progressive folding of bulbous bows. *6th Intl Symposium on Practical Design of Ships and Mobile Units*, 1995.

[43] Lloyds Register. *Rules for the manufacture, testing and certification of materials 1993*. Lloyds Register of Shipping, 2018.

[44] M Lutzen. Ship collision damage. *PhD Thesis, Department of Mechanical Engineering, Technical University of Denmark*, 2001.

[45] A Mansour, D Liu, and J R Paulling. *The Principles of Naval Architecture Series*. The Society of Naval Architects and Marine Engineers, 2008.

[46] V U Minorsky. An Analysis of Ship Collision to Protection of Nuclear Power Plant. Technical report, 1959.

[47] NEN. *NEN-EN 1991-1-7: Eurocode 1: Actions on structures - Part 1-7: General actions - Accidental actions*. Nederlands Normalisatie-instituut, 2015.

[48] J K Nunez. 28 January 1980, Blackthorn and Capricorn: Collision with History in Tampa Bay. 2003.

[49] E Onate. *Structural analysis with the finite element method. Linear statics: volume 2: beams, plates and shells*. Springer Science & Business Media, 2013.

[50] J K Paik. Practical techniques for finite element modeling to simulate structural crashworthiness in ship collisions and grounding (Part I: Theory). *Ships and Offshore Structures*, 2(1), 2007.

[51] J K Paik. *Ultimate limit state analysis and design of plated structures*. Wiley Online Library, 2018.

[52] J K Paik. *Advanced structural safety studies: with extreme conditions and accidents*, volume 37. Springer, 2019.

[53] J K Paik and J Y Chung. A basic study on static and dynamic crushing behavior of a stiffened tube. *Transactions of the Korean Society of Automotive Engineers*, 7(1), 1999.

[54] J K Paik and O F Hughes. Modeling complex engineering structures. *Ship structures*, 2006.

[55] J K Paik and A K Thayamballi. *Ultimate limit state design of steel-plated structures*. John Wiley & Sons, 2003.

[56] J K Paik, K J Kim, J H Lee, B G Jung, and S J Kim. Test database of the mechanical properties of mild, high-tensile and stainless steel and aluminium alloy associated with cold temperatures and strain rates. *Ships and Offshore Structures*, 12(sup1), 2017.

[57] P T Pedersen, S Valsgård, D Olsen, and S Spangenberg. Ship impacts: Bow collisions. *International Journal of Impact Engineering*, 13(2), 1993. ISSN 0734-743X.

[58] S R Reid and T Y Reddy. Experimental investigation of inertia effects in one-dimensional metal ring systems subjected to end impact—I. Fixed-ended systems. *International Journal of Impact Engineering*, 1(1), 1983.

[59] Rijkswaterstaat. Richtlijnen Ontwerpen Kunstwerken (ROK) 1.4, apr 2017. URL `http://publicaties.minienm.nl/documenten/richtlijnen-ontwerp-kunstwerken-rok-1-4`.

[60] R G Sargent. Verification and validation of simulation models. *Journal of simulation*, 7(1), 2013.

[61] Y Sha and H Hao. Nonlinear Finite Element Analysis of Barge Collision with a Single Bridge Pier. *Engineering Structures*, 41, 2012. ISSN 0141-0296.

[62] SIMULIA. *ABAQUS, "Version 6.13 user's manual,"*. SIMULIA, 2013.

[63] Simulia. Support case 4326 "Artificial Energy in Crashworthiness Analysis". 2014.

[64] A Soderberg and U Sellgren. Modelling of strain hardening and strain rate hardening of dual phase steels in finite element analysis of energy-absorbing components. In *NAFEMS World Congress*, number 69, 2005.

[65] Y Song and J Wang. Development of the impact force time-history for determining the responses of bridges subjected to ship collisions. *Ocean Engineering*, 187, 2019.

[66] NORSOK Standard. Design of steel structures. *N-004, Rev*, 2, 2004.

[67] M Storheim and J Amdahl. Design of offshore structures against accidental ship collisions. *Marine Structures*, 37, 2014.

[68] M Storheim and J Amdahl. On the sensitivity to work hardening and strain-rate effects in nonlinear FEM analysis of ship collisions. *Ships and Offshore Structures*, 12(1), 2017.

[69] M Storheim, G Notaro, A Johansen, and J Amdahl. Comparison of ABAQUS and LS-DYNA in simulations of ship collisions. *Proceedings of the ICCGS 2016*, 2016.

[70] M Storheim, H S Alsos, and J Amdahl. Evaluation of Nonlinear Material Behavior for Offshore Structures Subjected to Accidental Actions. *Journal of Offshore Mechanics and Arctic Engineering*, 140(4), 01 2018. ISSN 0892-7219.

[71] R Sual and H Svensson. On the theory of ship collision against bridge piers. *IABSE Proc. No. 2*, 1982.

[72] S Timoshenko and J M Gere. *Theory of Elastic Stability*. Dover Publications Inc., New York, second edition edition, 1963.

[73] R Toernqvist and B C Simonsen. Safety and structural crashworthiness of ship structures; modelling tools and application in design. *Society of Naval Architects of Japan*, 2004.

[74] Photographer unknown. I40 bridge collapse kills 14, 2002. URL `http://www.tulsaworld.com/may-i--bridge-collapse-kills/article_07ba4d68-68a1-11e6-a2e0-eb01ff3cedc9.html`.

[75] Photographer unknown. I40 bridge disaster, 2017. URL `https://commons.wikimedia.org/wiki/File:I40_Bridge_disaster.jpg`.

[76] Photographer unknown. Gehavende schelpenzuiger die tegen oosterscheldekering knalde naar sluiskil versleept, 2018. URL `https://www.pzc.nl/zeeuws-nieuws/gehavende-schelpenzuiger-die-tegen-oosterscheldekering-knalde-naar-sluiskil`.

[77] Photographer unknown. Schelpenzuiger botst met oosterscheldekering, 2018. URL `https://www.knrm.nl/nieuws/knrm-reddingstation-neeltje-jans/schelpenzuiger-botst-met-oosterscheldekering`.

[78] Vereniging de Binnenvaart. Database debinnenvaart.nl. URL `https://www.debinnenvaart.nl/schepen_a_z/`.

[79] A Vredeveldt and E Feenstra. Crashworthy side structures for improved collision damage survivability of coasters and medium sized Ro-Ro cargo ship. Technical report, Report GRD1-1999-10566, TNO/UNI, Netherlands, 2001.

[80] A C W M Vrouwenvelder, U Stieffel, and G Harding. Accidental actions background document, 3rd draft, februari. *Eurocode 1, Part 1.7*, 2010.

[81] T Vrouwenvelder. Joint Committee on Structural Safety. *Structural Safety*, 19(3), 1997.

[82] T Vrouwenvelder. Stochastic modelling of extreme action events in structural engineering. *Probabilistic Engineering Mechanics*, 15(1), 2000. ISSN 0266-8920.

[83] G Wang and J Spencer. Ultimate Limit State Design of Steel-Plated Structures. *Marine Technology and SNAME News*, 40(3), 2003.

[84] G Wang, J Spencer, and Y Chen. Assessment of a ship's performance in accidents. *Marine structures*, 15 (4-5), 2002.

[85] T Wierzbicki and W Abramowicz. On the crushing mechanics of thin-walled structures. *Journal of Applied Mechanics*, 50, 1983.

[86] G Woisin. Design against Collision. *Advances in Marine Technology*, 1979.

[87] G Woisin. Structures Against the Effects of Ship Collision. *Shift und Hafen/Kommando-Brucke*, 31, 1979.

[88] F Wu, R Spong, and G Wang. Using numerical simulation to analyze ship collision. In *Third International Conference on Collision and Grounding of Ships (ICCGS)*, 2004.

[89] Y Yamada. Bulbous buffer bows: a measure to reduce oil spill in tanker collisions. 2006. (PhD Thesis, Department of Mechanical Engineering. Technical University of Denmark, Lyngby, Denmark.

[90] P. D.C. Yang and J. B. Caldwell. Collision energy absorption of ships' bow structures. *International Journal of Impact Engineering*, 1988.

[91] J Zhang, X Chen, D Liu, and X Li. Analysis of bridge response to barge collision: Refined impact force models and some new insights. *Advances in Structural Engineering*, 19(8), 2016.

[92] S Zhang, P T Pedersen, and R Villavicencio. *Probability and mechanics of ship collision and grounding*. Butterworth-Heinemann, 2019.